Immobilization of functionalized glycosaminoglycans to regulate protein adsorption and cell behavior

Dissertation

zur Erlangung des
Doktorgrades der Naturwissenschaften (Dr. rer. nat.)

der

Naturwissenschaftlichen Fakultät I – Biowissenschaften –

der Martin-Luther-Universität
Halle-Wittenberg,

vorgelegt

von Herrn Dipl. Chem. Alexander Köwitsch

geb. am 17.08.1982 in Salzwedel

Gutachter: Prof. Dr. rer. nat. habil. Thomas Groth
Prof. Dr. rer. nat. habil. Karsten Mäder
Prof. Dr. Gloria Gallego Ferrer

Datum der öffentlichen Verteidigung: 30.08.2016

Meiner Familie

Table of contents

Abstract

Surface modification in the micro- and nanoscale can be used to control material properties. The application of glycosaminoglycans (GAG) for the coating and structuration of material surfaces offers great potential in the field of biomaterial research. GAG represents a unique class of bioactive polysaccharides that are able to specifically bind a multitude of natural binding partners like growth factors and adhesive proteins. Thus, it is possible to control cell behavior such like adhesion, growth and differentiation. The stability of material coatings and its biocompatibility display crucial features for the intended application of each particular biomaterial. Therefore, a covalent attachment of GAG to material surfaces provides an appropriate approach to create stable material coatings with suitable properties.

Hence, two different approaches (oxidation and thiolation) were used for the chemical activation of the GAG heparin, chondroitin sulfate, hyaluronic acid (HA) and sulfated HA by introducing reactive functional groups into their glycan structure. The degree of modification was varied to investigate a possible impact on the GAG`s reactivity and biocompatibility. The activated GAG were subsequently immobilized to different model substrata by covalent reactions. This surface grafting could be achieved in a homogeneous approach as well as in a heterogeneous manner via microcontact printing. In addition, oxidized heparin was used as a cross-linker for succinylated gelatin to generate nanoparticles which were successfully applied as a template for the mineralization of hydroxyapatite.

The homogeneously coated substrata showed distinguishable surface properties, such as surface topography and coating thickness. Moreover, the wettability and the surface zeta potential were directly related to the sulfation degree of the immobilized GAG and similarly supported the successful surface grafting. An increase of reactive groups also enhanced the amount of immobilized GAG and the resulting surface roughness.

Protein adsorption experiments revealed the specific binding capability of immobilized HA to its natural binding partner aggrecan. Further, fibronectin adsorption was clearly correlated to the degree of sulfation of the immobilized GAG, which both indicated the maintenance of bioactivity of the modified GAG.

Abstract

Cell experiments with human fibroblasts showed an increasing number of adhering cells in dependence on the sulfation degree of the immobilized GAG. Finally, cell growth and viability tests demonstrated that cell proliferation was higher for the substrata coated with sulfated GAG and not hampered by the modification of the GAG in general, which was taken as another evidence for the bioactivity of the activated GAG. Overall, oxidized and thiolated GAG are useful as building blocks for bioactive surface coatings of 3D-structures like nanoparticles useful in different tissue engineering applications.

Zusammenfassung

Zur Steuerung von Materialeigenschaften können Oberflächenmodifizierungen im Mikro- und Nanometerbereich eingesetzt werden. Die Anwendung von Glykosaminoglykanen (GAG) für die Beschichtung und Strukturierung von Materialoberflächen besitzt ein großes Potenzial im Bereich der Biomaterialentwicklung. GAG stellen eine einzigartige Klasse von biologisch aktiven Polysacchariden dar, die fähig sind, spezifische Wechselwirkungen mit einer Vielzahl von natürlichen Bindungspartnern wie Wachstumsfaktoren und adhäsive Proteine einzugehen. Somit ist es möglich, das Zellverhalten, wie Adhäsion, Wachstum und Differenzierung zu steuern. Die Beständigkeit der Beschichtung und ihre Biokompatibilität spielen eine entscheidende Rolle für das beabsichtigte Anwendungsgebiet der entsprechenden Biomaterialien. Folglich bildet die kovalente Bindung von GAG an Materialoberflächen einen vielversprechenden Ansatz für die Erzeugung von beständigen Materialbeschichtungen mit genau definierten Eigenschaften.

Daher wurden die GAG Heparin, Chondroitinsulfat, Hyaluronsäure (HA) und sulfatierte HA mittels zweier unterschiedlicher Ansätze (Oxidation und Thiolierung) chemisch aktiviert. Dabei wurde der Umsetzungsgrad beider Methoden variiert um eine mögliche Auswirkung auf die Reaktivität und die Biokompatibilität der GAG feststellen zu können. Die aktivierten GAG wurden anschließend durch kovalente Reaktionen auf verschiedenen Materialien immobilisiert. Neben der homogenen Beschichtung konnte die Immobilisierung auch in strukturierter Weise mittels Mikrokontaktdrucken durchgeführt werden. Desweiteren wurde das oxidierte Heparin als Vernetzer für Gelatine verwendet um Nanopartikel zu erzeugen, die anschließend als Vorlage für die Mineralisierung von Hydroxylapatit eingesetzt wurden.

Je nachdem welches GAG aufgebracht wurde, zeigten die homogen beschichteten Oberflächen charakteristische Unterschiede in ihrer Oberflächenbeschaffenheit und der Beschichtungsdicke. Darüber hinaus waren die Benetzbarkeit und das Zetapotential der Oberflächen direkt mit dem Sulfatierungsgrad der immobilisierten GAG korreliert und bestätigten ebenfalls die erfolgreiche Immobilisierung der GAG. Eine höhere Konzentration an reaktiven Gruppen steigerte auch die Menge an immobilisiertem GAG und erhöhte die Oberflächenrauhigkeit.

Untersuchungen zur Proteinadsorption zeigten die spezifische Bindungsfähigkeit von immobilisierter HA zu seinem natürlichen Bindungspartner Aggrecan. Ferner machten Untersuchungen mit Fibronektin deutlich, dass mit steigender Sulfatierung des immobilisierten GAG auch die Bindung von Fibronektin zunahm. Demzufolge, konnte gezeigt werden, dass die spezifische Bioaktivität der modifizierten GAG erhalten blieb.

Das Adhäsionsverhalten von humanen Fibroblasten zeigte eine Zunahme von Zellen mit ansteigendem Sulfatierungsgrad der immobilisierten GAG. Ferner zeigten auch Untersuchungen zum Zellwachstum, dass Substrate, welche mit höher sulfatierten GAG beschichtet waren, erhöhte Wachstumsraten aufwiesen. Letzteres kann als weiterer Nachweis für die Aufrechterhaltung der Bioaktivität der aktivierten GAG angesehen werden. Folglich stellen die oxidierten und thiolierten GAG vielversprechende Komponenten für die Bildung von bioaktiven Materialbeschichtungen dar. Darüber hinaus können sie auch als Bestandteil von 3D-Strukturen wie Nanopartikeln dienen und in verschiedenen Anwendungen des Tissue Engineerings genutzt werden.

Chapter 1

Introduction

This cumulative thesis consists of six papers. The first manuscript is a review which is used as a general introduction to glycosaminoglycans and their medical application. The remaining five published papers are assembled as chapters 2-6 including a summary at the beginning of each chapter.

Medical application of glycosaminoglycans - A review

Alexander Köwitsch, Guoying Zhou, Thomas Groth*

Biomedical Materials Group, Institute of Pharmacy, Martin Luther University Halle-Wittenberg, Heinrich-Damerow-Str. 4, 06099 Halle (Saale), Germany

E-mail: thomas.groth@pharmazie.uni-halle.de

Phone: +49(0)345 55 28460

Fax: +49(0)345 55 27379

Abstract

The characteristic molecular composition of the different glycosaminoglycans (GAG) is related to their role as structural components and regulators of a multitude of functions of proteins, cells and tissues in the human body. Therefore it is not surprising that GAG are widely used as coating materials for implants, components of 3D-constructs like tissue engineering scaffolds and hydrogels, but also as diagnostic devices like biosensors and in controlled release applications. Beside a physisorption or encapsulation of GAG, these applications often require their chemical modification to allow a stable covalent attachment on surfaces or cross-linking reactions with other molecules. Then, the preservation of the functionality of GAG under maintenance of their biocompatibility is a challenging task and has to be addressed in accordance with the designated field of application. Here, we will give a brief overview on structure and biological functions of GAG, different methods of their activation and immobilization, the recent progress in GAG-related biomaterials development as well as some examples of their application in the field of tissue engineering and regenerative medicine.

Keywords: Tissue engineering, Biomaterials, Glycosaminoglycans, Chemical modifications, Immobilization, Hydrogels, Proteoglycans, Extracellular matrix

Content:

1. General introduction to structure and function of glycosaminoglycans

Glycosaminoglycans (GAG) are long-chain, unbranched polysaccharides that are present on the cell surface and as components of the extracellular matrix. They are consisting of repeating disaccharides linked by glycosidic bonds creating individual complex structures. Whereas proteins and nucleic acids are copied from a template in a series of identical steps applying the same enzymes, GAG, like other oligo- and polysaccharides, are assembled by different enzymes during each specific step of polymerization. Activated monosaccharides are polymerized by glycosyltranferases followed by a deacetylation/N-sulfation through N-deacetylase/N-sulfotransferase and epimerization by epimerases completed by O-sulfation via specific sulfotransferases [1]. Sulfated GAG are synthesized by specific enzymes in the Golgi apparatus of the cell, whereas hyaluronan (HA) is synthesized by transmembrane proteins called HA synthases. While HA is not linked to a protein and synthesized from its reducing end, the sulfated GAG are build up from the non-reducing end and synthesized as side chains attached to a protein forming so called proteoglycans (PG) [2]. The protein core is assembled and released from the endoplasmic reticulum (ER). Beforehand, a specific tetrasaccharide (for Hep/HS, CS/DS: Xyl-Gal-Gal-GlcA) is connected to a serine residue of the core protein as a linker region in the ER [3]. For sulfated GAG, an alternating polymerization of glucuronic acid (GlcA) or galactose (KS) and a glucosamine is accomplished by designated glycosyltransferases. Henceforth, deacetylation/N-sulfation and epimerization of GlcA to iduronic acid (IdoA) is followed by O-sulfation of the growing GAG chain performed by epimerases and sulfotransferases, respectively [4]. This individual processing of the GAG leads to distinctive patterns of functionalization which is also reflected by their unique structures (Figure 1).

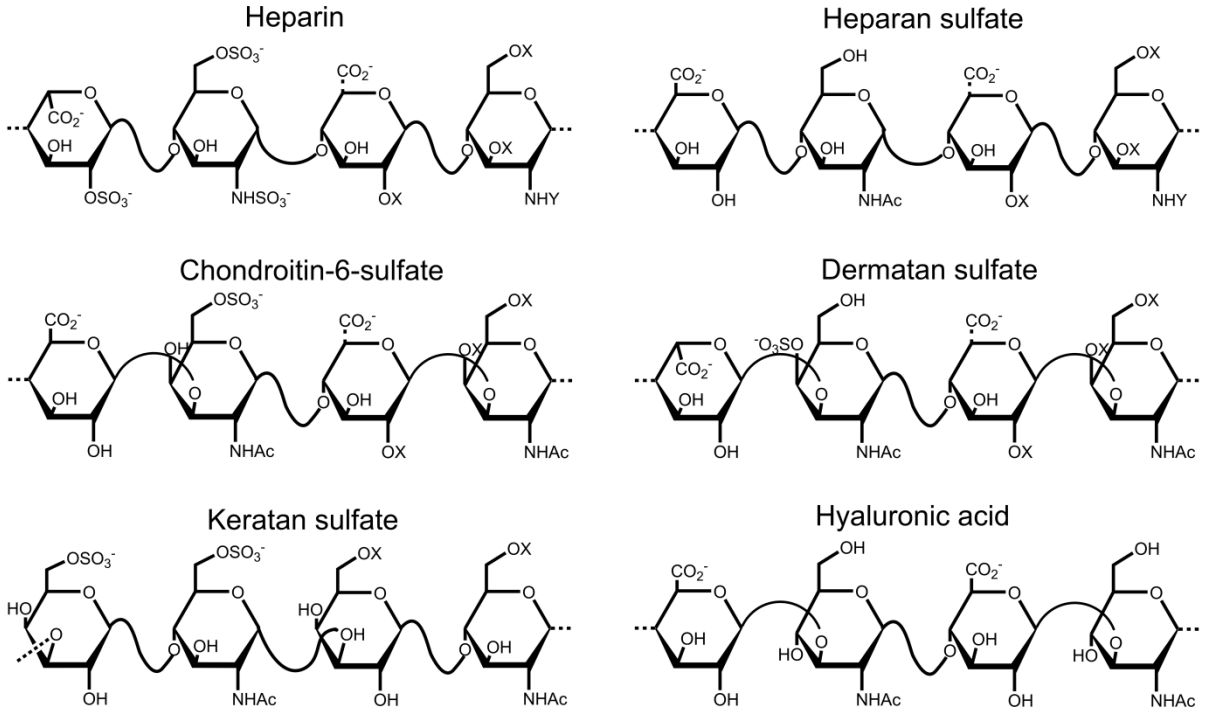

Figure 1: Major and variable disaccharide repeating unit of glycosaminoglycans. (X = -OH or $–OSO_3^-$; Y = -Ac or $-OSO_3^-$)

In contrast to glycoproteins that also exhibit carbohydrate side chains, the covalently attached GAG side chains make up most of the molecular weight (MW) of the PG and are principally responsible for most of their physiological functions [5]. In addition to intracellular and cell-surface PG found on almost all mammalian cell surfaces, they are components of the extracellular matrix (ECM) [6]. Structurally, PG can be categorized regarding their attached GAG into heparan sulfate PG (HSPG), chondroitin sulfate PG (CSPG), dermatan sulfate proteoglycans (DSPG), keratan sulfate PG (KSPG) and hyalectans which are aggregates of HA and extracellular PG that can also bind to lectins [7]. Moreover, one core protein is often linked to two different GAG like aggrecan carrying multiple CS and KS chains. According to their functions, PG can be also summarized in four groups (Table 1). Extracellular PG can be classified into three groups according to their protein structure (Figure 2a). Firstly, there are the high molecular weight PG aggrecan, versican, brevican and neurocan that are responsible for the compressive-resistant properties of cartilage, the tensile strength of skin and tendon as well as the mineralization of the bone matrix [2]. These PGs are able to bind to lectins with a specific CRD (carbohydrate-recognition domain) at the C-terminus and also to HA with a specific link module at their N-terminal domain and thus are often referred as lecticans or hyalectans [8, 9].

Furthermore, they can influence inflammation processes by the binding and regulation of inflammatory cytokines [10]. Secondly, small leucine-rich repeat PG (SLRP) like decorin and biglycan are supporting ECM components like collagens and are able to bind growth factors influencing several signaling cascades [11]. In addition, three testicans belong to the group of extracellular PG which possess a calcium-binding domain [12]. The pericellular or basement membrane PG (perlecan, agrin, collagen XV and XVIII, Figure 2b) are able to bind and cross-link many matrix components and cytokines like vascular endothelial growth factor (VEGF) and interleukin-2 (IL-2), thus, exhibiting multiple regulatory functions like maintenance of vascular homeostasis and control of cancer cell invasion [13, 14]. The transmembrane or cell-surface PG (Figure 2c) like syndecans and glypicans function as co-receptors for growth factors (GF) and adhesive proteins like fibronectin and mediate cell-cell and cell-matrix adhesions [15-17]. They can directly (binding of GF through HS or CS) or indirectly (in concert with integrins or GF receptors) activate cellular signaling cascades [18]. Furthermore, syndecans interact with other PG to execute endocytosis processes [19]. Inflammatory cytokines can shed the ectodomain of syndecans and further activate matrix metalloproteinases (MMPs), thus, controlling the number of active cell surface receptors [20]. Syndecans are also able to influence tumor growth and progression, e.g. syndecans-1 is a prognostic marker for several cancer types because it is solubilized by an increased heparanase activity [21, 22]. Serglycin, the only known intracellular PG, can also include Hep as GAG-side chains when assembled in mast cells of connective tissue [1, 23]. It is implicated in the binding and activation of inflammatory mediators [24, 25]. The degradation of PG usually takes place in the ECM and is executed by proteases like MMPs from the ADAMTS-family (a disintegrin and metalloproteinase with thrombospondin type I motifs), while the final breakdown of GAG takes place inside the lysosomes of the cell in the reverse sequence of their synthesis [26-28]. The latter breakdown of GAG is catalyzed either by hydrolases (e.g. heparin hydrolase, different exoglycosidases), which process hydrolytic cleavage or by lyases (heparinases, chondroitinases, hyaluronidases) that catalyze the eliminative cleavage of glycosidic bonds [29, 30]. A comprehensive summary of PG structure and function was recently published by Iozzo and Schaefer [31].

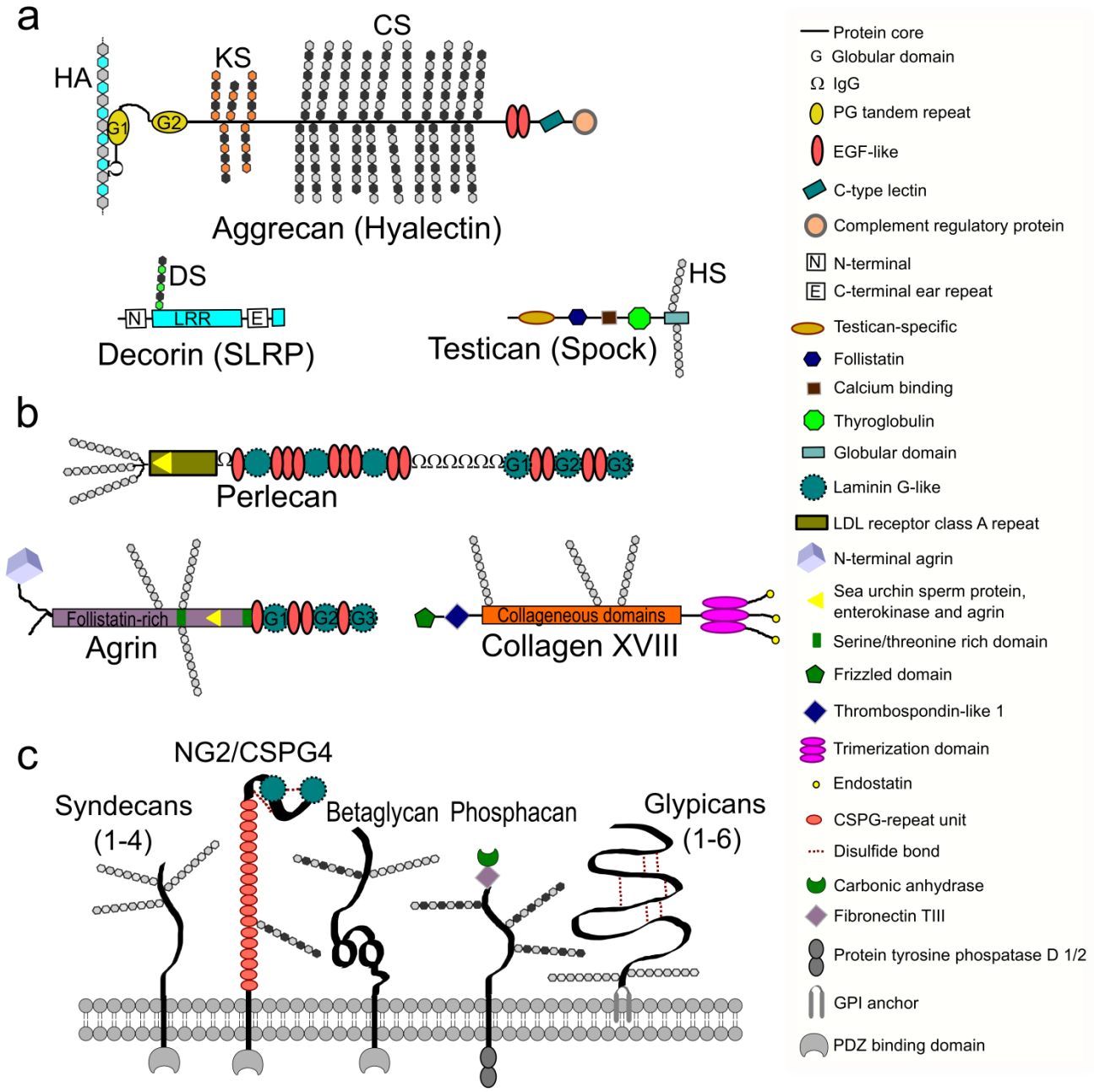

Figure 2: Schematic representation of extracellular matrix proteoglycans (PG) (a), pericellular PG (b) and transmembrane PG (c). SLRP - Small leucine-rich repeat PG; LRR - Leucine-rich repeat (Adapted from [31]).

Table 1: Glycosaminoglycan-containing proteoglycans divided into their four main classes. (Adapted from [31])

Location/Class	***PG***	***Predominant GAG component(s)***
Intracellular:		
Secretory Granules	Serglycin	Heparin
Cell surface:		
Transmembrane	Syndecans (1-4)	Heparan sulfate
	NG2, Phosphacan	Chondroitin sulfate
	Betaglycan	Chondroitin sulfate/ Heparan sulfate
GPI-Anchored	Glypicans (1-6)	Heparan sulfate
Pericellular:		
Basement membrane	Perlecan, Agrin, Collagen XVIII	Heparan sulfate
	Collagen XV	Chondroitin sulfate/ Heparan sulfate
Extracellular:		
Hyalectans	Aggrecan	Chondroitin sulfate/ Keratan sulfate
	Versican, Neurocan, Brevican	Chondroitin sulfate
SLRPS (small leucine-rich repeat proteoglycans)	Biglycan	Chondroitin sulfate
	Decorin	Dermatan sulfate
	Fibromodulin, Lumican, Keratocan, Osteoadherin	Keratan sulfate
	Epiphycan	Chondroitin sulfate/ Dermatan sulfate
Spock	Testican (1-3)	Heparan sulfate

2. Classification of glycosaminoglycans

2.1. Heparin (Hep)/Heparan sulfate (HS)

Hep and HS are composed of alternating saccharide units of N-acetylated or N-sulfated D-glucosamine that are α(1-4)- or β(1-4)-linked to uronic acids (L-iduronic or D-glucuronic acid). In particular, the main disaccharide of Hep is composed of iduronic acid (IdoA), which is sulfated at the carbon 2 (C2) and N-sulfated glucosamine (GlcNS). The latter is additionally sulfated at C6. On the other hand, the main disaccharide of HS consists of glucuronic acid (GlcA) and N-acetylated glucosamine (GlcNAc). The degree of sulfation of Hep is much higher than that of HS resulting in the highest negative charge density of all known biomacromolecules [32]. The sulfation pattern of Hep is more equally distributed over the whole GAG chain while HS shows distinct regions of high sulfation as well as segments that are lower or non-sulfated [33]. Hep and HS are synthesized as PG with Hep being processed only in connective-tissue-type mast cells or basophils while HSPG are produced in almost all mammalian cells [1, 34]. Thereby, Hep is synthesized on a specific core protein (serglycin) with a MW of up to 1000 kDa with Hep having a MW of 60-100 kDa [35]. Upon degranulation of mast cells or basophils, Hep chains are cleaved resulting in MW of 5-25 kDa and stored in secretory mast cell granules from where they are secreted into the extracellular space [36, 37]. Hep is released from mast cells by exocytosis of the mast cell granules upon exogenous stimulation, e.g. by the interaction of antigens with cell-surface bound IgE antibodies [38]. In contrast, HS is attached to PG, which assemble in the basement membrane (perlecan) or as cell-surface PG (e.g. several syndecans). Syndecans can act as co-receptors for growth factor (GF) binding or as direct signal transducers and are involved in the assembly of focal adhesions [39, 40]. Moreover, HSPG, like syndecans and glypicans, modulate different endocytosis pathways controlling the uptake of macromolecular cargo [19]. Hep is also essential for the storage of proteases in mast cell granules and also plays an important role in the prevention of autolysis of these proteases [41]. Because of their structural similarity, HS and Hep might also have similar regulative effects as they are able to bind a variety of GF, and thus, induce GF-mediated signal transduction [42, 43]. HS and Hep play also a role during inflammatory reactions [44]. HSPG like perlecan are presenting chemokines to integrins of leukocytes that promote the transmigration of leukocytes, while Hep is

capable to bind L- and P-selectin to inhibit leukocyte adhesion [45-47]. Hep can also inhibit leukocyte adhesion by direct binding to the integrin Mac-1 [48]. Depending on its specific sulfation motifs, HS can activate FGF- and FGFR-signaling pathways [49, 50]. Furthermore, HS is able to activate or inhibit cytokines like interleukins and tumor necrosis factor α (TNF-α) [51].

2.2. Chondroitin sulfate (CS)/Dermatan sulfate (DS)

CS comprises of alternating β(1-4) GlcA and β(1-3) N-acetylgalactosamine (GalNAc) that can be sulfated at the carbon 4 and/or 6 of the galactosamine and additionally at C2 and/or C3 of the GlcA. CS is named depending on the position of sulfation, e.g. CS-A for single sulfation at C4 of the GalNAc or CS-C for single sulfation at C6 of the GalNAc [52]. DS, also known as CS-B, is composed of alternating D-GlcA or L-IdoA (partly sulfated at C2) and GalNAc that can be sulfated at C4 or C6 [53]. CS and DS vary significantly in chain length and MW from 5-70 kDa with strong deviations even when isolated from a single source [29, 54]. Together with the sulfation pattern, this might directly impact on the biological functions [54, 55]. CS and DS are essential elements of various PG like SLRP or transmembrane PG, e.g. phosphacan (CSPG), which is able to interact with neurons and neural cell adhesion molecules (NCAM) [56]. SLRP like decorin (DSPG) and biglycan (CSPG) interact with collagen in the regulation of fibrillogenesis by the association of collagens as well as protecting them from enzymatic cleavage [57-59]. In cartilage and skin, CS-containing PG like aggrecan, that is bound to long hyaluronan chains, functions as shock absorber by resisting compressive forces via the uptake of water or influence the tissue elasticity, respectively [60, 61]. The role of CS in the pathogenesis of osteoarthritis is still frequently discussed [62-65]. CS and DS, as major (phosphacan, NG2) or minor (syndecans 1 and 4) GAG component of cell-surface PG, can specifically interact with GF like fibroblasts growth factors FGF-1, FGF-2 and transforming growth factors (TGFs) that possess a heparin-binding domain [53, 66, 67]. Thus, CS/DS influence signaling processes in cells making them important regulators during inflammation, wound healing and tumor development and progression [68-70]. The sulfation of CS/DSPG in cancer cells was found to be significantly decreased at C4 while it was increased at C6 resulting in a decrease of total sulfation compared to normal cells of the same tissue [71]. In addition, the chain length of CS/DS and the GAG content of the PG, decorin and versican, was decreased significantly.

2.3. Keratan sulfate (KS)

KS is composed of disaccharides of β(1-4) GlcNAc and β(1-3) galactose which both might be sulfated at C6. Therefore, KS is the only GAG lacking a carboxyl group. The MW of KS ranges from 5-25 kDa and is highly dependent on the tissue origin [72]. The main source of KS is the cornea where the highest concentration is found. Unlike other sulfated GAG, KS is synthesized as differently assembled saccharide chains connected to its core proteins [73]. Hence, three main classes of KS can be distinguished; in KS-I the KS is N–linked through GlcNAc to asparagine of the core protein, in KS-II it is O-linked through GalNAc to serine or threonine residues and in KS-III it is O-linked through mannose to serine [74, 75]. KS-I and KS-II can be distinguished by their enzymatic sensitivity, since KS-I is prone to digestion by keratanase I and II while KS-II is only sensitive to keratanase II [76]. Generally, KS-II is found in cartilage and characterized by a higher degree of sulfation and a shorter chain length than KS-I, which is the main KS in cornea and responsible for tissue hydration and corneal transparency. KS-III is found preferentially in PG of the brain and nervous tissue [75]. KS is a GAG component of several PG, as part of aggrecan in cartilage or in different SLRPs (e.g. lumican, keratocan, fibromodulin) but can be also found attached to proteins in brain and bone. Apart from the ECM, KS-I is also found intracellularly in eosinophil-specific granules [76]. A lack of lumican lead to a decrease in skin elasticity and opacity of the cornea by influencing the fibrillization of collagen [77]. Furthermore, SLRPs like fibromodulin and lumican are involved in osteoarthritic processes by the modulation of collagen fibrillogenesis and TGF-β signaling [78, 79]. Thereby, corneal KS is able to bind and interact with a multitude of proteins like ephrin and semaphorin [80]. Like other SLRPs, fibromodulin is able to bind to bone morphogenic protein BMP-2 resulting in an increased expression of the transcription factor RunX and Ca^{2+} accumulation leading to an ossification of tendon [81]. Lumican is able to modulate the TLR4 (Toll-like receptor 4) signal pathway in lumican-deficient macrophages leading to a decrease of the pro-inflammatory response [82]. However, KS occurrence is not limited to interstitial connective tissue like cartilage and can be also found as part of cell trans-membrane proteins like CD44 and MUC1 [74].

2.4. Hyaluronan (Hyaluronic acid, HA)

In contrast to sulfated GAG, HA is synthesized by integral membrane proteins (HA-synthases) from its reducing end and released to the extracellular space [83]. HA represents the only non-sulfated GAG and is not linked to a protein core. HA consists of alternating GlcA and GlcNAc monosaccharides, which are connected by β(1-4) and β(1-3) glycosidic bonds, respectively. The molecular weight of HA depends on the tissue and species origin and can reach up 12×10^6 Da in naked mole rats [84, 85]. In humans the MW of HA is correlated to age, especially the MW of cartilage HA is decreasing from 2×10^6 Da to 5×10^5 Da within a lifetime [86]. The highest HA concentrations in humans are found in umbilical cord, synovial fluid, skin and the vitreous body of the eye [61]. HA has distinct biological properties depending on its molecular weight (distribution). High molecular weight HA has anti-angiogenic, immunosuppressive and anti-inflammatory properties, while low molecular weight HA is highly angiogenic, immunostimulatory and exhibits pro-inflammatory properties [87]. In the extracellular space HA is typically bound to matrix proteins (PG), which are called hyaladherins [88]. This connection is often accomplished via linker modules of the proteins that specifically bind to a decasaccharide sequence of HA [89]. Thus, HA is able to bind to proteoglycans like aggrecan and versican building up large aggregates to provide structural integrity of cartilage, skin and other tissues by the inclusion of water [90]. Furthermore, the viscoelastic properties of HA solutions are the basis of the viscous and elastic properties of the synovial fluid [91, 92]. HA is a key regulator in inflammation as it is cross-linked by different hyaladherins like CD44 and TSG-6 (tumor necrosis factor-stimulated gene-6) building up a pericellular coating of cells, which not only protects from inflammatory mediators but also acts also as immunosuppressor as it prevents ligand access and inhibits phagocytosis by macrophages and monocytes [87, 93]. On the other hand, HA species of lower MW are known to promote inflammation processes by the interactions with TLR, the activation and maturation of dendritic cells and by inducing the release of pro-inflammatory cytokines [94]. A decrease of the mean MW of HA in synovial fluid by reactive oxygen species that are generated during inflammation processes is found in osteoarthritis (OA) patients [95]. Here, HA interactions with specific cell-surface receptors, notably CD44 and RHAMM (receptor for HA-mediated motility) play an essential role in immune response as they can lead to the internalization of

HA [96, 97]. The turnover of HA and its CD44-mediated endocytosis by macrophages is upregulated in inflammation [98]. Notably, extracellular HA binds to TLR-2 and TLR-4 of T cells and macrophages to induce the expression of pro-inflammatory cytokines and chemokines [99, 100]. Elevated serum levels of HA are also associated with a faster OA progression and a higher incidence of rheumatoid arthritis [101, 102]. HA interactions with cell surface receptors, primarily CD44 and RHAMM, are also associated with indispensable signaling processes regulating cancer cell motility, tumor progression and metastasis [103]. High HA levels in tumor tissue are often correlated to a poor prognosis for cancer patients [104, 105]. This is likely originated to the association of inflammation and cancer [106]. In detail, HA is capable to alter macrophage polarization to secrete pro-inflammatory factors and to prevent the extravasation of leukocytes leading to a chronic inflammation, which favours tumor proliferation and metastasis [107, 108]. Inflammatory stimuli give also rise to an enhanced HA synthesis as well as to the cleavage of HA via hyaluronidases that are most active at acidic pH, and thus, to higher extracellular HA concentrations, which attract more leukocytes [109, 110]. This increased distribution of HA in inflammation was also shown in patients with inflammatory disorders like asthma and Crohn`s disease [109].

3. Survey on medical application of native glycosaminoglycans

In the emerging field of glycobiology, GAG play a vital and evolving role [111]. In particular, their multiple effects as signaling molecules, regulatory effects on protein activity, as structural components and effectors on cellular activity are unmatched [114]. Thus, GAG are extensively used in different medical applications because of their multiple regulatory functions, e.g. in anticoagulation of blood, inhibition of tumor growth and metastasis, but also control of inflammatory processes. Also, in the design of biomaterials the application of GAG, is a promising approach because they display specific interactions with a plethora of proteins and cells [112, 113].

3.1. Application of glycosaminoglycans as anticoagulants

Heparin (Hep) and dermatan sulfate (DS) are two main GAG having profound anticoagulant and antithrombotic activities [114]. Hep, the classic anticoagulant, has been used to interfere with blood coagulation for over 60 years. The anticoagulant activity of Hep was firstly reported by Mclean in 1916 and was confirmed by many

other studies afterwards [115]. Nowadays, it is still the major drug for routine in patients during hospitalization, extracorporeal blood circulation, but also treatment of thrombotic diseases, such as venous thromboembolism (VTE) and as adjuvant therapies for atherothrombotic syndromes [116] [117]. The anticoagulant activity of Hep is due to its unique binding of antithrombin (ATIII) with a pentasaccharide sequence, which amplifies ATIII affinity to thrombin and inhibits thrombin and other coagulation enzymes, thus preventing blood coagulation [114]. Therefore, Hep is widely used as an anticoagulant in a variety of clinical applications [44, 118]. However, besides ATIII, it was found recently that the heparin cofactor II (HCII) is also an important effector component involved in inhibition of blood coagulation. Importantly, HCII can be activated by Hep, forming a 1:1 stable complex to inactivate thrombin [119]. Therefore, the blood coagulation inhibiting property of Hep is attributed to both the binding of ATIII as well as the activation of HCII. On the other hand, DS was also successfully used as anticoagulant for hemodialysis patients because of its property to act as an activator of HCII [120, 121]. By sulfation, it is also possible to add anticoagulant activity to HA [122]. However, it should be mentioned that the misuse of chemically modified GAG (other than Hep), as an alternative to overly used heparin, can lead to severe side reactions as happened in 2007/08 when heparin that was contaminated with oversulfated CS led to numerous death of patients [123, 124]. Nowadays, different methods can be applied to uncover the type of saccharide sequences that are responsible for the specific binding to proteins and particularly if this ability is maintained after modification of the GAG. The utilization of arrays that use specific saccharide sequences (oligosaccharides, OS) is frequently utilized for this purpose [125, 126]. The production of OS via enzymatic synthesis or the *de novo* synthesis of OS are both well-established and can be possibly applied to replace Hep by synthetic GAG [127, 128].

3.2. Application of glycosaminoglycans as anti-inflammatory agents

Apart from their anticoagulant activity, GAG are also implicated in inflammatory processes, exhibiting an anti-inflammatory potential, as demonstrated in many experimental studies and clinical trials (Figure 3) [55, 129-131]. For instance, Hep has shown beneficial effects in the treatment of asthma and ulcerative colitis diseases [132, 133], while CS can help patients with knee and hand osteoarthritis [55]. In general, GAG can bind and interact with a wide range of proteins including

ECM adhesive proteins (e.g. collagen, fibronectin, laminin), as well as cytokines, growth factors, chemokines and enzymes to modulate biological processes such as migration, homing, growth and differentiation of leukocytes, which are associated with inflammation [134, 135]. For example, both CS and Hep can bind to L- and P-selectin, which impairs leukocyte adhesion, activation and transmigration activities [136]. Furthermore, both CS and Hep can mediate anti-inflammatory effects by inhibition of nuclear factor-κB (NF-κB) translocation, which is a crucial transcription factor of many pro-inflammatory mediators, leading to suppression of pro-inflammatory cytokine production [137]. By contrast, high molecular weight HA (HMW-HA) prevents inflammatory responses through interactions with CD44, which translates the signals from HA to down-regulate leukocyte activation, growth, and differentiation [94]. Although there is great potential of above-mentioned GAG as anti-inflammatory agents, it should be noted that some GAG also exhibited pro-inflammatory effects, depending on their specific structures or under specific conditions. For example, HS on the endothelial surface can interact with selectins and presents chemoattractants, promoting leukocyte recruitment, activation and transmigration [138]. The effects of HA in modulating inflammation are even depending on its molecular weight [94]. Upon injury, the production of HMW-HA increases immediately serving as anti-inflammatory molecules via specific interactions with CD44. However, the HMW-HA is rapidly cleaved into fragmented low-molecular weight HA (LMW-HA), which functions as pro-inflammatory effector through interactions with toll-like receptors (TLR) on leukocytes, which activate the release of pro-inflammatory effectors [94]. Thus, the involvement of various GAG in inflammation is complex and represents both pro- and anti-inflammatory mediators (Figure 3).

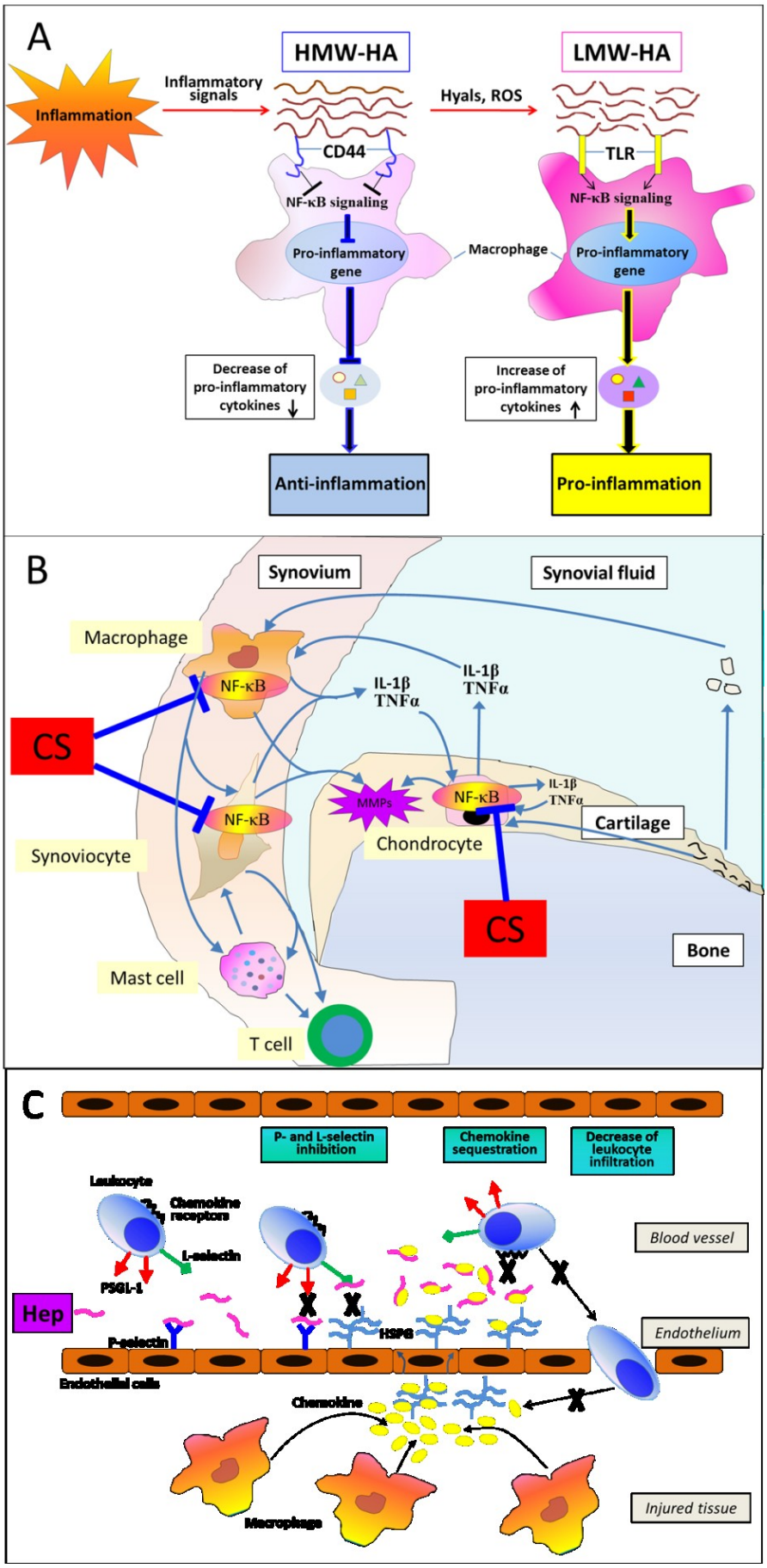
A
Inflammation
Inflammatory signals
HMW-HA
CD44
NF-κB signaling
Pro-inflammatory gene
Macrophage
Hyals, ROS
LMW-HA
TLR
NF-κB signaling
Pro-inflammatory gene
Decrease of pro-inflammatory cytokines
Increase of pro-inflammatory cytokines
Anti-inflammation
Pro-inflammation
B
Synovium
Synovial fluid
Macrophage
NF-κB
IL-1β
TNFα
CS
NF-κB
MMPs
NF-κB
IL-1β
TNFα
Cartilage
Chondrocyte
Synoviocyte
CS
Bone
Mast cell
T cell
C
P- and L-selectin inhibition
Chemokine sequestration
Decrease of leukocyte infiltration
Leukocyte
Chemokine receptors
L-selectin
PSGL-1
Hep
P-selectin
HSPG
Endothelial cells
Blood vessel
Endothelium
Chemokine
Macrophage
Injured tissue

Figure 3: Schematic diagrams of anti- and pro-inflammatory effects of hyaluronic acid (HA), chondroitin sulfate (CS) and heparin (Hep). **(A)** Functions of HA. During inflammation, the inflammatory stimuli trigger increased production levels of high molecular-weight HA (HMW-HA). However, HMW-HA can be catabolized into fragmented low molecular-weight HA (LMW-HA) in the presence of mediators such as hyaluronidases and reactive oxygen species (ROS). HMW-HA can bind to CD44 receptor and down-regulate pro-inflammatory cytokine production, exhibiting anti-inflammatory activities; LMW-HA promotes inflammatory responses through toll-like receptors (TLRs) on macrophages and regulates pro-inflammatory gene expression [94]. **(B)** Anti-inflammatory activities of CS in osteoarthritis. Cartilage damage results in extracellular matrix fragments (EMFs) that can activate chondrocytes by increasing the translocation of nuclear factor-κB (NF-κB) in chondrocytes, synovial macrophages and synoviocytes. The activated cells will release pro-inflammatory cytokines and matrix metalloproteinases (MMPs), exacerbating inflammation and cartilage destruction. CS can elicit anti-inflammatory effects by inhibition of the NF-κB translocation, leading to suppression of pro-inflammatory cytokine production and decrease of osteoarthritis (adapted from [137]). **(C)** Anti-inflammatory effects of Hep. In response to inflammatory stimuli, macrophages can produce chemokines that attract more leukocytes into the inflamed tissues. Hep can bind to L- and P-selectin, but also the chemokines, which can impair leukocyte adhesion, activation and transmigration activities. As a consequence, the lesser activation and infiltration of leukocytes results in attenuation of chemokine and pro-inflammatory cytokine release (adapted from [139]).

3.3. Application of glycosaminoglycans as antitumor agents

Due to the specific biologic roles of GAG in regulating growth factor signalling, cancer cell behaviour, inflammation and tumor progression and metastasis, GAG are involved in multiple cancer-related processes [21, 140]. Thus, they also play an important role in the prognosis and progress of cancer as their composition, distribution, molecular weight and sulfation display distinct changes [141]. Expression changes in GAG and their related enzymes can contribute to different steps of tumor progression, which have been endowed a predictive value for the clinical outcome of cancer [27]. For instance, high levels of HA expression are normally correlated to a poor prognosis for cancer patients [104, 105]. On the other hand, GAG and GAG-

based molecules have been considered as promising molecules for antitumor therapeutics, in particular Hep and CS [21, 142]. The antitumor effects of Hep are linked to its anticoagulant activity that can decrease thrombin generation and fibrin formation around tumor cells, but also by inhibition of heparanase as well as interfering with P-selectin-HSPG interactions to suppress cancer growth and metastasis [140]. Therefore, Hep and also HS are promising biomolecules for the development of anticancer therapeutics because they play a decent role in GF-driven signaling processes involved in tumor onset and progression [143]. Consequently, modified LMW-Hep was introduced as an orally active anti-cancer drug for prevention of lung cancer [144, 145]. By contrast, CS has been proven a potential anticancer therapeutics because of its anti-angiogenic effects during tumor progression [146]. On the other hand, HA has been exploited as tumor-specific targeting molecular for chemotherapy delivery of anti-cancer agents to CD44-expressing tumor cells owing to the HA-CD44 interactions [103].

3.4. Application of glycosaminoglycans as promoter of cell growth and differentiation in tissue engineering

The proliferation and differentiation of cells within artificial scaffolds is required for the engineering of functional tissues. GAG, as natural ECM components, have attractive properties such as nontoxicity, excellent biocompatibility, anticoagulant and antitumor activity, as well as being regulators of cell growth and differentiation, making them great candidates for tissue engineering applications [147-149]. Various studies reported that GAG support proliferation and differentiation of different cell types, but affect also remodeling of tissues like bone mineralization and osteoclastogenesis [150, 151]. It was also shown that the incorporation of GAG like Hep into collagen scaffolds significantly enhanced osteoblastic differentiation of mesenchymal stem cells (MSCs) both in vitro and in vivo situations [152, 153]. Because of affinity of GF to heparin, Hep-based hydrogels have been increasingly employed as growth factor carriers and scaffolds for tissue regeneration [148]. By contrast, HS has been shown to act as a substitute for exogenously applied GF in driving rat bone marrow stem cells into osteogenic lineage [151]. In addition, HA and CS are potent regulators in dealing with skeletal and skin diseases owing to their modulation of skin and bone precursor cell activation and their subsequent differentiation and gene expression [150]. Overall, the multiple biological activities of GAG bear promising prospects for

pure GAG and GAG-based materials in tissue engineering applications ranging from *in vitro* to *in vivo* generation of functional substitutes for tissue regeneration [147].

4. Chemical alteration and bioactivity of modified glycosaminoglycans

4.1. Chemical modification of glycosaminoglycans for covalent and physical immobilization

Application of GAG in sensing devices, as bioactive coating of implants and tissue engineering scaffolds or for formation of hydrogels by covalent linkage or physical interactions often requires chemical modifications. GAG exhibit several functional groups that can be used for chemical modifications (Figure 4). The *reducing end* of the GAG chain, an aldehyde functionality (open saccharide ring) in equilibrium with a hemiacetal (closed saccharide ring), can be used to attach GAG chains to nucleophiles like amine- or hydrazide-functionalized substrata (substances and surfaces), which results in *end-on* (single point) attached GAG [2]. The latter option is highly depending on the MW of the GAG and the ionic strength of the applied medium. The possibility of reaction is declining with an increase in chain length and the presence of a closed conformation which becomes entropically favoured with the decrease of repelling negative charges that can be screened by counterions in dependence on the ionic strength of the aqueous solvent [154, 155]. For this reason, the reducing end is not extensively used for chemical reactions of native GAG with larger molecular weight. However, the covalent reaction of the reducing end of low MW (degraded GAG) or *de novo* synthesized OS is an efficient way to immobilize them via the reactions described above to solid substrata [156, 157]. An advantage of the attachment of GAG in an end-on configuration is the maintenance of their bioactivity as they are not altered in their native structure and thus be able to interact with their natural binding partners, e.g. growth factors, adhesive proteins and enzymes [158, 159]. For example, the reducing end of CS was alkynated and linked to poly(lactid acid) (PLA) by click chemistry to form a copolymer that can form micelles in water which could be used as drug delivery systems [160].

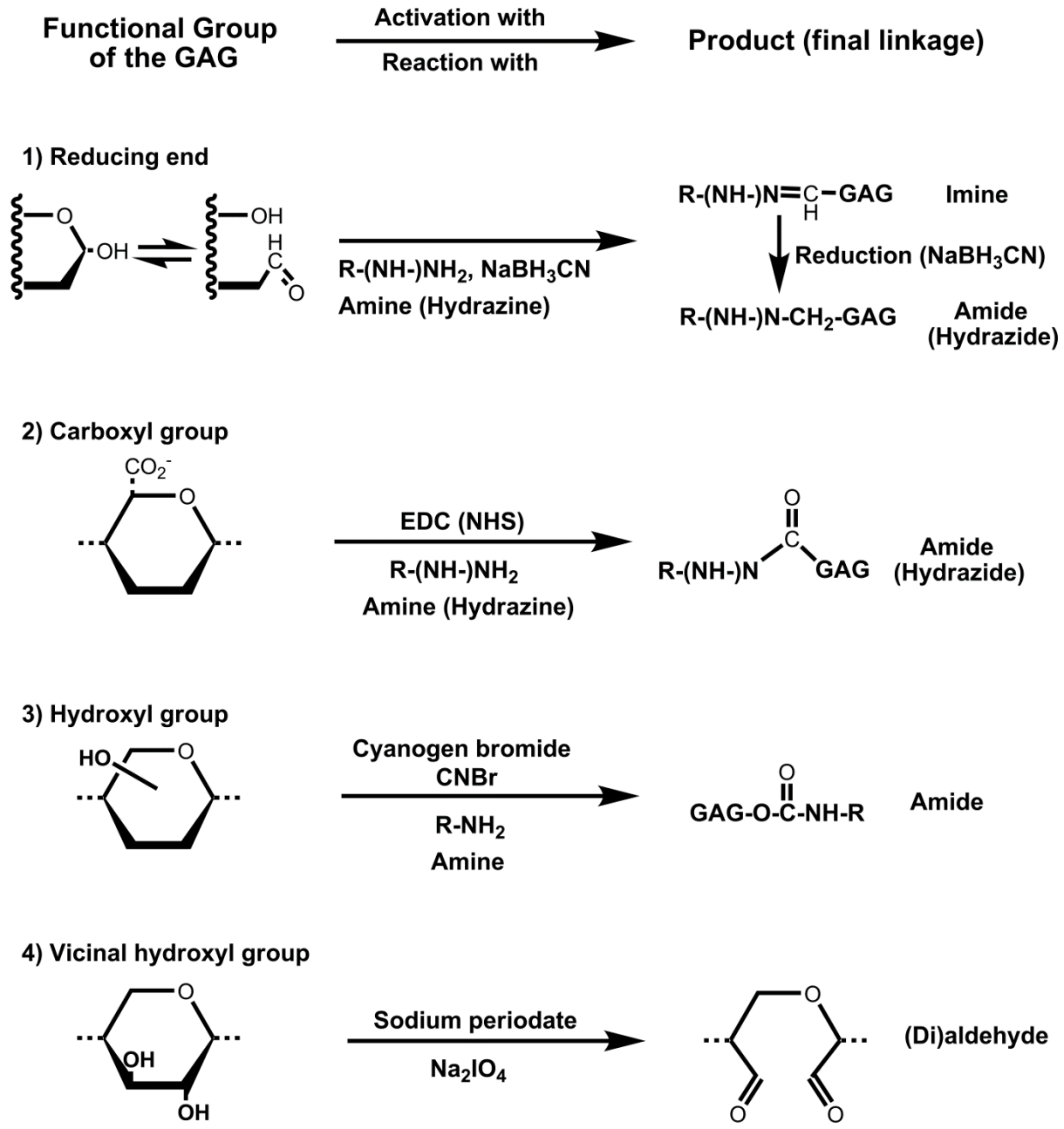

Figure 4: Summary of major chemistries used for the modification and coupling of glycosaminoglycans (GAG).

Apart from KS, GAG present carboxyl moieties that can be used for a variety of chemical modifications. Naturally, GAG are present in aqueous solutions but for modifications of the carboxylates it is also possible to use polar organic solvents like dimethylformamide (DMF), which was used for esterification of HA, resulting in products like HYAFF that represents HA with benzoyl side group [161]. The esterification of the carboxyl groups with alkyl halides in dimethylsulfoxide (DMSO) resulted in amphiphilic hyaluronic acid derivatives [162]. Most importantly, carboxyl

groups of GAG are functionalized with carbodiimide-mediated reactions, which allow to introduce specific functionalities or cross-linkers via reaction with an amine or a hydrazide [163]. EDC- or EDC/NHS-mediated reactions can be used for chemical modification and to covalently link GAG to scaffolds or matrices to alter mechanical properties or facilitate the binding of bioactive molecules like GF [164, 165]. As an alternative route, the use of triazine mediated functionalization of carboxyl groups has been considered, as well [166].

The hydroxyl groups of the polysaccharide structure are also frequently used for further chemical modification that may help to immobilize them on substrata or cross-linking them with other molecules by physical interactions. In addition, such modifications may affect the bioactivity of GAG. The sulfation of GAG`s hydroxyl groups and especially its specific sulfation pattern play an essential role in the ability to bind GF as it was shown for sulfated HA and oversulfated CS towards TGF-β1 [167] and with specific OS of CS for neuronal growth factors, respectively [168]. Additionally, the sulfation of HA been shown to promote stem cell differentiation [169]. However, sulfation is mainly applied to the non-sulfated HA to mimic the capacity of the sulfated GAG. On the other hand, sulfation is leading to an increased negative charge of the GAG chain, which further increases ionic interaction relevant for coating methods like layer-by-layer technique (LbL) [170]. The sulfation can be also tailored to obtain a desired sulfation degree and distinguished sulfation pattern [171]. Furthermore, cyanogen bromide can be applied to modify the vicinal hydroxyls of the uronic acid units in GAG like HA applying an amidation reaction [172]. The hydroxyls of GAG can be also modified to generate free aldehyde moieties by peroxidate-mediated cleavage of the carbon-carbon bond [173]. The latter can be functionalized with amine- or hydrazide-containing substrata [174-176]. Moreover, it is possible to obtain free amino groups by the deacetylation of the N-acetylated glucosamine by hydrazinolysis, which will also result in a degradation of GAG [177, 178]. Thereafter, the free amino groups can be used for covalent attachment to aldehydes and carboxyl moieties, respectively. Basically, the reaction with a substrate can be performed after previous functionalization of GAG or *in situ* by applying the reagent together with the GAG, e.g. when using EDC/NHS mediated coupling reactions of GAG with amino-modified surfaces [179, 180].

4.2. Bioactivity and functionality of activated glycosaminoglycans

The preservation of the bioactivity of GAG including the specific interaction with numerous cytokines, matrix proteins and cell surface receptors is a major prerequisite for their use in various biomedical applications. Furthermore, the functionality of GAG which have been modified to have additional functions has to be determined. Thus, the testing of bioactivity of chemically altered GAG is of major importance. Studies on measuring the affinity of protein ligands to GAG and experiments with cells can be used as a benchmark to compare the bioactivity of natural and functionalized GAG.

There are several tools to obtain information about the GAG binding affinity to their native binding partners (NBP). Qualitative information can be derived from simple characterization methods like fluorescence microscopy, when a label is introduced to a distinct target protein or the GAG, which are specifically binding to each other [181]. Quantitative fluorometric methods exploit changes of the intrinsic fluorescence of tryptophan and tyrosine in proteins upon binding of GAG and can be used for affinity measurements in solution [182]. Furthermore, toluidine blue can be utilized to quantify polyanions like GAG which are immobilized to solid substrates [183]. More sophisticated methods like high performance liquid chromatography (HPLC), electrophoresis and mass spectrometry can be used and combined to quantify the amount of GAG [184-186]. Mass spectrometry, especially in tandem with liquid chromatography, can be used to obtain the precise amount and composition of the GAG`s disaccharide content [187-189]. Generally, a prerequisite for the latter methods is the depolymerisation of the GAG. Other methods like surface plasmon resonance (SPR) and quartz-crystal microbalance (QCM) are applied to generate comprehensive quantitative data by the studying the adsorption of GAG to a NBP or vice versa. The measured signal is directly related to the amount of adsorbed binding partner of the GAG and thus revealing the GAG`s activity. For instance, ATIII, growth factors like FGFs or adhesive proteins like FN, which all possess Hep-binding domains can be used to assay the bioactivity of Hep and its derivatives [159, 190, 191]. Likewise, the activity of degrading enzymes like hyaluronidase towards functionalized GAG can uncover their remaining bioactivity [158]. The measurement of anticoagulant activity of Hep (as a complex with ATIII) can be performed by using thrombin and activated factor X (FXa) and specific chromogenic peptides [192].

In clinic, the effectiveness of heparin can be monitored with coagulation test like activated clotting time or thrombin time [193]. More complex trials and the combination of different cell types are used to investigate multifaceted process like inflammation [194].

The biodegradability of native GAG is also limiting certain biomedical applications as they can be degraded quickly within 24 h like in the case of HA [195]. Thus, chemical modifications can also lead to a desired prolongation of the half-life in tissue engineering applications especially because carboxyls are active sites of eliminative degradation mechanism by lyases [29, 196, 197]. Further, an additional sulfation of hydroxyls of GAG like HA can delay their degradation by enzymes like hyaluronidase [198]. Recently, *end-on* immobilized HA has shown to be easily degradable by hyaluronidase while side-on immobilized HA with higher degree of conjugation was not digested at all [158]. Adsorption studies with aggrecan and the adhesion of fibroblasts on surface-immobilized thiolated and oxidized HA showed the maintenance of bioactivity of such modified HAs [199].

The application of modified GAG is closely related to their designated function which might be most notable in case of Hep. Periodate-oxidized Hep was found to have reduced or no anticoagulant activity because an additional cleavage of the glycosidic bond is occurring adjacent to the N-sulfated glucosamine residues (GlcNS3S or GlcNS3S6S) which is crucial for the binding of ATIII [200, 201]. Thus, the manner of immobilization (end-on or side-on) of Hep plays a crucial role for its anticoagulant property [159]. On the other hand, LMW-Hep can be used as well because beside its specific anticoagulant activity, it is still able to bind GF like FGF2, e.g. for promoting vascularization *in vivo* [202, 203]. It was also shown that the utilization of a part of the carboxyl groups of Hep does not seem to hamper the antithrombotic properties as shown for EDC/NHS-immobilized Hep to amino groups of collagen, which inhibited platelet adhesion [204]. Furthermore, the ability of Hep to bind and protect GF from proteolysis or denaturation was proven in a similar EDC/NHS-cross-linked Hep-collagen scaffold, which was successfully loaded with VEGF and FGF2 and significantly supported early vascularization *in vivo* [205].

Importantly, the toxicity of the activated GAG towards cells has to be determined as well. In general, this is conducted by *in vitro* cell studies as any cytotoxic effect can

be revealed by comparative studies with functionalized and native GAG (or a positive control, in case the native GAG is not applicable) [160, 199].

5. Applications of glycosaminoglycans in 2D and 3D systems in tissue engineering and regenerative medicine

To utilize the beneficial properties of GAG for TE applications, they are usually immobilized on different material surfaces or integrated into various scaffold and hydrogel systems. The rationale behind the application of GAG as biomaterials is justified by their potential function as a matrix component and/or as a binding partner of cytokines and cell receptors. On the one hand, PG containing CS and DS are able to bind water and interact with collagens contributing greatly to the structural organization in most tissues [60]. Moreover, PG can bind matrix components like GF and other cytokines protecting them from proteolysis, thus playing an important role in signal transduction [16, 31]. Furthermore, the interaction with cellular receptors like integrins can regulate cell adhesion, proliferation and motility [1, 17]. The specific binding capacity of PG is mostly based on the attached GAG, although the protein core itself is able to interact with binding partners like HA [206]. The functionalization of GAG is usually required to generate stable GAG-coated implants and/or functional scaffolds. Furthermore, functionalized GAG can be used to cross-link forming hydrogels, which can be used for microscopic and macroscopic encapsulation of labile bioactive factors like cytokines and cells for the replacement and regeneration of tissues. Therefore, different experimental set-ups have been designed to immobilize or cross-link GAG. The application of GAG as biomaterials can be distinguished between more fundamental research strategies, e.g. changing material properties for the interaction with NBP or cells *in vitro*, and subsequent clinical research which results in an *in vivo* application. The employment of GAG *in vitro* encompass all surface modifications that are performed to transfer GAG properties to the material itself as homogeneous or heterogeneous (structured) surface coatings. The intended *in vivo* application is then tested in living organisms to obtain the efficacy and its overall effect in the proposed biological system. Another classification is presented by their way of immobilization/linkage into covalently attached (chemisorbed) GAG and physically linked (physisorbed) GAG. Depending on its application, a permanent coating of biomaterial surfaces requires an immobilization procedure that results in a sufficiently stable attachment of the GAG. Therefore, it is

important to know the bonding forces that are present at different interfaces depending on the type of surface, the solvent and GAG. An overview of selected GAG-related utilization as biomaterials and for tissue engineering applications can be found in Table 2.

Table 2: Summery of glycosaminoglycan application in biomedical applications.

Glycosaminoglycan conjugate	**Type of application**	**Target tissue / Application method**	**Reference**
Biotinylated HA/CS	Material coating	In vitro Biosensor	[158]
Carbodiimide-immobilized Hep	Material coating	Increase of blood compatibility	[204]
Carbodiimide-immobilized HA	Surface structuring	In vitro Biosensor	[180]
CHI / HA-Paclitaxel multilayers	Implant coating	Drug delivery	[224]
CHI / GAG multilayers	Implant coating	Reduction of platelet adhesion and inflammation	[129, 209]
CHI / HA multilayers	Implant coating	Antibacterial / anti-adhesive	[225]
Collagen / HA multilayers	Implant coating	Decrease of foreign body response	[218]
Gelatin methacrylate + HA-/CS-methacrylate	Hydrogel	Cartilage regeneration	[226]
Chemically cross-linked Hep + Hep-binding GFs	Hydrogel	GF delivery, synthetic ECM	[191, 227]
Cross-linked thiolated HA, CS, Hep, gelatin	Biodegradable hydrogel	Drug / GF delivery, Tissue regeneration	[228-230]
Cross-linked CS-tyramine	Hydrogel	Drug delivery	[231, 232]

Cross-linked aldehyde HA	Hydrogel	Vocal cord/fold regeneration	[174, 233]
Gelatin – aldehyde Hep +FGF-2	Injectable hydrogel	Neovascularization	[203]
Chemically cross-linked HA/CS	Hydrogel matrix/particles	Wound dressing, skin regeneration	[174, 234-236]
Chemically cross-linked HA (+ stem cells, HyStem®)	Injectable/ Implantable hydrogels	Osteoarthritis (Synvisc®), Cartilage regeneration (Hyalograft®), bone regeneration / vascular graft (HYAFF®)	[237-242]
Maleimide-crosslinked thiolated Hep	Hydrogel	Glutathione-sensitive release of Hep	[243]
Collagen-Hep	Porous scaffold	Subcutaneous / Neovascularization	[205]
Collagen-CS	Porous scaffold	Neovascularization, Bone regeneration	[244]
Collagen-HA	Porous scaffold	Bone regeneration	[223]
Genipin cross-linked HA, CS	Porous scaffold	Cartilage regeneration	[245]
Carbodiimide-crosslinked HA, CS, DS, CHI, gelatin	Porous scaffold	Cartilage regeneration	[246, 247]
Electrospun collagen-GAG (HA, CS)	Porous mesh	Artificial ECM, Cartilage regeneration	[248-250]
Crosslinked Collagen-HS matrices + bFGF	Porous scaffold	Enhancement of angiogenesis / regeneration	[165]
Hep/poly-L-arginine	Microcapsules	GF delivery	[211, 212]

CHI-CS	Nanoparticles	GF delivery, bone regeneration	[251]
HA-DEAP	Nanoparticles	pH-responsive drug delivery	[252]
HA-lipid vesicles	Nanoparticles	Drug delivery, cancer therapy	[253]
Thiolated Hep-gold	Nanoparticles	Drug delivery, cancer therapy, biosensor	[254]
HA-Hep	Nanoparticles (Nano-/microgels)	GF delivery	[255]
Thiolated Hep-PEG	Nanoparticles (Nanogels)	Drug delivery, cancer therapy	[256]

Abbreviations: GAG – Glycosaminoglycans; Hep – Heparin; HS – Heparan sulfate; CS – Chondroitin sulfate; DS – Dermatan sulfate; HA – Hyaluronic acid; CHI – Chitosan; ECM – Extracellular matrix; GF – Growth factor; bFGF – Basic fibroblast growth factor; DEAP - 3-(diethylamino)propyl amine; PEG – Poly(ethylene glycol).

5.1. Immobilization of glycosaminoglycans on implants, scaffolds and other surfaces

The physisorption of GAG to charged or functionalized substrata is related to their molecular weight and the inherent negative charge density, which can be used for electrostatic attraction to and ion pairing with the charged material surface. Even a simple physical adsorption of GAG to cell culture substrata may also improve the response of cells. For example, it was shown that sulfated HA, which was physically adsorbed to tissue culture plastic can promote keratinocyte differentiation and modulated the expression of Wnt and Notch3 [207]. The alternating adsorption of oppositely charged polyelectrolytes to generate multilayers on various material surfaces like inorganic materials, metals and polymers by the so called Layer-by-Layer method (LbL) was introduced by Decher et al. [208] and also applied for GAG like HA, Hep and others [175, 209, 210]. One benefit of the multilayer approach is the possible inclusion of bioactive molecules like GF and other chemokines to support adhesion, proliferation or differentiation of cells as also reported for microcapsules applying biodegradable GAG like heparin [211-214]. Furthermore, the mechanical properties like stiffness can be controlled not only by

the choice of GAG but also by application of chemically functionalized GAG and *in situ* or subsequent chemical cross-linking [215]. Recently, this was achieved by reversible disulfide bridging for thiolated HA/PLL (Poly-L-lysine) multilayers [216] and by the Schiff base formation between collagen and aldehyde containing GAG [175]. Another application, especially of multilayer-assembled or -coated microcapsules/-beads, represents the transport of drugs since the association with specific binding molecules like GAG can prevent drugs from fast release and degradation and act as a target-oriented delivery system [217]. Multilayer coatings made of GAG showed *in vitro* and *in vivo* macrophage activation and decrease of capsule formation *in vivo*, which is related to their anti-inflammatory properties [129, 218].

For biomedical applications, a certain durability of the coating plays a crucial role. Thus, the chemical surface grafting of GAG is desired for a majority of TE applications in 2D. On the other hand, also the physically adsorbed build-up of polymer as multilayers can lead to adsorption of considerable amounts of GAG which might be further stabilized by covalent cross-linking [216]. For both methods it might be necessary to change the inherent substrate properties for the interaction with the GAG. The latter can be achieved by different surface treatments, e.g. the application of plasma treatment [219], the adsorption via coating techniques like spin-coating [220], the preadsorption of a specific polymer like poly(ethylene) imine (PEI) [210], the chemical grafting of self-assembled monolayers of silanes to glass and silicon or thiols to gold [221, 222]. For instance, a prior treatment of glass or silicon with an amino-terminated silane is allocating amino groups to the surface which can be used for the carbodiimide-initiated coupling of carboxyl groups of GAG to create covalently immobilized GAG surfaces. The latter procedure was applied to specifically couple HA to a surface which was structured by microcontact printing of the amino silane to study the interaction of cancer cells *in vitro* [180]. Another example is the EDC-driven biotinylation of HA and CS which enables specific binding to streptavidin-modified surfaces for the fabrication of biosensing tools [158].

As major components of the ECM of bone and skin exhibiting unique functions, GAG in combination with collagen I are widely used for the design of implant materials [150, 165, 223].

5.2. Glycosaminoglycans as building blocks for formation of hydrogels and porous scaffolds

Hydrogels present a promising type of biomaterial because they can host labile factors like cytokines, but also cells for transplantation without any damage. In addition, *in situ* gelling systems can be injected into the pathological site allowing minimal invasive procedures. The requirements for hydrogel properties are closely related to its location and its mode of action in the body [257]. The application of natural polymers like GAG as building blocks for hydrogels is especially desirable with regard to their utilization *in vivo* as drug or GF release system and as scaffold for the regeneration of soft tissue which both require biocompatibility, bioactivity and a specific biodegradability [258].

For example, maleimide-functionalized Hep was cross-linked with different PEG-thiols to form glutathione-sensitive reversible hydrogels [243]. Hydrogels prepared from methacrylated HA and CS together with methacrylated gelatin provided a supportive environment for the deposition of cartilage-like matrix [226].

GAG-based hydrogels can be used as drug release system as shown for cross-linked CS, tyramine-cross-linked CS or various Hep hydrogels [148, 231, 259]. In a different approach, methacrylated Hep was copolymerized with PEG-methacrylate to form hydrogels that are able to bind basic FGF to induce hMSC differentiation [191]. Aldehyde-containing Hep was cross-linked with chitosan to obtain hydrogels which were utilized for the controlled release of FGF2 to induce vascularization *in vivo* [203]. Also, injectable hydrogels composed of thiolated GAG and acrylated PEG-polymers could be used for the controlled release of GF like FGFs [228].

Cell-supportive, *in situ* cross-linking GAG-gelatin hydrogels with varying mechanical properties showed tissue-like properties 8 weeks after injection with fibroblasts *in vivo* [229]. Furthermore, vinyl ester composites of HA as thiol-ene component were successfully applied for two-photon polymerization to create 3D hydrogel scaffolds with specific mechanical properties [260]. Aldehyde-HA was cross-linked to form tuneable viscoelastic hydrogels which showed improved restoration of rabbit vocal cord [174, 233]. HA or HA-based hydrogels are extensively used for cartilage regeneration and replacement. Cross-linked HA (Hylan GF 20, Synvisc®) has been

used for two decades to relieve pain of osteoarthritis patients with modest success [237, 238]. An alkylated HA-alginate hydrogel was used to treat cartilage defects in a rat model [261]. Esterified HA (HYAFF®) scaffolds in combination with (stem) cells are promising materials for bone regeneration and as vascular graft [240, 241, 262]. HYAFF® combined with autologous chondrocytes (Hyalograft® C) was successfully applied to repair cartilage defects [239]. Moreover, chemically cross-linked HA and CS hydrogel films were used to make wound dressings [234, 235]. *In situ* cross-linkable hydrogels of HA (HyStem®) mimicking the ECM can be customized with different cells from various tissue origin to be applied *ex vivo* and in vivo [263]. In addition, hydrazide-functionalized HA was cross-linked with a bifunctional PEG-ketone to obtain hydrogel scaffolds with potential use in TE of bone [242].

The fabrication of porous scaffolds can be achieved by the lyophilization of a (mixed) polymer-containing solution [264, 265]. The pore size and interconnectivity of porous scaffolds is closely related to the implicated application, e.g. for the TE of bone and skin. The porosity and pore size of GAG based scaffolds can be controlled by the cooling rate, the total time and the final temperature of the freeze-drying process [266]. Porous collagen-GAG scaffolds seeded with endothelial cells and hMSCs have shown improved vascularization *in vitro* and *in vivo* with potential application for bone defects [244]. Biocompatible and porous collagen-GAG (CS, HA) nanofiber scaffolds have been generated by electrospinning, an electrostatic technique which generates polymer fibers with nanometer diameter, to mimic the structural properties of the ECM [248, 249, 267]. HA and CS were coupled to collagen II sponges with genipin to obtain cross-linked scaffolds which represent promising candidates for cartilage regeneration [245]. It was also shown that covalently attached CS increased the water binding capacity and decreased the tensile strength of porous collagen matrices [268]. Furthermore, photo-cross-linked fibrous meshes of thiolated HA and acrylated PEG were used to produce HA-scaffolds for different TE applications [250].

GAG-based biomaterials can be also constituted of more than two main components, especially when a scaffold should allow cell proliferation and differentiation to replace damaged tissue [269]. Hence, CS, HA and silk fibroin were cross-linked by carbodiimide chemistry to obtain porous scaffolds which were successfully applied for skin regeneration together with fibroblasts in a rat model [236]. By making use of

the same chemistry, CS and HA were cross-linked with gelatin and chitosan to obtain scaffolds for the replacement of cartilage defects in a rabbit model [247].

Similarly, CS and DS were coupled to chitosan scaffolds which exhibited a synergistic effect of CS and DS in increasing ECM synthesis when seeded with chondrocytes [246].

5.3. Glycosaminoglycans as a component of micro- and nanoparticles

Micro- and nanoparticles (NP) can be administered to the blood circulation of patients and pass through capillary vessels allowing their systemic distribution in the body of patients, but also a targeted delivery to penetrate tissue barriers, particularly with nano-sized particles [270]. Different types of NP have been used for drug encapsulation and surface immobilization. The NP itself can be a product of a component (e.g. metal, synthetic polymers) which is coated with one or more biopolymers (e.g. GAG) or it can be formed directly by the physical or chemical cross-linking of one (or more) component(s) which can be considered as nano- or microparticles as they are colloidally stable systems with a diameter up to the micrometer range [217, 271, 272]. In addition to the intended target site, the nanoparticle activity, stability and body distribution is highly depending on the size and the surface zeta potential, e.g. larger NP tend to aggregate and a lower (negative) zeta potential increases the half-life of NP [273, 274]. Notably, in cancerous tissue the vascularization is abnormal resulting in large vessel junctions (<1200 nm) which can be penetrated by NP that cannot invade into normal tissue (5-10 nm junctions) [274, 275]. Hence, GAG-NP are applied as transport and release system for GF and drugs but also as inducers of apoptosis in cancer cells [252, 254]. Nanogels with a mean diameter of around 200 nm were prepared by cross-linking of thiolated Hep, followed by induction of glutathione mediated release of Hep that lead to the inhibition of cancer cell proliferation [256]. Moreover, HA was conjugated to lipid-based NP for the specific delivery of siRNA to cancer cells that overexpress CD 44 to induce gene silencing [253]. Physically formed NP of chitosan and CS were successfully used for the release of platelet lysate which represents a promising system for bone-TE [251]. Interestingly, NP consisting of a cross-linked hydrogel of HA and Hep can be also used as controlled release system for Hep binding GF like BMP-2 [255]. A microgel formed by the cross-linking of oxidized HA and a

bifunctional hydrazide linker is a promising candidate for vocal fold regeneration [174]. In a combined approach, Hep-poly-L-arginine capsules were assembled by applying a multilayer coating of Hep and poly-L-arginine to Hep-$CaCO_3$ particles and further used for the delivery of TGF-β1 [211].

6. Summary and future aspects

GAG have been used so far in a variety of biomedical applications primarily for drug delivery and tissue engineering (TE) purposes. Because of their multifunctional properties playing a crucial role in a multitude of biological processes, but also their biocompatibility and biodegradability they are attractive to promote stem cell differentiation and tissue regeneration. Although, the current adoption of these properties to biomaterials and tissue engineering scaffolds is very promising, the translation from *in vitro* systems to clinical applications still remains a demanding mission.

Thereby, the biomedical application of GAG is still confronted partly with the animal origin leading to varying batch-to-batch composition regarding degree of sulfation and a broad molecular weight distribution of GAG, but also a potential risk of contaminations with infectious agents. On the other hand, some of them like HA can be already produced by biotechnological approaches with high purity and better controlled chemical composition. Moreover, several approaches exist to synthesize bioactive oligosaccharides that represent active domains of GAG [128] or to make semi-synthetic GAG based on natural polysaccharides occurring in plants and animals in larger quantities [276, 277]. In addition, the possibility to combine GAG with a multitude of other materials, being it biological derived or synthetically manufactured ones, gives rise to diverse adjustments to aim for various tissue and for different functions. In our opinion, despite the increasing amount of commercially available GAG-based products, this is not yet mirroring their peerless capability as biomaterials for drug delivery or TE applications. Therefore, it is important to support the continual efforts in research and development of GAG-based biomaterials to cope with the needs of an increasingly aging society and improved medical care for treatment of traumata and cancer.

7. Acknowledgements

This work was funded partly by a grant from European Union under FP-7-PEOPLE-2012_IAPP, "FIBROGELNET" and from Deutsche Forschungsgemeinschaft Gr 1290/10-1 to TG and a grant from Chinese Scholarship Council to GZ.

8. References

1. Varki, A., *Essentials of glycobiology*. 1999, Cold Spring Harbor, NY: Cold Spring Harbor Laboratory Press. xvii, 653 p.
2. Gabius, H.J., *The sugar code: fundamentals of glycosciences*. 2009, Weinheim, Chichester: Wiley-VCH; John Wiley distributor. xxviii, 569 p.
3. Lodish, H.F., *Molecular cell biology*. 4th ed. 2000, New York: W.H. Freeman. xxxvi, 1084, G-17, I-36 p.
4. Prydz, K. and K.T. Dalen, *Synthesis and sorting of proteoglycans.* Journal of cell science, 2000. **113**(2): p. 193-205.
5. Victor, X.V., et al., *Investigating the elusive mechanism of glycosaminoglycan biosynthesis.* Journal of Biological Chemistry, 2009. **284**(38): p. 25842-25853.
6. Hay, E.D., *Cell biology of extracellular matrix*. 2013: Springer Science & Business Media.
7. Day, A.J. and G.D. Prestwich, *Hyaluronan-binding proteins: tying up the giant.* Journal of Biological Chemistry, 2002. **277**(7): p. 4585-4588.
8. Wu, Y.J., et al., *The interaction of versican with its binding partners.* Cell research, 2005. **15**(7): p. 483-494.
9. Day, A., *The C-type carbohydrate recognition domain (CRD) superfamily.* Biochemical Society Transactions, 1994. **22**(1): p. 83-88.
10. Wight, T.N., I. Kang, and M.J. Merrilees, *Versican and the control of inflammation.* Matrix Biology, 2014. **35**: p. 152-161.
11. Iozzo, R.V. and L. Schaefer, *Proteoglycans in health and disease: novel regulatory signaling mechanisms evoked by the small leucine-rich proteoglycans.* Febs Journal, 2010. **277**(19): p. 3864-3875.
12. Kohfeldt, E., et al., *Properties of the extracellular calcium binding module of the proteoglycan testican.* FEBS letters, 1997. **414**(3): p. 557-561.
13. Kawahara, R., et al., *Agrin and Perlecan Mediate Tumorigenic Processes in Oral Squamous Cell Carcinoma.* PloS one, 2014. **9**(12): p. e115004.
14. Whitelock, J.M., J. Melrose, and R.V. Iozzo, *Diverse Cell Signaling Events Modulated by Perlecan.* Biochemistry, 2008. **47**(43): p. 11174-11183.
15. Kwon, M.-J., et al., *Syndecans play dual roles as cell adhesion receptors and docking receptors.* FEBS letters, 2012. **586**(16): p. 2207-2211.
16. Mythreye, K. and G.C. Blobe, *Proteoglycan signaling co-receptors: roles in cell adhesion, migration and invasion.* Cellular signalling, 2009. **21**(11): p. 1548-1558.
17. Choi, Y., et al., *Syndecans as cell surface receptors: unique structure equates with functional diversity.* Matrix Biology, 2011. **30**(2): p. 93-99.

18. Kim, S.-H., J. Turnbull, and S. Guimond, *Extracellular matrix and cell signalling: the dynamic cooperation of integrin, proteoglycan and growth factor receptor.* Journal of Endocrinology, 2011. **209**(2): p. 139-151.
19. Christianson, H.C. and M. Belting, *Heparan sulfate proteoglycan as a cell-surface endocytosis receptor.* Matrix Biology, 2014. **35**: p. 51-55.
20. Teng, Y.H.-F., R.S. Aquino, and P.W. Park, *Molecular functions of syndecan-1 in disease.* Matrix Biology, 2012. **31**(1): p. 3-16.
21. Yip, G.W., M. Smollich, and M. Götte, *Therapeutic value of glycosaminoglycans in cancer.* Molecular cancer therapeutics, 2006. **5**(9): p. 2139-2148.
22. Yang, Y., et al., *Heparanase Enhances Syndecan-1 Shedding a novel mechanism for stimulation of tumor growth and metastasis.* Journal of Biological Chemistry, 2007. **282**(18): p. 13326-13333.
23. Kolset, S., K. Prydz, and G. Pejler, *Intracellular proteoglycans.* Biochem. J, 2004. **379**: p. 217-227.
24. Reine, T.M., et al., *Serglycin secretion is part of the inflammatory response in activated primary human endothelial cells in vitro.* Biochimica et Biophysica Acta (BBA)-General Subjects, 2014. **1840**(8): p. 2498-2505.
25. Douaiher, J., et al., *Development of mast cells and importance of their tryptase and chymase serine proteases in inflammation and wound healing.* Advances in immunology, 2014. **122**: p. 211.
26. Stanton, H., et al., *Proteoglycan degradation by the ADAMTS family of proteinases.* Biochimica et Biophysica Acta (BBA)-Molecular Basis of Disease, 2011. **1812**(12): p. 1616-1629.
27. Reiland, J., et al., *Heparanase degrades syndecan-1 and perlecan heparan sulfate functional implications for tumor cell invasion.* Journal of Biological Chemistry, 2004. **279**(9): p. 8047-8055.
28. Harvey, R.A. and D.R. Ferrier, *Biochemistry*. 5th ed. Lippincott's illustrated reviews. 2011, Philadelphia: Wolters Kluwer Health/Lippincott Williams & Wilkins. 520 p.
29. Linhardt, R.J., et al., *CS lyases: structure, activity, and applications in analysis and the treatment of diseases.* Advances in pharmacology, 2006. **53**: p. 187-215.
30. Ernst, S., et al., *Enzymatic degradation of glycosaminoglycans.* Critical Reviews in Biochemistry and Molecular Biology, 1995. **30**(5): p. 387-444.
31. Iozzo, R.V. and L. Schaefer, *Proteoglycan form and function: A comprehensive nomenclature of proteoglycans.* Matrix Biology, 2015. **42**: p. 11-55.
32. Nelson, D.L., A.L. Lehninger, and M.M. Cox, *Lehninger principles of biochemistry*. 2008: Macmillan.
33. Powell, A.K., et al., *Interactions of heparin/heparan sulfate with proteins: appraisal of structural factors and experimental approaches.* Glycobiology, 2004. **14**(4): p. 17R-30R.

34. Rabenstein, D.L., *Heparin and heparan sulfate: structure and function.* Natural product reports, 2002. **19**(3): p. 312-331.
35. Conrad, H.E., *Heparin-binding proteins*. 1998, San Diego: Academic Press. xx, 527 p.
36. Jacobsson, K.-G. and U. Lindahl, *Degradation of heparin proteoglycan in cultured mouse mastocytoma cells.* Biochem. J, 1987. **246**: p. 409-415.
37. Hileman, R.E., et al., *Glycosaminoglycan-protein interactions: definition of consensus sites in glycosaminoglycan binding proteins.* Bioessays, 1998. **20**(2): p. 156-167.
38. Mekori, Y.A. and D.D. Metcalfe, *Mast cells in innate immunity.* Immunological reviews, 2000. **173**(1): p. 131-140.
39. Kirkpatrick, C.A. and S.B. Selleck, *Heparan sulfate proteoglycans at a glance.* Journal of Cell Science, 2007. **120**(11): p. 1829-1832.
40. McQuade, K.J., et al., *Syndecan-1 regulates αvβ5 integrin activity in B82L fibroblasts.* Journal of cell science, 2006. **119**(12): p. 2445-2456.
41. Humphries, D.E., et al., *Heparin is essential for the storage of specific granule proteases in mast cells.* Nature, 1999. **400**(6746): p. 769-772.
42. Eswarakumar, V., I. Lax, and J. Schlessinger, *Cellular signaling by fibroblast growth factor receptors.* Cytokine & growth factor reviews, 2005. **16**(2): p. 139-149.
43. Lindahl, U., et al., *More to Heparin Than Anticoagulation.* Thrombosis Research, 1994. **75**(1): p. 1-32.
44. Li, J.-p. and I. Vlodavsky, *Heparin, heparan sulfate and heparanase in inflammatory reactions.* Thromb Haemost, 2009. **102**(5): p. 823-828.
45. Nelson, R.M., et al., *Heparin Oligosaccharides Bind L-Selectin and P-Selectin and Inhibit Acute-Inflammation.* Blood, 1993. **82**(11): p. 3253-3258.
46. Springer, T.A., *Traffic signals for lymphocyte recirculation and leukocyte emigration: the multistep paradigm.* Cell, 1994. **76**(2): p. 301-314.
47. Parish, C.R., *The role of heparan sulphate in inflammation.* Nature Reviews Immunology, 2006. **6**(9): p. 633-643.
48. Peter, K., et al., *Heparin inhibits ligand binding to the leukocyte integrin Mac-1 (CD11b/CD18) in vitro and in patients.* Circulation, 1998. **98**(17): p. 242-242.
49. Guimond, S.E. and J.E. Turnbull, *Fibroblast growth factor receptor signalling is dictated by specific heparan sulphate saccharides.* Current Biology, 1999. **9**(22): p. 1343-1346.
50. Xu, D. and J.D. Esko, *Demystifying heparan sulfate-protein interactions.* Annual review of biochemistry, 2014. **83**: p. 129-157.
51. Whitelock, J.M. and R.V. Iozzo, *Heparan sulfate: a complex polymer charged with biological activity.* Chemical reviews, 2005. **105**(7): p. 2745-2764.
52. Lauder, R.M., *Chondroitin sulphate: a complex molecule with potential impacts on a wide range of biological systems.* Complementary therapies in medicine, 2009. **17**(1): p. 56-62.

53. Trowbridge, J.M. and R.L. Gallo, *Dermatan sulfate: new functions from an old glycosaminoglycan.* Glycobiology, 2002. **12**(9): p. 117R-125R.
54. Volpi, N., *Analytical aspects of pharmaceutical grade chondroitin sulfates.* Journal of Pharmaceutical Sciences, 2007. **96**(12): p. 3168-3180.
55. Volpi, N., *Quality of different chondroitin sulfate preparations in relation to their therapeutic activity.* Journal of pharmacy and pharmacology, 2009. **61**(10): p. 1271-1280.
56. Maurel, P., et al., *Phosphacan, a chondroitin sulfate proteoglycan of brain that interacts with neurons and neural cell-adhesion molecules, is an extracellular variant of a receptor-type protein tyrosine phosphatase.* Proceedings of the National Academy of Sciences, 1994. **91**(7): p. 2512-2516.
57. Rühland, C., et al., *The glycosaminoglycan chain of decorin plays an important role in collagen fibril formation at the early stages of fibrillogenesis.* Febs Journal, 2007. **274**(16): p. 4246-4255.
58. Dunkman, A.A., et al., *The injury response of aged tendons in the absence of biglycan and decorin.* Matrix Biology, 2014. **35**: p. 232-238.
59. Kadler, K.E., A. Hill, and E.G. Canty-Laird, *Collagen fibrillogenesis: fibronectin, integrins, and minor collagens as organizers and nucleators.* Current opinion in cell biology, 2008. **20**(5): p. 495-501.
60. Hardingham, T.E. and A.J. Fosang, *Proteoglycans - many forms and many functions.* Faseb Journal, 1992. **6**(3): p. 861-870.
61. Fraser, J., T. Laurent, and U. Laurent, *Hyaluronan: its nature, distribution, functions and turnover.* Journal of internal medicine, 1997. **242**(1): p. 27-33.
62. Reichenbach, S., et al., *Meta-analysis: chondroitin for osteoarthritis of the knee or hip.* Annals of internal medicine, 2007. **146**(8): p. 580-590.
63. Campbell, E.J. and C.A. Owen, *The sulfate groups of chondroitin sulfate-and heparan sulfate-containing proteoglycans in neutrophil plasma membranes are novel binding sites for human leukocyte elastase and cathepsin G.* Journal of Biological Chemistry, 2007. **282**(19): p. 14645-14654.
64. Tat, S.K., et al., *Chondroitin and glucosamine sulfate in combination decrease the pro-resorptive properties of human osteoarthritis subchondral bone osteoblasts: a basic science study.* Arthritis Research and Therapy, 2007. **9**(6): p. R117.
65. Wildi, L.M., et al., *Chondroitin sulphate reduces both cartilage volume loss and bone marrow lesions in knee osteoarthritis patients starting as early as 6 months after initiation of therapy: a randomised, double-blind, placebo-controlled pilot study using MRI.* Annals of the rheumatic diseases, 2011. **70**(6): p. 982-989.
66. Holzmann, J., et al., *Assorted effects of TGFβ and chondroitinsulfate on p38 and ERK1/2 activation levels in human articular chondrocytes stimulated with LPS.* Osteoarthritis and cartilage, 2006. **14**(6): p. 519-525.

67. Bandtlow, C.E. and D.R. Zimmermann, *Proteoglycans in the developing brain: new conceptual insights for old proteins.* Physiological reviews, 2000. **80**(4): p. 1267-1290.
68. Afratis, N., et al., *Glycosaminoglycans: key players in cancer cell biology and treatment.* Febs Journal, 2012. **279**(7): p. 1177-1197.
69. Thelin, M.A., et al., *Biological functions of iduronic acid in chondroitin/dermatan sulfate.* FEBS Journal, 2013. **280**(10): p. 2431-2446.
70. Volpi, N., *Anti-inflammatory activity of chondroitin sulphate: new functions from an old natural macromolecule.* Inflammopharmacology, 2011. **19**(6): p. 299-306.
71. Theocharis, A.D., et al., *Altered content composition and structure of glycosaminoglycans and proteoglycans in gastric carcinoma.* The international journal of biochemistry & cell biology, 2003. **35**(3): p. 376-390.
72. Hopwood, J.J. and H.C. Robinson, *The molecular-weight distribution of glycosaminoglycans.* Biochem J, 1973. **135**(4): p. 631-7.
73. Funderburgh, J.L., *Keratan sulfate biosynthesis.* IUBMB life, 2002. **54**(4): p. 187-194.
74. Funderburgh, J.L., *MINI REVIEW Keratan sulfate: structure, biosynthesis, and function.* Glycobiology, 2000. **10**(10): p. 951-958.
75. Uchimura, K., *Keratan Sulfate: Biosynthesis, Structures, and Biological Functions*, in *Glycosaminoglycans*. 2015, Springer. p. 389-400.
76. Ohmori, J., et al., *Keratan sulfate glycosaminoglycans in murine eosinophil-specific granules.* Journal of Histochemistry & Cytochemistry, 1999. **47**(4): p. 481-488.
77. Chakravarti, S., et al., *Lumican regulates collagen fibril assembly: skin fragility and corneal opacity in the absence of lumican.* The Journal of cell biology, 1998. **141**(5): p. 1277-1286.
78. Ni, G.-X., Z. Li, and Y.-Z. Zhou, *The role of small leucine-rich proteoglycans in osteoarthritis pathogenesis.* Osteoarthritis and Cartilage, 2014. **22**(7): p. 896-903.
79. Jepsen, K.J., et al., *A syndrome of joint laxity and impaired tendon integrity in lumican-and fibromodulin-deficient mice.* Journal of Biological Chemistry, 2002. **277**(38): p. 35532-35540.
80. Conrad, A.H., et al., *Proteomic analysis of potential keratan sulfate, chondroitin sulfate A, and hyaluronic acid molecular interactions.* Investigative ophthalmology & visual science, 2010. **51**(9): p. 4500.
81. Bi, Y., et al., *Identification of tendon stem/progenitor cells and the role of the extracellular matrix in their niche.* Nature medicine, 2007. **13**(10): p. 1219-1227.
82. Amjadi, S., et al., *The role of lumican in ocular disease.* ISRN ophthalmology, 2013. doi:10.1155/2013/632302.

83. Weigel, P.H. and P.L. DeAngelis, *Hyaluronan synthases: a decade-plus of novel glycosyltransferases.* Journal of Biological Chemistry, 2007. **282**(51): p. 36777-36781.
84. Tian, X., et al., *High-molecular-mass hyaluronan mediates the cancer resistance of the naked mole rat.* Nature, 2013. **499**(7458): p. 346-349.
85. Laurent, T.C. and J. Fraser, *Hyaluronan.* The FASEB Journal, 1992. **6**(7): p. 2397-2404.
86. Holmes, M., M. Bayliss, and H. Muir, *Hyaluronic acid in human articular cartilage. Age-related changes in content and size.* Biochem. J, 1988. **250**: p. 435-441.
87. Stern, R., A.A. Asari, and K.N. Sugahara, *Hyaluronan fragments: an information-rich system.* European journal of cell biology, 2006. **85**(8): p. 699-715.
88. Toole, B., *Hyaluronan and its binding proteins, the hyaladherins.* Current opinion in cell biology, 1990. **2**(5): p. 839-844.
89. Seyfried, N.T., et al., *Expression and Purification of Functionally Active Hyaluronan-binding Domains from Human Cartilage Link Protein, Aggrecan and Versican Formation of Ternary Complexes with Defined Hyaluronan Oligosaccharides.* Journal of Biological Chemistry, 2005. **280**(7): p. 5435-5448.
90. Knudson, C.B. and W. Knudson, *Hyaluronan-binding proteins in development, tissue homeostasis, and disease.* The FASEB Journal, 1993. **7**(13): p. 1233-1241.
91. Ogston, A. and J. Stanier, *The physiological function of hyaluronic acid in synovial fluid; viscous, elastic and lubricant properties.* The Journal of physiology, 1953. **119**(2-3): p. 244-252.
92. Fung, Y.-C., *Biomechanics: mechanical properties of living tissues*. 2013: Springer Science & Business Media.
93. Day, A.J. and A. Carol, *Hyaluronan cross-linking: a protective mechanism in inflammation?* Trends in immunology, 2005. **26**(12): p. 637-643.
94. Ruppert, S.M., et al., *Tissue integrity signals communicated by high-molecular weight hyaluronan and the resolution of inflammation.* Immunologic Research, 2014. **58**(2-3): p. 186-192.
95. Band, P., et al., *Hyaluronan molecular weight distribution is associated with the risk of knee osteoarthritis progression.* Osteoarthritis and Cartilage, 2015. **23**(1): p. 70-76.
96. Turley, E.A., P.W. Noble, and L.Y. Bourguignon, *Signaling properties of hyaluronan receptors.* Journal of Biological Chemistry, 2002. **277**(7): p. 4589-4592.
97. Lee-Sayer, S.S., et al., *The where, when, how, and why of hyaluronan binding by immune cells.* Frontiers in immunology, 2015. **6**.
98. Teder, P., et al., *Resolution of lung inflammation by CD44.* Science, 2002. **296**(5565): p. 155-158.

99. Jiang, D., et al., *Regulation of lung injury and repair by Toll-like receptors and hyaluronan.* Nature medicine, 2005. **11**(11): p. 1173-1179.
100. Winkler, C.W., et al., *Hyaluronan oligosaccharides perturb lymphocyte slow rolling on brain vascular endothelial cells: implications for inflammatory demyelinating disease.* Matrix Biology, 2013. **32**(3): p. 160-168.
101. Pavelka, K., et al., *Hyaluronic acid levels may have predictive value for the progression of knee osteoarthritis.* Osteoarthritis and Cartilage, 2004. **12**(4): p. 277-283.
102. Kogan, G., et al., *Hyaluronic acid: a natural biopolymer with a broad range of biomedical and industrial applications.* Biotechnology letters, 2007. **29**(1): p. 17-25.
103. Toole, B.P., *Hyaluronan-CD44 Interactions in Cancer: Paradoxes and Possibilities.* Clinical Cancer Research, 2009. **15**(24): p. 7462-7468.
104. Toole, B.P., *Hyaluronan: from extracellular glue to pericellular cue.* Nature Reviews Cancer, 2004. **4**(7): p. 528-539.
105. Schmaus, A., J. Bauer, and J.P. Sleeman, *Sugars in the microenvironment: the sticky problem of HA turnover in tumors.* Cancer and Metastasis Reviews, 2014. **33**(4): p. 1059-1079.
106. Mantovani, A., et al., *Cancer-related inflammation.* Nature, 2008. **454**(7203): p. 436-444.
107. Tammi, R.H., et al. *Hyaluronan in human tumors: pathobiological and prognostic messages from cell-associated and stromal hyaluronan*. in *Seminars in cancer biology*. 2008. **18**(4): p. 288-295.
108. Kuang, D.-M., et al., *Tumor-derived hyaluronan induces formation of immunosuppressive macrophages through transient early activation of monocytes.* Blood, 2007. **110**(2): p. 587-595.
109. Hascall, V.C., et al., *Intracellular hyaluronan: a new frontier for inflammation?* Biochimica et Biophysica Acta (BBA)-General Subjects, 2004. **1673**(1): p. 3-12.
110. Kreil, G., *Hyaluronidases--a group of neglected enzymes.* Protein science: a publication of the Protein Society, 1995. **4**(9): p. 1666.
111. Werz, D.B., et al., *Exploring the structural diversity of mammalian carbohydrates ("glycospace") by statistical databank analysis.* ACS chemical biology, 2007. **2**(10): p. 685-691.
112. Pashkuleva, I. and R.L. Reis, *Sugars: burden or biomaterials of the future?* Journal of Materials Chemistry, 2010. **20**(40): p. 8803-8818.
113. Baldwin, A.D. and K.L. Kiick, *Polysaccharide-modified synthetic polymeric biomaterials.* Peptide Science, 2010. **94**(1): p. 128-140.
114. Pavao, M.S.G., *Structure and anticoagulant properties of sulfated glycosaminoglycans from primitive Chordates.* Anais Da Academia Brasileira De Ciencias, 2002. **74**(1): p. 105-112.
115. McLean, J., *The thromboplastic action of cephalin.* Am J Physiol, 1916. **41**(2): p. 250-7.

116. Merli, G.J. and J.B. Groce, *Pharmacological and clinical differences between low-molecular-weight heparins: implications for prescribing practice and therapeutic interchange.* Pharmacy and Therapeutics, 2010. **35**(2): p. 95.
117. Fransson, F., et al., *Rinsing the extra corporeal circuit with a heparin and albumin solution reduces the need for systemic anticoagulant in hemodialysis.* The International journal of artificial organs, 2013. **36**(10): p. 725-729.
118. Gray, E., B. Mulloy, and T.W. Barrowcliffe, *Heparin and low-molecular-weight heparin.* THROMBOSIS AND HAEMOSTASIS-STUTTGART-, 2008. **99**(5): p. 807.
119. Hirsh, J., et al., *Guide to anticoagulant therapy: Heparin a statement for healthcare professionals from the American Heart Association.* Circulation, 2001. **103**(24): p. 2994-3018.
120. Vitale, C., et al., *Dermatan sulfate: an alternative to unfractionated heparin for anticoagulation in hemodialysis patients.* J Nephrol, 2013. **26**: p. 158-163.
121. Liaw, P.C., et al., *Molecular basis for the susceptibility of fibrin-bound thrombin to inactivation by heparin cofactor II in the presence of dermatan sulfate but not heparin.* Journal of Biological Chemistry, 2001. **276**(24): p. 20959-20965.
122. Chen, G., et al., *Photoimmobilization of sulfated hyaluronic acid for antithrombogenicity.* Bioconjugate chemistry, 1997. **8**(5): p. 730-734.
123. Ramacciotti, E., et al., *Review: contaminants in heparin: review of the literature, molecular profiling, and clinical implications.* Clinical and Applied Thrombosis/Hemostasis, 2011. **17**(2): p. 126-135.
124. Liu, H., Z. Zhang, and R.J. Linhardt, *Lessons learned from the contamination of heparin.* Natural product reports, 2009. **26**(3): p. 313-321.
125. Shin, I., S. Park, and M.r. Lee, *Carbohydrate microarrays: an advanced technology for functional studies of glycans.* Chemistry-A European Journal, 2005. **11**(10): p. 2894-2901.
126. Rillahan, C.D. and J.C. Paulson, *Glycan microarrays for decoding the glycome.* Annual review of biochemistry, 2011. **80**: p. 797.
127. Bhaskar, U., et al., *Engineering of routes to heparin and related polysaccharides.* Applied microbiology and biotechnology, 2012. **93**(1): p. 1-16.
128. Seeberger, P.H., *Automated oligosaccharide synthesis.* Chemical Society Reviews, 2008. **37**(1): p. 19-28.
129. Zhou, G., et al., *Reducing the inflammatory responses of biomaterials by surface modification with glycosaminoglycan multilayers.* J Biomed Mater Res A, 2016. **104**(2): p. 493-502.
130. Reichenbach, S., et al., *Meta-analysis: Chondroitin for osteoarthritis of the knee or hip.* Annals of Internal Medicine, 2007. **146**(8): p. 580-590.
131. Zhou, G., H. Al-Khoury, and T. Groth, *Covalent immobilization of glycosaminoglycans to reduce the inflammatory effects of biomaterials.* The International journal of artificial organs, 2016. **39**(1): p. 37-44.

132. Ahmed, T., J. Garrigo, and I. Danta, *Preventing bronchoconstriction in exercise-induced asthma with inhaled heparin.* New England Journal of Medicine, 1993. **329**(2): p. 90-95.
133. Torkvist, L., et al., *Low molecular weight heparin as adjuvant therapy in active ulcerative colitis.* Alimentary Pharmacology & Therapeutics, 1999. **13**(10): p. 1323-1328.
134. Gandhi, N.S. and R.L. Mancera, *The Structure of Glycosaminoglycans and their Interactions with Proteins.* Chemical Biology & Drug Design, 2008. **72**(6): p. 455-482.
135. Taylor, K.R. and R.L. Gallo, *Glycosaminoglycans and their proteoglycans: host-associated molecular patterns for initiation and modulation of inflammation.* Faseb Journal, 2006. **20**(1): p. 9-22.
136. Young, E., *The anti-inflammatory effects of heparin and related compounds.* Thrombosis Research, 2008. **122**(6): p. 743-752.
137. Iovu, M., G. Dumais, and P. du Souich, *Anti-inflammatory activity of chondroitin sulfate.* Osteoarthritis and Cartilage, 2008. **16**: p. S14-S18.
138. Li, J.P. and I. Vlodavsky, *Heparin, heparan sulfate and heparanase in inflammatory reactions.* Thrombosis and Haemostasis, 2009. **102**(5): p. 823-828.
139. Pomin, V.H., *Fucanomics and galactanomics: Current status in drug discovery, mechanisms of action and role of the well-defined structures.* Biochimica et Biophysica Acta (BBA)-General Subjects, 2012. **1820**(12): p. 1971-1979.
140. Sasisekharan, R., et al., *Roles of heparan-sulphate glycosaminoglycans in cancer.* Nature Reviews Cancer, 2002. **2**(7): p. 521-528.
141. Lv, H., et al., *Elevate level of glycosaminoglycans and altered sulfation pattern of chondroitin sulfate are associated with differentiation status and histological type of human primary hepatic carcinoma.* Oncology, 2008. **72**(5-6): p. 347-356.
142. Jeney, A., et al., *Glycosaminoglycans as novel target in antitumor therapy.* The Tokai journal of experimental and clinical medicine, 1990. **15**(2-3): p. 167-177.
143. Knelson, E.H., J.C. Nee, and G.C. Blobe, *Heparan sulfate signaling in cancer.* Trends in biochemical sciences, 2014. **39**(6): p. 277-288.
144. Lee, E., et al., *Polyproline-type helical-structured low-molecular weight heparin (LMWH)-taurocholate conjugate as a new angiogenesis inhibitor.* International Journal of Cancer, 2009. **124**(12): p. 2755-2765.
145. Kim, J.-y., et al., *Antiangiogenic and anticancer effect of an orally active low molecular weight heparin conjugates and its application to lung cancer chemoprevention.* Journal of Controlled Release, 2015. **199**: p. 122-131.
146. Liu, Y., et al., *Effects of vascular endothelial growth factor (VEGF) and chondroitin sulfate A on human monocytic THP-1 cell migration.* Colloids and Surfaces B: Biointerfaces, 2005. **43**(3): p. 216-220.

147. Harley, B.A. and L.J. Gibson, *In vivo and in vitro applications of collagen-GAG scaffolds.* Chemical Engineering Journal, 2008. **137**(1): p. 102-121.
148. Liang, Y. and K.L. Kiick, *Heparin-functionalized polymeric biomaterials in tissue engineering and drug delivery applications.* Acta biomaterialia, 2014. **10**(4): p. 1588-1600.
149. Tognana, E., et al., *Hyalograft® C: hyaluronan-based scaffolds in tissue-engineered cartilage.* Cells Tissues Organs, 2007. **186**(2): p. 97-103.
150. Salbach, J., et al., *Regenerative potential of glycosaminoglycans for skin and bone.* Journal of molecular medicine, 2012. **90**(6): p. 625-635.
151. Dombrowski, C., et al., *Heparan sulfate mediates the proliferation and differentiation of rat mesenchymal stem cells.* Stem cells and development, 2009. **18**(4): p. 661-670.
152. Farrell, E., et al., *A collagen-glycosaminoglycan scaffold supports adult rat mesenchymal stem cell differentiation along osteogenic and chondrogenic routes.* Tissue Engineering, 2006. **12**(3): p. 459-468.
153. Tierney, C.M., M.J. Jaasma, and F.J. O'Brien, *Osteoblast activity on collagen-GAG scaffolds is affected by collagen and GAG concentrations.* Journal of Biomedical Materials Research Part A, 2009. **91A**(1): p. 92-101.
154. Servaty, R., et al., *Hydration of polymeric components of cartilage—an infrared spectroscopic study on hyaluronic acid and chondroitin sulfate.* International journal of biological macromolecules, 2001. **28**(2): p. 121-127.
155. Schönhoff, M., *Layered polyelectrolyte complexes: physics of formation and molecular properties.* Journal of Physics: Condensed Matter, 2003. **15**(49): p. R1781.
156. Takada, W., et al., *A sulfated glycosaminoglycan array for molecular interactions between glycosaminoglycans and growth factors or anti-glycosaminoglycan antibodies.* Analytical biochemistry, 2013. **435**(2): p. 123-130.
157. Zhi, Z.-l., A.K. Powell, and J.E. Turnbull, *Fabrication of carbohydrate microarrays on gold surfaces: direct attachment of nonderivatized oligosaccharides to hydrazide-modified self-assembled monolayers.* Analytical chemistry, 2006. **78**(14): p. 4786-4793.
158. Altgärde, N., et al., *Probing the biofunctionality of biotinylated hyaluronan and chondroitin sulfate by hyaluronidase degradation and aggrecan interaction.* Acta biomaterialia, 2013. **9**(9): p. 8158-8166.
159. Gore, S., et al., *Heparin surfaces: Impact of immobilization chemistry on hemocompatibility and protein adsorption.* Journal of Biomedical Materials Research Part B: Applied Biomaterials, 2014. **102**(8): p. 1817-1824.
160. Fajardo, A.R., et al., *Sulfated glycosaminoglycan-based block copolymer: preparation of biocompatible chondroitin sulfate-b-poly (lactic acid) micelles.* Biomacromolecules, 2014. **15**(7): p. 2691-2700.

161. Benedetti, L., et al., *Biocompatibility and biodegradation of different hyaluronan derivatives (Hyaff) implanted in rats.* Biomaterials, 1993. **14**(15): p. 1154-1160.
162. Della Valle, F., A. Romeo, and S. Lorenzi, *Salts and mixtures of hyaluronic acid with pharmaceutically active substances, pharmaceutical compositions containing the same and methods for administration of such compositions*. 1995, US 5442053.
163. Pouyani, T., G.S. Harbison, and G.D. Prestwich, *Novel hydrogels of hyaluronic acid: synthesis, surface morphology, and solid-state NMR.* Journal of the American Chemical Society, 1994. **116**(17): p. 7515-7522.
164. Daamen, W., et al., *Preparation and evaluation of molecularly-defined collagen–elastin–glycosaminoglycan scaffolds for tissue engineering.* Biomaterials, 2003. **24**(22): p. 4001-4009.
165. Pieper, J., et al., *Loading of collagen-heparan sulfate matrices with bFGF promotes angiogenesis and tissue generation in rats.* Journal of biomedical materials research, 2002. **62**(2): p. 185-194.
166. Bergman, K., et al., *Hyaluronic acid derivatives prepared in aqueous media by triazine-activated amidation.* Biomacromolecules, 2007. **8**(7): p. 2190-2195.
167. Hintze, V., et al., *Sulfated hyaluronan and chondroitin sulfate derivatives interact differently with human transforming growth factor-β1 (TGF-β1).* Acta biomaterialia, 2012. **8**(6): p. 2144-2152.
168. Gama, C.I., et al., *Sulfation patterns of glycosaminoglycans encode molecular recognition and activity.* Nature chemical biology, 2006. **2**(9): p. 467-473.
169. Hintze, V., et al., *Artificial extracellular matrices of collagen and sulphated hyaluronan enhance the differentiation of human mesenchymal stem cells in the presence of dexamethasone.* Journal of tissue engineering and regenerative medicine, 2014. **8**(4): p. 314-324.
170. Liu, Z.-M., et al., *Biocompatibility of poly (l-lactide) films modified with poly (ethylene imine) and polyelectrolyte multilayers.* Journal of Biomaterials Science, Polymer Edition, 2010. **21**(6-7): p. 893-912.
171. Becher, J., et al. *Synthesis of new regioselectively sulfated hyaluronans for biomedical application*. in *Macromolecular symposia*. 2010. **296**: p. 446-452.
172. Mlčochová, P., et al., *Synthesis and characterization of new biodegradable hyaluronan alkyl derivatives.* Biopolymers, 2006. **82**(1): p. 74-79.
173. Reyes, J.M., et al., *A modified chondroitin sulfate aldehyde adhesive for sealing corneal incisions.* Investigative ophthalmology & visual science, 2005. **46**(4): p. 1247-1250.
174. Jia, X., et al., *Hyaluronic acid-based microgels and microgel networks for vocal fold regeneration.* Biomacromolecules, 2006. **7**(12): p. 3336-3344.
175. Zhao, M., et al., *Improved Stability and Cell Response by Intrinsic Cross-Linking of Multilayers from Collagen I and Oxidized Glycosaminoglycans.* Biomacromolecules, 2014. **15**(11): p. 4272-4280.

176. Yang, Y., et al., *Functionality of surface-coupled oxidised glycosaminoglycans towards fibroblast adhesion.* Journal of Bioactive and Compatible Polymers: Biomedical Applications, 2015. **31**(2): p. 191-207.
177. Conrad, H.E., *Nitrous acid degradation of glycosaminoglycans.* Current Protocols in Molecular Biology, 2001: p. 17.22. 1-17.22. 5.
178. Dahl, L.B., T.C. Laurent, and B. Smedsrød, *Preparation of biologically intact radioiodinated hyaluronan of high specific radioactivity: Coupling of 125 I-tyramine-cellobiose to amino groups after partial N-deacetylation.* Analytical biochemistry, 1988. **175**(2): p. 397-407.
179. Jeon, O., et al., *Long-term and zero-order release of basic fibroblast growth factor from heparin-conjugated poly (L-lactide-co-glycolide) nanospheres and fibrin gel.* Biomaterials, 2006. **27**(8): p. 1598-1607.
180. Dickinson, L.E., et al., *Functional surfaces for high-resolution analysis of cancer cell interactions on exogenous hyaluronic acid.* Biomaterials, 2010. **31**(20): p. 5472-5478.
181. Ingham, K.C., S. Brew, and D.H. Atha, *Interaction of heparin with fibronectin and isolated fibronectin domains.* Biochemical journal, 1990. **272**(3): p. 605-611.
182. Bürgermeister, J., et al., *LaPSvS1, a (1→ 3)-β-galactan sulfate and its effect on angiogenesis in vivo and in vitro.* Carbohydrate research, 2002. **337**(16): p. 1459-1466.
183. Smith, P., A. Mallia, and G. Hermanson, *Colorimetric method for the assay of heparin content in immobilized heparin preparations.* Analytical Biochemistry, 1980. **109**(2): p. 466-473.
184. Studelska, D.R., et al., *Quantification of glycosaminoglycans by reversed-phase HPLC separation of fluorescent isoindole derivatives.* Glycobiology, 2006. **16**(1): p. 65-72.
185. Volpi, N. and F. Maccari, *Electrophoretic approaches to the analysis of complex polysaccharides.* Journal of Chromatography B, 2006. **834**(1): p. 1-13.
186. Frazier, S.B., et al., *The quantification of glycosaminoglycans: a comparison of HPLC, carbazole, and alcian blue methods.* Open glycoscience, 2008. **1**: p. 31.
187. Zaia, J., *Glycosaminoglycan glycomics using mass spectrometry.* Molecular & Cellular Proteomics, 2013. **12**(4): p. 885-892.
188. Sun, X., et al., *Analysis of total human urinary glycosaminoglycan disaccharides by liquid chromatography–tandem mass spectrometry.* Analytical chemistry, 2015. **87**(12): p. 6220-6227.
189. Osago, H., et al., *Quantitative analysis of glycosaminoglycans, chondroitin/dermatan sulfate, hyaluronic acid, heparan sulfate, and keratan sulfate by liquid chromatography–electrospray ionization–tandem mass spectrometry.* Analytical biochemistry, 2014. **467**: p. 62-74.

190. Liu, S., et al., *A heparin-binding synthetic peptide of heparin/heparan sulfateinteracting protein modulates blood coagulation activities.* Proceedings of the National Academy of Sciences, 1997. **94**(5): p. 1739-1744.
191. Benoit, D.S. and K.S. Anseth, *Heparin functionalized PEG gels that modulate protein adsorption for hMSC adhesion and differentiation.* Acta biomaterialia, 2005. **1**(4): p. 461-470.
192. Groth, T. and W. Wagenknecht, *Anticoagulant potential of regioselective derivatized cellulose.* Biomaterials, 2001. **22**(20): p. 2719-2729.
193. Bjornsson, T.D., K.M. Wolfram, and B.B. Kitchell, *Heparin kinetics determined by three assay methods.* Clinical pharmacology and therapeutics, 1982. **31**(1): p. 104-113.
194. Zhou, G., H. Loppnow, and T. Groth, *A macrophage/fibroblast co-culture system using a cell migration chamber to study inflammatory effects of biomaterials.* Acta biomaterialia, 2015. **26**: p. 54-63.
195. Brown, T. and U. Laurent, *Turnover of hyaluronan in synovial joints: elimination of labelled hyaluronan from the knee joint of the rabbit.* Experimental physiology, 1991. **76**(1): p. 125-134.
196. Oliveira, G., L. Carvalho, and M. Silva, *Properties of carbodiimide treated heparin.* Biomaterials, 2003. **24**(26): p. 4777-4783.
197. Zhong, S., et al., *Biodegradation of hyaluronic acid derivatives by hyaluronidase.* Biomaterials, 1994. **15**(5): p. 359-365.
198. Abatangelo, G., et al., *Biocompatibility and enzymatic degradation studies on sulphated hyaluronic acid derivatives.* Biomaterials, 1997. **18**(21): p. 1411-1415.
199. Köwitsch, A., et al., *Bioactivity of immobilized hyaluronic acid derivatives regarding protein adsorption and cell adhesion.* Biotechnology and applied biochemistry, 2011. **58**(5): p. 376-389.
200. Islam, T., et al., *Further evidence that periodate cleavage of heparin occurs primarily through the antithrombin binding site.* Carbohydrate research, 2002. **337**(21): p. 2239-2243.
201. Kusche, M., et al., *Biosynthesis of heparin. O-sulfation of the antithrombin-binding region.* Journal of Biological Chemistry, 1988. **263**(30): p. 15474-15484.
202. Capila, I. and R.J. Linhardt, *Heparin–protein interactions.* Angewandte Chemie International Edition, 2002. **41**(3): p. 390-412.
203. Fujita, M., et al., *Vascularization in vivo caused by the controlled release of fibroblast growth factor-2 from an injectable chitosan/non-anticoagulant heparin hydrogel.* Biomaterials, 2004. **25**(4): p. 699-706.
204. Wissink, M., et al., *Immobilization of heparin to EDC/NHS-crosslinked collagen. Characterization and in vitro evaluation.* Biomaterials, 2001. **22**(2): p. 151-163.

205. Nillesen, S.T., et al., *Increased angiogenesis and blood vessel maturation in acellular collagen–heparin scaffolds containing both FGF2 and VEGF.* Biomaterials, 2007. **28**(6): p. 1123-1131.
206. Ruoslahti, E. and Y. Yamaguchi, *Proteoglycans as modulators of growth factor activities.* Cell, 1991. **64**(5): p. 867-869.
207. Nagira, T., M. Nagahata-Ishiguro, and T. Tsuchiya, *Effects of sulfated hyaluronan on keratinocyte differentiation and Wnt and Notch gene expression.* Biomaterials, 2007. **28**(5): p. 844-850.
208. Decher, G., J. Hong, and J. Schmitt, *Buildup of ultrathin multilayer films by a self-assembly process: III. Consecutively alternating adsorption of anionic and cationic polyelectrolytes on charged surfaces.* Thin solid films, 1992. **210**: p. 831-835.
209. Thierry, B., et al., *Bioactive coatings of endovascular stents based on polyelectrolyte multilayers.* Biomacromolecules, 2003. **4**(6): p. 1564-1571.
210. Aggarwal, N., et al., *Tuning Cell Adhesion and Growth on Biomimetic Polyelectrolyte Multilayers by Variation of pH During Layer-by-Layer Assembly.* Macromolecular bioscience, 2013. **13**(10): p. 1327-1338.
211. De Cock, L.J., et al., *Engineered (hep/pARG) 2 polyelectrolyte capsules for sustained release of bioactive TGF-β1.* Soft Matter, 2012. **8**(4): p. 1146-1154.
212. She, Z., et al., *Encapsulation of basic fibroblast growth factor by polyelectrolyte multilayer microcapsules and its controlled release for enhancing cell proliferation.* Biomacromolecules, 2012. **13**(7): p. 2174-2180.
213. Costa, R.R., M. Alatorre-Meda, and J.F. Mano, *Drug nano-reservoirs synthesized using layer-by-layer technologies.* Biotechnology advances, 2015. **33**(6): p. 1310-1326.
214. Neto, A.I., et al., *Nanostructured Polymeric Coatings Based on Chitosan and Dopamine-Modified Hyaluronic Acid for Biomedical Applications.* Small, 2014. **10**(12): p. 2459-2469.
215. Gribova, V., R. Auzely-Velty, and C. Picart, *Polyelectrolyte multilayer assemblies on materials surfaces: from cell adhesion to tissue engineering.* Chemistry of Materials, 2011. **24**(5): p. 854-869.
216. Wang, L., et al., *Dynamic stiffness of polyelectrolyte multilayer films based on disulfide bond for in situ control of cell adhesion.* Journal of Materials Chemistry B, 2015. **3**, 7546-7553.
217. De Koker, S., R. Hoogenboom, and B.G. De Geest, *Polymeric multilayer capsules for drug delivery.* Chemical Society Reviews, 2012. **41**(7): p. 2867-2884.
218. Hsieh, C.Y.C., et al., *Reducing the Foreign Body Reaction by Surface Modification with Collagen/Hyaluronic Acid Multilayered Films.* ISRN Biomaterials, 2014. doi:10.1155/2014/718432.
219. Liston, E., L. Martinu, and M. Wertheimer, *Plasma surface modification of polymers for improved adhesion: a critical review.* Journal of Adhesion Science and Technology, 1993. **7**(10): p. 1091-1127.

220. Hall, D.B., P. Underhill, and J.M. Torkelson, *Spin coating of thin and ultrathin polymer films.* Polymer Engineering & Science, 1998. **38**(12): p. 2039-2045.
221. Ulman, A., *Formation and structure of self-assembled monolayers.* Chemical reviews, 1996. **96**(4): p. 1533-1554.
222. Love, J.C., et al., *Self-assembled monolayers of thiolates on metals as a form of nanotechnology.* Chemical reviews, 2005. **105**(4): p. 1103-1170.
223. Liu, L.-S., et al., *An osteoconductive collagen/hyaluronate matrix for bone regeneration.* Biomaterials, 1999. **20**(12): p. 1097-1108.
224. Thierry, B., et al., *Delivery platform for hydrophobic drugs: prodrug approach combined with self-assembled multilayers.* Journal of the American Chemical Society, 2005. **127**(6): p. 1626-1627.
225. Richert, L., et al., *Layer by layer buildup of polysaccharide films: physical chemistry and cellular adhesion aspects.* Langmuir, 2004. **20**(2): p. 448-458.
226. Levett, P.A., et al., *A biomimetic extracellular matrix for cartilage tissue engineering centered on photocurable gelatin, hyaluronic acid and chondroitin sulfate.* Acta biomaterialia, 2014. **10**(1): p. 214-223.
227. Zieris, A., et al., *FGF-2 and VEGF functionalization of starPEG–heparin hydrogels to modulate biomolecular and physical cues of angiogenesis.* Biomaterials, 2010. **31**(31): p. 7985-7994.
228. Cai, S., et al., *Injectable glycosaminoglycan hydrogels for controlled release of human basic fibroblast growth factor.* Biomaterials, 2005. **26**(30): p. 6054-6067.
229. Shu, X.Z., et al., *Synthesis and evaluation of injectable, in situ crosslinkable synthetic extracellular matrices for tissue engineering.* Journal of Biomedical Materials Research Part A, 2006. **79**(4): p. 902-912.
230. Elia, R., et al., *Silk–hyaluronan-based composite hydrogels: A novel, securable vehicle for drug delivery.* Journal of biomaterials applications, 2013. **27**(6): p. 749-762.
231. Jin, R., B. Lou, and C. Lin, *Tyrosinase-mediated in situ forming hydrogels from biodegradable chondroitin sulfate–tyramine conjugates.* Polymer International, 2013. **62**(3): p. 353-361.
232. Ni, Y., et al., *Tough and elastic hydrogel of hyaluronic acid and chondroitin sulfate as potential cell scaffold materials.* International journal of biological macromolecules, 2015. **74**: p. 367-375.
233. Thibeault, S.L., et al., *In vivo engineering of the vocal fold ECM with injectable HA hydrogels—late effects on tissue repair and biomechanics in a rabbit model.* Journal of Voice, 2011. **25**(2): p. 249-253.
234. Kirker, K.R., et al., *Glycosaminoglycan hydrogel films as bio-interactive dressings for wound healing.* Biomaterials, 2002. **23**(17): p. 3661-3671.
235. Philandrianos, C., et al., *Comparison of five dermal substitutes in full-thickness skin wound healing in a porcine model.* Burns, 2012. **38**(6): p. 820-829.
236. Yan, S., et al., *Silk fibroin/chondroitin sulfate/hyaluronic acid ternary scaffolds for dermal tissue reconstruction.* Acta biomaterialia, 2013. **9**(6): p. 6771-6782.

237. Adams, M.E., et al., *The role of viscosupplementation with hylan GF 20 (Synvisc®) in the treatment of osteoarthritis of the knee: a Canadian multicenter trial comparing hylan GF 20 alone, hylan GF 20 with non-steroidal anti-inflammatory drugs (NSAIDs) and NSAIDs alone.* Osteoarthritis and Cartilage, 1995. **3**(4): p. 213-225.
238. Chevalier, X., et al., *Single, intra-articular treatment with 6 ml hylan GF 20 in patients with symptomatic primary osteoarthritis of the knee: a randomised, multicentre, double-blind, placebo controlled trial.* Annals of the rheumatic diseases, 2010. **69**(01): p. 113-119.
239. Marcacci, M., et al., *Articular Cartilage Engineering with Hyalograft (R) C: 3-Year Clinical Results.* Clinical orthopaedics and related research, 2005. **435**: p. 96-105.
240. Remuzzi, A., et al., *Vascular smooth muscle cells on hyaluronic acid: culture and mechanical characterization of an engineered vascular construct.* Tissue engineering, 2004. **10**(5-6): p. 699-710.
241. Muscari, C., et al., *Restored perfusion and reduced inflammation in the infarcted heart after grafting stem cells with a hyaluronan-based scaffold.* Journal of cellular and molecular medicine, 2013. **17**(4): p. 518-530.
242. Cui, N., et al., *Hyaluronic acid hydrogel scaffolds with a triple degradation behavior for bone tissue engineering.* Carbohydrate polymers, 2015. **126**: p. 192-198.
243. Baldwin, A.D. and K.L. Kiick, *Reversible maleimide–thiol adducts yield glutathione-sensitive poly (ethylene glycol)–heparin hydrogels.* Polymer chemistry, 2013. **4**(1): p. 133-143.
244. McFadden, T., et al., *The delayed addition of human mesenchymal stem cells to pre-formed endothelial cell networks results in functional vascularization of a collagen–glycosaminoglycan scaffold in vivo.* Acta biomaterialia, 2013. **9**(12): p. 9303-9316.
245. Ko, C.-S., et al., *Type II collagen-chondroitin sulfate-hyaluronan scaffold cross-linked by genipin for cartilage tissue engineering.* Journal of bioscience and bioengineering, 2009. **107**(2): p. 177-182.
246. Chen, Y.-L., et al., *Composite chondroitin-6-sulfate/dermatan sulfate/chitosan scaffolds for cartilage tissue engineering.* Biomaterials, 2007. **28**(14): p. 2294-2305.
247. Kuo, C.-Y., et al., *Incorporation of chitosan in biomimetic gelatin/chondroitin-6-sulfate/hyaluronan cryogel for cartilage tissue engineering.* Carbohydrate polymers, 2015. **117**: p. 722-730.
248. Fischer, R.L., M.G. McCoy, and S.A. Grant, *Electrospinning collagen and hyaluronic acid nanofiber meshes.* Journal of Materials Science: Materials in Medicine, 2012. **23**(7): p. 1645-1654.
249. Zhong, S.P., et al., *Development of a novel collagen–GAG nanofibrous scaffold via electrospinning.* Materials Science and Engineering: C, 2007. **27**(2): p. 262-266.

250. Ji, Y., et al., *Dual-Syringe Reactive Electrospinning of Cross-Linked Hyaluronic Acid Hydrogel Nanofibers for Tissue Engineering Applications.* Macromolecular bioscience, 2006. **6**(10): p. 811-817.
251. Santo, V.E., et al., *Chitosan–chondroitin sulphate nanoparticles for controlled delivery of platelet lysates in bone regenerative medicine.* Journal of tissue engineering and regenerative medicine, 2012. **6**(S3): p. s47-s59.
252. Kim, S.W., et al., *Hyaluronated nanoparticles with pH-and enzyme-responsive drug release properties.* Colloids and Surfaces B: Biointerfaces, 2014. **116**: p. 359-364.
253. Landesman-Milo, D., et al., *Hyaluronan grafted lipid-based nanoparticles as RNAi carriers for cancer cells.* Cancer letters, 2013. **334**(2): p. 221-227.
254. Lee, K., et al., *Heparin immobilized gold nanoparticles for targeted detection and apoptotic death of metastatic cancer cells.* Biomaterials, 2010. **31**(25): p. 6530-6536.
255. Xu, X., et al., *Heparin-decorated, hyaluronic acid-based hydrogel particles for the controlled release of bone morphogenetic protein 2.* Acta biomaterialia, 2011. **7**(8): p. 3050-3059.
256. Bae, K.H., H. Mok, and T.G. Park, *Synthesis, characterization, and intracellular delivery of reducible heparin nanogels for apoptotic cell death.* Biomaterials, 2008. **29**(23): p. 3376-3383.
257. Burdick, J.A. and G.D. Prestwich, *Hyaluronic acid hydrogels for biomedical applications.* Advanced materials, 2011. **23**(12): p. H41-H56.
258. Kharkar, P.M., K.L. Kiick, and A.M. Kloxin, *Designing degradable hydrogels for orthogonal control of cell microenvironments.* Chemical Society Reviews, 2013. **42**(17): p. 7335-7372.
259. Wang, S.-C., et al., *Characterization of chondroitin sulfate and its interpenetrating polymer network hydrogels for sustained-drug release.* International journal of pharmaceutics, 2007. **329**(1): p. 103-109.
260. Qin, X.-H., et al., *Enzymatic synthesis of hyaluronic acid vinyl esters for two-photon microfabrication of biocompatible and biodegradable hydrogel constructs.* Polymer Chemistry, 2014. **5**(22): p. 6523-6533.
261. Dausse, Y., et al., *Cartilage repair using new polysaccharidic biomaterials: macroscopic, histological and biochemical approaches in a rat model of cartilage defect.* Osteoarthritis and cartilage, 2003. **11**(1): p. 16-28.
262. Lisignoli, G., et al., *Basic fibroblast growth factor enhances in vitro mineralization of rat bone marrow stromal cells grown on non-woven hyaluronic acid based polymer scaffold.* Biomaterials, 2001. **22**(15): p. 2095-2105.
263. Prestwich, G.D., *Hyaluronic acid-based clinical biomaterials derived for cell and molecule delivery in regenerative medicine.* Journal of controlled release, 2011. **155**(2): p. 193-199.
264. Madihally, S.V. and H.W. Matthew, *Porous chitosan scaffolds for tissue engineering.* Biomaterials, 1999. **20**(12): p. 1133-1142.

265. Davidenko, N., et al., *Collagen–hyaluronic acid scaffolds for adipose tissue engineering.* Acta biomaterialia, 2010. **6**(10): p. 3957-3968.
266. Murphy, C.M., M.G. Haugh, and F.J. O'Brien, *The effect of mean pore size on cell attachment, proliferation and migration in collagen–glycosaminoglycan scaffolds for bone tissue engineering.* Biomaterials, 2010. **31**(3): p. 461-466.
267. Khorshidi, S., et al., *A review of key challenges of electrospun scaffolds for tissue-engineering applications.* Journal of tissue engineering and regenerative medicine, 2015, DOI: 10.1002/term.1978.
268. Pieper, J., et al., *Preparation and characterization of porous crosslinked collagenous matrices containing bioavailable chondroitin sulphate.* Biomaterials, 1999. **20**(9): p. 847-858.
269. Collins, M.N. and C. Birkinshaw, *Hyaluronic acid based scaffolds for tissue engineering—A review.* Carbohydrate polymers, 2013. **92**(2): p. 1262-1279.
270. Hubbell, J.A. and A. Chilkoti, *Nanomaterials for drug delivery.* Science, 2012. **337**(6092): p. 303-305.
271. Nayak, S. and L.A. Lyon, *Soft nanotechnology with soft nanoparticles.* Angewandte chemie international edition, 2005. **44**(47): p. 7686-7708.
272. Oh, J.K., et al., *The development of microgels/nanogels for drug delivery applications.* Progress in Polymer Science, 2008. **33**(4): p. 448-477.
273. Hans, M. and A. Lowman, *Biodegradable nanoparticles for drug delivery and targeting.* Current Opinion in Solid State and Materials Science, 2002. **6**(4): p. 319-327.
274. Wang, A.Z., R. Langer, and O.C. Farokhzad, *Nanoparticle delivery of cancer drugs.* Annual review of medicine, 2012. **63**: p. 185-198.
275. Hobbs, S.K., et al., *Regulation of transport pathways in tumor vessels: role of tumor type and microenvironment.* Proceedings of the National Academy of Sciences, 1998. **95**(8): p. 4607-4612.
276. Peschel, D., et al., *Modulation of osteogenic activity of BMP-2 by cellulose and chitosan derivatives.* Acta biomaterialia, 2012. **8**(1): p. 183-193.
277. Silva, J.M., et al., *Nanostructured 3D constructs based on chitosan and chondroitin sulphate multilayers for cartilage tissue engineering.* PloS one, 2013. **8**(2): p. e55451.

Chapter 2

Summary - Bioactivity of immobilized hyaluronic acid derivatives regarding protein adsorption and cell adhesion:

The first paper was aimed to show the possibility to immobilize hyaluronic acid (HA) covalently onto different model substrata and study the bioactivity of immobilized HA towards the specific binding of aggrecan and cell adhesion to human fibroblasts. Therefore, HA was chemically modified either by oxidation to obtain aldehyde-HA (aHA) or by thiolation to obtain thiol-HA (tHA). The oxidation process of HA was carried out applying a specific amount of sodium periodate to cleave the C-C-bond between the vicinal hydroxyl groups of the glucuronic acid residues. The tHA was prepared by using the disulfide-containing, dihydrazide cross-linker 3,3`-dithiobis(propanoic hydrazide) that was attached to the carboxyl groups of the glycans backbone by carbodiimide chemistry. Subsequently, the reducing agent dithiothreitol was applied to generate the free thiols. The aldehyde group concentration of aHA was determined by Schiff`s reagent while the thiol group concentration of tHA was quantified by Ellman assay. Furthermore, the chemical structure, degree of modification and molecular weight of aHA and tHA were obtained from FT-IR, ^{1}H-NMR and field-flow fractionation, respectively. The modified HA derivatives were covalently immobilized on model surfaces like amino-terminated self assembled monolayers (SAM) for aHA or vinyl-terminated SAM and gold for tHA. The HA-coated substrata were analyzed by different physical methods such as water contact angle measurements, ellipsometry and atomic force microscopy. The bioactivity of aHA and tHA towards their natural binding partner aggrecan was studied by surface plasmon resonance. The obtained binding constants demonstrate that the immobilized modified HA is still capable to bind aggrecan when compared to native HA. Dermal human fibroblasts were used as a model cell to study the influence of chemical modification and immobilization of HA on cell adhesion and spreading. A lower number of cells and a more round cell shape were observed on HA-modified surfaces compared to amino and vinyl-terminated glass and silicon surfaces. Immunofluorescence staining revealed that adhesion of fibroblast seeded on HA-modified surfaces was mediated primarily by HA receptor CD44 indicating that bioactivity of HA was not significantly reduced by its chemical modification.

In this study it was found that modification of HA, either by oxidation or thiolation, and subsequent immobilization did not impair the binding activity to aggrecan or the interaction with natural receptor CD44. Thus, the results support the further use of this kind of chemical conjugation to other biomolecules especially glycosaminoglycans.

Biotechnology and Applied Biochemistry

Bioactivity of immobilized hyaluronic acid derivatives regarding protein adsorption and cell adhesion

*Alexander Köwitsch, Yuan Yang, Ning Ma, Judith Kuntsche, Karsten Mäder, and Thomas Groth**

Department of Pharmaceutical Technology and Biopharmacy, Institute of Pharmacy, Martin Luther University Halle–Wittenberg, Halle (Saale), Germany

Abstract.

Hyaluronic acid (HA) was chemically modified either by oxidation to obtain aldehyde-HA (aHA) or 3,3′-dithiobis(propanoic hydrazide) to obtain thiol-HA (tHA) that was covalently immobilized on model substrata such as amino-terminated surfaces or gold. Knowledge about the effect of modification with HA on physicochemical surface properties of these substrata and estimates of the quantities of immobilized HA were obtained by different physical methods such as contact angle measurements, ellipsometry, and atomic force microscopy. The bioactivity of aHA and tHA toward their natural binding partner aggrecan was studied by comparing surface plasmon resonance to native HA; this shows that binding of aggrecan was achieved in a similar way. Dermal human fibroblasts were used as a model cell to study how chemical modification and immobilization of HA impact adhesion and spreading of cells, which also affects cell growth and differentiation. A lower number and spreading of cells were observed on HA-modified surfaces compared to amino- and vinyl-terminated glass and silicon surfaces. Immunofluorescence microscopy also revealed that adhesion of fibroblast plated on HA-modified surfaces was mediated primarily by HA receptor CD44, indicating that bioactivity of HA was not significantly reduced by chemical modification.

Volume 58, Number 5, September/October 2011, Pages 376–389 •
E-mail: thomas.groth@pharmazie.uni-halle.de

Keywords: hyaluronic acid, bioactivity, aggrecan, cell adhesion, protein adsorption, CD44

1. Introduction

Hyaluronic acid (HA) represents a linear, nonsulfated polysaccharide, which is composed of repeating disaccharide units consisting of (β-1,4)-D-glucuronic acid and (β-1,3)-*N*-acetyl-D-glucosamine [1]. Being abundant in connective tissue, HA interacts with linker proteins, such as hyalectans/lecticans and calreticulin, and HA-binding proteoglycans, such as aggrecan and versican, resulting in large aggregates that are important in the assembly of an extracellular and pericellular matrix [2]. These large aggregates also possess remarkable hydrodynamic characteristics, especially for tissue homeostasis and biomechanical integrity, which are essential to maintain the physiological structure of connective tissue. As a major component of the extracellular matrix (ECM), HA also serves as a coregulator for adhesion, proliferation, motility, signaling, gene expression, metastasis, and morphogenesis [3]. The inherent bioactivity, biocompatibility, and biodegradability of HA make it a particularly attractive starting material for the fabrication of synthetic matrices with widespread uses as scaffold [4],[5], hydrogel-encapsulated cells [6],[7], or drug delivery system [8] in tissue engineering.

Cell adhesion of anchorage-dependent cells is usually mediated through the binding of integrin cell-surface receptors to ECM molecules, such as collagens, fibronectin, and laminin, which give rise to signals that mediate cellular responses, such as spreading, motility, growth, and survival [9]. However, recent studies have revealed that HA also promotes cell attachment even preceding the integrin-related adhesions, which is achieved by binding specific cell-surface receptors, such as CD44, hyaluronan-mediated motility receptor [RHAMM (CD168)], and intercellular adhesion molecule-1, to induce the transduction of a range of intracellular signals, either directly or by activating other receptors [7],[8]. CD44 is a cell-surface glycoprotein of 85–100 kDa, which recognizes a six sugar sequence

Abbreviations: AFM, atomic force microscopy; aHA, aldehyde-hyaluronic acid; APTES, 3-aminopropyltriethoxysilane; BSA, bovine serum albumin; cHA, covalently attached hyaluronic acid; DTPHY, 3,3′-dithiobis(propanoic hydrazide); DTT, dithiothreitol (Cleland's reagent); DMEM, Dulbecco's modified Eagle's medium; ECM, extracellular matrix; EDC, 1-ethyl-3-(3-dimethylaminopropyl) carbodiimide; FBS, fetal bovine serum; FFF, field-flow fractionation; FTIR, Fourier transform infrared spectroscopy; GAG, glycosaminoglycan; HA, hyaluronic acid, hyaluronan; HF, human dermal fibroblasts; LMWHA, low-molecular-weight hyaluronic acid; MES, 2-(*N*-morpholino)ethanesulfonic acid monohydrate; M_w, weight average molecular weight; NH_2-GL, amino-modified glass; NH_2-Si, amino-modified silicon; NHS, *N*-hydroxysuccinimide; PBS, phosphate-buffered saline; PDI, polydispersity index; pHA, physically adsorbed hyaluronic acid; RHAMM, hyaluronan-mediated motility receptor; RI, refractive index; RT, room (ambient) temperature; SPR, surface plasmon resonance; TBC, *tert*-butyl carbazate; tHA, thiol(ated)-hyaluronic acid; WCA, water contact angle.

*Address for correspondence: Professor Dr. Thomas Groth, PhD, Biomedical Materials Group, Institute of Pharmacy, Martin Luther University Halle–Wittenberg, Heinrich–Damerow–Strasse 4, 06120 Halle (Saale), Germany. Tel.: +49-345-55-28460; Fax: +49-345-55-27379; e-mail: thomas.groth@pharmazie.uni-halle.de.
Alexander Köwitsch and Yuan Yang contributed equally to this work.
Received 02 June 2011; accepted 13 July 2011
DOI: 10.1002/bab.41
Published online 20 September 2011 in Wiley Online Library (wileyonlinelibrary.com)

of HA [10] via hydrogen bonds and van der Waals forces [11]. CD44 is involved in the initial binding of HA to the cell surface before its internalization and degradation by acidic hydrolysis in lysosomes [10]. CD44 is also a mediator for HA-induced cell proliferation and survival pathways [1]. RHAMM is mainly involved in HA-induced cell locomotion [1],[12]. Nevertheless, RHAMM also interacts intracellularly with actin filaments and microtubules, inducing focal adhesion kinase phosphorylation and dephosphorylation, which also play significant roles in the activation during integrin-mediated cell adhesion [13]. Therefore, HA has been utilized to maintain and self-renew human embryonic stem cells [7] or as the milieu to which adhesive motifs are incorporated to enable cellular attachment and growth [14].

The multiple roles of HA in biological information transfer and control of cellular behavior in health and disease have drawn increasing attention to the study of HA glycoconjugates. For a better understanding of the biological functions of HA, a series of analytical procedures, such as atomic force microscopy (AFM), microarrays, and surface plasmon resonance (SPR), have been used to quantify the recognition of its natural binding partners, such as aggrecan, CD44, and RHAMM. In most of these studies, HA needs to be immobilized on a surface to be available to its binding partners. Chemically modified HA is available as a biocompatible and versatile biomolecule such as hydrazide–HA [15], biotinylated–HA [16], or methacrylamide–HA [17]. Being immobilized on functionalized surfaces, they might provide a model to characterize and study the carbohydrate–protein interaction [18], as well as a way to investigate cellular behavior. Because of its exceptional high hydrophilicity, HA can also be used as a highly hydrated coating of biomaterials, which can reduce the undesired protein adsorption or act as binding sites for specific biomolecules to elicit specific and controllable biological responses [19]. Furthermore, conjugated HA, such as thiol-HA (tHA) [20] or aldehyde-HA (aHA) [21], used as a precursor can react with other activated molecules to establish three-dimensional (3D) hydrogel systems that apply to controlled drug release or growth factor systems [22], or implants for the repair and regeneration of cartilage and bone [23],[24], and even for reconstruction of vocal cords [21].

A common approach toward the immobilization of glycans is the reaction of their reducing end with amino- or hydrazide-derived surfaces via reductive amination [25]. However, the immobilization of polysaccharides in an oriented manner via covalent bonding remains a challenging task due to the difficulty to address the reducing end of long saccharide chains. The unpredictable folding of polysaccharides and the problematic access of the reducing end makes a covalent binding of polysaccharides difficult. Therefore, this method is utilized solely to monosaccharides, disaccharides, or oligosaccharides [25],[26]. The generation of aldehydes on the backbone of HA by oxidation [21] or the partial modification of carboxylic acid functionalities of HA with a disulfide containing cross-linker as a thiol precursor [27] may provide sufficient reaction sites to immobilize such large molecular chains on solid substrata.

Therefore, it was the aim of this study to explore two different routes of one-step immobilization of HA on model substrata that are used in different sensing techniques and cell adhesion studies. Moreover, it was investigated by comparison to native HA physisorbed or covalently linked by conventional 1-ethyl-3-(3-dimethylaminopropyl) carbodiimide (EDC)/*N*-hydroxysuccinimide (NHS) chemistry how the chemical modification of HA affects its bioactivity. Results of the study show that tHA and aHA immobilized on surfaces possess a similar bioactivity such as native HA toward aggrecan and human dermal fibroblasts (HFs). Results are reported herein.

2. Materials and methods

2.1. Materials

Hyaluronic acid sodium salt [weight average molecular weight (M_w) 1.3 MDa] was provided by Kraeber & Co. GmbH (Ellerbek, Germany). Bovine serum albumin (BSA) and sodium cyanoborohydride ($NaBH_3CN$) were purchased from Merck KGaA (Darmstadt, Germany). Aggrecan (from bovine articular cartilage), sodium periodate, *tert*-butyl carbazate (TBC), Schiff's fuchsin–sulfite reagent, NHS, glutaric dialdehyde, and Triton X–100 were obtained from Sigma–Aldrich (Schnelldorf, Germany). The dialysis bag (Spectra/Por membrane, M_w cut-off = 3,500), glycine, and organic solvents were provided by Roth (Karlsruhe, Germany). 3,3′-dithiobis(propanoic hydrazide) (DTPHY) was synthesized as stated before [15]. Other used compounds were: 3-aminopropyltriethoxysilane (APTES), 7-octenyldimethychlorosilane (ABCR GmbH & Co., KG, Karlsruhe, Germany), 2-(*N*-morpholino)ethanesulfonic acid monohydrate (MES), dithiothreitol (DTT) (VWR International, Poole, England), 5,5′-dithiobis-(2-nitrobenzoic acid) (Ellman's reagent), and EDC hydrochloride from Alfa Aesar (Karlsruhe, Germany). Phosphate-buffered saline (PBS) was prepared according to the following formulation: 2.7 mM KCl, 137 mM NaCl, 1.4 mM KH_2PO_4, 4.3 mM $Na_2HPO_4 \times 2H_2O$, pH 7.4.

2.2. Synthesis and characterization of oxidized and thiolated HA

2.2.1. Preparation of low-molecular-weight hyaluronic acid

High-molecular weight HA (1.5 g, M_w 1.3 MDa) was dissolved in distilled water (350 mL) and the pH of the solution was adjusted to 1.0 with HCl. The degradation process was carried out at a temperature of 60°C with a constant stirring speed for 24 H. After that, the pH was adjusted to 7.0 with NaOH and the solution was dialyzed against water for 3 days. The following lyophilization resulted in 1.1 g of low-molecular-weight HA (LMWHA).

2.2.2. Preparation of tHA

The procedure (Fig. 1B) was described previously and carried out at room temperature (RT) [27]. In brief, LMWHA (500 mg, 1.25 mmol) was dissolved in Milli-Q water (80 mL). Then, DTPHY (74 mg, 0.31 mmol) was added to the stirred solution. Thereafter, EDC (96 mg, 0.5 mmol) was added while maintaining the pH at 4.75. After additional 3 H of incubation, 1M NaOH was used to increase the pH to 7.0. Then, DTT (386 mg, 2.5 mmol) was added in portions and the pH was raised to 8.5. The solution was stirred overnight. Then, the pH of the reaction mixture was lowered to 3.5 before the solution was dialyzed exhaustively

Reprinted with permission from Journal of Bioactivity and Applied Biochemistry, Alexander Köwitsch, Yuan Yang, Ning Ma, Judith Kuntsche, Karsten Mäder, and Thomas Groth (2011), Bioactivity of immobilized hyaluronic acid derivatives regarding protein adsorption and cell adhesion, 58 (5), 376–389.
 DOI: 10.1002/bab.41

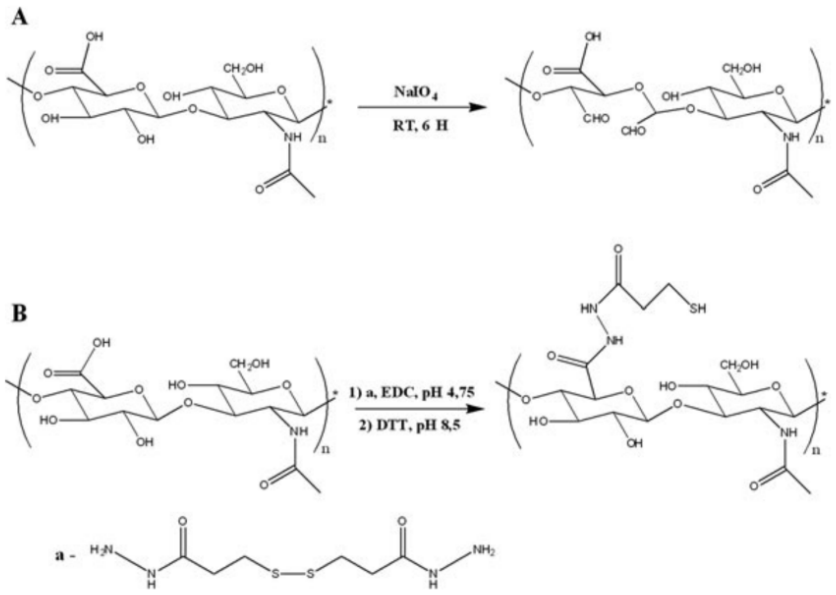

Fig. 1. Reaction scheme for the preparation of hyaluronic acid derivatives: (A) aldehyde-hyaluronic acid (aHA) and (B) thiol-hyaluronic acid (tHA).

against diluted HCl containing 100 mM NaCl firstly, and then against diluted HCl (pH 3.5). Finally, the solution was freeze-dried to obtain a white reaction product.

2.2.3. Preparation of aHA

The method used here (Fig. 1A) was slightly modified compared with the previously described report [28]. HA (M_w 1.3 MDa, 1.0 g, 2.5 mmol) was dissolved in 100 mL of H_2O in a flask that was wrapped with aluminum foil. Sodium periodate (0.6 mmol, 0.2 M in H_2O) was added dropwise. The reaction mixture was stirred for 6 H at RT in the dark. The solution was purified by dialysis in distilled water for 3 days. The final dry product was obtained by freeze-drying.

2.2.4. Characterization of aHA and tHA

The quantity of functional groups, such as aldehydes and thiols, was determined using Schiff's and Ellman's reagents, respectively, using ultraviolet–visible (UV–Vis) spectroscopy. For determination of aldehydes, the calibration curve was established using glutaric dialdehyde as a standard to calculate the extinction coefficient of aldehyde groups. The procedure was carried out by adding 2.5 mL of Schiff's reagent to a sample of 0.5 mL of an aldehyde-containing substance. The absorbance of the colored complex was measured at 550 nm within 40 Min [29]. The thiol content of tHA was determined according to the results of the UV measurement using Ellman's reagent [30]. The molar absorption coefficient of 14,150 at 412 nm was used for the calculation of the total thiol concentration [31].

The chemical structures of oxidized and thiolated HA were analyzed by Fourier transform infrared (FTIR) spectroscopy (IFS 28, Bruker, Ettlingen, Germany) and ^{1}H NMR (Varian Gemini 2000, Varian Inc., Palo Alto, CA, USA). The degree of substitution of the tHA with the cross-linker DTPHY was accessible by comparing the corresponding peak area of the hydrogens belonging to the cross-linker with the peak area of the acetamide methyl group. The identification of aldehyde groups was achieved by the conversion with TBC, which resulted in a stable product that could be visualized with ^{1}H NMR. Thus, the periodate-oxidized HA (aHA) was dissolved in acetate buffer (pH 5.14) at a concentration of 10 mg/mL. Then, a fivefold excess of TBC and $NaBH_3CN$ were dissolved in buffer and added subsequently. The mixture was allowed to react for 24 H at RT. The product was purified by thorough dialysis in 100 mM NaCl solution and distilled H_2O. The freeze-dried product was used for ^{1}H NMR examination.

The molecular weight and polydispersity of aHA and tHA were measured by asymmetrical flow field–flow fractionation (FFF) equipped with a Dawn EOS detector (Wyatt Technology Corporation, Santa Barbara, CA, USA) and a refractive index (RI)-detector (Shodex RI–101, Showa Denko Europe GmbH, Munich, Germany). All samples were measured in 50 mM NaCl containing 0.02% NaN_3 (w/v) to prevent bacterial growth. Molecular weights were calculated using Astra software (Wyatt Technology Corporation).

2.3. Functionalization and characterization of substrata

2.3.1. Preparation of model substrata

2.3.1.1. Cleaning procedures

Glass cover slips (Menzel GmbH + Co KG, Braunschweig, Germany) were cleaned either by immersion in piranha solution of a mixture of H_2O_2 and H_2SO_4 (30/70, v/v) for 1 H or by the treatment with 0.5 M NaOH in ethanol for 2 H. Afterward, the

Reprinted with permission from Journal of Bioactivity and Applied Biochemistry, Alexander Köwitsch, Yuan Yang, Ning Ma, Judith Kuntsche, Karsten Mäder, and Thomas Groth (2011), Bioactivity of immobilized hyaluronic acid derivatives regarding protein adsorption and cell adhesion, 58 (5), 376–389.
 DOI: 10.1002/bab.41

glass surfaces were washed with Milli-Q water (0.055 mS/cm, 10 cycles with 6 Min each) and dried in a stream of nitrogen. Silicon wafers (Silicon Materials, Kaufering, Germany) with each size of 15 × 15 mm² were treated with a solution of NH_4OH (27%), H_2O_2 (30%), and water (1:1:5, v/v/v) at 70°C for 15 Min and subsequently washed with Milli-Q water. Afterward, the silicon wafers were also dried with a stream of nitrogen. New gold-coated glass sensors for SPR (IBIS Technologies BV, Enschede, Netherlands, 16 × 16 mm²) were cleaned with ethanol and extensive rinsing with ultrapure water followed by drying with nitrogen.

2.3.1.2. Amino-terminated glass and silicon surfaces
The amino-terminated surfaces were generated by immersion of clean glass or silicon in a solution of APTES in ethanol (1%, v/v) for 1 H at RT. Catalytic amounts of concentrated acetic acid were added to the solution to accelerate the condensation reaction. Fresh solution was prepared right before the silanization was started. After that, the surfaces were rinsed extensively with ethanol and Milli-Q water, and then dried with streaming nitrogen.

2.3.1.3. Vinyl-terminated glass and silicon surfaces
The vinyl-terminated surfaces were prepared by immersion of cleaned glass or silicon in an ethanolic solution of 7-octenyldimethychlorosilane (3%, v/v) for 24 H while the solution was warmed to 35°C in a water bath for at least 3 H. Then the surfaces were rinsed with copious amounts of ethanol, washed with Milli-Q water (10 × 6 Min), and dried by nitrogen.

2.3.1.4. Amino-terminated gold
The clean gold sensors were put into a solution of cysteamine hydrochloride in ethanol (20 mM) at RT overnight to obtain amino-terminated gold. Before use, the sensors were carefully rinsed with ethanol and Milli-Q water and dried in a stream of nitrogen.

2.3.2. Immobilization of HA

2.3.2.1. Immobilization of aHA
The immobilization of aHA on NH_2-terminated surfaces (glass, silicon, or gold) was achieved by reductive amination. A solution of 1 mL aHA (4.0 mg/mL in PBS) was applied to NH_2–modifed surfaces and kept for 24 H at RT. Then, 1 mL $NaBH_3CN$ (3.0 mg/mL in PBS) was added to the same solution to create a stable bond by reducing the Schiff's base. The solution was kept at 4°C for 24 H [21]. Then, the HA-coated surface was rinsed by copious amounts of PBS and Milli-Q water and then dried with a stream of nitrogen. This was also done during the other immobilization variants described below.

2.3.2.2. Immobilization of tHA
The reaction of tHA with the vinyl-terminated glass or silicon surfaces was carried out in a UV light chamber (Bio-Link BLX, LTF Labortechnik GmbH & Co. KG, Wasserburg, Germany) at 365 nm in Tris–HCl (10 mM, pH 7.4) for 4 H at a concentration of 2 mg/mL. The modified surfaces were washed and dried.

2.3.2.3. Physically adsorbed native HA (pHA) and covalently attached LMWHA (cHA)
As control surfaces, native pHA on NH_2- or vinyl-terminated surfaces and covalently attached LMWHA on amino-terminated gold were utilized, respectively. To obtain pHA, native HA (4.0 mg/mL in PBS) was applied to NH_2 terminated for 48 H, then rinsed and dried. Similarly, native HA was applied to vinyl-terminated surfaces in Tris–HCl (10 mM, pH 7.4) for 4 H, washed with water (10 × 6 Min), and also dried. To obtain cHA, the amino-terminated gold was immersed in a MES-buffered solution (50 mM, pH 4.7) containing LMWHA (10 mg/mL), EDC (5 mg/mL), and NHS (3 mg/mL) for 24 H. To inactivate the remaining reactive carboxyl species of the EDC linker, the sensor was then immersed in a 1 M solution of ethanolamine, followed by ethanol rinsing and washing with Milli-Q water.

After HA immobilization, modified glass substrata were used for contact angle measurement and a cell adhesion experiment, silicon substrata were applied to ellipsometry and AFM, and gold sensors were used for the SPR experiments.

2.3.3. Physical characterization of HA-modified surfaces

2.3.3.1. Water contact angle (WCA)
Static WCA measurements were performed with OCA 15Plus device from Dataphysics (Filderstadt, Germany) applying the sessile drop method to measure the wetting changes after surface modification of substrata and immobilization of HA. Five droplets of 3 μL ultrapure water was applied to each sample and the obtained values were used to calculate means and standard deviations.

2.3.3.2. Ellipsometry
Changes in layer thickness of the modified silicon surfaces was determined by ellipsometry (M-2000V, J.A. Woollam Company, Lincoln, NE, USA) at the range of angles from 65° to 85°. A RI of 1.45 was used for all samples because it is recommended for such surfaces [32]. Measurements were performed three times in different locations on the surface and averaged. The experimental data were analyzed with the WVase32 software provided with the equipment.

2.3.3.3. Atomic force microscopy (AFM)
AFM was performed with a 3D molecular force probe (MFP-3D-BIO, Asylum Research, Santa Barbara, CA, USA) and ACT cantilevers (Applied NanoStructures Inc., Santa Clara, CA, USA) with a resonance frequency of 300 kHz and a spring constant of 40 N/m to monitor the surface morphology. Roughness analysis was performed using the software SPIP v5.0.1 (Scanning Probe Image Processor, Image Metrology A/S, Hørsholm, Denmark). Modified silicon surfaces were probed in tapping mode under ambient (air) laboratory conditions. Scans were carried out on a 0.7 μm² sized window.

Reprinted with permission from Journal of Bioactivity and Applied Biochemistry, Alexander Köwitsch, Yuan Yang, Ning Ma, Judith Kuntsche, Karsten Mäder, and Thomas Groth (2011), Bioactivity of immobilized hyaluronic acid derivatives regarding protein adsorption and cell adhesion, 58 (5), 376–389.
 DOI: 10.1002/bab.41

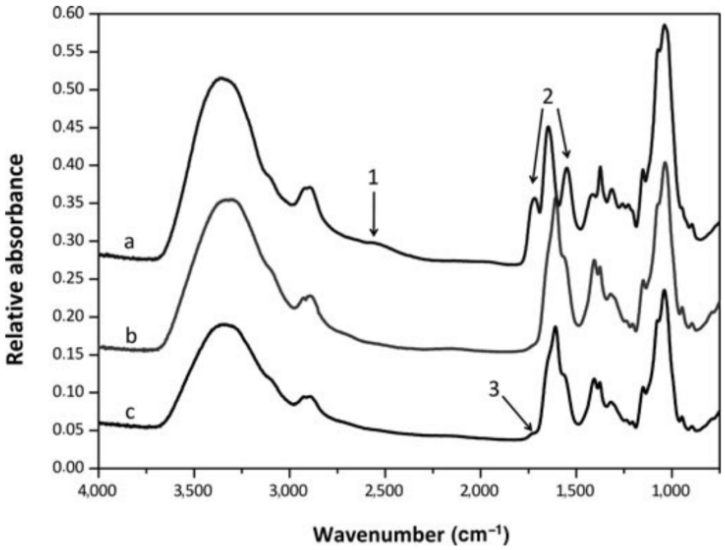

Fig. 2. FTIR spectra of HA (b), thiol-HA (a) and aldehyde-HA (c) and their significant adsorption bands: (1) —SH stretching vibration, (2) —C=O— stretching vibration of amide/hydrazide, (3) —C=O— stretching vibration of aldehyde.

2.4. Aggrecan binding to immobilized HA analyzed by SPR

The adsorption of aggrecan—the natural ligand of HA in cartilage—was measured by SPR using an imaging SPR instrument (IBIS Technologies BV, Enschede, Netherlands). All relevant SPR substrata were first equilibrated with PBS (pH 7.4). All solutions were injected with a flow rate of 3 μL/Min at a constant temperature of 25°C. The solution of interest (aHA, pHA at 4.0 mg/mL in PBS, and tHA at 2 mg/mL in PBS) was applied to the surface and allowed to immobilize for 1 H (aHA and pHA) or 2 H (tHA). An additional glycine rinsing step was used to inactivate free aldehyde groups after the injection of aHA. Then, the surface was rinsed with running buffer for 12 Min and aggrecan was injected in rising concentrations from 5 to 100 μg/mL (for 30 Min each), alternated by PBS rinsing steps (6 Min each). Finally, the surface was rinsed with PBS again for 12 Min to remove unbound protein.

The resulting change in the angle shift (m°) before and after each injection is proportional to the mass of molecules adsorbed on the surface (122 m° corresponds to approximately 1 ng/mm²) [33]. Adsorption isotherms were established by plotting the adsorbed amount as a function of solution concentration (Fig. 2). Results were analyzed applying the Langmuir adsorption model to calculate the binding constant K and the possible maximum amount of protein adsorbed Γ_{max}.

2.5. Cell adhesion studies on HA-modified surfaces

2.5.1. Cell culture

Human dermal fibroblasts were grown in Dulbecco's modified Eagle's medium (DMEM, Biochrom AG, Berlin, Germany) supplemented with 10% fetal bovine serum (FBS, Biochrom AG), 1% antibiotic–antimycotic solution (Sigma–Aldrich) at 37°C in a humidified 5% CO_2/95% air atmosphere using a NUAIRE DH Autoflow incubator (NuAire Corporation, Plymouth, MN, USA). Cells from almost confluent cultures were harvested by 0.25% Trypsin/ethylenediaminetetraacetic acid (Biochrom AG). Trypsin was neutralized with DMEM containing 10% FBS. After centrifugation of cell suspension for 5 Min at 200 × g, HFs were resuspended in culture medium without FBS and seeded on the plain or HA-modified surfaces at a density of 2.5 × 10^4 cells/mL.

2.5.2. Cell adhesion studies

The test surfaces (different types of modified glass slides) were placed into 12-well tissue culture plates (Greiner Bio-One GmbH, Frickenhausen, Germany) and rinsed with sterile PBS twice. Amino- and vinyl-terminated glass as well as pHA on either surfaces were used as controls. aHA-modified surfaces were pretreated with 200 mM glycine dissolved in PBS for 30 Min, then with 1% (w/v) BSA for 60 Min at RT before cell seeding. HFs were seeded on the different modified surfaces and incubated for 4 H at 37°C in a humidified 5% CO_2/95% air atmosphere. The morphology of human fibroblasts was visualized by staining with crystal violet (5%, v/v in methanol), followed by extensive washing with water and drying. Cells were photographed by a transmitted light microscope (Axiovert 100, Carl Zeiss MicroImaging GmbH, Germany) equipped with a CCD camera (Sony, MC-3254, AVT-Horn, Aalen, Germany) and image analyzing software KS 300 (Carl Zeiss, Oberkochen, Germany). Cell number, area, and form factor were evaluated by image analysis software.

2.5.3. Immunostaining of cells

After 4 H of incubation, the cells attached to the different surfaces were fixed with 4% (w/v) paraformaldehyde in PBS for

Reprinted with permission from Journal of Bioactivity and Applied Biochemistry, Alexander Köwitsch, Yuan Yang, Ning Ma, Judith Kuntsche, Karsten Mäder, and Thomas Groth (2011), Bioactivity of immobilized hyaluronic acid derivatives regarding protein adsorption and cell adhesion, 58 (5), 376–389.
 DOI: 10.1002/bab.41

15 Min. Then, the cells were permeabilized with 0.1% (v/v) Triton X–100 for 10 Min. After rinsing the samples with PBS three times, the nonspecific binding sites were blocked by incubation with 1% BSA for 30 Min. CD44, the cell-surface receptor of HA, was stained by incubation with a mouse monoclonal antibody raised against CD44 (Dianova, Hamburg, Germany) for 30 Min at RT. Specific antibody binding was revealed by the incubation with a Cy2–conjugated anti-mouse secondary antibody (Dianova). Antibodies were diluted in PBS containing 1% BSA. Filamentous actin was stained by incubation with BODIPY phalloidin (Invitrogen, Darmstadt, Germany) at RT for 30 Min. Cell nuclei were stained with To–Pro3 Iodide (Invitrogen) at RT for 30 Min. The samples were then washed with PBS, distilled water, and finally mounted with Mowiol (Calbiochem, Darmstadt, Germany). Samples were examined with confocal laser scanning microscopy (LSM 710, Carl Zeiss MicroImaging GmbH, Jena, Germany) using a 40 × oil immersion objective.

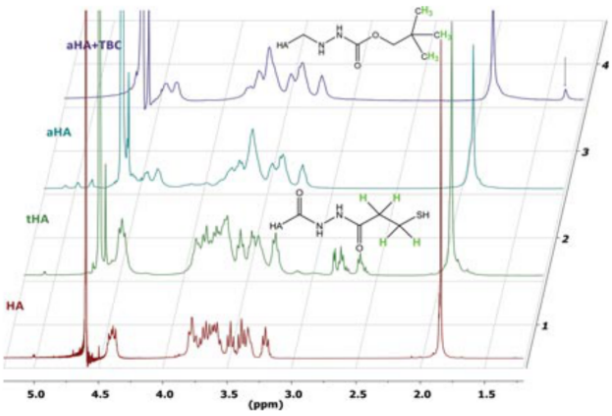

Fig. 3. ^{1}H NMR spectra (400 MHz, D_2O) of HA (line 1) and HA derivatives: thiol-HA (line 2), aldehyde-HA (line 3), aldehyde-HA modified with TBC (line 4). TBC, *tert*-butyl carbazate.

3. Results and Discussion

3.1. Synthesis and characterization of HA derivatives

Chemical modification of HA has been studied for a variety of applications. Here, either reactive aldehydes or thiol groups were introduced into the HA chain to different degrees. Vicinal hydroxyl groups of HA can be oxidized to dialdehydes in the presence of sodium periodate, which introduces the reactive groups to the sugar backbone (see Fig. 1A). Another option of HA activation/conjugation is the generation of reactive thiol groups. To achieve this, carboxylic acid groups of HA were partially conjugated with DTPHY, a disulfide containing cross-linker, and subsequently reacted with the reducing agent DTT to generate free thiol groups.

Native HA and its derivatives were characterized by FTIR as shown in Fig. 2. HA is distinguished by saccharide alkyls at 2,920 and 1,415 cm^{-1}, and alkoxyls at 1,030 cm^{-1} (see Fig. 2b). After oxidation, the spectrum of aHA shows a new weak absorption peak at around 1,733 cm^{-1} (Fig. 2c), which corresponds to the stretching vibration of the aldehyde's carbonyl group [28]. The spectrum of tHA (Fig. 2a) shows two new stretching vibrations (1,550 cm^{-1}; 1,715 cm^{-1}), which are attributed to the carbonyl absorbance of the newly created amide bonds. Additionally, a weak broad absorbance at 2,500—2,600 cm^{-1} is visible that corresponds to the —SH stretching vibration [34].

Nuclear magnetic resonance spectroscopy was applied to detect the molecular changes resulting from the modification of HA. The ^{1}H NMR spectrum of HA before and after oxidation is compared in Fig. 3. However, the new peaks of dialdehydes were not detectable by ^{1}H NMR due to a fast equilibrium of aldehydes and the corresponding hydrated form. To improve the identification of aldehydes, the oxidized HA (Fig. 3, aHA) was reacted with an excess of TBC in the presence of the reducing agent $NaBH_3CN$. The unreacted carbazate and $NaBH_3CN$ were removed by dialysis. A well-resolved singlet peak was found at 1.4 ppm in the ^{1}H NMR spectrum of TBC-conjugated HA (Fig. 3, aHA + TBC), which is attributed to the *tert*-butyl group introduced by the aldehyde–hydrazide reaction. This was used to qualitatively determine the free aldehyde groups. The successful thiolation of HA can be also extracted from Fig. 3. The amount of cross-linker inserted to the carboxylic acid groups of HA can be calculated by comparing the peak areas of the new adsorptions of the four hydrogens belonging to the introduced cross-linker DTPHY (m, 4H, —CH_2CH_2—S, 2.5–2.8 ppm) and the well-separated singlet of the acetamide (s, 3H, Ac, 1.9 ppm) (Fig. 3, tHA). The results indicate that a total amount of 26% of carboxyl groups was reacted with the cross-linker. These observations are attributed to the fact that every DTPHY has two reactive sites. For the influence of higher molar amounts of the cross-linker on the reaction, the reader is referred to the findings of Prestwich and coworkers [27].

As aldehydes cannot be quantitatively determined by simple ^{1}H NMR techniques, the quantification was realized utilizing Schiff's reagent, which indicated a yield of 10% of dialdehyde groups per disaccharide unit. The amount of free thiols was determined to 19% by quantification with Ellman's reagent. The latter value also refers to disaccharide units because the carboxyl group is only available in glucuronic acid rings. Taking into account the degree of substitution, it is apparent that about 70% of introduced cross-linker was cleaved by the reducing agent DTT. It is not known whether the cross-linker was attached on both sides or with one active group only, so this value could be only estimated by dividing the thiol content by the percentage of introduced cross-linker. The results of the determination of reactive groups via UV–Vis spectroscopy are listed in Table 1. The molecular weight of HA and its derivatives were determined by FFF with aqueous NaCl solution (50 mM) as the mobile phase. Applying 25% molar amount of $NaIO_4$ for 6 H led to a decrease of the M_w from 1.3 MDa to 92 kDa. Because the thiolation was derived from a cross-linking reaction, the molecular weight of the resulting tHA increased from 15 kDa for LMWHA to 70 kDa, which was reasonable because there were still unconverted disulfides remaining in the tHA.

Reprinted with permission from Journal of Bioactivity and Applied Biochemistry, Alexander Köwitsch, Yuan Yang, Ning Ma, Judith Kuntsche, Karsten Mäder, and Thomas Groth (2011), Bioactivity of immobilized hyaluronic acid derivatives regarding protein adsorption and cell adhesion, 58 (5), 376–389.
 DOI: 10.1002/bab.41

Table 1
Theoretical (D_{th}) and experimental (D_{exp}) degree of modification (related to repeating disaccharide units) and weight average molecular weight (M_w), number average molar mass (M_n), and polydispersity index (PDI) of HA and HA derivatives

	Amount of active groups D(%)		Molecular weight (Da)[a]		
Sample	D_{th}	D_{exp}	M_w	M_n	PDI
HA	–	–	1.3×10^6	–	11.5
LMWHA	–	–	15,000	11,500	1.3
aHA[b]	25	10	92,000	57,000	1.6
tHA[c]	25	19	70,000	17,000	4.1

[a]Molecular weights and PDI of oxidized HA determined by field–flow fractionation with mobile phase of NaCl 50 mM.
[b]Molar amount of aldehyde groups (determined by UV–Vis spectroscopy) in relation to the molar amount of HA disaccharide repeating units.
[c]Thiol groups determined by reaction with Ellman's reagent, monitored via UV–Vis at 412 nm.
LMWHA , low-molecular-weight hyaluronic acid; aHA, aldehyde-HA; tHA, thiol-HA.

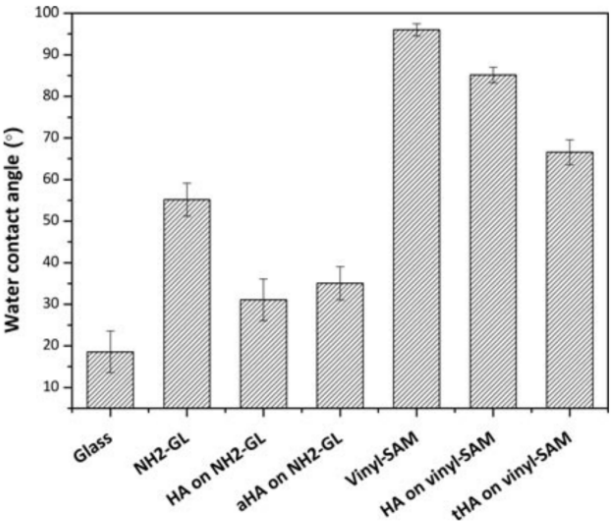

Fig. 4. Water contact angle of immobilized hyaluronic acid (HA) derivatives on glass. NH2—GL, amino-terminated glass; aHA, aldehyde-HA; vinyl-SAM, vinyl-terminated glass; tHA, thiol-HA.

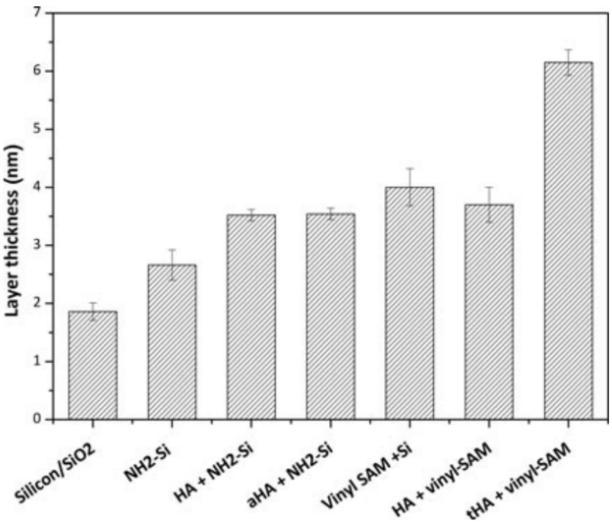

Fig. 5. Cumulative thickness of immobilized hyaluronic acid (HA) derivatives on silicon determined by ellipsometry (NH2–Si, amino-terminated silicon; aHA, aldehyde-HA; vinyl-SAM, vinyl-terminated silicon; tHA, thiol-HA.

3.2. Characterization of HA–modified surfaces

Interaction between implants and host tissue is greatly influenced by physicochemical surface properties of implants. In contrast, carbohydrate–protein interactions have been used to elucidate fundamental biochemical processes and identify new pharmaceutical substances in a living cell system [35]. To fully study the specific interaction of glycosaminoglycans (GAGs) with both biomolecules, such as proteins or DNA, and cell behavior, we applied conjugated HA and immobilization methods addressing gold or amine- and vinyl-modified substrata, which shall retain the functional sites of polysaccharide structures so that the immobilized molecules can mimic the specific biomolecular interactions.

Wettability of surfaces is an important factor that influences protein adsorption and cell behavior. Wetting properties of the different substrata were measured here by the WCA method. The results of the WCA measurements depicted in Fig. 4 show a reasonable increase of WCA, when the cleaned glass cover slips (WCA $<20^\circ$) were modified with APTES to generate amino-modified glass (NH_2–GL, WCA $= 55^\circ$). It was also visible that modification of this surface with pHA or aHA decreased the WCA to about 30°, which should be related to the immobilization of hydrophilic HA. In contrast, a steep rise in WCA was monitored when clean glass was modified with vinyl-terminated self-assembled monolayers (SAM), resulting in a WCA of about 95°. Immobilization of native HA (pHA) and tHA decreased the WCA to 85° and 67°, respectively. The lower change of wetting properties indicates that coverage of the vinyl-terminated SAM with HA was not complete. Overall, the WCA values of the plain, NH_2–GL, and vinyl-modified glass correspond well to previous work [36]. The observed changes of WCA after physical adsorption of HA or covalent binding of aHA and tHA indicate the presence of HA, although no complete surface coverage can be expected.

Reprinted with permission from Journal of Bioactivity and Applied Biochemistry, Alexander Köwitsch, Yuan Yang, Ning Ma, Judith Kuntsche, Karsten Mäder, and Thomas Groth (2011), Bioactivity of immobilized hyaluronic acid derivatives regarding protein adsorption and cell adhesion, 58 (5), 376–389.

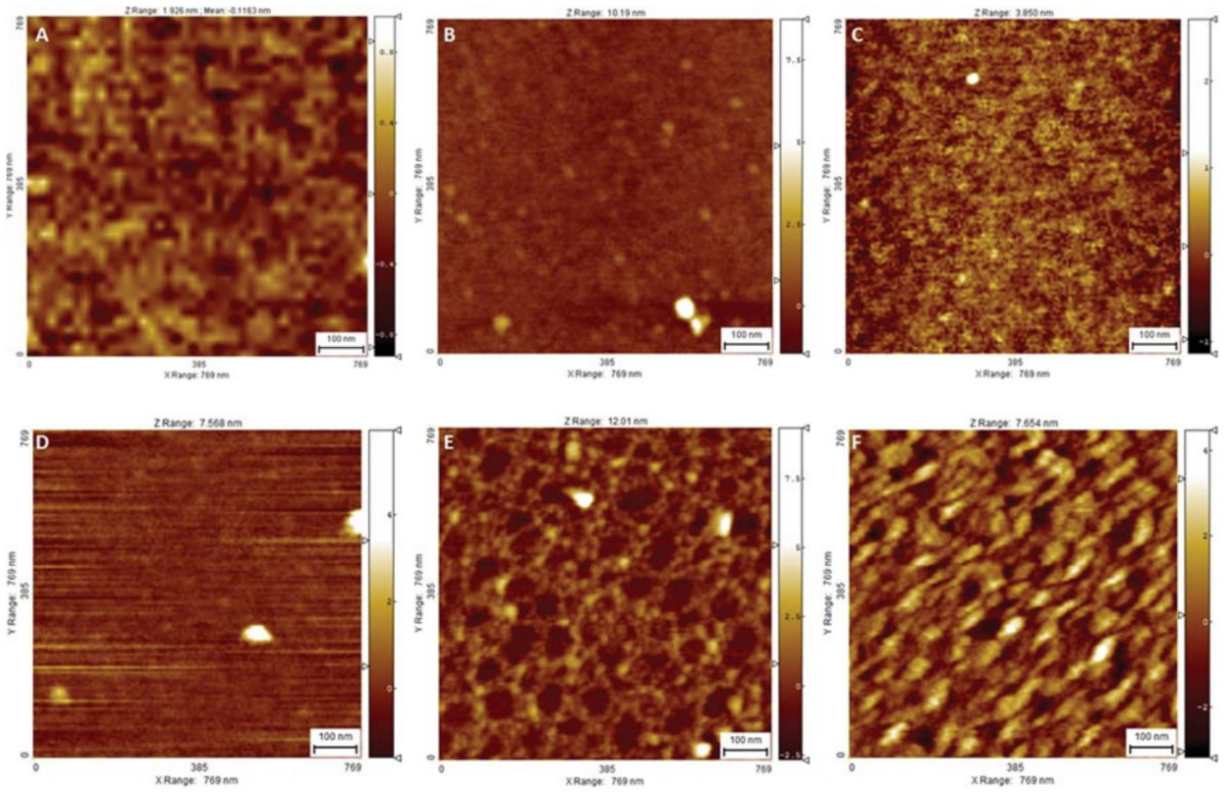

Fig. 6. Topographic AFM images of HA and its derivatives immobilized on modified silicon (image size: 0.7 × 0.7 μm²), (A) amino-terminated silicon (NH_2–Si), (B) physically adsorbed HA (pHA) on NH_2–Si, (C) aldehyde-HA on NH_2–Si, (D) vinyl-terminated silicon, (E) pHA on vinyl-terminated silicon, and (F) thiol-HA on vinyl-terminated silicon.

Ellipsometry is a useful method to determine the thickness of bound material on reflective substrata such as silicon, which is measured by the induced change of the polarization state of light reflected on a surface. All measurements were executed under dry conditions. The oxide layer of silicon was measured and set as the basal layer. The thickness of the following layers, that is, the chemical modification with silanes and binding of HA, was then added to the value of the oxide layer to obtain the thicknesses depicted in Fig. 5. The thickness of APTES–silanized layer (NH_2–Si) was about 0.78 nm, which corresponds well to the results of other groups [36],[37]. When pHA or aHA was measured on NH_2–Si, the layer thickness increased approximately 1 nm again. Compared with the molecular dimensions of HA, assuming a random coil, one comes to the conclusion that HA is attached side-on in a single layer in these cases [38]. A different behavior was observed in the case of tHA. The thickness of the vinyl-terminated SAM of about 2.1 nm was predictably higher than that of NH_2–Si, also corresponding well to previous results of other groups [36]. The immobilization of tHA on vinyl-SAM resulted in a thickness increase of about 2 nm, which confirms the immobilization of tHA, but probably also resulted in a side-on configuration, which might be extended by the length of the cross-linker as shown previously in a similar study [39]. In contrast, the physical adsorption of HA on vinyl-terminated silicon did not result in an increase in layer thickness, which would lead to the conclusion that no binding of HA takes place under these conditions. The thickness of HA layers strongly depends on the surrounding medium and can increase up to 100 nm because HA is able to take up a huge amount of water [40]. The measurements were carried out in a dry state, so the observed layer thickness is generally lower because no swelling of the HA can be expected in such a case.

The AFM images depicted in Fig. 6 and the results of the surface roughness calculation reveal the successful immobilization of HA and its conjugated derivatives. The roughness of NH_2–Si with (Fig. 6B) and without (Fig. 6A) pHA were similar to each other, which might be explained by a similar surface density of the immobilized molecules. When aHA (Fig. 6C) was covalently attached to the amino-modified silicon, average roughness and root mean square increased (see Table 2).

The monolayer of the vinyl silane (Fig. 6D) appeared rather unstructured, which points to a nice packing of the molecules as self-assembled monolayer. The native pHA on vinyl-terminated silicon (Fig. 6E) is visible as a honeycomb-like texture, which indicates an incomplete surface coverage. The estimation of the width of these visual structures (15–30 nm) does not match with

Reprinted with permission from Journal of Bioactivity and Applied Biochemistry, Alexander Köwitsch, Yuan Yang, Ning Ma, Judith Kuntsche, Karsten Mäder, and Thomas Groth (2011), Bioactivity of immobilized hyaluronic acid derivatives regarding protein adsorption and cell adhesion, 58 (5), 376–389.
 DOI: 10.1002/bab.41

Table 2
Surface roughness of differently immobilized layers on silicon calculated from AFM data

	Surface parameters (nm)	
Sample	R_a[a]	R_q[a]
NH_2-Si	0.268	0.355
Vinyl-SAM	0.322	0.516
HA on NH_2	0.267	0.338
HA on vinyl-SAM	0.840	1.143
aHA on NH_2–Si	0.318	0.504
tHA on vinyl-SAM	0.845	1.060

[a]Surface roughness: R_a, average roughness; R_q, root mean square roughness.
NH_2–Si, amino-terminated silicon; vinyl-SAM, vinyl-terminated silicon; aHA, aldehyde-HA; tHA, thiol-HA.

simulated or experimental data (~1 nm) for HA helices [38],[41]. These findings indicate a rather aggregated structure of multiple HA chains or helices. Taking into account the film thickness measured by ellipsometry, which is not increased compared with the vinyl-SAM, we speculate that the nonhomogeneous coating may have an impact on the analyzing method itself. The characteristic structures observed might be attributed to the aggregation of the hydrophilic HA chains during the drying process. A similar phenomenon was recently observed with AFM after adsorption of fibronectin on different polymer films by Salmeron-Sanchez and coworkers [42].

In general, the AFM images indicate a dense surface coverage for aHA- (Fig. 6C) and tHA-modified (Fig. 6F) surfaces. In comparison with aHA, the rise in layer thickness as well as the higher surface roughness of tHA reveals the influence of the different attaching modes. Because tHA is attached via a short linker molecule, the thickness of the HA layer is expected to be larger than that of the more closely bound aHA, which is more flexible than native HA because some of the sugar rings were cleaved by the oxidation reaction. Also, the formation of aggregates by the creation of disulfides between remaining thiols of immobilized tHA and free thiols of the dissolved tHA could make a contribution to the increased layer thickness. The surface topography of the tHA-modified surface (R_a = 0.85 nm; R_q = 1.06 nm) is similar to previous results where a comparable linker was used to attach HA onto solid substrates [39].

3.2.1. SPR studies on HA binding and subsequent aggrecan adsorption

To evaluate the immobilization of the native and activated HAs, the adsorption process was monitored by SPR. aHA and native HA were applied to amino-terminated gold (Fig. 7a). After equilibration of the sensor with PBS, the respective solution (4 mg/mL) was allowed to immobilize for 1 H followed by rinsing with PBS to remove unbound molecules. After a steep increase of angle shift, the adsorption was nearly constant after a few minutes for native HA, whereas the adsorption of aHA was slightly increasing for an additional 30 Min. In both cases, rinsing with PBS led to a decrease of the adsorbed amount of about 50%. The results show that after rinsing there was 0.53 ng/mm² of aHA attached to the amino-terminated gold, whereas only 0.34 ng/mm² of native HA remained after washing. This indicates that a substantial portion of aHA is covalently bound. In addition, one must take into account that the molecular weight of aHA is about 10 times lower than that of HA. Hence, a higher molar quantity of aHA was bound.

The immobilization of tHA was performed directly on bare gold with a concentration of 2 mg/mL for 2 H. At first, a strong increase of the associated angle shift could be observed when

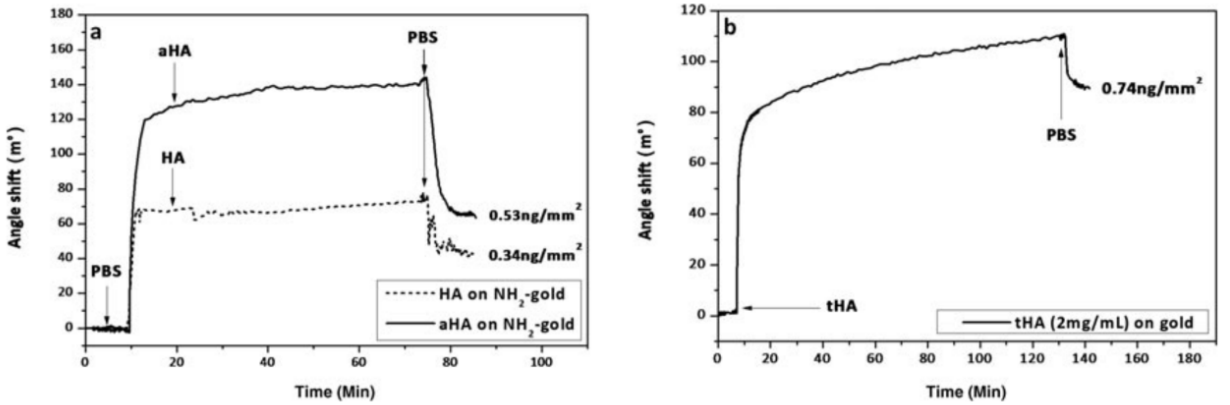

Fig. 7. The binding of aldehyde-HA (aHA, 4.0 mg/mL in PBS, straight line) and HA (4.0 mg/mL in PBS, dotted line) [graph (a)] on amino-modified gold (NH2-gold) for 1 H and of thiol-HA (tHA, 2.0 mg/mL in PBS) [graph (b)] on plain gold for 2 H was studied by surface plasmon resonance (SPR).

Reprinted with permission from Journal of Bioactivity and Applied Biochemistry, Alexander Köwitsch, Yuan Yang, Ning Ma, Judith Kuntsche, Karsten Mäder, and Thomas Groth (2011), Bioactivity of immobilized hyaluronic acid derivatives regarding protein adsorption and cell adhesion, 58 (5), 376–389.

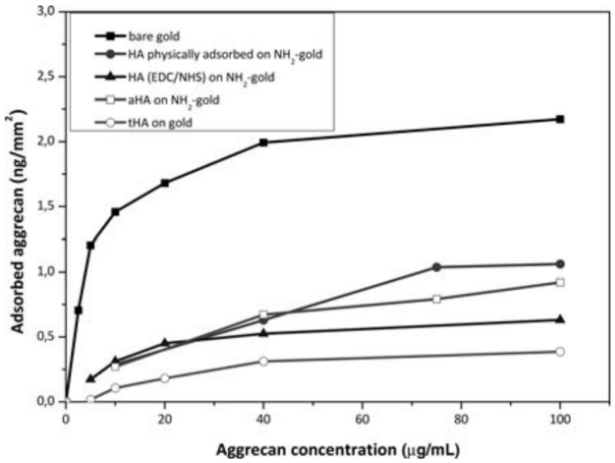

Fig. 8. Adsorbed amount of aggrecan per surface area on different modified gold surfaces; increasing protein concentrations were used and immobilized for 30 Min for each concentration with PBS (running buffer) rinsing steps in between. NH_2–gold, amino-terminated gold; aHA, aldehyde-HA; tHA, thiol-HA.

the solution of tHA reached the sensor surface (Fig. 7b) under flow conditions. After that, the slope of the adsorption curve decreased strongly but still remained weakly rising for the remaining incubation time. After rinsing with PBS only, a small quantity of tHA was lost, which indicates a strong binding of the hydrophilic HA to the hydrophobic gold via the thiol groups.

Aggrecan consists of a 250 kDa core protein that has three globular domains (G1, G2, and G3) and a GAG-attachment domain, to which approximately 100 chondroitin sulfate and approximately 60 keratan sulfate chains are bound [43]. In cartilage, aggrecan is anchored to high-molecular-weight HA and stabilized by small linker protein through the tandem repeats of G1, which forms the large aggregate that has the compressive properties of cartilage and can mediate the interactions between chondrocyte and the matrix network [43],[44].

Aggrecan adsorbed on bare gold, surface was set as a control for the HA-modified surfaces. Aggrecan binding to aHA and tHA was used to monitor the bioactivity of modified HA and compared with native HA that was physically adsorbed. Kinetic measurements with aggrecan of increasing concentrations between 5 and 100 μg/mL were then performed in PBS as running buffer. For all five surfaces, the adsorption of aggrecan increased with the rise of concentration. The amount of aggrecan adsorbed on HA-modified surfaces was much less than that on bare gold, where nonspecific adsorption occurred probably via hydrophobic interaction and chemisorption of sulfur species, which are able to bind to gold (e.g., cysteine residues or disulfides). The adsorbed amount on natural HA approached a constant value, when the protein concentration was higher than 75 μg/mL, indicating the saturation of aggrecan binding. It was reported that every aggrecan molecule can specifically bind to HA in an aggregate's initial formation if at least five disaccharide units are available [2],[44]. As shown in Fig. 8, the behavior of aggrecan adsorbed on aHA is slightly different from that on the natural HA. The curve of aHA continues to increase after the concentration of 75 μg/mL has been achieved. The behavior of aggrecan adsorption on HA (bound covalently via EDC/NHS) and tHA is quite similar to each other, approaching respective constant values after reaching the concentration of 40 μg/mL. However, one must note that the adsorbed quantity of bound aggrecan on native HA is about two times higher than that on tHA, indicating also a higher bioactivity.

We have applied the Langmuir equation [45] to fit our experimental data, which relates to the coverage or adsorption of molecules on a solid surface in comparison to the concentration in solution at a constant temperature.

$$\Gamma = \Gamma_{max}\frac{K c}{1 + K c} \quad (1)$$

where K is the Langmuir equilibrium constant, that is, affinity constant, a parameter that describes the strength of the interaction between molecules and solid surfaces; c is the protein concentration; Γ is the adsorbed quantity per unit area; and Γ_{max} is the maximal adsorbed quantity per unit area. The Langmuir equation can be fitted to data either by linear or nonlinear regression methods. Here also the coefficient of determination R^2, which is the square of correlation coefficient between the experimental data and their predicted values, was calculated. The result of the fitting is presented in Table 3.

With the values of R^2, it seems justifiable to use the Langmuir equation for description of experimental data. The affinity constant of plain gold is almost 10-fold higher than the value of the other HA-modified surfaces, suggesting the adsorptive forces become much weaker after the immobilization of HA. On the hydrophobic surfaces (bare gold), aggrecan has a compact conformation in which the hydrophobic ends serve as surface anchors, thus resulting in higher adsorption, which is in accordance with the study of lubricin on hydrophobic CH_3–terminated surfaces [46]. In contrast to that, on the modified-HA surfaces, aggrecan is fixed only by the linkage to disaccharide units of HA in a specific manner via side-on G1 domain [43], which means that the probability for adsorption must be consequently reduced. Affinity constants of physically adsorbed HA, aHA, and tHA are close to one other, falling in the range of 2.4 to 2.8 $\times$ 10^{-2} $mm^3/\mu g$, whereas those of the native HA (bound covalently via EDC/NHS linker chemistry) sample are approximately two times higher. This finding might indicate that the HA structure undergoes only a minor change when using EDC/NHS as an immobilized linker. HA samples of high-molecular weight (M_w of pHA = 1.3 MDa, M_w of aHA = 92k Da) might provide more binding sites for aggrecan, whose adsorption is therefore higher than that of low-molecular weight derivatives (M_w of LMWHA = 15 kDa, M_w of tHA = 70 kDa). Among all samples, tHA has the highest immobilization density of 0.74 ng/mm² but has the lowest capacity to bind aggrecan. This is in accordance with findings of Dhayal and Ratner [47] on the interaction between ConA and thiol–functionalized trimannoside. From our point of view, there are two possible interpretations for this phenomenon: (1) high density bound HA might increase steric hindrance at the

Reprinted with permission from Journal of Bioactivity and Applied Biochemistry, Alexander Köwitsch, Yuan Yang, Ning Ma, Judith Kuntsche, Karsten Mäder, and Thomas Groth (2011), Bioactivity of immobilized hyaluronic acid derivatives regarding protein adsorption and cell adhesion, 58 (5), 376–389.
 DOI: 10.1002/bab.41

Table 3
Parameters for the fit of experimental data from aggrecan adsorption on different modified surfaces with the Langmuir Eq. (1)

Parameter	Gold[a]	pHA on NH_2–gold[b]	aHA on NH_2–gold[b]	HA(EDC/NHS) on NH_2–gold[b]	tHA on gold[c]
K ($mm^3/\mu g$)	1.7×10^{-1}	2.5×10^{-2}	2.8×10^{-2}	5.6×10^{-2}	2.4×10^{-2}
Γ_{max} (ng/mm^2)	2.2899	1.4133	1.2234	0.8083	0.5660
R^2	0.999	0.982	0.998	0.986	0.973

[a]Using Langmuir linear regression.
[b]Using Lineweaver–Burk linear regression.
[c]Using vertical nonlinear least squares method (v–NLLS).

surface due to repulsive interaction between surface-bound HA and GAG-attached domain of aggrecan; (2) aggrecan's cystein residues of G3 domain might bind to tHA's free thiol groups and subsequently form a loop-like structure via disulfide bonds [48]. Their occupation over the binding sites at the surface might account for the reduction of adsorption. Therefore, tHA may also represent a promising candidate to bind to growth factors or proteins, which exhibit cysteine residues for the fabrication of a 3D hydrogel system.

3.3. Cell adhesion studies

Surfaces modified by oligosaccharides via reductive amination or various thiol compounds have been widely used as a well–defined model system to study protein–surface interactions [25],[46],[47] and cell adhesion [49]. In this study, we employed the reductive amination and thiolene chemistry to immobilize HA molecules covalently on model substrata surfaces. Prior to cell adhesion experiments, NH_2–GL and vinyl-SAM surfaces were functionalized with aHA and tHA, respectively, and then transferred to 12-well plates. Native HA and HA of low molecular weight were also physically adsorbed on NH_2–GL and vinyl-SAM and used as control groups. Fibroblasts plated on the different surfaces under protein-free conditions were stained with crystal violet and are shown in Fig. 9. After 4 H incubation, cells on NH_2–GL were most widely spread compared with all other surfaces including clean glass or vinyl-SAM. Considering the absence of proteins, the initial attachment of fibroblasts was only affected by the physicochemical features of the surfaces. The appearance of either rounded cells or cells elongated with pseudopodia, after immobilization of HA and its derivatives on the surfaces, indicates that the adhesion and spreading of cells is suppressed by HA. These findings correspond to observations of others that also found a decrease of cell adhesion and spreading on HA-modified surfaces [50]. The effect of HA immobilization on cell shape was also studied quantitatively with image analyzing software. The form factor of 1 represents here a perfectly round cell, whereas lower values indicate an increasing elongation (polarization) of cells. Results in Fig. 10B show that the form factor was 0.76 for cells plated on clean glass and

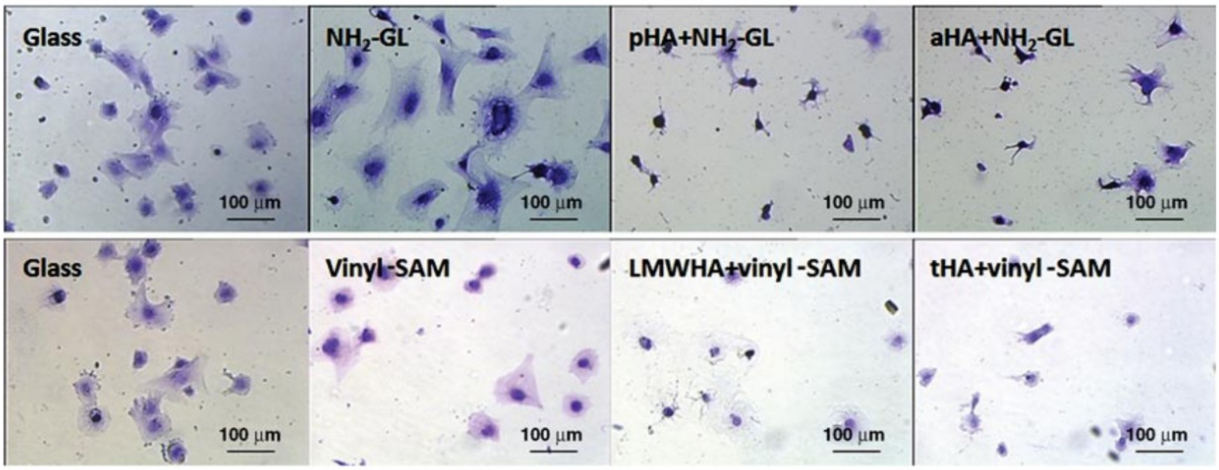

Fig. 9. Transmitted light microscopic images of HF adhesion on different modified surfaces stained by crystal violet (5%, v/v in methanol). NH2–GL, amino-terminated glass; pHA, physically adsorbed HA; aHA, aldehyde-HA; vinyl-SAM, vinyl-terminated glass; tHA, thiol-HA [scale bar: 100 m].

Reprinted with permission from Journal of Bioactivity and Applied Biochemistry, Alexander Köwitsch, Yuan Yang, Ning Ma, Judith Kuntsche, Karsten Mäder, and Thomas Groth (2011), Bioactivity of immobilized hyaluronic acid derivatives regarding protein adsorption and cell adhesion, 58 (5), 376–389.
 DOI: 10.1002/bab.41

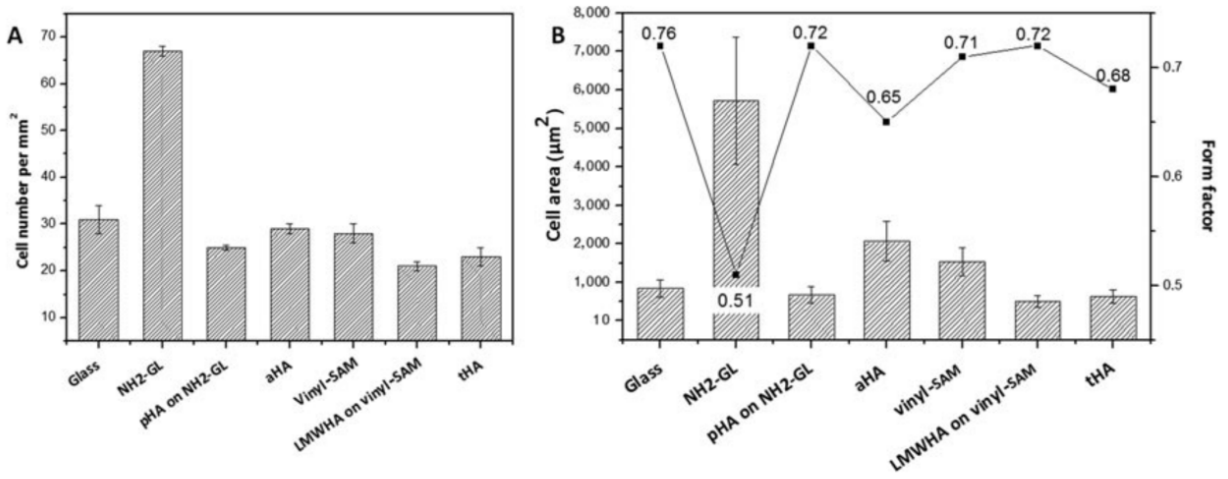

Fig. 10. Cell adhesion numbers (A), area (B), and form factor (B) of human fibroblasts after 4 H incubation on different immobilized surfaces. NH_2–GL, amino-terminated glass; aHA, aldehyde-HA; vinyl-SAM, vinyl-terminated glass; tHA, thiol-HA.

became 0.51 on NH_2–GL and 0.71 on vinyl-SAM. The form factor increased in relation to NH_2–GL, to 0.72 and 0.65 on physically adsorbed HA and covalently bound aHA, respectively. Cells on LMWHA and tHA surfaces had a form factor of 0.72 and 0.68 respectively, which was close to that on vinyl-SAM. Native HA had the strongest effect on cell shape with the smallest size of cells being most rounded. The slightly increased spreading and polarization of cells of aHA and tHA revealed that the chemical modification might have caused a certain loss of bioactivity.

Figures 10A and 10B demonstrate that the number and area of adhering human fibroblasts strongly depended on the type of modified surfaces. Analysis of initial cellular behavior showed that adhesion and spreading of human fibroblasts was highest on NH_2–GL compared with clean glass and vinyl-terminated glass, which is in accordance with previous studies using dermal fibroblasts as well [36]. After surface modification with HA and its derivatives, the number and area of adhered cells decreased significantly. Compared with NH_2–GL, the cell number on pHA and aHA was reduced by approximately 63% and 57%, respectively, and the mean cellular area by 76% and 71%, respectively. Compared with vinyl-SAM, the cell number on LMWHA and tHA decreased by approximately 25% and 18%, respectively, and the cellular area by 74% and 54%, respectively. The fact that the observed effects on cells were stronger when native HA (pHA and LMWHA) was used indicates a certain loss of functional activity of HA due to the chemical modification (aHA and tHA) of HA. In addition, the filopodia formation of cells seen in the corresponding images of "hyaluronized" surfaces (Fig. 9) might result from an incomplete surface coverage with HA or modified HA that enables cells to find some areas at which to attach.

Surface wettability also strongly influences the cell adhesion and spreading [3]. Cells prefer to adhere on a moderately hydrophilic surface (NH_2–GL, WCA $= 55^\circ$) compared to highly hydrophilic (clean glass, WCA $= 18^\circ$) or hydrophobic (vinyl-SAM, WCA $= 96^\circ$) surfaces. However, after the immobilization of HA and its derivatives, the factors that influence cell adhesion become more complicated; not only wettability but also biospecific interactions of cell-surface receptors with HA may become involved. In general, the observed spreading of cells is low due to the lack of integrin ligands on the surfaces. The increased spreading on NH_2–GL can be also explained by the electrostatic interactions between cells (with their negatively charged receptors) and the positively charged amino-terminated surface [51].

In addition, this study examined whether receptors recognizing HA such as CD44 are involved in the adhesion process. HFs were seeded on the different modified surfaces. Cell morphology was analyzed by immunofluorescence microscopy staining CD44, actin polymerization, and cell nuclei using anti–CD44–Cy2 (green), BODIPY–Ph (red), and To–Pro3 (blue) labeling. Figure 11 shows micrographs of HF cultured on the different surfaces. The upper images represent cells plated on NH_2–GL, pHA on NH_2–GL, and aHA on NH_2–GL (Figs. 11A–11C), whereas the lower panel illustrates cells on vinyl-SAM, pHA on vinyl-SAM, and tHA on vinyl-SAM (Fig. 11D–11F). Figure 11A shows that cells on NH_2–GL adhered strongly with full spreading after 4 H. The actin cytoskeleton was fully polymerized in a circumferential manner. CD44 staining was predominantly perinuclear as indicated by the green background around the blue stained nucleus of the cells. Cells plated on vinyl-SAM had a rather irregular shape with lower spreading and less actin polymerization, which goes along with the hydrophobic nature of this substratum. No peripheral staining of CD44 in the adhesion-related areas of spread cells was detected on both NH_2–GL and vinyl-SAM. In contrast to this, adhesion and spreading were significantly suppressed on HA-modified surfaces (Figs. 11B, 11C, 11E, and 11F). Cell shapes were largely irregular with the formation of pseudopodia. Actin polymerization was reduced or absent, indicated by the lack of stress fibers. However, it was found that CD44 was present in peripheral regions of cells. In

Reprinted with permission from Journal of Bioactivity and Applied Biochemistry, Alexander Köwitsch, Yuan Yang, Ning Ma, Judith Kuntsche, Karsten Mäder, and Thomas Groth (2011), Bioactivity of immobilized hyaluronic acid derivatives regarding protein adsorption and cell adhesion, 58 (5), 376–389.
 DOI: 10.1002/bab.41

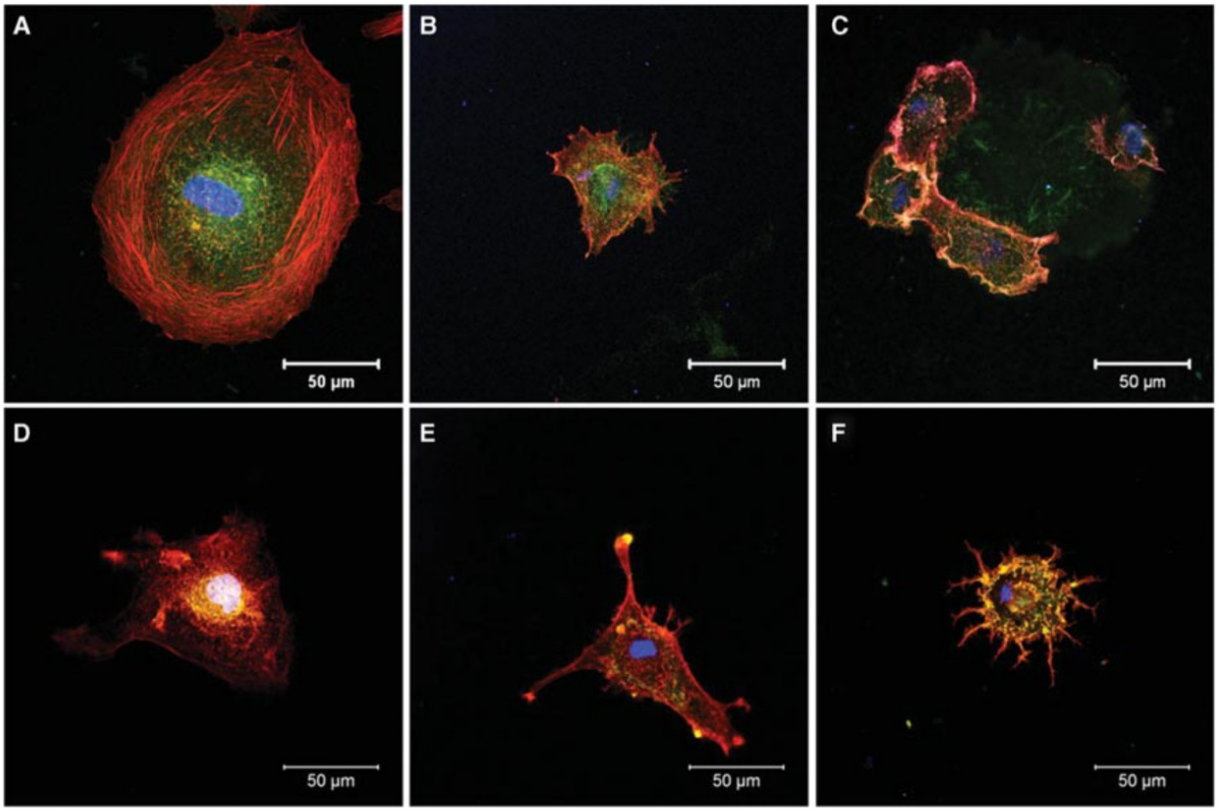

Fig. 11. Scanning confocal photomicrographs of human fibroblasts incubated under serum-free conditions on the different immobilized surfaces: (A) amino-terminated glass (NH_2–GL), (B) physically adsorbed HA (pHA) on NH_2–GL, (C) aldehyde-HA on NH_2–GL, (D) vinyl-terminated-glass (vinyl-SAM), (E) pHA on vinyl-SAM, (F) thiol-HA on vinyl-SAM. Staining of CD44 (green), filamentous actin (red), and To-Pro3 (blue) after 4 H incubation time [scale bar: 500 m].

particular, on LMWHA samples (Fig. 11E), there was a high assembly of CD44 in the pseudopodia, which indicates that the adhesion of cells might be mediated via CD44–HA interaction. CD44–HA complex formation was also visible on pHA (Fig. 11B) and aHA (Fig. 11C) surfaces, suggesting that HA–CD44 mediated adhesion may also prevail after chemical modification of HA [52].

Wettability of the immobilized HA surfaces was dependent on the properties of the substrata and the immobilized molecules. When pHA and aHA were adsorbed on NH_2–GL surfaces, relatively hydrophilic surfaces resulted (WCA of pHA = 31°, WCA of aHA = 35°), whereas LMWHA and tHA adsorbed on vinyl-SAM surfaces were still relatively hydrophobic surfaces (WCA of LMWHA = 85°, WCA of tHA = 67°). Nevertheless, these two types of surfaces differ significantly in surface wettability as shown in contact angle measurement; their biological effects on cellular adhesion and spreading were very similar. This indicates that the features of modified HA and not general wetting properties of substrata dominate the initial adhesion process, which points to the remaining biological activity of immobilized HA derivatives. The chemical modification of immobilized HA impacts adhesion and spreading of cells at the initial stage; this also affects cell growth and differentiation in the long term. This is supported by findings of Liu et al. [50] who showed that differentiation of mesenchymal stem cells was related to initial spreading of cells on polyelectrolyte multilayers made of HA and chitosan.

4. Conclusion

This work investigated the covalent immobilization of conjugated HAs, aHA, and tHA, as well as protein–HA and cell–HA interactions to clarify the biological function, of chemical modified HA and its potential application in tissue engineering. Conjugated HAs were successfully synthesized and immobilized onto different substrata. SPR analysis demonstrated that immobilized HA molecules still maintain bioactivity comparable to native HA in terms of aggrecan binding, their natural binding partner. Studies on adhesion of human fibroblast were conducted to learn about the bioactivity of modified HA toward cells. A significant decrease in cell number and spreading was observed on

Reprinted with permission from Journal of Bioactivity and Applied Biochemistry, Alexander Köwitsch, Yuan Yang, Ning Ma, Judith Kuntsche, Karsten Mäder, and Thomas Groth (2011), Bioactivity of immobilized hyaluronic acid derivatives regarding protein adsorption and cell adhesion, 58 (5), 376–389.
 DOI: 10.1002/bab.41

HA-modified glass, compared with amino- and vinyl-modified glass. Immunofluorescence microscopy also revealed that fibroblast adhesion plated on HA-modified surfaces was mediated by HA receptor CD44, which indicates that modified HA may still exert effects on cells and rules the adhesion process. Because HA has distinct effects on cell adhesion, motility and subsequent growth and differentiation, chemical modification of HA either with aldehydes or thiols may be useful for direct immobilization on biomaterial surfaces, which may be interesting for applications in tissue engineering of cartilage and other tissues [5], [53].

Acknowledgements

This work was supported by the European Union Seventh Framework Programme (FP7/2007–2013) under grant agreement no. NMP4–SL–2009–229292 ("Find & Bind").

References

[1] Toole, B. P. (2004) *Nat. Rev. Cancer* **4**, 528–539.
[2] Hardingham, T. E. and Fosang, A. J. (1992) *FASEB J.* **6**, 861–870.
[3] Morra, M. (2005) *Biomacromolecules* **6**, 1205–1223.
[4] Ji, Y., Ghosh, K., Shu, X. Z., Li, B. Q., Sokolov, J. C., Prestwich, G. D., Clark, R. A. F., and Rafailovich, M. H. (2006) *Biomaterials* **27**, 3782–3792.
[5] Raghunath, J., Rollo, J., Sales, K. M., Butler, P. E., and Seifalian, A. M. (2007) *Biotechnol. Appl. Biochem.* **46**, 73–84.
[6] Davidenko, N., Campbell, J. J., Thian, E. S., Watson, C. J., and Cameron, R. E. (2010) *Acta Biomater.* **6**, 3957–3968.
[7] Gerecht, S., Burdick, J. A., Ferreira, L. S., Townsend, S. A., Langer, R., and Vunjak-Novakovic, G. (2007) *Proc. Natl. Acad. Sci. U. S. A.* **104**, 11298–11303.
[8] David, L., Dulong, V., Le Cerf, D., Cazin, L., Lamacz, M., and Vannier, J. P. (2008) *Acta Biomater.* **4**, 256–263.
[9] Hynes, R. O. (2002) *Cell* **110**, 673–687.
[10] Culty, M., Nguyen, H. A., and Underhill, C. B. (1992) *J. Cell Biol.* **116**, 1055–1062.
[11] Banerji, S., Wright, A. J., Noble, M., Mahoney, D. J., Campbell, I. D., Day, A. J., and Jackson, D. G. (2007) *Nat. Struct. Mol. Biol.* **14**, 234–239.
[12] Turley, E. A., Noble, P. W., and Bourguignon, L. Y. W. (2002) *J. Biol. Chem.* **277**, 4589–4592.
[13] Hall, C. L., Wang, C., Lange, L. A., and Turley, E. A. (1994) *J. Cell Biol.* **126**, 575–588.
[14] Lutolf, M. P., Gilbert, P. M., and Blau, H. M. (2009) *Nature* **462**, 433–441.
[15] Vercruysse, K. P., Marecak, D. M., Marecek, J. F., and Prestwich, G. D. (1997) *Bioconjugate Chem.* **8**, 686–694.
[16] Segura, T., Anderson, B. C., Chung, P. H., Webber, R. E., Shull, K. R., and Shea, L. D. (2005) *Biomaterials.* **26**, 359–371.
[17] Park, Y. D., Tirelli, N., and Hubbell, J. A. (2003) *Biomaterials* **24**, 893–900.
[18] Barbucci, R., Magnani, A., Chiumiento, A., Pasqui, D., Cangioli, I., and Lamponi, S. (2005) *Biomacromolecules* **6**, 638–645.
[19] Tian, H., Lin, L., Chen, J., Chen, X., Park, T. G., and Maruyama, A. *J. Control Release* in press, doi:10.1016/j.jconrel.2011.01.025.
[20] Dhanasingh, A., Salber, J., Moeller, M., and Groll, J. (2010) *Soft Matter* **6**, 618.
[21] Jia, X. Q., Burdick, J. A., Kobler, J., Clifton, R. J., Rosowski, J. J., Zeitels, S. M., and Langer, R. (2004) *Macromolecules* **37**, 3239–3248.
[22] Riley, C. M., Fuegy, P. W., Firpo, M. A., Shu, X. Z., Prestwich, G. D., and Peattie, R. A. (2006) *Biomaterials* **27**, 5935–5943.
[23] Ossipov, D. A., Piskounova, S., Varghese, O. P., and Hilborn, J. (2010) *Biomacromolecules* **11**, 2247–2254.
[24] Jha, A. K., Xu, X. A., Duncan, R. L., and Jia, X. Q. (2011) *Biomaterials* **32**, 2466–2478.
[25] Song, X. Z., Xia, B. Y., Stowell, S. R., Lasanajak, Y., Smith, D. F., and Cummings, R. D. (2009) *Chemi. Biol.* **16**, 36–47.
[26] Seo, J. H., Adachi, K., Lee, B. K., Kang, D. G., Kim, Y. K., Kim, K. R., Lee, H. Y., Kawai, T., and Cha, H. J. (2007) *Bioconjugate Chem.* **18**, 2197–2201.
[27] Shu, X. Z., Liu, Y. C., Luo, Y., Roberts, M. C., and Prestwich, G. D. (2002) *Biomacromolecules* **3**, 1304–1311.
[28] Wang, D. A., Varghese, S., Sharma, B., Strehin, I., Fermanian, S., Gorham, J., Fairbrother, D. H., Cascio, B., and Elisseeff, J. H. (2007) *Nat. Mater.*, **6**, 385–392.
[29] Korzhikov, V., Rocker, S., Vlakh, E., Kasper, C., and Tennikova, T. (2008) *Bioconjugate Chem.* **19**, 617–625.
[30] Ellman, G. L. (1959) *Arch. Biochem. Biophys.* **82**, 70–77.
[31] Riddles, P. W., Blakeley, R. L., and Zerner, B. (1979) *Anal. Biochem.* **94**, 75–81.
[32] Booth, B. D., Vilt, S. G., McCabe, C., and Jennings, G. K. (2009) *Langmuir* **25**, 9995–10001.
[33] Schasfoort, R. B. M. and Tudos, A. J. (2008) Handbook of Surface Plasmon Resonance. 1st ed. RSC Publishing, Cambridge.
[34] Hesse, M., Meier, H., and Zeeh, B. (2005) Spektroskopische Methoden in der Organischen Chemie. 7th ed. Georg Thieme Verlag, Stuttgart.
[35] Lasky, L. A. (1995) *Annu. Rev. Biochem.* **64**, 113–139.
[36] Faucheux, N., Schweiss, R., Lutzow, K., Werner, C., and Groth, T. (2004) *Biomaterials* **25**, 2721–2730.
[37] Seitz, O., Fernandes, P. G., Tian, R., Karnik, N., Wen, H.-C., Stiegler, H., Chapman, R. A., Vogel, E. M., and Chabal, Y. J. (2011) *J. Mater. Chem.* **21**, 4384.
[38] Yeh, M. L. and Luo, Z. P. (2004) *Scanning* **26**, 273–276.
[39] Pasqui, D., Atrei, A., and Barbucci, R. (2007) *Biomacromolecules* **8**, 3531–3539.
[40] Albersdorfer, A. and Sackmann, E. (1999) *Eur. Phys. J. B* **10**, 663–672.
[41] Almond, A., Brass, A., and Sheehan, J. K. (2000) *J. Phys. Chem. B* **104**, 5634–5640.
[42] Guerra, N. B., Gonzalez-Garcia, C., Llopis, V., Rodriguez-Hernandez, J. C., Moratal, D., Rico, P., and Salmeron-Sanchez, M. (2010) *Soft Matter* **6**, 4748–4755.
[43] Kiani, C., Chen, L., Wu, Y. J., Yee, A. J., and Yang, B. B. (2002) *Cell Res.* **12**, 19–32.
[44] Bonnet, F., Dunham, D. G., and Hardingham, T. E. (1985) *Biochem. J.* **228**, 77–85.
[45] Tzoneva, R., Heuchel, M., Groth, T., Altankov, G., Albrecht, W., and Paul, D. (2002) *J. Biomat. Sci.-Polym. E*, **13**, 1033–1050.
[46] Chang, D. P., Abu-Lail, N. I., Guilak, F., Jay, G. D., and Zauscher, S. (2008) *Langmuir* **24**, 1183–1193.
[47] Dhayal, M. and Ratner, D. A. (2009) *Langmuir* **25**, 2181–2187.
[48] Chen, L. W., Yang, B. L., Wu, Y. J., Yee, A., and Yang, B. B. (2003) *Biochem.-Us* **42**, 8332–8341.
[49] Bengali, Z. and Shea, L. D. (2005) *Mrs. Bull* **30**, 659–662.
[50] Liu, Z. M., Gu, Q. Y., Xu, Z. K., and Groth, T. (2010) *Macromol. Biosci.* **10**, 1043–1054.
[51] Dubiel, E. A., Martin, Y., and Vermette, P. (2011) *Chem. Rev.* **111**, 2900–2936.
[52] Mori, H., Tomari, T., Koshikawa, N., Kajita, M., Itoh, Y., Sato, H., Tojo, H., Yana, I., and Seiki, M. (2002) *Mol. Biol. Cell* **13**, 208a–208a.
[53] Wegener, B., Schrimpf, F. M., Pietschmann, M. F., Milz, S., Berger-Lohr, M., Bergschmidt, P., Jansson, V., and Muller, P. E. (2009) *Biotechnol. Appl. Biochem.* **53**, 63–70.

Reprinted with permission from Journal of Bioactivity and Applied Biochemistry, Alexander Köwitsch, Yuan Yang, Ning Ma, Judith Kuntsche, Karsten Mäder, and Thomas Groth (2011), Bioactivity of immobilized hyaluronic acid derivatives regarding protein adsorption and cell adhesion, 58 (5), 376–389.
 DOI: 10.1002/bab.41

Chapter 3

Summary - Synthesis of thiolated glycosaminoglycans and grafting to solid surfaces:

In this publication the glycosaminoglycans (GAG) hyaluronic acid (HA), sulfated HA, chondroitin sulfate (CS) and heparin were chemically thiolated and subsequently immobilized to model substrata. The aim of this study was to investigate and characterize the capability of thiolated GAG (tGAG) modified by two different degree of thiolation to be covalently attached to vinyl-terminated self-assembled monolayers via thiol-ene reaction. For the thiolation, GAG were conjugated with different ratios of a disulfide containing cross-linker which was subsequently reduced by dithiothreitol (DTT) to generate free thiols. The tGAG were characterized in terms of chemical composition, chemical structure and molecular weight by ^{1}H-NMR, Raman spectroscopy and field-flow fractionation, respectively. The results of ^{1}H-NMR showed that the cross-linker was successfully introduced in two distinguishable extents to the GAG. The latter was also confirmed by Ellman`s assay which was used to quantify the thiol concentration of tGAG. Moreover, the thiolation led to an increase of the molecular weight of the tGAG as not all of the introduced disulfides were cleaved by the reducing agent DTT. The tGAG were immobilized onto vinyl-terminated substrata by homogeneous immobilization from solution as well as in a structured manner with microcontact printing. The tGAG-treated surfaces showed a significant decrease in wetting behavior assessed by water contact angle measurements. The wettability was always more increased with an increase in thiolation of the tGAG but also seemed to be dependent on the molecular weight and sulfation of the tGAG. Furthermore, ellipsometry showed an increase in layer thickness after immobilization of the tGAG. The results showed that the surface coverage was improved with a higher degree of thiolation and increasing molecular weight of the tGAG. Confocal laser scanning microscopy was used to demonstrate that the microcontact printing of fluorescein-labeled tCS to vinyl-terminated glass could be used to create microstructured surfaces for biosensor applications to detect specific binding partners or to monitor the mobility of cells.

Carbohydrate Polymers 114 (2014) 344–351

Contents lists available at ScienceDirect

Carbohydrate Polymers

journal homepage: www.elsevier.com/locate/carbpol

Synthesis of thiolated glycosaminoglycans and grafting to solid surfaces

Alexander Köwitsch[a], Mauricio Jurado Abreu[a], Ankur Chhalotre[a], Martin Hielscher[b], Steffen Fischer[b], Karsten Mäder[c], Thomas Groth[a,*]

[a] Biomedical Materials Group, Institute of Pharmacy, Martin Luther University Halle-Wittenberg, Heinrich-Damerow-Strasse 4, D-06099 Halle Saale, Germany
[b] Institute of Plant and Wood Chemistry, Dresden University of Technology, Pienner Strasse 19, D-01737 Tharandt, Germany
[c] Pharmaceutical Technology Group, Institute of Pharmacy, Martin Luther University Halle-Wittenberg, Wolfgang-Langenbeck-Strasse 4, D-06099 Halle Saale, Germany

ARTICLE INFO

Article history:
Received 11 March 2014
Received in revised form 4 August 2014
Accepted 5 August 2014
Available online 23 August 2014

Keywords:
Glycosaminoglycan
Thiol-ene chemistry
Surface grafting
Microcontact printing (μcp)
Ellipsometry
Water contact angle measurements (WCA)

ABSTRACT

Glycosaminoglycans (GAGs) with varying degree of sulfation were chemically modified to obtain thiolated analogues (tGAGs) for subsequent surface grafting on vinyl-terminated self-assembled monolayers. Thiolation was achieved by the use of the disulfide containing crosslinker 3,3'-dithiobis(propanoic hydrazide) and subsequent reduction of the disulfide with dithiothreitol. Two different molar ratios of the crosslinker were used for conjugation. The tGAGs were characterized by ^{1}H-NMR, Raman and flow-field-flow-fractionation (A4F) to determine the chemical composition, structure and molecular weight of the products. Ellman's reagent was used to quantify the thiol concentration of tGAGs. The tGAGs were immobilized onto vinyl-terminated glass and silicon via thiol-ene reaction. This was achieved by homogeneous immobilization from solution as well as with microcontact printing and exposure to UV light. The results of water contact angle measurement (WCA), ellipsometry and confocal laser scanning microscopy (CLSM) demonstrated that the resulting surface coverage was dependent on the degree of thiolation of GAGs.

1. Introduction

Glycosaminoglycans (GAGs) are charged polysaccharides that contribute to tissue structure and function in vertebrates by their partly large molecular weight and ability to bind huge quantities of water, but also because of their inherent bioactivity (Varki, 2009). Heparin, hyaluronic acid (HA) and chondroitin sulfate (CS) represent linear, unbranched GAGs that are widely used in different biomedical applications. Heparin is composed of different disaccharide units mainly of D–glucuronic acid or L–iduronic acid linked to a D–glucosamine by a α (1–4) bond. The hexuronic acid can be sulfated at 2–*O* position whereas the glucosamine unit primarily carries a *N*–sulfation and a sulfation at 6–*O* position (Murugesan, Xie, & Linhardt, 2008). Heparin is found in secretory granula of mast cells and released during tissue injury. Heparin is well–known for its anticoagulant properties due to amplification of activity of anti–thrombin III, which plays a major role in clinical use. On the other hand, heparin binds also to adhesive proteins, cytokines and growth factors, which may affect their activity (Capila & Linhardt, 2002). Chondroitin sulfate is composed of disaccharides consisting of β (1–4) D–glucuronic acid and β (1–3) *N*–acetyl–D–galactosamine with potential *O*–sulfation. CS is the most abundant GAG in human body as a component of many different proteoglycans like aggrecan, versican, etc. (Kjellen & Lindahl, 1991). Besides the important role of chondroitin sulfate for compressive resistance of cartilage and other tissues (Nishimura et al., 1998), it plays also a role during fibrilization of collagen (Kvist et al., 2006) and may also interact with regulatory proteins for development and homeostasis of the nerve system (Rogers et al., 2011). In addition, it was also found that CS is a negative regulator of apoptosis by binding of tumor necrosis factor TNF–α (Xu et al., 2008). Hyaluronic acid consists of two repeating saccharide units β (1–4) D–glucuronic acid and β (1–3) *N*–acetyl–D–glucosamine. HA represents the only non–sulfated glycosaminoglycan and is widely used in medical approaches and cosmetic applications (Beasley, Weiss, & Weiss, 2009; Falcone & Berg, 2008; Volpi, Schiller, Stern, & Soltes,

* Corresponding author. Tel.: +49 0345 55 28460; fax: +49 0345 55 27379.
E-mail addresses: Alexander.Koewitsch@pharmazie.uni-halle.de (A. Köwitsch), Jurado.Abreu@hotmail.com (M. Jurado Abreu), Ankurchhalotre@gmail.com (A. Chhalotre), Martin.hielscher@forst.tu-dresden.de (M. Hielscher), Sfischer@forst.tu-dresden.de (S. Fischer), Karsten.maeder@pharmazie.uni-halle.de (K. Mäder), Thomas.groth@pharmazie.uni-halle.de (T. Groth).

http://dx.doi.org/10.1016/j.carbpol.2014.08.027
0144-8617/

2009). While CS is always linked to a core protein, HA is synthesized as a polysaccharide chain, which can be composed by thousands of disaccharide units which are able to bind to multiple aggrecan units which can lead to the formation of huge proteoglycan aggregates (Fraser, Laurent, & Laurent, 1997; Prehm, 1983). Beside the mechanical function of high molecular HA, this GAG has also important regulatory functions during inflammation, tumor progression and metastasis (Toole, 2009). Recently, HA has been chemically sulfated to alter its biological functions because sulfation has shown to be an important precondition for the interaction with growth factors and proteins of the extracellular matrix (Cencetti, Bellini, Longinotti, Martinelli, & Matricardi, 2011; Hintze et al., 2009).

The bioactivity of GAGs is connected to the interaction with a plethora of proteins that possess specific binding regions to bind them (Kjellen & Lindahl, 1991). Particularly adhesion and growth of cells is also regulated by the presence of GAGs in the surrounding extracellular matrix, but also on the surface of cells (Guillame-Gentil et al., 2010; Kuschert et al., 1999). Hence, surface modification of biomaterials with GAGs can provide specific adhesive cues for cells, like HA or CS to cell surface receptors CD 44 (Knudson, Aguiar, Hua, & Knudson, 1996; Iida et al., 1998) or act indirectly by binding of adhesive proteins with heparin–binding domains and integrins (Haugen, Mccarthy, Roche, Furcht, & Letourneau, 1992). The alteration of surface composition is often applied to control interaction of biomaterials with proteins and to mediate adhesion, proliferation and differentiation (Guillame-Gentil et al., 2010; Lee et al., 2013; Murugesan et al., 2008).

Hence, immobilization of some GAGs has been introduced to control the bioactivity of surfaces to promote binding of growth factors, adhesive proteins and direct behaviour of cells in scaffolds (Baldwin & Kiick, 2010; Gribova, Auzely-Velty, & Picart, 2012). However, different methods have been applied for GAG immobilization. Some require rather harsh methods of surface modification and subsequent covalent grafting of GAGs to the surface (Huang, Guduru, Xu, Vienken, & Groth, 2010). Other approaches use physical forces to adsorb GAGs that may lead to more loosely or irreversible immobilization (Aggarwal et al., 2013). For most of the recent techniques for covalent immobilization of GAGs several steps for surface modification or GAG treatment are necessary (Edlund, Danmark, & Albertsson, 2008). Another disadvantage might be that some methods are limited to oligosaccharides of GAGs (Chuang & Masters, 2009; Seo et al., 2007). We have shown recently that covalent grafting of pre–activated hyaluronan leads to functional material surfaces that guide binding of protein ligands like aggrecan but also adhesion of cells (Köwitsch et al., 2011). Here we focus on the use of free thiols as active moieties that allow direct covalent linkage of GAGs via click chemistry to vinyl groups or gold and expand the range of GAGs from hyaluronan to chondroitin sulfate, heparin and one sulfated hyaluronan. For thiolation of GAGs a disulfide containing crosslinker which exposes reactive hydrazide groups is applied. The latter has the benefit that the thiol group can be released or reactivated with a thiol-reducing agent and also uses less material than direct application of unprotected thiolation agents, which have to be used in excess thus resulting in a less effective thiolation (Hermanson, 1996; Shu, Liu, Luo, Roberts, & Prestwich, 2002). Beside the details of synthesis and characterization of derivates that differ also in degree of thiolation, we show their grafting to self–assembled monolayers via thiol–ene reaction and the generation of 2–D–structured surfaces via microcontact printing (μCP).

2. Materials and methods

2.1. Materials

Heparin (Hep) from porcine intestinal mucosa was purchased from Serva Electrophoresis GmbH (Heidelberg, Germany). Hyaluronic acid (HA) sodium salt (Mw 1.3 MDa) was provided by Kraeber & Co GmbH (Ellerbek, Germany). Low molecular weight HA (Mw 15 kDa) was obtained by acidic hydrolysis as reported previously (Köwitsch et al., 2011). Sulfated HA with a sulfation degree (D_{Sulf}) of 1.3 was provided by Innovent e.V. (Jena, Germany) (Hintze et al., 2009). Chondroitin sulfate A (from bovine trachea), N–Hydroxysuccinimide (NHS) and 6–aminofluorescein were obtained from Sigma–Aldrich (Schnelldorf, Germany). The dialysis bag (Spectra/Por membrane, Mw cutoff = 3500), D_2O and organic solvents were provided by Carl Roth GmbH (Germany). 3,3‘–dithiobis(propanoic hydrazide) (DTPH) was synthesized and analyzed as described before (Vercruysse, Marecak, Marecek, & Prestwich, 1997). 7–octenyldimethychlorosilane was purchased from ABCR GmbH & Co. KG (Karlsruhe, Germany), dithiothreitol (DTT) and 2–(N–Morpholino)ethanesulfonic acid monohydrate (MES) from VWR International GmbH (Dresden, Germany), tris(hydroxymethyl)aminomethane (TRIS) from Merck KGaA (Karlsruhe, Germany), 5,5′–dithiobis–(2–nitrobenzoic acid) (DTNB, Ellman‘s reagent) and 1–ethyl–3–(3–dimethylaminopropyl) carbodiimide hydrochloride (EDC) from Alfa Aesar (Karlsruhe, Germany).

2.2. Synthesis of thiolated glycosaminoglycans (tGAGs)

The synthesis of thiolated GAGs was performed with some modification according to a recent paper (Shu et al., 2002). All reactions were conducted at room temperature (RT). Briefly, 0.8 mmol of GAG (Hep, CS, HA, sHA) was dissolved in micropure water (80 mL). Then, 3,3‘–dithiobis(propanoic hydrazide) (DTPH, 0.2 mmol (representing 0.25 equivalents of the available —COOH groups) or 0.04 mmol (0.05 eq.)) was added to the stirring solution and the pH was adjusted to 4.75. Thereafter, EDC (0.5 mmol (for 0.25 eq.)/0.1 mmol (for 0.05 eq.)) was added while the pH was maintained at 4.75. After additional 3 h incubation 1 M NaOH was used to increase the pH to 7.0. Then, DTT (2.0 mmol) was added and the pH was raised to 8.5. The solution was stirred over night. Then, the pH of the reaction mixture was lowered to 3.5 before the solution was dialyzed against diluted HCl (pH 3.5) containing 100 mM NaCl for 2 days and against diluted HCl (pH 3.5) for 2 days. Finally, the solution was freeze–dried and a white product was obtained.

For the visualization via fluorescence microscopy the thiolated CS (tCS1.16) was labelled with 6–aminofluorescein. Therefore, 0.35 mmol of tCS1.16 was dissolved in 50 mL MES buffer (50 mM, pH 4.7). Then EDC (0.7 mmol) and NHS (0.7 mmol) were added and the solution was stirred for 1 h. The pH was adjusted to 7.0 and 9 mg of 6–aminofluorescein in 4 mL of DMSO was added. The container was wrapped in aluminium foil and stirred over night. Afterwards, the solution was acidified and dialyzed against diluted HCl (pH 3.5) for 5 days. Finally, the solution was freeze–dried and a pale yellow product was obtained.

2.3. Characterization of thiolated glycosaminoglycans (tGAGs)

The chemical structure of the thiolated GAGs was analyzed by ^{1}H–NMR (Varian Gemini 2000, Palo Alto, CA, USA). ^{1}H–NMR samples were dissolved in D_2O and measured with 256 repetitive scans at a frequency of 400 MHz to obtain the corresponding spectra.

Raman spectroscopy was performed with a Bruker MultiRam spectrometer (Ettlingen, Germany) equipped with a germanium diode as detector that is cooled with liquid nitrogen. A cw–Nd:YAG–laser with an exciting line of 1024 nm was applied as light source for the excitation of Raman scattering. The spectra were recorded over a range of 3500–0 cm^{-1} using an operating spectral resolution of 3 cm^{-1} and a laser power output of 125 mW. The thiol content of tGAGs was determined according to the results of the

UV–VIS (Specord 200, Analytik Jena AG, Jena, Germany) measurement using Ellman's reagent (Ellman, 1959). The molar absorption coefficient of 14,150 $M^{-1}cm^{-1}$ at 412 nm was used for the calculation of the total thiol concentration of the thiolated GAGs (Riddles, Blakeley, & Zerner, 1979). The thiol content was calculated by dividing the resulting thiol concentration (c_{SH}) by the theoretical thiol concentration ($c_{SH}{}^{th}$). The latter can be derived from the concentration of the solution used for the Ellman's assay (2 mg/mL) and the expected molecular weight of the thiolated GAG per disaccharide unit (Mw^{th}) ($c_{SH}{}^{th}$ = 2 mg/(Mw^{th} × 1 mL). The molecular weight and polydispersity of native and thiolated GAGs were determined by asymmetrical flow field–flow–fractionation (A4F) equipped with a Dawn EOS detector (Wyatt Technology, Santa Barbara, CA, USA) and a RI–Detector (Shodex, RI–101 Showa Denko Europe GmbH, Munich, Germany). All samples were measured at a concentration of 1 mg/mL in 50 mM NaCl. Molecular weights were calculated using Astra software (Wyatt Tech., Santa Barbara, CA, USA).

2.4. Surface modification

Glass cover slips (Menzel GmbH + Co KG, Braunschweig, Germany) were cleaned with 0.5 M NaOH in 96% ethanol for 2 h followed by excessive washing with micropure water (7 × 5 min) and dried in a stream of nitrogen. Silicon wafers (Silicon Materials, Kaufering, Germany) were treated with a solution of NH_4OH (27%), H_2O_2 (30%) and micropure water (1:1:5, v/v/v) at 70 °C for 15 min and subsequently washed with micropure water (7 × 5 min). Afterwards, the silicon wafers were also dried with a stream of nitrogen.

The vinyl–terminated surfaces were prepared according to manufacturer's instructions by the immersion of cleaned glass or silicon in an ethanolic solution of 7–octenyldimethychlorosilane (3%, v/v) for 24 h at room temperature. Thereafter, the solution was warmed to 35 °C for 3 h. Then the surfaces were rinsed with ethanol and washed with micropure water.

The reaction of the tGAGs with the vinyl–terminated glass or silicon surfaces was carried out in a UV light chamber (Bio–Link BLX, LTF Labortechnik GmbH & Co. KG, Wasserburg, Germany) at 365 nm (50 J cm^{-2}) in TRIS–HCl (50 mM, pH 7.4) for 4 h with a tGAG concentration of 2 mg/mL. The modified surfaces were washed and dried as mentioned above. A comparable approach was already used to create protein patterns on thiol–functionalized supports (Weinrich et al., 2010).

After immobilization of tGAGs, modified glass substrata were used for water contact angle measurements while the silicon substrata were employed for ellipsometry measurements.

2.5. Physical characterization of modified substrata

Static WCA measurements were performed with OCA 15+ device (Dataphysics, Filderstadt, Germany) utilizing the sessile drop method to measure the changes in wettability after surface modification of substrata and immobilization of tGAGs. Five droplets of 3 μL micropure water were applied to each sample and the obtained values were used to calculate means and standard deviations. The values mentioned herein represent the mean of at least two independent measurements which are composed of a minimum of three different samples each.

The layer thickness of the surface coatings with silane and GAGs on silicon was determined by ellipsometry (M–2000 V, J.A. Woollam Co. Inc., Lincoln, NE, USA) at the range of angles from 65° to 85°. A refractive index of 1.45 was used for the vinylsilane monolayer, while 1.41 was used for the tGAG coated samples (Booth, Vilt, McCabe, & Jennings, 2009) (Boddohi, Killingsworth, & Kipper, 2008; Booth et al., 2009). Measurements were performed three times on different locations of each surface (of three replicates) and averaged. The experimental data were analyzed with the WVase32 software provided with the equipment.

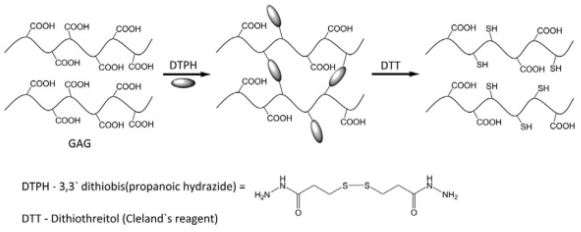

Fig. 1. Reaction scheme for the thiolation of glycosaminoglycans (GAGs).

2.6. Preparation and characterization of microcontact–printed surfaces

The polydimethylsiloxane (PDMS) stamps were made with Sylgard® 184 silicone elastomer kit (Dow Corning GmbH, Wiesbaden, Germany) according to the following conditions, which turned out to be most suitable for our experiments. The oven was preheated to 100 °C, whilst the curing agent and elastomer base were mixed for 5 min at a volume proportion of 1:10. The PDMS mixture was degassed in a vacuum chamber for 20 min to remove bubbles. The elastomer mix was injected into a mounted polycarbonate body, which was set on a casting station together with the silicon master (circular structures with ø = 80 μm, depth = 10 μm, elaborated by Tekniker, Eibar, Spain). The stamp was cured for 2 h at 100 °C. The cured stamp was cleaned with ethanol and micropure water. PDMS stamps were treated with oxygen plasma for 5 min (70 W/40 kHz, 0.08 mbar, 160 sccm/min O_2) (Walther et al., 2010). The plasma treated PDMS stamps were stored in micropure water to keep the wettability (Zhou, Ellis, & Voelcker, 2010).

For a reproducible microcontact printing a μcp–PVM–A printing module (GeSiM GmbH, Grosserkmannsdorf, Germany) was used, mounted on an inverted microscope (BIOLAB, Müller, Erfurt, Germany). The plasma treated stamp was inked by allowing 30 μL (5 mg/mL in 10 mM TRIS–HCl, pH 7.4) of fluorescein labelled tCS1.16 (FL–tCS1.16) to wet the stamp surface for 10 min in a closed humid chamber. Afterwards the stamp was blown dry with compressed air to remove excess of ink. Now the wetted stamp was mounted to the printing head of the PVM–A and the vinyl–terminated glass substrata was placed onto the printing stage. The printing time was set to 10 min according to previous findings in our lab. The former contact of the stamp and the glass substrate was assured by monitoring with an inverted microscope. After the stamp was removed from the surface, the printed substrate was irradiated at 365 nm for 10 min. Then the printed surface was washed with micropure water and TRIS–HCl. All microcontact printing steps were performed at room temperature.

3. Results and discussion

Here, a method that introduces thiol groups into the backbone of several glycosaminoglycans (GAGs) having different degree of sulfation was applied. To achieve thiolation of GAGs, the carboxylic acid groups of GAG were partly conjugated with DTPH, a disulfide containing crosslinker. Since the conjugation with DTPH results in a product that contains a disulfide bond and can lead also to crosslinking of GAGs, reduction with DTT is required to generate free thiol groups (Fig. 1). To explore the effect of the amount of applied crosslinker DTPH on thiolation degree and subsequent surface grafting, two different molar ratios of DTPH to GAG (1:4 and 1:20) were applied. Thiol–ene chemistry was used to generate

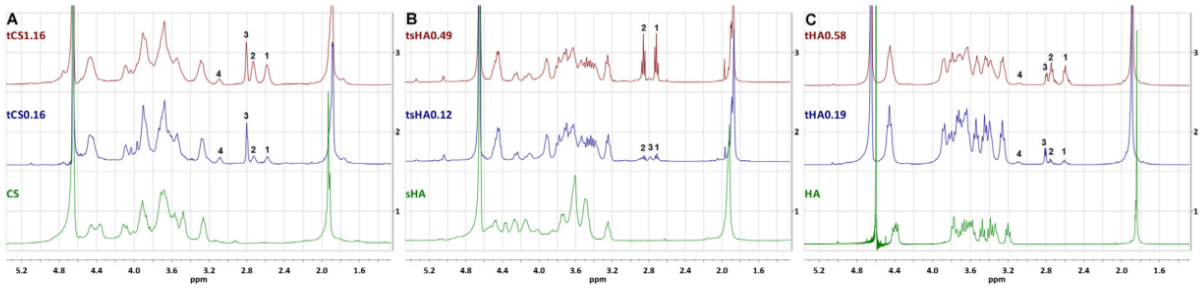

Fig. 2. ^{1}H–NMR spectra (400 MHz, D_2O) of derivatives of chondroitin sulfate (A), sulfated hyaluronic acid (B) and hyaluronic acid (C).

covalently immobilized GAG–substrata. Thus, we grafted the tGAGs to vinyl–terminated surfaces by means of homogeneous immobilization from solution or by microcontact printing (μcp) to generate microstructured substrata. The obtained surfaces were characterized by physical methods, such as wettability and coating thickness, to show the change of surface properties.

3.1. Synthesis and characterization of thiolated glycosaminoglycans

Nuclear magnetic resonance spectroscopy (NMR) was utilized to detect the molecular changes resulting from the grafting of DTPH to the GAGs. The exemplary spectra of the thiolated and native GAG derivatives are depicted in Fig. 2. ^{1}H–NMR spectra can be used to calculate the amount of crosslinker conjugated to the carboxylic acid groups of GAGs comparing the peak areas of the singlet of the methyl group of the acetamide (δ 1.9) with the new adsorptions of the four hydrogens belonging to the methylene groups (—CH_2CH_2S—) of the introduced crosslinker DTPH. When the disulfide was successfully cleaved by DTT, then the methylene groups have a chemical shift at δ 2.60 for HA (—CH_2CH_2SH, 1 in Fig. 2C) and δ 2.75 for HA (—CH_2CH_2SH, 2 in Fig. 2C), respectively. If the disulfide was not cleaved the methylene groups show peaks at δ 2.80 (–CH_2CH_2S–, 3 in Fig. 2C) and at δ 3.08 (—CH_2CH_2S—, 4 in Fig. 2C) in case of HA. Since the peak with a chemical shift around δ 3.08 is very broad and cannot be integrated with accuracy for the tGAGs, the resulting degree of substitution (DS) is probably slightly smaller for all tGAGs. Nevertheless, the DS was calculated from ^{1}H–NMR spectra for HA, sHA and CS, which have a constant repetition of the same disaccharide units in the carbohydrate chain. By contrast, heparin does not have exactly one acetyl group per disaccharide unit, which did not allow the calculation of DS. It has been shown previously that DS can be controlled by the variation of the molar ratios of GAG/DTPH/EDC and different reaction times. For example, 27–67% substitution of the carboxylic acid groups of a HA with a molecular weight of 250 kDa has been reported by Shu et al. (2002).

The results of ^{1}H—NMR spectroscopy of tHA0.58 indicate that a total amount of 31% of carboxyl groups reacted with DTPH of the sample with a ratio of 1:4 of DTPH/—COOH and 13% of the sample with ratio of 1:20 of DTPH/—COOH, respectively. The results of calculations of DS from ^{1}H—NMR spectra are shown in Table 1. It is clearly evident that all DTPH molecules seem to react with the corresponding GAG when a DTPH/—COOH ratio of 1:20 was used for the thiolation since the resulting DS was between 10–13%. By contrast, in case of a starting DTPH/—COOH ratio of 1:4, a lower than expected DS between 31–41% was obtained, without consideration of heparin. This implies that the access of the carboxylic acid groups is hindered when a higher DS shall be achieved. One reason for that could be the sterical hindrance because of aggregation of GAGs or the crosslinking with DTPH.

A common method for the analysis of free thiols is Raman spectroscopy. The S—H stretching vibration is located between 2600–2535 cm^{-1} and gives a strong signal in Raman spectra (Socrates, 2001). During investigations with Raman spectroscopy the specific adsorption band at 2585–2560 cm^{-1} (* in Fig. 3) in the spectra of tCS1.16 and tHA0.58 were found, but not for the other tGAG. This might be explained by the lower sensitivity of Raman compared to the UV–VIS measurements with Ellman's reagent. Nevertheless, the introduction of the disubstituted hydrazide by the reaction with DTPH was detected by a specific adsorption of the carbonyl double bond (Amide I) in the region 1750–1700 cm^{-1} (+ in Fig. 3) whereas for the native GAGs the adsorption bands visible in the region 1680–1600 cm^{-1} (o in Fig. 3) are attributed to the carbonyl stretch of the free carboxylic acid (full spectra in supplementary data). This new band was also visible for tHep0.29, which confirmed the successful conjugation of DTPH to heparin.

Since the Raman spectroscopy was not sensitive enough to verify the presence of free thiols in all tGAGs, Ellman's Reagent (DTNB) was used to measure the exact thiol concentration of the products by UV–VIS spectrometry (Table 1). The thiol content was calculated as mentioned in the methods section. Thus, the thiol content directly displays how many free thiols exist per repeating disaccharide of the corresponding GAG. If the bifunctional crosslinker DTPH would react quantitatively and on both ends it would be expected to obtain tGAGs with a substitution of 50% (DTPH/—COOH ratio = 1:4) or 10% (DTPH/—COOH ratio = 1:20), respectively. The results in Table 1 show that with a rising amount of DTPH not only a higher DS but also an increase in free thiols was obtained. After conjugation with the two different DTPH ratios, most thiols were found for tCS in both cases. In case of lower starting amounts of DTPH all resulting tGAGs had similar thiol concentrations. This

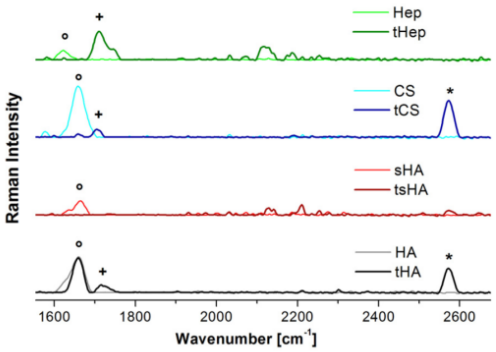

Fig. 3. FT Raman spectra (2600–1600 cm^{-1}) of thiolated GAGs showing the–SH stretch (*) and the C = O adsorption bands of the free carboxylic acid groups (°) and the disubstituted hydrazide (+).

Table 1
Degree of substitution (DS) and thiol concentration (c_{SH})of thiolated glycosaminoglycans calculated based on results of ^{1}H–NMR and Ellman's assay.

Sample	tHep0.11	tHep0.29	tCS0.16	tCS1.16	tsHA0.12	tsHA0.49	tHA0.19	tHA0.58
Degree of substitution (DS)	n.d.	n.d.	10%	41%	13%	40%	13%	31%
Thiol conc.	0.11/	0.29/	0.16/	1.16/	0.12/	0.49/	0.19/	0.58/
[x10^{-3}mol/L]/thiol content	3.7%	10.0%	4.4%	30.7%	3.2%	13.3%	3.9%	12.2%

was even more prominent when comparing the thiol content (3.2–4.4%), which also includes the different molecular weights of GAGs. For tGAGs with a higher DS significantly more free thiols were obtained in case of tCS1.16, while the other tGAGs gathered in a rather comparable range. Considering the DS that resulted from the ^{1}H–NMR the proportion of disulfides of DTPH can be estimated that was cleaved by DTT to generate free thiol groups. For tCS1.16 a thiol content of 30.7% and a DS of 41% was obtained, which means that around 75% of the introduced disulfides of DTPH were reduced to free thiols by DTT. Since the DS for tHep could not obtained by spectroscopy, this ratio is highest for the tCS samples (44%/75%) and lowest for the tsHA analogues (25%/33%). An important factor that controls DS could be the conformation of the GAG prior to reduction of the disulfide by DTT. The fact that not all of the disulfides could be cleaved to free thiols by reduction with DTT led obviously to an increase in molecular weight as a result of the intermolecular crosslinking of GAG chains (Table 2). It can be concluded that an increase of DS resulted in a product with a higher molecular weight (Mw). This trend is more pronounced when the above mentioned ratio of the thiol content and the DS is decreasing. The lowest increase in Mw and also polydispersity was shown for tCS1.16 which is comprehensible taking into account the fact that the ratio of the thiol content and the DS was highest (75%) in this sample. The less disulfides are cleaved, the higher the conjugation of tGAGs and the resulting Mw. In particular, tHA0.58 with a high degree of substitution (DS) showed a large increase in molecular weight even it had a comparable thiol content/DS ratio as tsHA0.49, which indicates that the sulfation influences the final Mw of the product. The presence of equally charged groups leads to more intra– and intermolecular repulsion. The non–sulfated HA is the least charged GAG and thus not repelling the hydrophobic part of DTPH as much as the more negatively charged sulfated GAGs. As a consequence the conformation of the crosslinked HA is more closed and inaccessible for the reduction of the disulfide by DTT.

3.2. Characterization of glycan-modified substrata

The immobilization of tGAGs was carried out on vinyl–terminated self–assembled monolayer (SAM) via the thiol–ene reaction that was initiated by UV–treatment. The covalent S—C—bond formation between the alkene and the thiol group is difficult to detect with spectroscopy due to their low concentration on the substrate and the high sulfur content of GAGs (except HA). Therefore, indirect measurement verifying the success of immobilization was performed with surface sensitive methods that measure wetting properties (water contact angle, WCA) and layer thickness (ellipsometry).

Table 2
Molecular weight and Polydispersity index (PDI) of glycosaminoglycans.

Sample	Mw (kDa)	PDI (Mw/Mn)
Heparin	15	1.1
tHep0.11	17	1.5
tHep0.29	28	1.5
CS	25	1.4
tCS0.16	27	1.4
tCS1.16	30	1.5
sHA (D_{Sulf} = 1.3)	12–17[a]	2.0[a]
tsHA0.12	24	1.9
tsHA0.49	38	1.9
LMWHA	12	1.2
tHA0.19	14	1.4
tHA0.58	64	2.7

[a] Determined by gel permeation chromatography (GPC)

The results of water contact angle (WCA) measurements depicted in Fig. 4 show a considerable increase of WCA, when the hydrophilic cleaned glass cover slips were modified with a vinyl–terminated SAM resulting in a WCA of about 95°. This result is in good accordance to a previous study on surface modification with silanes having the same functional group (Faucheux, Schweiss, Lutzow, Werner, & Groth, 2004). The subsequent immobilization of tGAGs decreased the WCA because of the hydrophilic nature of GAGs, but to a different extent. First of all, only a moderate decrease of WCA was observed. This was rather unexpected due to the presence of polar hydroxyl and charged carboxylic and sulfate groups in the GAGs. However, a part of the carboxylic groups was converted and the introduction of DTPH will also decrease the hydrophilicity of GAGs to some extent. In addition steric hindrance during grafting–to may also limit surface density of GAG to some extent as it has been described previously for other molecules (Zajac & Chakrabarti, 1995). A strong evidence for thiol–ene reaction during the immobilisation of tGAG was that the observed decrease of WCA was always more pronounced in case of the higher thiolated GAGs. This indicates that a higher concentration of reactive thiols leads to more surface coverage due to the increased covalent binding of GAGs. When the degree of sulfation of tGAGs was compared it was also evident that heparin (D_{Sulf} = 1.6), which is the most sulfated GAG, yielded the lowest WCA were measured. Nevertheless, the tCS immobilization produced more wettable substrata than tsHA even the sulfation degree of sHA (D_{Sulf} = 1.3) was higher than that of CS (D_{Sulf} = 0.8). It was assumed that the higher concentration of free thiols in tCS samples compared to tsHA samples might lead to an enhanced surface coverage. Despite the conjugation of DTPH to the carboxylic groups of all GAGs also non–sulfated HA led to more hydrophilic surfaces indicating that tHA0.58 was able to cover the surface to a higher extent than sHA0.49, which

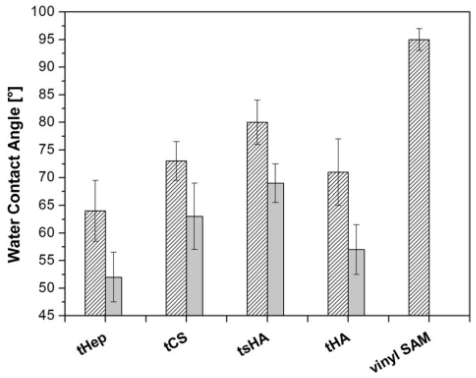

Fig. 4. Change of wettability for thiolated GAGs with different degree of substitution compared to vinyl–terminated glass (thiol concentration of tGAGs: hatched–tHep0.11, tCS0.16, tsHA0.12, tHA0.19; grey–tHep0.29, tCS1.16, tsHA0.49, tHA0.58).

Reprinted from Carbohydrate Polymers, 114, Alexander Köwitsch, Mauricio Jurado Abreu, Ankur Chhalotre, Martin Hielscher, Steffen Fischer, Karsten Mäder, Thomas Groth, Synthesis of thiolated glycosaminoglycans and grafting to solid surfaces (2014), 344-351.
 http://dx.doi.org/10.1016/j.carbpol.2014.08.027

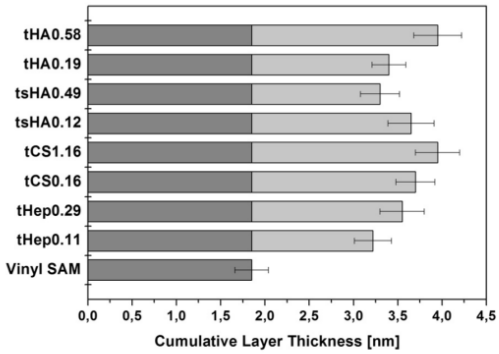

Fig. 5. Cumulative layer thickness of thiolated GAGs compared to vinyl–terminated silicon measured by ellipsometry.

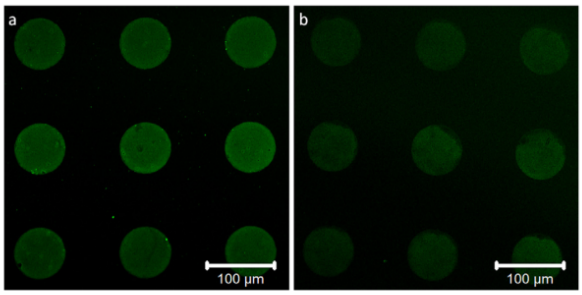

Fig. 6. Confocal laser scanning microscopy micrographs of FL–tCS1.16 printed onto vinyl–terminated glass before (a) and after (b) additional washing with TRIS–HCl (pH 7.4).

should be more hydrophilic because of sulfate groups. The molecular weight of tGAGs directly influences the wettability too, because a larger molecule can cover a larger surface area than a smaller one. Here, tHA0.58 possessed the highest Mw which may explain the lower WCA compared to the sulfated GAGs. Overall, it seems that the immobilization of tGAGs on vinyl–terminated SAM did not lead to complete surface coverage. This may be due to steric hindrance of adjacent GAG molecules during the grafting to the vinyl SAM, which could prevent the attachment of additional molecules. Another obstacle may also be the more hydrophobic nature of the surface that may also reduce the interaction with hydrophilic GAGs and last but not least a lower efficiency of the UV–initiated thiol–ene reaction (Jeyachandran, Mielezarski, Rai, & Mielczarski, 2009; Karlsson, Edfors-Lilja, & Bjornsson, 2000; Rouse, Whateley, Thomas, & Eccleston, 2007).

Ellipsometry is a useful tool to determine the thickness of coatings on reflective substrata like silicon, which is measured by the induced change of the polarization state of light reflected on the surface (Tompkins & Irene, 2005). All measurements were conducted under dry laboratory conditions at room temperature. Therefore, no swelling of the coating material can be expected. The oxide layer of silicon was measured and set as the basal layer. The thickness of the following layers includes the vinyl–terminated SAM plus tGAG layer and is shown in Fig. 5. The thickness of the vinyl–terminated SAM of 1.85 nm is in correspondence with results of silanes with similar length (Wasserman, Tao, & Whitesides, 1989). In general, the immobilization of the tGAGs resulted in surface coatings with a thickness between 1.37 nm (tHep0.11) and 2.1 nm (tCS1.16). There were no major differences in layer thickness between the different GAGs, which might be due to the fact that the experiments were performed in a dry state. Nevertheless, a higher thiol content of the tGAGs led also to higher layer thickness except for the tsHA substrata. Ellipsometry is based on an integral measurement of a comparatively large surface area. Hence, the resulting layer thickness always incorporates also vacant areas due to the incomplete surface coverage that has been also deduced from WCA measurements. The immobilization of tCS1.16 and tHA0.58 on vinyl–terminated silicon resulted in the most pronounced thickness increase of about 2.1 nm. This could be correlated to the concentration of free thiols, which are highest for these tGAGs. The lowest thickness was measured for substrata coated with the tHep0.11 (1.37 nm) surfaces. To get an idea of the dimensions of thickness measured with ellipsometry one has to consider that a single saccharide ring has a diameter of around 1 nm. Yeh et al. determined the height of HA in dry state with AFM measurements to 0.54 nm (Yeh & Luo, 2004). Layer by layer studies of heparin and chitosan also showed that single heparin layers had a concentration dependent thickness between 0.5 nm and 2 nm when measured by ellipsometry (Boddohi et al., 2008). In the present study one has to consider also the size of the crosslinker (DTPH) that was introduced to the GAGs. From these considerations one can assume that the surface grafting of tGAGs resulted in a side–on configuration perhaps including some loopy conformation of GAGs. This is also more probable for tGAGs with lower thiol content, because they have less covalent links to the substratum. On the other hand, it is conceivable that tGAGs might not be strictly immobilized in monolayers because they can still present free thiol groups after immobilization enabling them to bind to other tGAGs chains in solution via disulfide formation.

In addition to the characterization of surface properties also bioactivity of the surface-immobilized tGAGs was characterized by studying adhesion and metabolic activity of fibroblasts seeded in serum containing medium. Here the idea was that sulfated GAGs like heparin can bind adhesive proteins like fibronectin and vitronectin present in plasma that possess heparin-binding domains and thus support cell adhesion (Steele, Johnson, & Underwood, 1992). On the other hand, cells possess also adhesion receptors like CD 44 that can recognize certain GAGs like HA directly (Dickinson, Ho, Wang, Stebe, & Gerecht, 2010). Since thiolation changes the chemical structure and also accessibility of GAG chains, it was assumed that reduced adhesion and spreading of cells indicates a lower bioactivity of thiolated GAGs. Accordingly, the adhesion of cells was studied with phase contrast microscopy while metabolic activity of cells was measured with Qblue® assay after 24 h and 48 h. Results of this study are shown in supplementary data with Figs. S1, S2 and S3. Fig. S1 shows that for most of tGAG-coated surfaces a significant increase in metabolic activity of fibroblasts was observed within this time period. However, it was found that substrata coated with highly thiolated tCS1.16 and tHA0.58 showed a noticeable lower metabolic activity than the other tGAGs. These findings were also confirmed by cell adhesion studies after 24 h (Fig. S2) and 48 h (Fig. S3). Here it was also evident that the number of adhering cells on highly thiolated tCS1.16 and tHA0.58 were lower at both time points. This indicates a potential lower bioactivity in case of too high thiolation of GAGs.

3.3. *Making of microcontact–printed surfaces with thiolated GAGs*

As an additional method we applied microcontact printing (μcp) to create GAG-textured substrata. In an exemplary approach we used fluorescein-labelled tCS (FL–tCS1.16) as ink for soft lithography and visualized the resulting prints by confocal laser scanning microscopy. In Fig. 6 the result of the print is depicted prior and after washing with TRIS–HCl (pH 7.4). It can be seen that also after the additional washing step with buffered solution the printed

Reprinted from Carbohydrate Polymers, 114, Alexander Köwitsch, Mauricio Jurado Abreu, Ankur Chhalotre, Martin Hielscher, Steffen Fischer, Karsten Mäder, Thomas Groth, Synthesis of thiolated glycosaminoglycans and grafting to solid surfaces (2014), 344-351.
 http://dx.doi.org/10.1016/j.carbpol.2014.08.027

structures remain on the glass surface, even some unbound FL–tCS1.16 from the periphery of the prints was removed. That makes them good candidates for subsequent cell migration or co–culture studies to explore the specific effect of the different printed tGAGs.

It was found that not only the FL–tCS1.16 could be easily transferred to the vinyl–terminated glass surfaces by μcp but also fluorescein labelled analogues of tHA and tHep. In addition to the result for a PDMS stamp with 80 μm circular structures which is depicted in Fig. 6 the labelled tGAGs can be also applied to stamps with smaller sized structures to generate other surface structures.

4. Conclusion

In this work four GAGs were thiolated with two different degrees of substitution. The accessibility of the carboxylic acid groups decreased when an increased amount of DTPH was used. The surface grafting of tGAGs could be achieved in a homogeneous manner as well as in a microstructured way by microcontact printing. It was found that the surface coverage was improved with a higher degree of thiolation and an increased molecular weight of the tGAGs. The resulting glycanized surfaces presented an increase in wettability and layer thickness. The wettability of the homogeneous coated substrata seemed to be dependent on the sulfation degree and molecular weight of the immobilized tGAGs. Studies with human fibroblasts showed also that surface coatings with tGAGs were bioactive although a higher thiolation degree of tCS and tHA reduced cell activity to some extent. In conclusion, the thiol–ene reaction seems to be a facile method to graft thiolated GAGs to vinyl–terminated or gold substrata. Such surface modified with different GAGs may be useful for quantitative studies of protein-GAG interaction with surface plasmon resonance or quartz microbalance (Altgarde et al., 2013; Yagi et al., 2012). On the other hand, the important role of GAGs during inflammation and tumor development may also open applications of GAG modified surfaces for studies on cell adhesion and migration (Dickinson et al., 2010). Furthermore, the detection of specific interaction partners or cell mobility is an interesting task that could be addressed with biosensing devices coated or structured with GAGs. HA, for instance, has shown to have a promoting effect on metastatic cancer cells that could be studied with such biosensors (Afify, Purnell, & Nguyen, 2009).

Acknowledgements

This work was supported by the European Union Seventh Framework Programme (FP7/2007–2013) under grant agreement no. NMP4–SL–2009–229292 ("Find & Bind"). The authors also want to thank the Interdisciplinary Center for Material Sciences in Halle (Germany) for the opportunity to use the ellipsometer and the plasma cleaner. We are grateful for support of this work by the micro and nano manufacture unit at IK4–Tekniker (Spain) for the silicon master preparation and Innovent e.V. (Germany) for providing the sulfated hyaluronic acid. The authors thank Ute Mentzel for her support of the A4F experiments.

Appendix A. Supplementary data

Supplementary data associated with this article can be found, in the online version, at http://dx.doi.org/10.1016/j.carbpol.2014.08.027.

References

Afify, A., Purnell, P., & Nguyen, L. (2009). Role of CD44s and CD44v6 on human breast cancer cell adhesion, migration, and invasion. *Experimental and Molecular Pathology*, *86*(2), 95–100.

Aggarwal, N., Altgarde, N., Svedhem, S., Zhang, K., Fischer, S., & Groth, T. (2013). Effect of molecular composition of heparin and cellulose sulfate on multilayer formation and cell response. *Langmuir*, *29*(45), 13853–13864.

Altgarde, N., Nileback, E., de Battice, L., Pashkuleva, I., Reis, R. L., Becher, J., et al. (2013). Probing the biofunctionality of biotinylated hyaluronan and chondroitin sulfate by hyaluronidase degradation and aggrecan interaction. *Acta Biomaterialia*, *9*(9), 8158–8166.

Baldwin, A. D., & Kiick, K. L. (2010). Polysaccharide-modified synthetic polymeric biomaterials. *Biopolymers*, *94*(1), 128–140.

Beasley, K. L., Weiss, M. A., & Weiss, R. A. (2009). Hyaluronic acid fillers: A comprehensive review. *Facial Plastic Surgery*, *25*(2), 86–94.

Boddohi, S., Killingsworth, C. E., & Kipper, M. J. (2008). Polyelectrolyte multilayer assembly as a function of pH and ionic strength using the polysaccharides chitosan and heparin. *Biomacromolecules*, *9*(7), 2021–2028.

Booth, B. D., Vilt, S. G., McCabe, C., & Jennings, G. K. (2009). Tribology of monolayer films: Comparison between n-alkanethiols on gold and n-alkyl trichlorosilanes on silicon. *Langmuir*, *25*(17), 9995–10001.

Capila, I., & Linhardt, R. J. (2002). Heparin—protein interactions. *Angewandte Chemie-International Edition*, *41*(3), 391–412.

Cencetti, C., Bellini, D., Longinotti, C., Martinelli, A., & Matricardi, P. (2011). Preparation and characterization of a new gellan gum and sulphated hyaluronic acid hydrogel designed for epidural scar prevention. *Journal of Materials Science-Materials in Medicine*, *22*(2), 263–271.

Chuang, T. W., & Masters, K. S. (2009). Regulation of polyurethane hemocompatibility and endothelialization by tethered hyaluronic acid oligosaccharides. *Biomaterials*, *30*(29), 5341–5351.

Dickinson, L. E., Ho, C. C., Wang, G. M., Stebe, K. J., & Gerecht, S. (2010). Functional surfaces for high-resolution analysis of cancer cell interactions on exogenous hyaluronic acid. *Biomaterials*, *31*(20), 5472–5478.

Edlund, U., Danmark, S., & Albertsson, A. C. (2008). A strategy for the covalent functionalization of resorbable polymers with heparin and osteoinductive growth factor. *Biomacromolecules*, *9*(3), 901–905.

Ellman, G. L. (1959). Tissue sulfhydryl groups. *Archives of Biochemistry and Biophysics*, *82*(1), 70–77.

Falcone, S. J., & Berg, R. A. (2008). Crosslinked hyaluronic acid dermal fillers: a comparison of rheological properties. *Journal of Biomedical Materials Research Part A*, *87A*(1), 264–271.

Faucheux, N., Schweiss, R., Lutzow, K., Werner, C., & Groth, T. (2004). Self-assembled monolayers with different terminating groups as model substrates for cell adhesion studies. *Biomaterials*, *25*(14), 2721–2730.

Fraser, J. R. E., Laurent, T. C., & Laurent, U. B. G. (1997). Hyaluronan: Its nature, distribution, functions and turnover. *Journal of Internal Medicine*, *242*(1), 27–33.

Gribova, V., Auzely-Velty, R., & Picart, C. (2012). Polyelectrolyte multilayer assemblies on materials surfaces: From cell adhesion to tissue engineering. *Chemistry of Materials*, *24*(5), 854–869.

Guillame-Gentil, O., Semenov, O., Roca, A. S., Groth, T., Zahn, R., Vörös, J., et al. (2010). Engineering the extracellular environment: Strategies for building 2D and 3D cellular structures. *Advanced Materials*, *22*(48), 5443–5462.

Haugen, P. K., Mccarthy, J. B., Roche, K. F., Furcht, L. T., & Letourneau, P. C. (1992). Central and peripheral neurite outgrowth differs in preference for heparin-binding versus integrin-binding sequences. *Journal of Neuroscience*, *12*(6), 2034–2042.

Hermanson, G. T. (1996). *Bioconjugate Techniques*. San Diego: Elsevier Science.

Hintze, V., Moeller, S., Schnabelrauch, M., Bierbaum, S., Viola, M., Worch, H., et al. (2009). Modifications of hyaluronan influence the interaction with human bone morphogenetic protein-4 (hBMP-4). *Biomacromolecules*, *10*(12), 3290–3297.

Huang, X. J., Guduru, D., Xu, Z. K., Vienken, J., & Groth, T. (2010). Immobilization of heparin on polysulfone surface for selective adsorption of low-density lipoprotein (LDL). *Acta Biomaterialia*, *6*(3), 1099–1106.

Iida, J., Meijne, A. M. L., Oegema, T. R., Yednock, T. A., Kovach, N. L., Furcht, L. T., et al. (1998). A role of chondroitin sulfate glycosaminoglycan binding site in alpha(4)beta(1) integrin-mediated melanoma cell adhesion. *Journal of Biological Chemistry*, *273*(10), 5955–5962.

Jeyachandran, Y. L., Mielezarski, E., Rai, B., & Mielczarski, J. A. (2009). Quantitative and qualitative evaluation of adsorption/desorption of bovine serum albumin on hydrophilic and hydrophobic surfaces. *Langmuir*, *25*(19), 11614–11620.

Karlsson, M., Edfors-Lilja, I., & Bjornsson, S. (2000). Binding and detection of glycosaminoglycans immobilized on membranes treated with cationic detergents. *Analytical Biochemistry*, *286*(1), 51–58.

Kjellen, L., & Lindahl, U. (1991). Proteoglycans—structures and interactions. *Annual Review of Biochemistry*, *60*, 443–475.

Knudson, W., Aguiar, D. J., Hua, Q., & Knudson, C. B. (1996). CD44-anchored hyaluronan-rich pericellular matrices: An ultrastructural and biochemical analysis. *Experimental Cell Research*, *228*(2), 216–228.

Köwitsch, A., Yang, Y., Ma, N., Kuntsche, J., Mäder, K., & Groth, T. (2011). Bioactivity of immobilized hyaluronic acid derivatives regarding protein adsorption and cell adhesion. *Biotechnology and Applied Biochemistry*, *58*(5), 376–389.

Kuschert, G. S. V., Coulin, F., Power, C. A., Proudfoot, A. E. I., Hubbard, R. E., Hoogewerf, A. J., et al. (1999). Glycosaminoglycans interact selectively with chemokines and modulate receptor binding and cellular responses. *Biochemistry*, *38*(39), 12959–12968.

Kvist, A. J., Johnson, A. E., Morgelin, M., Gustafsson, E., Bengtsson, E., Lindblom, K., et al. (2006). Chondroitin sulfate perlecan enhances collagen fibril formation—Implications for perlecan chondrodysplasias. *Journal of Biological Chemistry*, *281*(44), 33127–33139.

Lee, S.-Y., Yun, Y.-P., Song, H.-R., Chun, H. J., Yang, D. H., Park, K., et al. (2013). The effect of titanium with heparin/BMP-2 complex for improving osteoblast activity. *Carbohydrate Polymers*, *98*(1), 546–554.
Murugesan, S., Xie, J., & Linhardt, R. J. (2008). Immobilization of heparin: Approaches and applications. *Current Topics in Medicinal Chemistry*, *8*(2), 80–100.
Nishimura, M., Yan, W. Q., Mukudai, Y., Nakamura, S., Nakamasu, K., Kawata, M., et al. (1998). Role of chondroitin sulfate hyaluronan interactions in the viscoelastic properties of extracellular matrices and fluids. *Biochimica Et Biophysica Acta-General Subjects*, *1380*(1), 1–9.
Prehm, P. (1983). Synthesis of hyaluronate in differentiated teratocarcinoma cells—Characterization of the synthase. *Biochemical Journal*, *211*(1), 181–189.
Riddles, P. W., Blakeley, R. L., & Zerner, B. (1979). Ellman's reagent: 5,5'-dithiobis(2-nitrobenzoic acid)—a reexamination. *Analytical Biochemistry*, *94*(1), 75–81.
Rogers, C. J., Clark, P. M., Tully, S. E., Abrol, R., Garcia, K. C., Goddard, W. A., et al. (2011). Elucidating glycosaminoglycan-protein-protein interactions using carbohydrate microarray and computational approaches. *Proceedings of the National Academy of Sciences of the United States of America*, *108*(24), 9747–9752.
Rouse, J. J., Whateley, T. L., Thomas, M., & Eccleston, G. M. (2007). Controlled drug delivery to the lung: Influence of hyaluronic acid solution conformation on its adsorption to hydrophobic drug particles. *International Journal of Pharmaceutics*, *330*(1–2), 175–182.
Seo, J. H., Adachi, K., Lee, B. K., Kang, D. G., Kim, Y. K., Kim, K. R., et al. (2007). Facile and rapid direct gold surface immobilization with controlled orientation for carbohydrates. *Bioconjugate Chemistry*, *18*(6), 2197–2201.
Shu, X. Z., Liu, Y. C., Luo, Y., Roberts, M. C., & Prestwich, G. D. (2002). Disulfide cross-linked hyaluronan hydrogels. *Biomacromolecules*, *3*(6), 1304–1311.
Socrates, G. (2001). *Infrared and Raman characteristic group frequencies: Tables and charts*. New York: Wiley. Chichester
Steele, J. G., Johnson, G., & Underwood, P. A. (1992). Role of serum vitronectin and fibronectin in adhesion of fibroblasts following seeding onto tissue-culture polystyrene. *Journal of Biomedical Materials Research*, *26*(7), 861–884.
Tompkins, H. G., & Irene, E. A. (2005). *Handbook of ellipsometry*. Heidelberg Germany: Norwich, NY,William Andrew Pub. Springer.
Toole, B. P. (2009). Hyaluronan-CD44 interactions in cancer: Paradoxes and possibilities. *Clinical Cancer Research*, *15*(24), 7462–7468.
Varki, A. (2009). *Essentials of glycobiology*. Cold Spring Harbor N. Y.: Harbor Laboratory Press.
Vercruysse, K. P., Marecak, D. M., Marecek, J. F., & Prestwich, G. D. (1997). Synthesis and in vitro degradation of new polyvalent hydrazide cross-linked hydrogels of hyaluronic acid. *Bioconjugate Chemistry*, *8*(5), 686–694.
Volpi, N., Schiller, J., Stern, R., & Soltes, L. (2009). Role, metabolism chemical modifications and applications of hyaluronan. *Current Medicinal Chemistry*, *16*(14), 1718–1745.
Walther, F., Drobek, T., Gigler, A. M., Hennemeyer, M., Kaiser, M., Herberg, H., et al. (2010). Surface hydrophilization of SU-8 by plasma and wet chemical processes. *Surface and Interface Analysis*, *42*(12–13), 1735–1744.
Wasserman, S. R., Tao, Y. T., & Whitesides, G. M. (1989). Structure and reactivity of alkylsiloxane monolayers formed by reaction of alkyltrichlorosilanes on silicon substrates. *Langmuir*, *5*(4), 1074–1087.
Weinrich, D., Kohn, M., Jonkheijm, P., Westerlind, U., Dehmelt, L., Engelkamp, H., et al. (2010). Preparation of biomolecule microstructures and microarrays by thiol-ene photoimmobilization. *ChemBioChem*, *11*(2), 235–247.
Xu, C. X., Jin, H., Chung, Y. S., Shin, J. Y., Woo, M. A., Lee, K. H., et al. (2008). Chondroitin sulfate extracted from the Styela clava tunic suppresses TNF-alpha-induced expression of inflammatory factors VCAM-1 and NOS by blocking Akt/NF-kappa B signal in JB6 cells. *Cancer Letters*, *264*(1), 93–100.
Yagi, M., Murray, J., Strand, K., Blystone, S., Interlandi, G., Suda, Y., et al. (2012). Heparin modulates the conformation and signaling of platelet integrin alpha IIb beta 3. *Thrombosis Research*, *129*(6), 743–749.
Yeh, M. L., & Luo, Z. P. (2004). The structure of proteoglycan aggregate determined by atomic force microscopy. *Scanning*, *26*(6), 273–276.
Zajac, R., & Chakrabarti, A. (1995). Irreversible polymer adsorption from semidilute and moderately dense solutions. *Physical Review E*, *52*(6), 6536–6549.
Zhou, J. W., Ellis, A. V., & Voelcker, N. H. (2010). Recent developments in PDMS surface modification for microfluidic devices. *Electrophoresis*, *31*(1), 2–16.

Reprinted from Carbohydrate Polymers, 114, Alexander Köwitsch, Mauricio Jurado Abreu, Ankur Chhalotre, Martin Hielscher, Steffen Fischer, Karsten Mäder, Thomas Groth, Synthesis of thiolated glycosaminoglycans and grafting to solid surfaces (2014), 344-351.
 http://dx.doi.org/10.1016/j.carbpol.2014.08.027

Supporting information – Synthesis of thiolated glycosaminoglycans and grafting to solid surfaces:

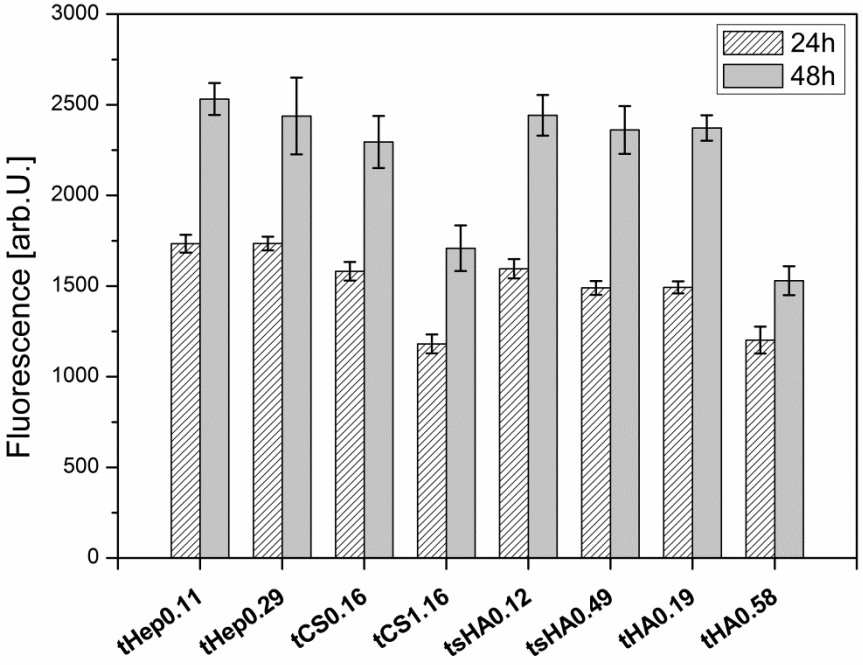

Figure S1: Metabolic activity of human fibroblasts seeded on surfaces coated with different thiolated glycosaminoglycans after 24 h and 48 h (tHep – thiolated heparin, tCS – thiolated chondroitin sulfate, tsHA – thiolated sulfated hyaluronic acid, tHA – thiolated hyaluronic acid).

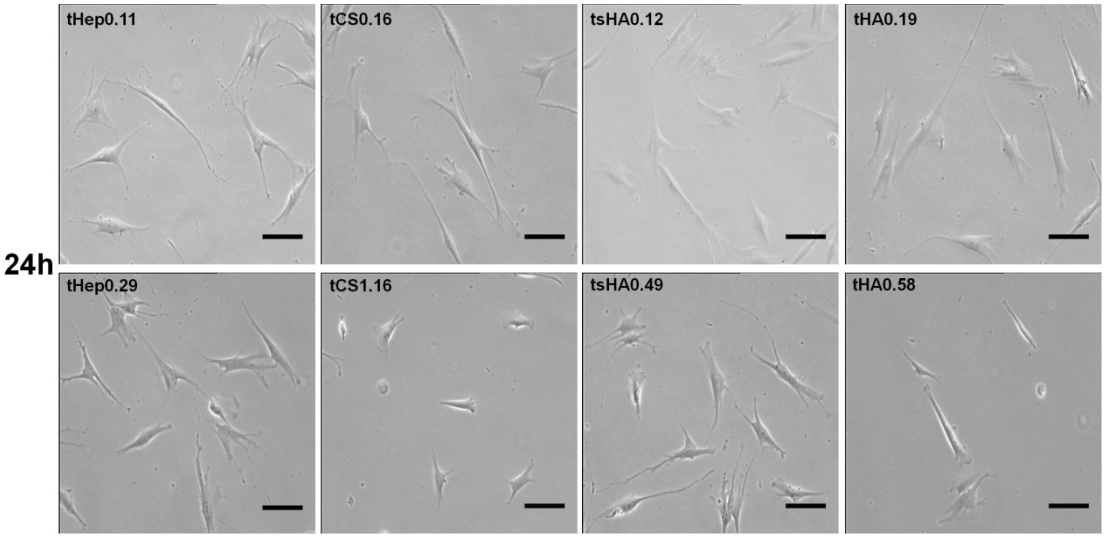

Figure S2: Phase contrast images of human fibroblasts after 24 h adhesion on surfaces coated with different thiolated glycosaminoglycans (tHep – thiolated heparin, tCS – thiolated chondroitin sulfate, tsHA – thiolated sulfated hyaluronic acid, tHA – thiolated hyaluronic acid).

Reprinted from Carbohydrate Polymers, 114, Alexander Köwitsch, Mauricio Jurado Abreu, Ankur Chhalotre, Martin Hielscher, Steffen Fischer, Karsten Mäder, Thomas Groth, Synthesis of thiolated glycosaminoglycans and grafting to solid surfaces (2014), 344-351.
 http://dx.doi.org/10.1016/j.carbpol.2014.08.027

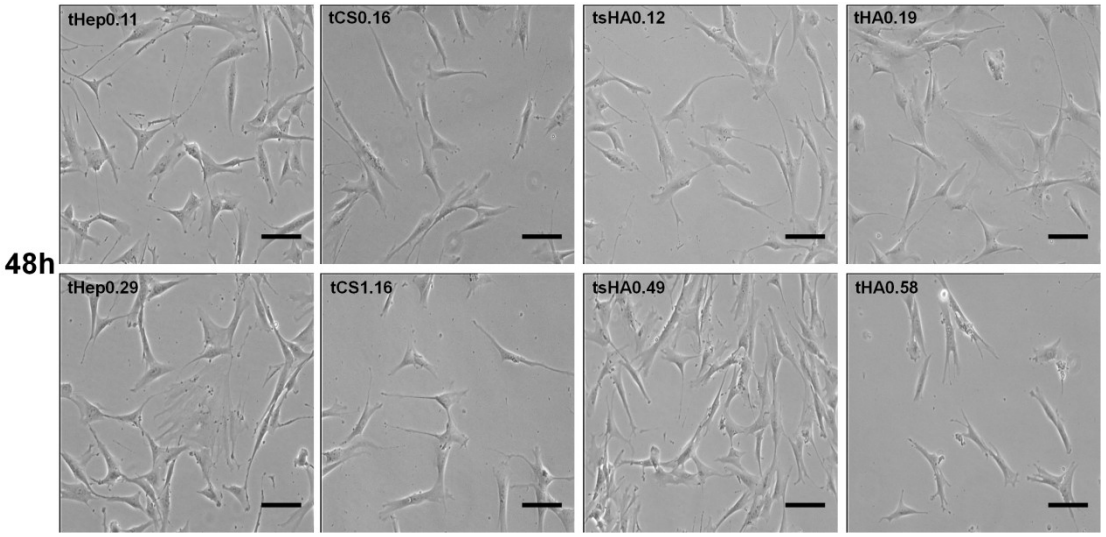

Figure S3: Phase contrast images of human fibroblasts after 48 h adhesion on surfaces coated with different thiolated glycosaminoglycans (tHep – thiolated heparin, tCS – thiolated chondroitin sulfate, tsHA – thiolated sulfated hyaluronic acid, tHA – thiolated hyaluronic acid).

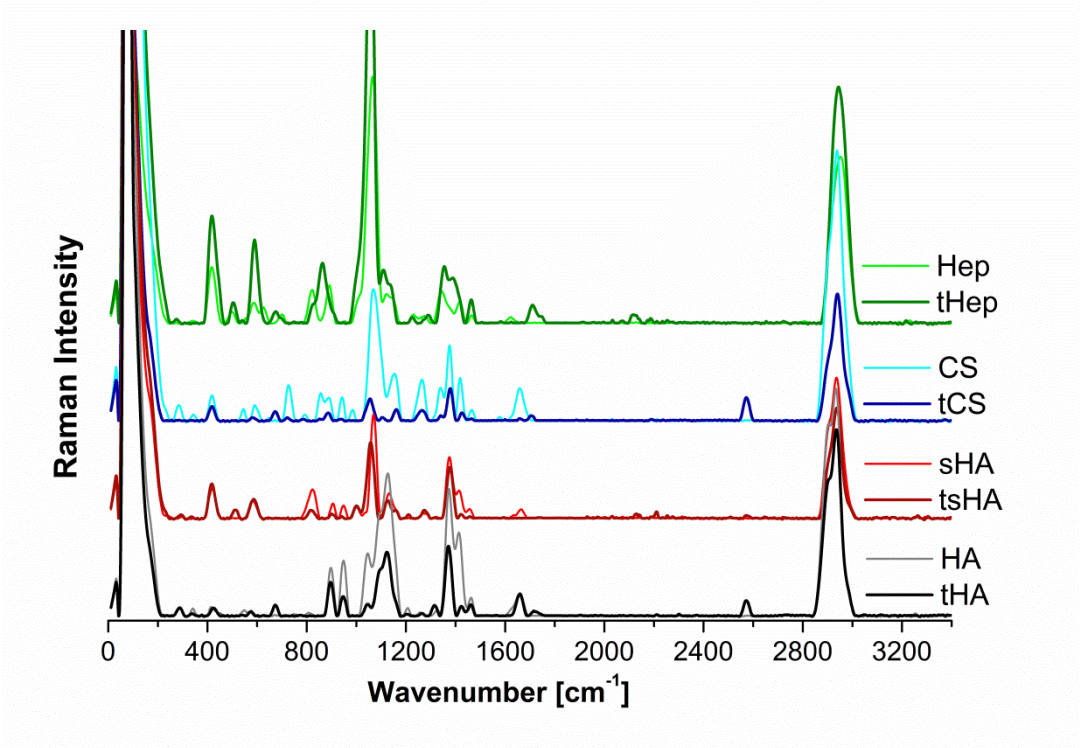

Figure S4: Full Raman spectra of thiolated and native glycosaminoglycans (tHep – thiolated heparin, tCS – thiolated chondroitin sulfate, tsHA – thiolated sulfated hyaluronic acid, tHA – thiolated hyaluronic acid).

Reprinted from Carbohydrate Polymers, 114, Alexander Köwitsch, Mauricio Jurado Abreu, Ankur Chhalotre, Martin Hielscher, Steffen Fischer, Karsten Mäder, Thomas Groth, Synthesis of thiolated glycosaminoglycans and grafting to solid surfaces (2014), 344-351.
 http://dx.doi.org/10.1016/j.carbpol.2014.08.027

Chapter 4

Summary – Effect of immobilized thiolated glycosaminoglycans on fibronectin adsorption and behavior of fibroblasts:

In this paper the biological activity of surface-coupled thiolated glycosaminoglycans (tGAG) was investigated in terms of fibronectin adsorption as well as adhesion and proliferation of fibroblasts.

The glycosaminoglycans (GAG) hyaluronic acid (HA), sulfated HA, chondroitin sulfate (CS) and heparin were chemically thiolated with two different degree of thiolation and subsequently immobilized to model substrata. The thiol concentration of the tGAG was determined by Ellman`s reagent. The tGAG were applied to vinyl-terminated surfaces (glass or silicon) and gold to create GAG-coated substrata.

Measurements of water contact angle (WCA), surface zeta potential (ZP) and atomic force microscopy (AFM) were used for surface characterization as biomaterial properties like wettability, charge and topography represent important modulators of protein adsorption and cellular adhesion. Water contact angle measurements revealed that the tGAG exhibiting a higher thiol concentration resulted in more wettable GAG-modified surfaces. The surface potential of GAG with a higher degree of sulfation possessed a more negative surface potential. Furthermore, AFM measurements showed that tGAG with higher thiol concentration and exhibited a higher surface roughness.

Fibronectin (FN) adsorption onto tGAG-coated gold sensors were used to obtain information about the capability of the immobilized tGAG to bind to FN. It was found that the amount of adsorbed FN increased with sulfation degree of tGAG having the most adsorbed FN on the heparinized surfaces. The tGAG-functionalized surfaces with higher degree of sulfation also promoted fibroblast adhesion under serum-free conditions. A pre-adsorption of FN supported the cell adhesion on all tGAG surfaces. Metabolic activity measurements showed that cell growth was enhanced for tGAG up to a certain thiolation degree. In the end, thiolation of GAG did not hamper their bioactivity towards proteins and cells, which make them highly interesting for biomimetic surface modification of implants and tissue engineering scaffolds.

Full Paper
Macromolecular Journals
Macromolecular Bioscience

Effect of Immobilized Thiolated Glycosaminoglycans on Fibronectin Adsorption and Behavior of Fibroblasts

Alexander Köwitsch, Marcus S. Niepel, Georgios P. A. Michanetzis, Yannis F. Missirlis, Thomas Groth*

Glycosaminoglycans (GAGs) chondroitin sulfate, heparin, hyaluronan, and sulfated hyaluronan are lower and higher thiolated to enable a one-step covalent modification of gold or vinyl-terminated surfaces. Measurements of water contact angle and zeta potentials reveal that sulfated GAG-modified surfaces are more wettable and possess a negative surface potential. Additionally, higher thiolated GAGs (tGAGs) exhibit increased wettability and higher surface roughness. Fibronectin (FN) adsorption increases with sulfation degree of tGAGs. The tGAG-functionalized surfaces with higher degree of sulfation promote fibroblast adhesion most under serum-free conditions. The preadsorption of FN allows for more cell adhesion on tGAG surfaces. Metabolic activity measurements show that cell growth is enhanced for tGAGs up to a certain thiolation degree. Overall, thiolation of GAGs does not hamper their bioactivity toward proteins and cells, which make them highly interesting for biomimetic surface modification of implants and tissue engineering scaffolds.

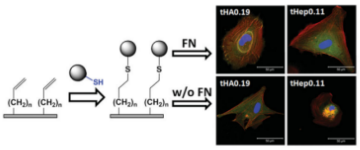

1. Introduction

Surface engineering is frequently used for the development and design of new biomaterials for application in a variety of tissue engineering approaches.[1] A major challenge is the combination of the required materials bulk properties and surface features to generate an appropriate interface for the desired biological response.[2,3] Hence, surface modification plays a key role in biomaterial science. Biocompatible surfaces can be prepared by mimicking the natural environment of cells either by the development and application of synthetic molecules or by direct use of biomolecules.[4] For example, the material functionalization with self-assembled monolayers (SAMs) is a facile and valuable approach to create specific surface properties and allow further chemical modification with bioactive oligopeptides but also larger molecules like proteins, proteoglycans and polysaccharides to guide cell adhesion.[5–8]

Glycosaminoglycans (GAGs) like heparin, heparan sulfate, and chondroitin sulfate (CS) are nonbranched, highly sulfated polysaccharides that are composed of different disaccharide units that contain a glucosamine or galactosamine and uronic acid. More specifically, heparin mainly consists of an (α-1,4)-2-O-sulfated iduronic acid and an (α-1,4)-6-O-sulfated, N-sulfated glucosamine,

A. Köwitsch, Dr. M. S. Niepel, Prof. T. Groth
Biomedical Materials Group
Institute of Pharmacy
Martin Luther University Halle-Wittenberg
06099 Halle (Saale), Germany
E-mail: thomas.groth@pharmazie.uni-halle.de
Dr. G. P. A. Michanetzis, Prof. Y. F. Missirlis
Biomedical Engineering Laboratory
Department of Mechanical Engineering
University of Patras, 26504 Rion-Patras, Greece

Macromol. Biosci. **2016**, *16*, 381–394

DOI: 10.1002/mabi.201500276

Macromolecular Bioscience
www.mbs-journal.de

although the particular ratio of disaccharide units highly depends on the animal origin.[9] CS is made of repeating (β-1,4)-D-glucuronic acid and (β-1,3)-*N*-acetyl-D-galactosamine units.[10] Hyaluronic acid (HA) represents the only nonsulfated GAG, which is composed of disaccharides consisting of one (β-1,4)-D-glucuronic acid and a (β-1,3)-*N*-acetyl-D-glucosamine.[11] HA can be chemically sulfated to acquire specific binding properties toward proteins like human bone morphogenetic protein-4.[12]

GAGs like heparan sulfate as less sulfated relative of heparin are able to specifically interact with a large variety of cytokines (fibroblast growth factor-2 (FGF-2), BMP-2), adhesive proteins (fibronectin (FN), vitronectin, etc.), and coagulation-related proteins (anti-thrombin III, factor IIa).[13,14] A common feature of these proteins is the presence of heparin-binding domains.[15] They play essential roles as co-factors in signaling transduction processes of cells like the FGF-2-related signal transduction.[16] Also other sulfated GAGs like CS as component of proteoglycans are able to interact with adhesive proteins like FN and are involved in signaling processes.[17,18] Previous studies reported that CS promotes the differentiation of osteoblasts.[19] On the other hand, nonsulfated HA interacts directly with the cell surface receptor CD44 in a lectin-like manner promoting initial adhesion of cells and influencing the cell motility.[20,21]

Therefore, GAGs represent highly interesting molecules that can be used to generate biomimetic surface coatings on implant materials,[22] to make biosensors,[23] but also to generate 3D environments as part of porous tissue engineering scaffolds[24,25] or hydrogels.[26,27] Here, it is particularly interesting to have preactivated GAGs that can undergo covalent reactions with surfaces or which cross-link to form hydrogels. Particularly in the latter case, bioactive factors and cells may be embedded without any damage when a biocompatible chemistry is applied. Such chemistry can be represented by the presence of thiol groups that may undergo covalent reactions with vinyl or other groups on pendant macromolecules. However, a modification of GAGs with thiol groups via grafting and subsequent reduction of dithiobis (propanoic hydrazide) (DTPHY) on carboxyl groups of the uronic acid components of GAGs might deteriorate the bioactivity. Therefore, the current work sought to study thiolated GAG (tGAG) heparin (Hep), CS, hyaluronan (HA), and sulfated hyaluronan (sHA) after photochemical immobilization on vinyl-terminated glass or silicon surfaces. The efficacy of immobilization and effects on surface properties were evaluated by water contact angle (WCA) and zeta potential (ZP) measurements, as well as by atomic force microscopy (AFM). Finally, the influence of the thiolation degree of GAGs on their bioactivity was investigated by adsorption of FN and adhesion and growth of human dermal fibroblasts.

2. Experimental Section

2.1. Materials

Heparin from porcine intestinal mucosa was purchased from Serva Electrophoresis GmbH (Heidelberg, Germany). High molecular weight HA (M_w 1.3 MDa) was provided by Kraeber & Co. GmbH (Ellerbek, Germany). Low molecular weight HA (M_w 15 kDa) was obtained by acidic hydrolysis as reported previously.[28] Sulfated HA with a sulfation degree (DS_S) of 1.3 was a kind gift from Innovent e.V. (Jena, Germany). Chondroitin sulfate A (from bovine trachea) and Triton X-100 were obtained from Sigma-Aldrich Chemie GmbH (Steinheim, Germany). The dialysis bag (Spectra/Por membrane, M_w cutoff = 3500 Da) and organic solvents were purchased from Carl Roth GmbH (Karlsruhe, Germany). 3,3′-dithiobis (propanoic hydrazide) (DTPHY) was synthesized and analyzed as described recently.[29] 7-octenyldimethylchlorosilane was purchased from ABCR GmbH &Co. KG (Karlsruhe, Germany), dithiothreitol (DTT) (VWR International GmbH, Dresden, Germany), 5,5′-dithiobis-(2-nitrobenzoic acid) (DTNB, Ellman's reagent), and 1-ethyl-3-(3-dimethylaminopropyl) carbodiimide hydrochloride (EDC) from Alfa Aesar (Karlsruhe, Germany). Phosphate buffered saline (PBS) was prepared according to the following formulation: 2.7 mmol L^{-1} KCl, 137 mmol L^{-1} NaCl, 1.4 mmol L^{-1} KH_2PO_4, 4.3 mmol L^{-1} $Na_2HPO_4 \times 2H_2O$, pH 7.4.

2.2. Synthesis and Characterization of tGAGs

The preparation of tGAGs was described previously and carried out at room temperature.[30] Briefly, 0.75 mmol of the GAG (heparin, CS, HA, sHA) was dissolved in micropure water (80 mL). Then, DTPHY (0.19 mmol (25%) or 0.04 mmol (5%)) was added to the stirred solution and the pH was adjusted to 4.75. Thereafter, EDC (96 mg, 0.4 mmol (25%) or 0.1mmol (5%)) was added while the pH was maintained at 4.75. After additional 3 h incubation at room temperature, 1 mol L^{-1} NaOH was used to increase the pH to 7.0. Then, DTT (2.0 mmol) was added raising the pH to 8.5 and stirring the solution overnight. Thereafter, the pH of the reaction mixture was lowered to 3.5 before the solution was dialyzed extensively at first against diluted HCl (pH 3.5) containing 0.1 mol L^{-1} NaCl, and then dialyzed against diluted HCl (pH 3.5) for another 3 d. Finally, the solution was freeze-dried to obtain a white sponge-like product.

The thiol content of tGAGs was determined using Ellman's reagent with UV absorption measurements.[31] The molar absorption coefficient of 14 150 L mol^{-1} cm^{-1} at 412 nm was used for the calculation of the total thiol concentration.[32] The thiol concentration obtained with Ellman's test was used for the nomenclature of the different samples. For example, the thiolated heparin with a thiol concentration of 0.11 mmol L^{-1} was named tHep0.11 (also see Table 1). In addition, Raman and FT-IR spectroscopy were used to characterize the tGAGs. The obtained

Table 1. Nomenclature and properties of thiolated glycosaminoglycans.

Sample	Material	DS_{Sulf}[a)]	Thiol conc. [10^{-3} mol L^{-1}][b)]	Thiol content [%][c)]	M_w [kDa]	PDI[d)]
tHep0.11	Thiolated heparin	1.6	0.11	3.7	17	1.5
tHep0.29			0.29	10.0	28	1.5
tCS0.16	Thiolated chondroitin sulfate	0.8	0.16	4.4	27	1.4
tCS1.16			1.16	30.7	30	1.5
tsHA0.12	Thiolated, sulfated hyaluronan	1.3	0.12	3.2	24	1.9
tsHA0.49			0.49	13.3	38	1.9
tHA0.19	Thiolated hyaluronan	0	0.19	3.9	14	1.4
tHA0.58			0.58	12.2	64	2.7

[a)]DS_{Sulf}: degree of sulfation (sulfate groups per disaccharide unit); [b)]Experimental thiol concentration $c_{SH}(exp) = A \times D/\varepsilon$ (A: UV-absorption at 412 nm; D: dilution factor; ε: molar absorption coefficient at 412 nm); [c)]Thiol content [%] = $c_{SH}(exp)/c_{SH}(th) \times 100$; $c_{SH}(th)$: theoretical thiol concentration (c_{tGAG}/M_{tGAG}); c_{tGAG}: concentration of tGAGs in solution; M_{tGAG}: molecular mass of repeating disaccharide of the tGAGs; [d)]PDI: polydispersity index (PDI = M_w/M_n).

results as well as the molecular weights of the tGAGs were reported in a recent publication.[30]

2.3. Functionalization and Characterization of Substrata

2.3.1. Preparation of Model Substrata

Glass cover slips (Menzel GmbH + Co KG, Braunschweig, Germany) were cleaned with 0.5 mol L^{-1} NaOH in 96% ethanol for 2 h followed by excessive washing with micropure water (7 × 5 min) and drying in a stream of nitrogen. Silicon wafers (Silicon Materials, Kaufering, Germany) were treated with a solution of NH_4OH (27%), H_2O_2 (30%), and micropure water (1:1:5, v/v/v) at 70 °C for 15 min, subsequently washed with micropure water (7 × 5 min) and also dried with a stream of nitrogen. New gold-coated glass sensors for surface plasmon resonance (SPR, IBIS Technologies BV, Enschede, Netherlands, 16 × 16 mm^2) were cleaned by repeated dipping into 0.5 mol L^{-1} NaOH in 96% ethanol and 99% ethanol followed by extensive rinsing with micropure water and drying with nitrogen.

The vinyl-terminated surfaces were prepared by immersion of cleaned glass or silicon in a solution of 7-octenyldimethylchlorosilane (3%, v/v) in ethanol (99%) for 24 h while the solution was warmed to 35 °C in a water bath for the last 3 h. Then, the surfaces were rinsed with copious amounts of ethanol, washed with micropure water (7 × 5 min), and dried with nitrogen.[30]

2.3.2. Immobilization of tGAGs

The reaction of tGAGs with the vinyl-terminated glass or silicon surfaces was carried out in a UV–VIS chamber (Bio-Link BLX, LTF Labortechnik GmbH & Co. KG, Wasserburg, Germany) at 365 nm in TRIS-HCl (50 mmol L^{-1}, pH 7.4) at a concentration of 2 mg mL^{-1} for 4 h.[33,34] The modified surfaces were washed and dried as mentioned above. After surface coating, modified glass substrata were used for WCA and ZP measurements as well as cell experiments, while silicon substrata were applied in AFM measurements. The cleaned gold sensors were used for the SPR experiments.

2.3.3. Physicochemical Characterization of Modified Surfaces

Static WCA measurements were performed with an OCA 15+ device (Dataphysics, Filderstadt, Germany) using the sessile drop method to determine the wetting properties after surface modifications. Five droplets of 2 µL micropure water were applied to each sample. The obtained values were used to calculate means and standard deviations. The values mentioned herein represent the mean of at least two independent experiments, which are composed of a minimum of three different samples each.

Surface ZPs were obtained from streaming potential measurements using a SurPASS Electrokinetic Analyzer (Anton Paar, Graz, Austria). Glass coverslips with specific dimensions (10 mm × 20 mm) for the measuring chamber were used for sample preparation and ZP measurements. Two identical modified coverslips were fixed on stamps, which were placed oppositely in the SurPASS flow cell. The width of the flow cell was adjusted to a distance that a flow rate of 100–150 mL min^{-1} was achieved at a maximum pressure of 300 mbar. Potassium chloride solution (1 mmol L^{-1}) was used as electrolyte and HCl (10 mmol L^{-1}) was used for pH titration. First, the pH value of the electrolyte was adjusted to pH 10 using 1 mol L^{-1} NaOH before starting the measurement. The measurements from pH 10 to 3 were performed by an automated titration program using titration steps of 0.02 mL and pH changes of ≈0.25 each step.

AFM of modified silicon surfaces was performed in a liquid environment with a Multimode AFM with a Nanoscope III controller (Digital Instruments, Veeco, Santa Barbara, CA, USA). NP-S10 cantilevers (Bruker, Santa Clara, CA, USA) with a resonant frequency of 18–80 kHz and a spring constant of 0.03–0.7 N m^{-1} were used. All measurements were performed using tapping mode in water. Roughness analysis was performed using the Nanoscope software v5.31r1 and Gwyddion 2.25. Scans were performed on an area of 1 μm^2. For representative measurements,

Reprinted with permission from Journal of Macromolecular Bioscience, Alexander Köwitsch, Marcus S. Niepel, Georgios P. A. Michanetzis, Yannis F. Missirlis, Thomas Groth (2016), Effect of immobilized thiolated glycosaminoglycans on fibronectin adsorption and behavior of fibroblasts, 16, 381–394.

Macromolecular Bioscience
www.mbs-journal.de

vinyl-terminated silicon surfaces coated with the tGAGs were swollen in micropure water for at least 30 min prior to the measurement.

2.4. Measurement of tGAG Quantity Bound on Gold and Subsequent FN Adsorption

SPR measurements were conducted with an IBIS-*i*SPR device (IBIS Technologies BV, Enschede, Netherlands) to measure the immobilization of tGAGs on gold and their subsequent interaction with human plasma FN (YO Proteins, Huddinge, Sweden). First, gold sensors mounted in a flow chamber were equilibrated with degassed PBS at 25°C to establish a stable baseline. Then the solution of tGAGs (4 mg mL^{-1} in PBS) was injected at a flow rate of 3 µL s^{-1} for 1 h followed by rinsing with PBS to remove loosely bound GAGs. Afterward, FN solutions with incremental concentrations (1, 2, 5, 10, 25, 50, 100, 200 µg mL^{-1} FN in PBS) were injected for 30 min each, followed by rinsing with PBS. The observed angle shifts (m°) before and after each injection step are proportional to adsorbed mass of molecules, whereby 122 m° corresponds to ≈1 ng mm^{-2}.[35] FN adsorption isotherms were plotted as a function of solution concentration and analyzed applying the Langmuir adsorption model (Equation (1)) which allows to calculate the binding constant K and the possible maximum amount of protein adsorbed (Γ_{max}) depending on the protein concentration c

$$\Gamma = \Gamma_{max} \frac{K_c}{1 + K_c} \quad (1)$$

2.5. Adhesion and Morphology of Fibroblasts on tGAG-Coated Surfaces

2.5.1. Cell Culture

Human dermal fibroblasts (HFs, Promocell, Heidelberg, Germany) were grown in Dulbecco's modified Eagle's medium (DMEM, Biochrom AG, Berlin, Germany) supplemented with 10% fetal bovine serum (FBS, Biochrom), 1% antibiotic-antimycotic solution (Biochrom) at 37 °C in a humidified 5%CO_2/95% air atmosphere using a NUAIRE DH Autoflow incubator (NuAire Corp., Plymouth, USA). Cells from almost confluent cultures were harvested by 0.25% Trypsin/EDTA (Biochrom). Trypsin was neutralized with DMEM containing 10% FBS. After centrifugation, HFs were resuspended in culture medium without FBS for adhesion and immunofluorescence studies and in serum-containing DMEM for cell proliferation experiments.

2.5.2. Fibroblast Adhesion Studies

Samples (different types of GAG-modified glass slides) were placed into 12-well tissue culture plates (Greiner Bio-One GmbH, Frickenhausen, Germany) and sterilized with 70% ethanol for 10 min followed by rinsing with sterile PBS twice. The ability of GAG-modified surfaces to bind FN and their effect on cell behavior was studied in comparative experiments with and without preadsorption of FN. Therefore, one fraction of the samples was treated with 2 µg mL^{-1} FN in PBS at 37 °C for 30 min and subsequently washed with PBS twice. Afterward, HFs were seeded at a density of 60 cells mm^{-2} on the different modified surfaces and incubated at 37 °C in a humidified 5%CO_2/95% air atmosphere for 4 h. Thereafter, adherent cells were fixed with 4% (w/v) paraformaldehyde in PBS for 15 min and permeabilized with 0.1% (v/v) Triton X-100 for 10 min. After rinsing the samples with PBS three times, nonspecific binding sites were blocked by incubation with 1% (w/v) bovine serum albumin (BSA, Merck, Darmstadt, Germany) for 30 min. Focal adhesions (FAs) were visualized by incubating the samples with a primary mouse antibody raised against vinculin (Sigma) and a CY2-conjugated secondary anti-mouse antibody (Dianova, Hamburg, Germany) at room temperature for 30 min each. Filamentous actin was stained by incubation with BODIPY-phalloidin (Invitrogen, Darmstadt, Germany) and cell nuclei were stained with TO-PRO3 Iodide (Invitrogen). All antibodies and dyes were diluted in PBS containing 1% BSA. The samples were then washed with PBS, micropure water and finally mounted with Mowiol (Calbiochem, Darmstadt, Germany) containing 25 mg mL^{-1} triethylenediamine (Carl Roth). Samples were examined with confocal laser scanning microscopy (LSM 710, Carl Zeiss MicroImaging GmbH, Jena, Germany) using a 63× oil immersion objective. The acquired images were processed with ZEN software (Carl Zeiss). Cell count and area were evaluated by image analysis software ImageJ (v1.49e9) from low magnification images.

2.5.3. Cell Growth

The metabolic activity (MA) of HF on the different substrata was examined with the fluorometric QBlue cell viability assay (Bio-Chain, Newark, USA). For that reason, HFs in DMEM containing 10% FBS were seeded at a density of 120 cells mm^{-2} in 24-well tissue culture plates (Greiner) containing the different GAG-coated, round cover slips with a diameter of 10 mm^2. After 24, 48, and 72 h, the old medium was removed and the surfaces were carefully washed with prewarmed colorless DMEM once. Afterward, colorless DMEM containing 10% of QBlue reagent was added to each well and incubated at 37 °C for 3 h. Then, 100 µL of the supernatant from each well was transferred to a 96-black well plate and the fluorescence was read out with a fluorescence plate reader (BMG Labtech, Fluostar Optima, Offenburg, Germany). The obtained values of two independent experiments with triplicate samples were used to calculate mean values and standard deviations.

2.6. Statistical Analysis

The significance of all means was calculated by one-way analysis of variance (ANOVA) followed by post-hoc Tukey's test. The significance level of $p \leq 0.05$ is indicated in the figures where applicable.

3. Results

3.1. Characterization of tGAGs

Biomolecule conjugation and surface modification is widely used in biomaterials and tissue engineering research. For the introduction of thiol groups, it was assumed that every disaccharide unit contains one carboxylic acid group,

which might not be completely correct for heparin, whose saccharide composition differs according to its animal origin.[9] The influence of the applied cross-linker amount on bioactivity and surface grafting density was evaluated using two different aliquots (0.25 aq./0.05 aq.) of the cross-linking agent to generate corresponding lower and higher tGAGs (Table 1).[30]

3.2. Characterization of Modified Surfaces

Biomaterial surface properties like wettability, charge, and topography are important parameters influencing protein adsorption and subsequent cellular interaction.[4,36] Here, WCA and ZP measurements as well as AFM were applied to study the successful immobilization of GAGs and the resulting surface properties.

The results of the static WCA measurements are depicted in Figure 1. A significant increase of WCA was found when the hydrophilic cleaned glass was modified with a vinyl-terminated SAM resulting in a WCA of about 95°.[8] The subsequent immobilization with tGAGs decreased the WCA because of the hydrophilic nature of GAGs. The observed decrease of WCA was always more pronounced in the case of GAGs with a higher thiolation degree. The lowest WCA was observed for the heparin coated surfaces with 57° for tHep0.29, while the sulfated HA substrata showed the highest WCA of the glycanized surfaces.

Zeta (ζ) potential measurements of modified surfaces were conducted to evaluate the surface potential in relation to the surface modification. Vinyl-terminated glass was used as reference and the results are depicted in Figure 2. ZPs increased from pH 10 to pH 3 independent of the modification and were negative for all measured samples over the entire measured pH range. The vinyl-terminated glass showed an almost linear dependence of the ZP on the pH value. The highest ZP

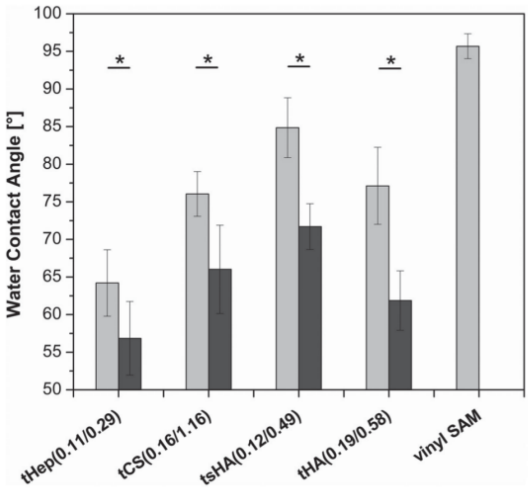

Figure 1. Change of wettability for thiolated GAGs with different degree of substitution compared to vinyl-terminated glass (lower/higher thiolation degree of tGAGs: light gray/black). tHep: thiolated heparin; tCS: thiolated chondroitin sulfate; tsHA: thiolated, sulfated hyaluronic acid; tHA: thiolated hyaluronic acid; vinyl SAM: vinyl-terminated self-assembled monolayer on glass. Data represent means, standard deviations, and significance (ANOVA) of different thiolated samples at a significance level of $p \leq 0.05$ indicated by the asterisks.

(least negative) was obtained for the tHA-coated substrata. The coatings of the sulfated GAGs resulted in more negative ZPs at pH 7.4 with tsHA0.49 and tCS1.16 showing the lowest values (Table 2). At pH 7.4, the ZP of the higher tGAGs was lower compared to the tGAGs with low degree of thiolation, except for tHep0.29 where a less negative ZP was observed. Further, a higher degree of thiolation always led to a lowered negative surface potential above pH 6.0, except for the tHA surfaces, where almost

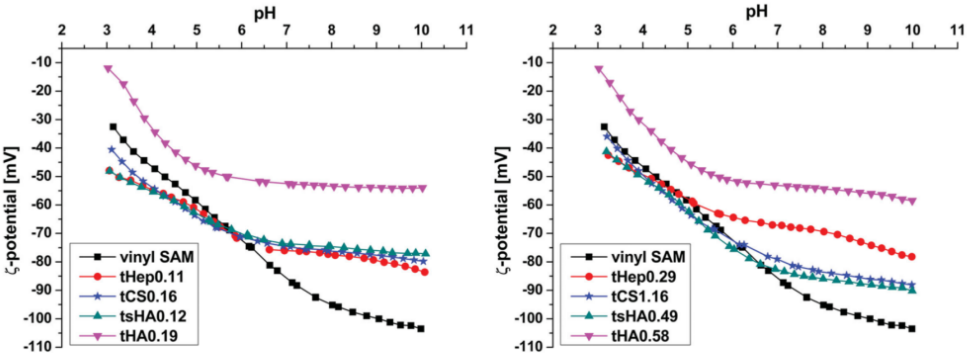

Figure 2. Comparison of the zeta potential of tGAG-coated glass with low degree of thiolation (left) and high degree of thiolation (right) in dependence on the solution pH value. tHep: thiolated heparin; tCS: thiolated chondroitin sulfate; tsHA: thiolated, sulfated hyaluronic acid; tHA: thiolated hyaluronic acid; vinyl SAM: vinyl-terminated self-assembled monolayer on glass. The graph shows one representative set out of three independent experiments.

Reprinted with permission from Journal of Macromolecular Bioscience, Alexander Köwitsch, Marcus S. Niepel, Georgios P. A. Michanetzis, Yannis F. Missirlis, Thomas Groth (2016), Effect of immobilized thiolated glycosaminoglycans on fibronectin adsorption and behavior of fibroblasts, 16, 381–394.

Table 2. Zeta potential of tGAG-coated glass at pH 7.4. Vinyl SAM: vinyl-terminated self-assembled monolayer on glass; tHep: thiolated heparin; tCS: thiolated chondroitin sulfate; tsHA: thiolated, sulfated hyaluronic acid; tHA: thiolated hyaluronic acid.

	Zeta potential at pH 7.4 [mV]
Vinyl SAM	–90.1
tHep0.11/0.29	–76.4/–68.0
tCS0.16/1.16	–75.5/–81.6
tsHA0.12/0.49	–74.0/–84.4
tHA0.19/0.58	–52.9/–53.6

no difference was observed. However, sulfated GAGs with a low thiolation degree (tHep0.11, tCS0.16, tsHA012) showed very similar curve progressions.

The surface topography of the different tGAGs on vinyl-terminated silicon surfaces was analyzed by AFM in micropure water to allow the hydration of the GAG. The images (Figure 3) showed distinctive topographies for each GAG immobilized to vinyl-terminated silicon as well as a specific surface roughness (Table 3). It can be seen that with increasing degree of thiolation also the surface roughness parameters were increasing. Generally, the GAG with a higher thiolation degree showed larger surface structures. The thiolated heparin revealed round structures, which increased in diameter with increased degree of thiolation indicated by an increased surface roughness. For the low thiolated CS-coated surfaces, a more fuzzy surface topography was found. On the high thiolated CS, the observed aggregates had a higher variety in size and shape. The tsHA0.12 showed also small round structures similar to the one found for the tHep0.11. In contrast, the tsHA0.49 had an increased surface topography without the domination of circular structures. Interestingly, the immobilized tHA showed characteristic donut-like structures of similar size and shape for both degrees of thiolation. The roughness parameters confirmed the visual observations on topography regarding size and number of aggregates. The average roughness (R_a) and root mean square (RMS) were highest on tHep0.29- and tCS1.16-coated silicon substrata while they were lowest for tHep0.11, tsHA0.12, and tCS0.16.

3.3. Measurement of tGAG Quantity Bound on Gold and Subsequent FN Adsorption

SPR was used as a surface sensitive analytical method to monitor the immobilization of different tGAGs and their interaction with the extracellular matrix protein FN. The adsorption of tGAGs was characterized by a strong increase in angle shift, which was proportional to the adsorption of the dry layer mass of the molecule (Figure 4). After 5–10 min, the initial increase equilibrated and only minor changes in angle shift were observed. However, tCS adsorption continued with a lowered slope during the residual time while the surface concentrations of other tGAGs remained constant. After an additional rinsing step with buffer (PBS), unbound molecules were removed. The amount of adsorbed biomolecules per area was calculated using the recorded angle shifts.[35] In general, the adsorbed amount of tGAGs varied from 0.63 ng mm^{-2} for tHA0.19 to 1.99 ng mm^{-2} for tsHA0.49 (Figure 4). The adsorption of tHep0.11 (1.39 ng mm^{-2}) was highest among the low tGAGs and also higher than the adsorption of tHep0.29 (1.14 ng mm^{-2}). The other tGAGs usually showed

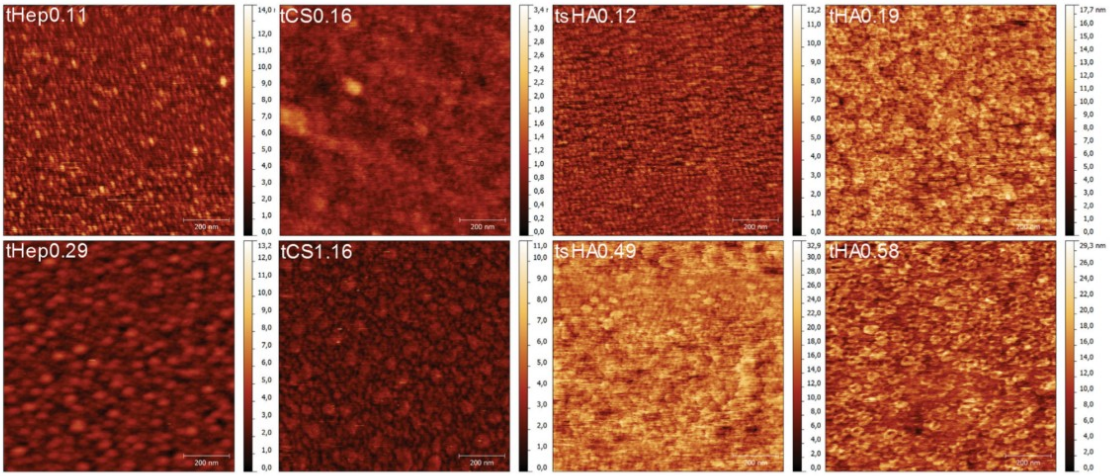

Figure 3. Surface morphology of tGAGs measured by AFM in water (scale bar = 200 nm). Representative images of at least three scans are displayed. tHep: thiolated heparin; tCS: thiolated chondroitin sulfate; tsHA: thiolated, sulfated hyaluronic acid; tHA: thiolated hyaluronic acid.

Reprinted with permission from Journal of Macromolecular Bioscience, Alexander Köwitsch, Marcus S. Niepel, Georgios P. A. Michanetzis, Yannis F. Missirlis, Thomas Groth (2016), Effect of immobilized thiolated glycosaminoglycans on fibronectin adsorption and behavior of fibroblasts, 16, 381–394.

Table 3. Roughness parameters of silicon surfaces coated with thiolated glycosaminoglycans. tHep: thiolated heparin; tCS: thiolated chondroitin sulfate; tsHA: thiolated, sulfated hyaluronic acid; tHA: thiolated hyaluronic acid.

	tHep0.11	tHep0.29	tCS0.16	tCS1.16	tsHA0.12	tsHA0.49	tHA0.19	tHA0.58
RMS[a)] [nm]	1.1	4.2	1.3	3.5	1.2	1.8	1.7	2.8
R_a[b)] [nm]	0.8	3.3	1.0	2.8	0.9	1.4	1.3	2.1

[a)]RMS: root mean square; [b)]R_a: average roughness.

a higher adsorption with an increased thiolation degree. The amount of adsorbed tCS0.16 was 0.99 ng mm^{-2} while for tCS1.16 it was 1.29 ng mm^{-2}. A significant increase from 1.14 ng mm^{-2} to 1.99 ng mm^{-2} was found during the immobilization of tsHA. The lowest values were found for tHA with only 0.63 ng mm^{-2} (tHA0.19) and 1.07 ng mm^{-2} (tHA0.58), respectively.

After tGAG immobilization, increasing concentrations of FN were applied to the sensor surface starting with 1 µg mL^{-1} up to 200 µg mL^{-1}. The obtained results indicated a strong dependence of the adsorbed FN amount on the type of immobilized GAGs. The highest amount of FN was found on tHep-coated surfaces (Figure 5, Table 4). It rose with increasing thiolation degree from 0.88 ng mm^{-2} to 1.12 ng mm^{-2}. In contrast, the amount of adsorbed FN decreased with enhanced thiolation degree on the remaining GAGs. While 0.75 ng mm^{-2} of FN was bound to the tCS0.16, only 0.39 ng mm^{-2} was adsorbed on tCS1.16. Such a decrease was similar on tsHA (0.51 ng mm^{-2} to 0.20 ng mm^{-2}) and on tHA (0.58 ng mm^{-2} to 0.21 ng mm^{-2}). In general, a Langmuir-like adsorption behavior was found for FN adsorption on tGAGs on gold substrata. At constant temperature, the surface coverage of adsorbed molecules from solution of a certain concentration can be described using the Langmuir equation (Equation (1). Here, a linear regression of the Langmuir equation was used and c/Γ was plotted against c, where Γ is the adsorbed amount of FN and c represents the concentration of FN in the applied solution. All calculated parameters are displayed in Table 4. The Γ_{max} value displays the possible maximum amount of FN that can be adsorbed on the surface and K represents the equilibrium constant of the adsorption process. The square of the correlation coefficient (R^2) indicates the precision of the fitting results. The calculated Γ_{max} values varied from 0.21 ng mm^{-2} for tHA0.58 to 1.15 ng mm^{-2} for tHep0.29. The maximum estimated FN values were found for tHep with a high thiolation degree, while lowest values were found on highly thiolated tsHA (0.25 ng mm^{-2}) and tHA. The equilibrium constant K correlates with the binding affinity of FN to the surface. However, it does not consider the interaction with already adsorbed FN or bare gold islands as such. Thus, the equilibrium constant should be always related to the surface coverage to avoid misinterpretation. Here, the K values fall in the same magnitude with the highest value for tHA0.19 and the lowest for tsHA0.49. Generally, the affinity of FN to the tsHA substrata was the lowest and increased for the tHep, tCS to tHA substrata.

3.4. Studies on the Bioactivity of tGAG-Modified Surfaces versus Cells

3.4.1. Fibroblast Adhesion and Spreading

Human fibroblasts (HFs) seeded on the different surfaces were stained for actin fibers, vinculin in FAs and nuclei after 4 h of incubation under protein-free conditions to ensure direct interaction between cells and surfaces.

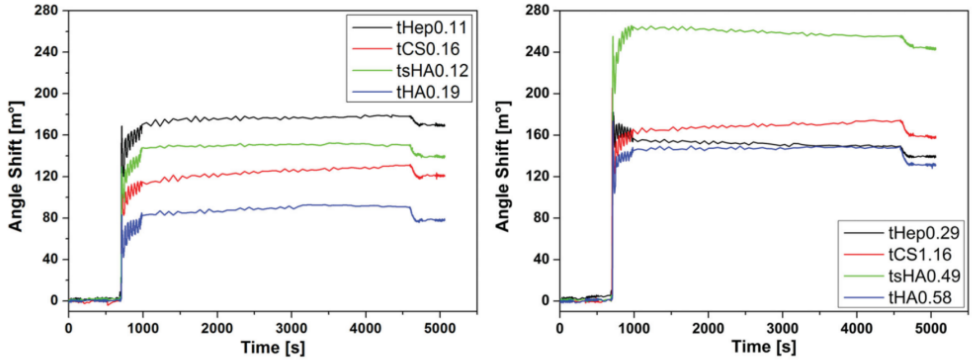

Figure 4. Results of real time adsorption of tGAGs on gold sensors determined with surface plasmon resonance (SPR). Left: thiolated GAGs with low degree of thiolation; right: thiolated GAGs with higher degree of thiolation. tHep: thiolated heparin; tCS: thiolated chondroitin sulfate; tsHA: thiolated, sulfated hyaluronic acid; tHA: thiolated hyaluronic acid.

Reprinted with permission from Journal of Macromolecular Bioscience, Alexander Köwitsch, Marcus S. Niepel, Georgios P. A. Michanetzis, Yannis F. Missirlis, Thomas Groth (2016), Effect of immobilized thiolated glycosaminoglycans on fibronectin adsorption and behavior of fibroblasts, 16, 381–394.

Macromolecular Bioscience
www.mbs-journal.de

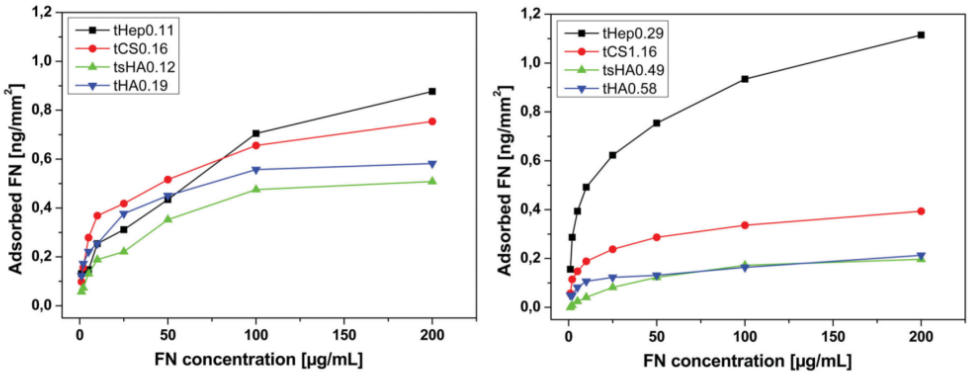

Figure 5. Results of fibronectin (FN) adsorption determined with surface plasmon resonance (SPR). Left: thiolated GAGs with low degree of thiolation; right: thiolated GAGs with higher degree of thiolation. tHep:- thiolated heparin; tCS: thiolated chondroitin sulfate; tsHA: thiolated, sulfated hyaluronic acid; tHA: thiolated hyaluronic acid.

After 4 h of adhesion, HFs were evenly distributed on the substrata. Lowest cell number was found on vinyl-terminated glass (Figure 6a). On both tHep substrata as well as on tCS1.16 and tsHA0.49 significantly more cells were found as compared to the vinyl-terminated surface ($p \leq 0.05$). Generally, surfaces coated with higher tGAGs promoted adhesion of HF to a higher extent than surfaces with tGAGs of lower thiolation degree. This effect was particularly pronounced on tCS and tsHA surfaces. In general, the tHA substrata showed the lowest cell adhesion from all GAGs. Images used for calculation of cell count per surface area were also used to assess the size of HF, which was about 2000 µm² for most of the investigated substrata (Figure 6b,c). Generally, cell size was not significantly different on all surfaces, except for tCS1.16, where cells were significantly larger than on tHep0.11, tHA0.58, and vinyl-terminated glass. A preadsorption of 2 µg mL^{-1} FN prior to cell seeding did not promote cell adhesion significantly, but showed a qualitative increase in cell number (Figure 6a). Here a significant increase was observed only on tCS0.16. Again, the lowest number of cells was found on vinyl-terminated glass, which was significantly lower than the cell counts on tHep and tCS substrata. Furthermore, significantly more cells were attached to tHep0.29 than on tsHA- and tHA-coated surfaces. The preadsorption of FN had also an effect on the spreading of cells. Here, HF significantly spread more on FN-coated vinyl-terminated glass and tHA0.58 in contrast to their noncoated counterparts. In addition, significantly smaller cells were found on tsHA0.12 compared to tHA- and tCS1.16-coated substrata after preadsorption of FN.

3.4.2. Cell Morphology

Cellular structures were stained to identify differences in overall cell morphology and organization of structures important for adhesion of cells, such as vinculin as part of FAs and filamentous actin as indicator for cell spreading and motility (Figure 7). HF seeded in the absence of FN and adherent on tHep0.11 and tsHA0.12 showed a round shape, while HF on tCS0.16 and tHA0.19 formed more filopodia (Figure 7, upper panel). In general, GAGs with a higher degree of thiolation promoted cell adhesion to a higher extent, resulting in larger cell size except for the tHA-coated substrata. Staining of the actin cytoskeleton (BODIPY-phalloidin, red) revealed elongated stress fiber

Table 4. Experimental results and theoretical parameters of the Langmuir linear regression for the adsorption of fibronectin on gold sensors coated with thiolated glycosaminoglycans. tHep: thiolated heparin; tCS: thiolated chondroitin sulfate; tsHA: thiolated, sulfated hyaluronic acid; tHA: thiolated hyaluronic acid.

	tHep0.11	tHep0.29	tCS0.16	tCS1.16	tsHA0.12	tsHA0.49	tHA0.19	tHA0.58
Γ_{exp} [a)] [ng mm^{-2}]	0.88	1.12	0.75	0.39	0.51	0.20	0.58	0.21
Γ_{max} [b)] [ng mm^{-2}]	0.95	1.15	0.78	0.40	0.55	0.25	0.61	0.21
K [c)] [×10^{-2}]	3.41	7.23	7.36	8.55	5.16	1.96	9.87	7.33
R^2 [d)]	0.92	0.98	0.99	0.99	0.98	0.99	0.99	0.97

[a)] Γ_{exp}: experimental surface coverage; [b)] Γ_{max}: maximum surface coverage; [c)] K: Langmuir equilibrium constant; [d)] R^2: square of the correlation coefficient.

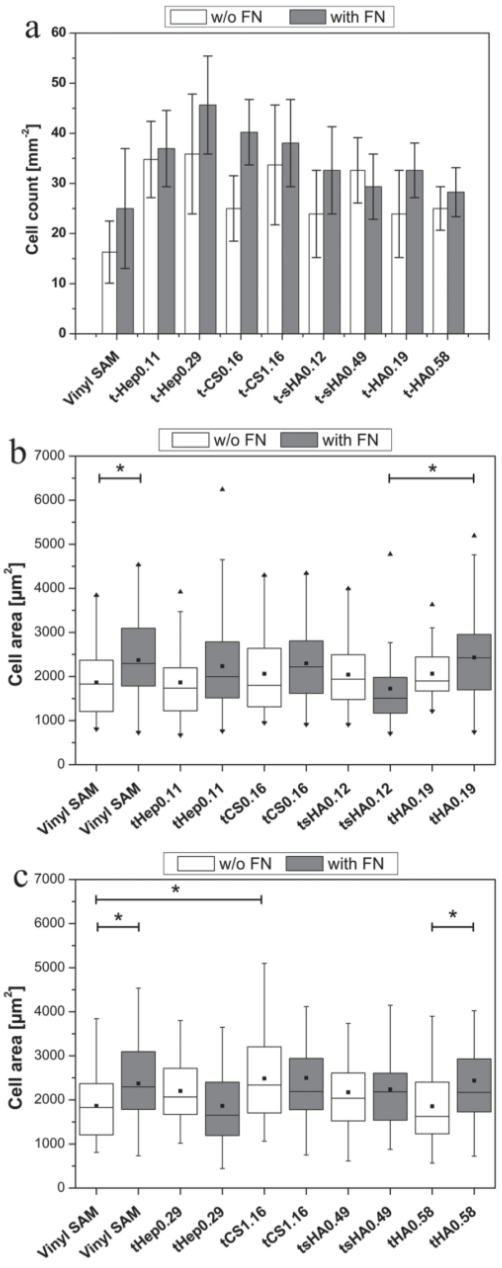

Figure 6. a) Count and b,c) area of HF after 4 h. The cells were seeded without (white) or with preadsorbed FN (2 µg mL^{-1}, gray). Box–whisker diagrams are used for cell area on b) low and c) high thiolated GAGs, where the box indicates the 25th and the 75th percentile, the median (dash) and mean (black square) values, respectively, whereas the 95%–5% confidence interval is represented by the whiskers. tHep: thiolated heparin; tCS: thiolated chondroitin sulfate; tsHA: thiolated, sulfated hyaluronic acid; tHA: thiolated hyaluronic acid; vinyl SAM: vinyl-terminated self-assembled monolayer on glass.

formation, especially for tHep0.29 and tCS1.16. FAs (vinculin, green) were almost absent on FN-free surfaces and primarily found at the end of the actin stress fibers in the cell periphery on tCS and tHep substrata. The preadsorption of FN had a promoting effect on actin fiber formation and cell size as well, particularly for surfaces that were modified with the low tGAGs. In addition, FA formation was enhanced on surfaces precoated with FN, indicated by the yellow spots in the merged images at the end of the actin fibers. On the tHA0.19-coated substrate with FN preadsorption, actin fibers were organized predominantly circumferentially with FA expressed at the periphery of the cells.

3.4.3. Cell Growth

Figure 8 shows the change in MA of cells on the different substrata using the QBlue viability assay. Here, the fluorescence signal is directly proportional to the quantity of viable cells and used to monitor the growth of cells from 24 to 72 h. Cells seeded on immobilized tHep surfaces showed similar MAs after 24, 48, and 72 h. The MA of HF on tCS surfaces was always higher for the low thiolation degree. Cells seeded on tsHA surfaces showed similar MA as cells on tHep-coated surfaces after 24 and 48 h. However, after 72 h almost no differences in MA were found in dependence on the thiolation degree. While cells on tHA0.19 had similar MA like cells on the other tGAGs with low degree of thiolation, cells on the high thiolated HA had the lowest MA of all substrata. Even after 72 h, the MA of HF on tHA0.58 was lower than for cells seeded on vinyl-terminated glass. In contrast, cell quantities on all other tGAGs were higher than on the primary vinyl-terminated surface. Along with that, cells on the highly conjugated samples of tCS1.16 and tHA0.58 show a considerably lower MA than HF on the other GAG samples. Overall, the quantity of HF cultured on tGAGs roughly doubled within 24 h.

4. Discussion

tGAGs with different degree of thiolation were covalently attached to vinyl-terminated glass or silicon surfaces to investigate if thiolation affects their bioactivity toward FN and HFs. Since a direct characterization of the covalent binding by spectroscopic methods is difficult to achieve due to the similar adsorption bands of thiols and sulfate groups, only indirect evidence for a covalent immobilization of tGAGs was delivered here by methods that characterize physical surface properties like wettability, surface potential, and topography of surfaces. Detailed information about these parameters is additionally useful since they have an impact on adsorption of proteins and adhesion of cells.[4,37] The determination of the surface

Reprinted with permission from Journal of Macromolecular Bioscience, Alexander Köwitsch, Marcus S. Niepel, Georgios P. A. Michanetzis, Yannis F. Missirlis, Thomas Groth (2016), Effect of immobilized thiolated glycosaminoglycans on fibronectin adsorption and behavior of fibroblasts, 16, 381–394.

Macromolecular
Bioscience
www.mbs-journal.de

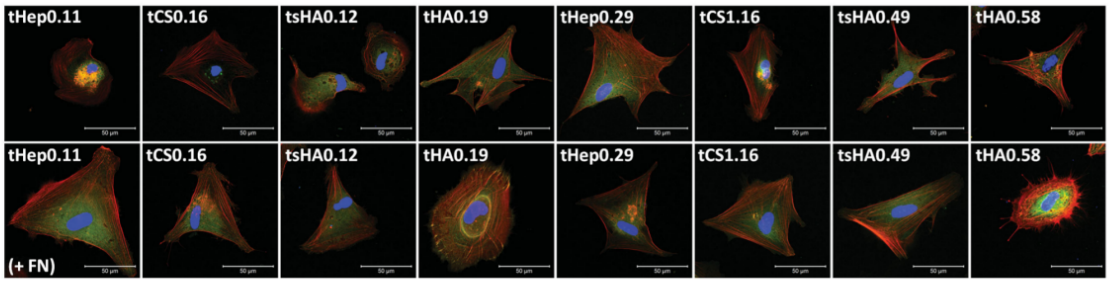

Figure 7. Cell morphology of HF on tGAGs without preadsorption of FN (upper panel) and precoated with 2 μg mL^{-1} FN (lower panel) after 4 h of incubation. Cells were stained for actin (red), vinculin (green), and nucleus (blue). [Scale: 50 μm] tHep: thiolated heparin; tCS: thiolated chondroitin sulfate; tsHA: thiolated, sulfated hyaluronic acid; tHA: thiolated hyaluronic acid.

wettability has shown that an immobilization of tGAGs to the underlying vinyl-SAM resulted in an increased wetting as it was expected because of the high charge density of GAGs. It was also observed that the surface wettability was further increased when GAGs of higher thiolation degree were immobilized. This indicates that additional free thiol groups led to an enhanced GAG coupling to the surface and, thus, a higher surface density of tGAGs. It is not surprising that the sulfation degree of the immobilized GAGs had also an effect on wetting properties, since heparin as the most sulfated GAGs exhibited the lowest WCA. On the other hand, the improved wettability of the immobilized tHA surfaces arose possibly due to the properties of HA to absorb large quantities of water.[38] Further, the higher molecular weight of the tHA0.58 (64 kDa, Table 1) compared to the other tGAGs could be a reason for higher surface coverage leading to a higher wettability of the system. Nevertheless, the tGAG surfaces were not as hydrophilic as expected since it was shown that substrata coated with native GAGs by adsorptive techniques as multilayers can have a WCA as low as 20°–40°.[39] A reason for that could be the insertion of the small, hydrophobic cross-linker DTPHY for thiolation of the GAGs.

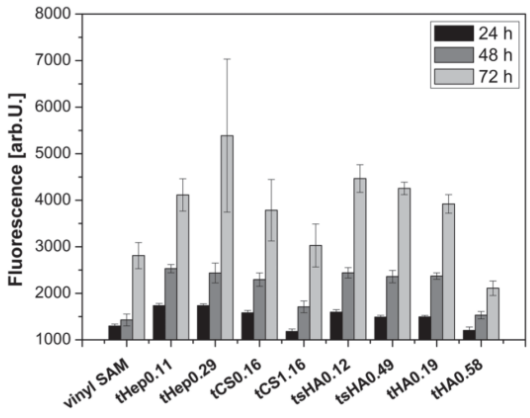

Figure 8. Metabolic activity of human dermal fibroblasts after 24 h (black), 48 h (dark gray), and 72 h (light gray) determined with QBlue assay. tHep: thiolated heparin; tCS: thiolated chondroitin sulfate; tsHA: thiolated, sulfated hyaluronic acid; tHA: thiolated hyaluronic acid.

ZP measurements were conducted to obtain information about surface charge density which also affects protein adsorption and cell attachment.[40] The linear dependence of the ZP of vinyl-terminated glass on the pH value is typical for nonpolar surfaces and indicates the adsorption of ions from solution which is driven by adsorption of hydroxyl ions at higher pH values.[41] Hence, tGAG-coated vinyl surfaces showed lesser negative ZP than vinyl-terminated glass at basic pH values. In addition, the sulfation of the immobilized molecules had a prominent effect on the ZP, since the nonsulfated tHA had the least negative potentials. Interestingly, the thiolation degree had no effect on the ZP of both tHA surfaces probably due to the high water absorption. Besides the sulfate groups, also the carboxylic acid groups are prone to be protonated resulting in less negative ZPs. A higher thiolation reduces the amount of carboxylic acid groups, hence, a less negative surface potential for tGAGs with a higher thiolation degree would be expected. However, such effect was only found for heparin-modified surfaces because a higher thiolation could also lead to more binding of tGAGs, which would increase the charge density and, thus, lower the ZP. In general, the sulfate degree seemed to have a stronger influence on the ZP of surfaces modified with sulfated GAGs, since the increased thiolation degree did not result in a lower negative potential. Since ZP measurements were started at pH 10, most of the remaining free thiols were present as negatively charged thiolates. Thus, it may explain why the highly thiolated tCS1.16 and tsHA0.49 had lower potentials at basic conditions compared to tHep0.29.

The AFM results in aqueous environment revealed tremendous differences in surface morphology between the different tGAGs depending on their thiolation degree.

Obviously, GAGs with a higher degree of thiolation showed larger surface structures, particularly the sulfated GAG. Here, it might be assumed that an excess of free thiol groups enables tGAGs to form disulfide bonds, leading to an increased intra- and intermolecular binding and resulting in the formation of larger aggregates.[42] Hence, the observed structures did not represent single, but aggregations of tGAG molecules. The larger diameter of the observed structures of higher tGAGs might be explained with a higher molecular weight (Table 1). Thus, the largest aggregates were found on tCS1.16 with a diameter of 20–80 nm, while on tHep0.11 (Ø = 15–30 nm) and tsHA0.12 (Ø = 20 nm) the smallest, sphere-like structures were found. However, the characteristic donut-like structures with similar dimensions (Ø = 30–50 nm) of both tHA-coated surfaces was unique and could be explained by the entanglement of HA chains which might be enhanced by disulfide formation.[43] In addition, the roughness parameters (Table 3) confirmed the visible results since they were increased for GAGs with a higher thiolation degree. The obtained surface roughness values might also explain the inconformity of WCA results with the sulfation of HA. In contrast to nanoroughness, an increased microroughness as obtained for tHA is known to increase the wettability of substrata.[44,45] Here, tHA displayed an increased roughness and is also showing a higher wettability than tsHA substrata. Overall, an almost complete surface coverage was observed on all immobilized GAG surfaces since no uncoated areas were detected with AFM.

Real-time adsorption measurements with SPR were used to estimate the amount of surface-bound tGAGs as well as FN adsorbed on tGAGs. It was expected that a higher thiol concentration results in a higher surface concentration of tGAGs. In fact, an increased immobilization of tGAGs on gold was observed for all tGAGs with the increased thiol content, except for tHep, which binding was slightly reduced from tHep0.11 (1.39 ng mm^{-2}) to tHep0.29 (1.14 ng mm^{-2}). For the native heparin molecule with a chain length of 25 disaccharides (0.85 nm per disaccharide) and a diameter of 1 nm a maximum surface coverage of 1.19 ng mm^{-2} can be calculated.[46] However, the tGAGs are not adsorbed in an ideal packed conformation which could be deduced from AFM images (Figure 3) that showed sphere-shaped aggregates. Furthermore, the larger aggregates found with AFM for tHep0.29 might have hindered the immobilization of additional tHep molecules onto adjacent surface areas. Hence, this would explain the high surface roughness in comparison to all other substrata. AFM results gave evidence that tHep0.29 assembled in an uneven manner. This would also explain the slight increase of the subsequent FN adsorption on tHep0.29 compared to tHep0.11 because the surface area for the interaction was much higher compared to the other sulfated GAGs, which were more evenly distributed. In general, the major adsorption of tGAGs already reached quasi-steady-state conditions after ≈10 min. Thereby, the tHep and tsHA samples showed a constant angle with no further shift, while tHA and, especially, tCS constantly increased with a reduced angle shift indicating that thermodynamic equilibrium conditions could not be reached within 60 min. Hence, additional molecules from solution might possibly be adsorbed by the formation of disulfide bonds with already adsorbed tGAGs that still have free thiol groups owing to the higher thiol concentration in comparison to tHep and tsHA.

The adsorption of FN was dependent on the type of GAGs immobilized on the gold surface. Always more FN adsorbed on tHep substrata due to its specific binding sites for heparin, even though the equilibrium constant was not the highest among the used GAGs.[47] Theoretically, an FN molecule (440 kDa) with a length of 120 nm and a diameter of 2 nm should result in a maximum surface coverage of 3.04 ng mm^{-2} if a monolayer of FN is adsorbed in a side-on conformation on 2D substrata.[48,49] Of course, the theoretic value does not consider repulsive or volume effects of adjacent molecules. Furthermore, an ideal, plane surface with no or negligible roughness would have to be assumed. However, the surface grafting of the tGAGs introduced a certain micro-roughness to the surface, which could increase the availability of adsorption sites for FN. Most importantly, all FN molecules would have to adsorb in a side-on conformation. The highest amount of FN was found on tHep0.29 with 1.12 ng mm^{-2} which represents 37% of the theoretical amount. Thiolated HAs as well as tsHA were not able to bind larger quantities because FN does not have a specific binding site for the immobilized HA-derivatives. The low amount of adsorbed FN on tsHA might be explained by an unequal sulfation pattern created by the chemical sulfation of HA. The sulfate groups could be distributed in a more uneven manner, resulting in regions of unsulfated HA and regions of highly sulfated HA. The latter could hamper the specific interaction with FN as observed for other biological processes like growth factor binding and neurite extension.[50,51] In contrast, the tCS-substrata showed a higher FN adsorption than the tHA surfaces because FN is capable to bind to CS at the high-affinity heparin binding site.[18,47] Here, the high degree of thiolation of tCS1.16 might have a negative effect on protein adsorption as well. The more carboxylic acid groups are consumed for thiolation, the less are available for ionic interactions with FN. Except for tHep0.29, tGAGs with higher thiolation degree always had reduced amounts of adsorbed FN, which indicated a loss of binding capacity at least for sulfated tGAGs due to a change of chemical structure. Further, FN could be bound in a conformation that might not be able

Reprinted with permission from Journal of Macromolecular Bioscience, Alexander Köwitsch, Marcus S. Niepel, Georgios P. A. Michanetzis, Yannis F. Missirlis, Thomas Groth (2016), Effect of immobilized thiolated glycosaminoglycans on fibronectin adsorption and behavior of fibroblasts, 16, 381–394.

of a reversible exchange or occupy a higher surface area, e.g., by unfolding processes.[49] Additionally, the material-induced fibrillogenesis of FN might play an important role during FN adsorption. An enhanced fibrillogenesis of FN was observed when the concentration of the applied FN solution was increased or the hydroxyl group density of the substrate was decreased. Others have also shown that sulfated material surfaces may drive fibrillogenesis of FN.[52]

Cell adhesion onto the tGAG substrata is guided by physicochemical interactions under protein-free conditions but will be also influenced by rapid secretion of proteins like FN from cells like fibroblasts.[53,54] In general, the surface wettability can strongly influence cell adhesion and cell spreading[55] and cells preferably adhere to moderately wettable surfaces (WCA ≈ 50°–60°) than to highly hydrophilic or hydrophobic surfaces.[28] Thus, the results of WCA can be used at least to some extent to explain initial cell adhesion behavior. Significantly, more cells adhered to the GAG-coated surfaces than to the vinyl-terminated glass due to the lowered hydrophobicity. In addition, the cell count on higher tGAGs was generally higher than on their lower thiolated counterparts because of obviously higher quantity of tGAG immobilization, leading to increased wettability as well as surface roughness. Moreover, the different tGAG-functionalized surfaces might have properties under protein-free conditions that enabled specific interaction with HF, thus, mediating adhesion, spreading, and proliferation. In general, cell count and cell area, which were increased under protein-free conditions for the tGAG surfaces with higher degree of thiolation, indicated that the increased amount of grafted tGAGs also supported cell attachment and spreading, which might also be a result of FN secreted by HF during culture.[53] One exception was tHA0.58 that showed a decrease in cell area caused probably by an increase in water binding and swelling, resulting in unfavorable conditions for cell adhesion and spreading.[56] Further, cell number and cell area were significantly increased on tCS1.16 compared to vinyl-SAM and tHA0.58 under protein-free conditions. The tHA-functionalized surfaces also showed the most prominent differences in actin polymerization and FA formation. Here, cells were round with a large fraction of circumferential actin fibers connected to FA plaques in the cell periphery. Further, the increased number of filopodia in cells on tHA0.58 in comparison to the other surfaces might be an additional indicator for the more soft nature of the underlying substrate, even though cell adhesion could be based on specific receptor–ligand interaction (CD44).[57,58] The increase in cell count and cell area induced by the preadsorption of FN was more prominent on the substrata with lower degree of thiolation, which initially displayed the lowest cell numbers. Hence, a lower thiolation degree results in a higher bioactivity in terms of protein adsorption. Particularly, the tCS0.16 showed a significant increase in cell number with FN present on the substrate. This is likely related to the ability of FN to bind to CS with one of its heparin-binding sites.[47] Interestingly, the highest cell numbers of all surfaces were found on tHep substrata, even when FN was absent. After preadsorption of FN, the cell size was increased on tHep0.11 but not on the tHep0.29-functionalized surface. On the other hand, HFs are able to secrete their own FN within 1 h after seeding, thus, leading to enhanced adsorption and making these substrata more cell supportive than the other tGAGs shown here.[53] Another significant effect on cell spreading was found when FN was applied to vinyl-terminated glass and tHA0.58 substrata. In all other cases, no such significant impact of the protein precoating was found since all coatings are biocompatible and receptor–ligand interactions could support adhesion of HF. However, the prominent effect of FN on cell spreading on hydrophobic surfaces is known.[59] Further, the type of hydrophobicity plays a crucial role for later bioactivity. In the case of the vinyl-terminated glass, the double bonds present on the surface might positively affect the FN conformation leading to improved cell spreading. Nevertheless, comparing hydrophilic and hydrophobic surfaces with similar amounts of FN resulted in pronounced cellular response on the hydrophilic material.[60] Although the amount of adsorbed FN was low on tsHA0.49 and tHA0.58 and the cell count did not reveal any significant differences, at least on the tHA0.58 FN seemed to adsorb in a conformation and amount favorable for cell adhesion. Further, the hydrophobic parts of the GAG chains might have contributed to FN adsorption.[61]

Cell growth experiments showed an increase in MA of HF on all GAG surfaces within the first 72 h, but in dependence on the sulfation and thiolation degree of the different GAGs. The low amount of metabolic active cells on tCS surfaces could have been due to its less hydrophilic nature together with a high negative charge. Even though tsHA was the least hydrophilic coating and exhibited the lowest initial cell numbers together with tHA, cell growth was increased in comparison to tCS surfaces. Here, proteins from the serum-containing medium possibly adsorbed in a sufficient amount and conformation favorable for cell adhesion and growth. Heparin surfaces were per se cell supportive in the presence of proteins[36] which was also initially represented in the highest cell count of all tGAGs. However, lowest growth of HF was found on the tHA0.59 surface, which along with the hydrophobic vinyl-SAM also had the lowest initial cell count after 4 h. For tHA, the low protein adsorption together with the high water uptake leading to highly viscoelastic coatings might be a reason for that.

Reprinted with permission from Journal of Macromolecular Bioscience, Alexander Köwitsch, Marcus S. Niepel, Georgios P. A. Michanetzis, Yannis F. Missirlis, Thomas Groth (2016), Effect of immobilized thiolated glycosaminoglycans on fibronectin adsorption and behavior of fibroblasts, 16, 381–394.
 DOI: 10.1002/mabi.201500276

5. Conclusion

tGAGs were used in this study to immobilize them on model surfaces and study their bioactivity toward FN and HF. The successful immobilization of tGAGs was shown by WCA and AFM measurements that also indicated an improved surface immobilization of higher tGAGs by an increase in wettability and surface roughness. Additionally, ZP measurements confirmed the surface immobilization of tGAGs to vinyl-terminated glass and showed a strong dependence on the presence of charged groups like sulfate and carboxylic acid groups of the immobilized tGAGs. Likewise, the immobilization of tGAGs on gold was increased for the higher tGAGs with the exception of tHep, which showed slight decrease. FN adsorption experiments showed that slightly more FN adsorbed on tHep0.29 than on tHep0.11 while other higher tGAGs could only bind half amount of FN compared to the lower tGAGs. This implied that a high degree of thiolation could deteriorate the biocompatibility of the GAG. Furthermore, the results of FN adsorption showed that naturally sulfated GAGs like heparin and CS adsorbed the highest amount of FN. Adhesion of HF under serum-free condition was guided by the sulfation of the immobilized tGAG. The highest cell counts were found on tHep-surfaces while tHA-functionalized substrata showed the lowest cell numbers. For tCS- and tsHA-surfaces, the cell count was increased for the higher thiolated samples while it was similar for tHep and tHA. Thus, a higher degree of thiolation did not negatively affect cell adhesion. In general, cells were able to sense FN adsorbed on the tGAG-substrata, which was also observed via immunofluorescence by an enhanced actin fiber formation and the development of FA. Interestingly, the cell shape on tHA-functionalized surfaces was also affected by FN adsorption and FA might have been generated by specific CD44-HA interactions. Even though HFs were proliferating over a time period of 72 h, the highly thiolated tCS1.16 and tHA0.58 showed an initial delay of cell growth attributed to a reduction of protein binding capability as indicated by FN adsorption measurements. Although to a different extent, the applied GAGs were highly biocompatible, enabling their application as coating materials for tissue engineering applications. The most prominent differences were found regarding their FN binding capability allowing an application as real-time detection unit (biosensor) for specific binding partners such as growth factors. The application range of the presented coatings is widespread as GAG–protein interactions play a key role in biochemical signaling processes in cell systems.[62] For example, HA could be used as nonadhesive biomaterial coating due to its anti-fouling properties. Further, it has a unique ability to interact specifically with cancer cells giving insight into different stages of cancer development.[63,64] Heparin coatings for implantable materials could prevent blood-mediated inflammation.[65] Additionally, the preparation of 3D-constructs like scaffolds or hydrogels by disulfide formation of the tGAGs or by cross-linking with reactive binding partners like vinyl sulfone species can open new application pathways.[66,67]

Acknowledgements: This work was supported by the European Union Seventh Framework Programme (FP7/2007-2013) under grant agreement no. NMP4-SL-2009-229292 ("Find & Bind"). The work was funded partly by German Academic Exchange Service and the Greek State Scholarships Foundation-IKY in the frame of bilateral cooperation between Germany and Greece. The authors are grateful for the provision of the sulfated hyaluronic acid by INNOVENT e.V. (Germany).

Received: July 22, 2015; Revised: October 10, 2015; Published online: November 30, 2015; DOI: 10.1002/mabi.201500276

Keywords: fibroblast adhesion; fibronectin adsorption; glycosaminoglycans; sulfation degree; surface modification

[1] S. Bauer, P. Schmuki, K. von der Mark, J. Park, *Prog. Mater. Sci.* **2013**, *58*, 261.
[2] M. P. Lutolf, P. M. Gilbert, H. M. Blau, *Nature* **2009**, *462*, 433.
[3] P. Roach, D. Eglin, K. Rohde, C. C. Perry, *J. Mater. Sci.: Mater. Med.* **2007**, *18*, 1263.
[4] E. A. Dubiel, Y. Martin, P. Vermette, *Chem. Rev.* **2011**, *111*, 2900.
[5] A. Ulman, *Chem. Rev.* **1996**, *96*, 1533.
[6] J. C. Love, L. A. Estroff, J. K. Kriebel, R. G. Nuzzo, G. M. Whitesides, *Chem. Rev.* **2005**, *105*, 1103.
[7] X.-L. Sun, C. L. Stabler, C. S. Cazalis, E. L. Chaikof, *Bioconjugate Chem.* **2006**, *17*, 52.
[8] N. Faucheux, R. Schweiss, K. Lutzow, C. Werner, T. Groth, *Biomaterials* **2004**, *25*, 2721.
[9] L. Fu, G. Y. Li, B. Yang, A. Onishi, L. Y. Li, P. L. Sun, F. M. Zhang, R. J. Linhardt, *J. Pharm. Sci.* **2013**, *102*, 1447.
[10] N. Volpi, *Chondroitin Sulfate: Structure, Role and Pharmacological Activity*, Elsevier, Amsterdam **2006**, p. xxvi.
[11] B. P. Toole, *Nat. Rev. Cancer* **2004**, *4*, 528.
[12] V. Hintze, S. Moeller, M. Schnabelrauch, S. Bierbaum, M. Viola, H. Worch, D. Scharnweber, *Biomacromolecules* **2009**, *10*, 3290.
[13] S. M. Opal, C. M. Kessler, J. Roemisch, S. Knaub, *Crit. Care Med.* **2002**, *30*, S325.
[14] L. Kjellen, U. Lindahl, *Annu. Rev. Biochem.* **1991**, *60*, 443.
[15] A. Woods, J. McCarthy, L. Furcht, J. Couchman, *Mol. Biol. Cell* **1993**, *4*, 605.
[16] O. A. Ibrahimi, F. Zhang, S. C. Lang Hrstka, M. Mohammadi, R. J. Linhardt, *Biochemistry* **2004**, *43*, 4724.
[17] C. J. Rogers, P. M. Clark, S. E. Tully, R. Abrol, K. C. Garcia, W. A. Goddard, L. C. Hsieh-Wilson, *Proc. Natl. Acad. Sci. USA* **2011**, *108*, 9747.
[18] F. J. Barkalow, J. E. Schwarzbauer, *J. Biol. Chem.* **1994**, *269*, 3957.
[19] S. Bierbaum, T. Douglas, T. Hanke, D. Scharnweber, S. Tippelt, T. K. Monsees, R. H. Funk, H. Worch, *J. Biomed. Mater. Res. Part A* **2006**, *77*, 551.
[20] B. Yang, B. L. Yang, R. Savani, E. A. Turley, *EMBO J.* **1994**, *13*, 286.

[21] S. Banerji, A. J. Wright, M. Noble, D. J. Mahoney, I. D. Campbell, A. J. Day, D. G. Jackson, *Nat. Struct. Mol. Biol.* **2007**, *14*, 234.
[22] P. K. Thalla, H. Fadlallah, B. Liberelle, P. Lequoy, G. De Crescenzo, Y. Merhi, S. Lerouge, *Biomacromolecules* **2014**, *15*, 2512.
[23] N. Altgärde, E. Nilebäck, L. De Battice, I. Pashkuleva, R. L. Reis, J. Becher, S. Möller, M. Schnabelrauch, S. Svedhem, *Acta Biomater.* **2013**, *9*, 8158.
[24] M. N. Collins, C. Birkinshaw, *Carbohydr. Polym.* **2013**, *92*, 1262.
[25] S. J. Hollister, *Nat. Mater.* **2005**, *4*, 518.
[26] L. Vodná, S. Bubenikova, D. Bakoš, *Macromol. Biosci.* **2007**, *7*, 629.
[27] X.-H. Qin, P. Gruber, M. Markovic, B. Plochberger, E. Klotzsch, J. Stampfl, A. Ovsianikov, R. Liska, *Polym. Chem.* **2014**, *5*, 6523.
[28] A. Köwitsch, Y. Yang, N. Ma, J. Kuntsche, K. Mäder, T. Groth, *Biotechnol. Appl. Biochem.* **2011**, *58*, 376.
[29] K. P. Vercruysse, D. M. Marecak, J. F. Marecek, G. D. Prestwich, *Bioconjugate Chem.* **1997**, *8*, 686.
[30] A. Köwitsch, M. Jurado Abreu, A. Chhalotre, M. Hielscher, S. Fischer, K. Mäder, T. Groth, *Carbohydr. Polym.* **2014**, *114*, 344.
[31] G. L. Ellman, *Arch. Biochem. Biophys.* **1959**, *82*, 70.
[32] P. W. Riddles, R. L. Blakeley, B. Zerner, *Anal. Biochem.* **1979**, *94*, 75.
[33] J. Amici, P. Allia, P. Tiberto, M. Sangermano, *Macromol. Chem. Phys.* **2011**, *212*, 1629.
[34] D. Weinrich, P. C. Lin, P. Jonkheijm, U. T. Nguyen, H. Schröder, C. M. Niemeyer, K. Alexandrov, R. Goody, H. Waldmann, *Angew. Chem. Int. Ed.* **2010**, *49*, 1252.
[35] R. B. M. Schasfoort, A. J. Tudos, *Handbook of Surface Plasmon Resonance*, 1st ed., RSC Publishing, Cambridge **2008**, p. 128.
[36] M. S. Niepel, D. Peschel, X. Sisquella, J. A. Planell, T. Groth, *Biomaterials* **2009**, *30*, 4939.
[37] M. S. Lord, M. Foss, F. Besenbacher, *Nano Today* **2010**, *5*, 66.
[38] A. Albersdorfer, E. Sackmann, *Eur. Phys. J. B* **1999**, *10*, 663.
[39] N. Aggarwal, N. Altgarde, S. Svedhem, G. Michanetzis, Y. Missirlis, T. Groth, *Macromol. Biosci.* **2013**, *13*, 1327.
[40] G. Altankov, K. Richau, T. Groth, *Materialwiss. Werkstofftech.* **2003**, *34*, 1120.
[41] C. Werner, H. J. Jacobasch, *Int. J. Artif. Organs* **1999**, *22*, 160.
[42] K. Yamamoto, S. Migita, *J. Biol. Chem.* **1983**, *258*, 7887.
[43] M. K. Cowman, C. Spagnoli, D. Kudasheva, M. Li, A. Dyal, S. Kanai, E. A. Balazs, *Biophys. J.* **2005**, *88*, 590.
[44] R. N. Wenzel, *Ind. Eng. Chem.* **1936**, *28*, 988.
[45] A. Cassie, S. Baxter, *Trans. Faraday Soc.* **1944**, *40*, 546.
[46] D. L. Rabenstein, *Nat. Prod. Rep.* **2002**, *19*, 312.
[47] R. Pankov, K. M. Yamada, *J. Cell Sci.* **2002**, *115*, 3861.
[48] H. P. Erickson, N. Carrell, J. McDonagh, *J. Cell Biol.* **1981**, *91*, 673.
[49] M. Bergkvist, J. Carlsson, S. Oscarsson, *J. Biomed. Mater. Res. Part A* **2003**, *64*, 349.
[50] R. J. Gilbert, R. J. McKeon, A. Darr, A. Calabro, V. C. Hascall, R. V. Bellamkonda, *Mol. Cell. Neurosci.* **2005**, *29*, 545.
[51] C. I. Gama, S. E. Tully, N. Sotogaku, P. M. Clark, M. Rawat, N. Vaidehi, W. A. Goddard, A. Nishi, L. C. Hsieh-Wilson, *Nat. Chem. Biol.* **2006**, *2*, 467.
[52] P. Rico, J. C. R. Hernández, D. Moratal, G. Altankov, M. M. Pradas, M. Salmerón-Sánchez, *Tissue Eng. Part A* **2009**, *15*, 3271.
[53] F. Grinnell, M. K. Feld, *Cell* **1979**, *17*, 117.
[54] L. Chou, J. D. Firth, V.-J. Uitto, D. M. Brunette, *J. Cell Sci.* **1995**, *108*, 1563.
[55] M. Morra, *Biomacromolecules* **2005**, *6*, 1205.
[56] R. J. Pelham, Y.-l. Wang, *Proc. Natl. Acad. Sci. USA* **1997**, *94*, 13661.
[57] J. A. Travis, M. G. Hughes, J. M. Wong, W. D. Wagner, R. L. Geary, *Circ. Res.* **2001**, *88*, 77.
[58] S. R. Hamilton, S. F. Fard, F. F. Paiwand, C. Tolg, M. Veiseh, C. Wang, J. B. McCarthy, M. J. Bissell, J. Koropatnick, E. A. Turley, *J. Biol. Chem.* **2007**, *282*, 16667.
[59] W. Norde, J. Lyklema, *J. Biomater. Sci., Poly. Ed.* **1991**, *2*, 183.
[60] G. K. Toworfe, R. J. Composto, C. S. Adams, I. M. Shapiro, P. Ducheyne, *J. Biomed. Mater. Res. Part A* **2004**, *71*, 449.
[61] J. E. Scott, *FASEB J.* **1992**, *6*, 2639.
[62] L. A. Lasky, *Annu. Rev. Biochem.* **1995**, *64*, 113.
[63] A. Afify, P. Purnell, L. Nguyen, *Exp. Mol. Pathol.* **2009**, *86*, 95.
[64] K. Williams, K. Motiani, P. V. Giridhar, S. Kasper, *Exp. Biol. Med.* **2013**, *238*, 324.
[65] S. Cabric, J. Sanchez, T. Lundgren, A. Foss, M. Felldin, R. Källen, K. Salmela, A. Tibell, G. Tufveson, R. Larsson, *Diabetes* **2007**, *56*, 2008.
[66] X. Z. Shu, Y. C. Liu, Y. Luo, M. C. Roberts, G. D. Prestwich, *Biomacromolecules* **2002**, *3*, 1304.
[67] R. Jin, L. M. Teixeira, A. Krouwels, P. Dijkstra, C. Van Blitterswijk, M. Karperien, J. Feijen, *Acta Biomater.* **2010**, *6*, 1968.

Reprinted with permission from Journal of Macromolecular Bioscience, Alexander Köwitsch, Marcus S. Niepel, Georgios P. A. Michanetzis, Yannis F. Missirlis, Thomas Groth (2016), Effect of immobilized thiolated glycosaminoglycans on fibronectin adsorption and behavior of fibroblasts, 16, 381–394.
 DOI: 10.1002/mabi.201500276

Chapter 5

Summary – Functionality of surface-coupled oxidised glycosaminoglycans towards fibroblast adhesion:

The aim of this work was to functionalize different glycosaminoglycans (GAG) by applying periodate-mediated oxidation to obtain reactive aldehydes which can be used to covalently attach the GAG to amino-terminated substrata. Moreover, the biological properties of the glycanized substrata should be examined towards fibroblast adhesion.

The GAG hyaluronan (HA), sulfated hyaluronan (HAS), chondroitin sulfate (CS) and heparin (HEP) were oxidized with sodium periodate to generate aldehydes (aGAG) by cleaving the C2-C3 bond of the uronic acid monomers of GAG. The chemical structure, molecular weight and the aldehyde concentration of the newly synthesized aGAG were determined with FT-IR, field-flow fractionation and UV-Vis spectroscopy applying Schiff`s reagent, respectively. A decrease of the molecular weight of aGAG compared to native GAG was found because periodate-oxidation also occurred at the glycosidic linkage between monosaccharides. The newly introduced aldehydes were confirmed by a new carbonyl shoulder in FT-IR and quantified by Schiff`s reagent to range from a concentration of 8.2×10^{-4} mol/g (aHAS) to 12.9×10^{-4} mol/g (aCS).

The aGAG were directly immobilized to amino-terminated model substrata from solutions with a concentration of 4 mg/mL for overnight and the formed imine bond was subsequently reduced by sodium cyanoborohydride to yield a stable secondary amine. The successful immobilization of aGAG was confirmed by water contact angle, zeta potential (ZP), ellipsometry measurements and atomic force microscopy (AFM). The wettability of the amino-terminated glass was significantly decreased by the immobilization of aGAG in relation to their sulfation. Also ZP of the surfaces were dependent on the sulfate content of the immobilized aGAG. Thus, aHEP was characterized as most wettable surface and displayed the most negative surface charge. The thickness of surface layers measured by ellipsometry indicated a predominant side-on immobilization of all aGAG as it was ranging between 0.36 nm for aHAS and 1.94 nm for aCS-coated substrata. AFM studies revealed that the

immobilization of aHA led to a rather smooth surface coating with a low surface roughness while immobilization of sulfated aGAG was characterized by surfaces exhibiting granular structures with higher roughness.

Human fibroblast adhesion was studied under serum-free conditions to learn about the bioactivity of the immobilized aGAG. It was found that the increase in sulfation degree of aGAG was accompanied by increased adhesion and spreading of cells. This was additionally confirmed by a stronger expression of focal adhesions and cytoskeletal structures visualized with immunofluorescence staining. By contrast, cell adhesion and spreading were lower on aHA. Moreover, it was shown that cells in contact with aHA revealed a stronger expression of CD44, which might represent an alternative mechanism of cellular adhesion.

The results show that aGAG can be successfully applied for the development of bioactive surface coatings which could be applied as a biomimetic microenvironment to engineer surfaces of implants and scaffolds for tissue regeneration.

JOURNAL OF
Bioactive
and
Compatible
Polymers

Original Article

Functionality of surface-coupled oxidised glycosaminoglycans towards fibroblast adhesion

Journal of Bioactive and
Compatible Polymers
1–17

DOI: 10.1177/0883911515599999
jbc.sagepub.com
SAGE

Yuan Yang[1], Alexander Köwitsch[1], Ning Ma[1], Karsten Mäder[2], Iva Pashkuleva[3,4], Rui L Reis[3,4] and Thomas Groth[1]

Abstract

Glycosaminoglycans are able to bind many growth factors and adhesive proteins, which affect cell activities such as adhesion, migration, growth and differentiation. Chondroitin sulphate, hyaluronan, sulphated hyaluronan and heparin were oxidised here (aldehyde glycosaminoglycans) to generate aldehydes on vicinal hydroxyl groups of the uronic monomers of glycosaminoglycans for subsequent direct covalent binding to amino-terminated model substrata. The properties of modified surfaces were monitored by water contact angle, zeta potential, ellipsometry measurements and atomic force microscopy showing successful immobilisation of aldehyde glycosaminoglycans. Wetting properties and zeta potentials were related to sulphate content of aldehyde glycosaminoglycans with aldehyde heparin as most wettable and negative surface and aldehyde hyaluronan as the least. The thickness of surface layers measured by ellipsometry indicated a predominant side-on immobilisation of all aldehyde glycosaminoglycans. Atomic force microscopy studies showed that immobilisation of aldehyde hyaluronan lead to a rather smooth surface coating while immobilisation of sulphated aldehyde glycosaminoglycans was characterised by a globular appearance of surfaces with higher roughness. The experiments with human fibroblast studying adhesion under serum-free conditions were carried out to learn about bioactivity of aldehyde glycosaminoglycans. It was observed that the increase in sulphation degree of aldehyde glycosaminoglycans was accompanied by increased adhesion and spreading of cells with stronger

[1]Biomedical Materials Group, Institute of Pharmacy, Martin Luther University Halle-Wittenberg, Halle (Saale), Germany
[2]Pharmaceutical Technology Group, Institute of Pharmacy, Martin Luther University Halle-Wittenberg, Halle (Saale), Germany
[3]3B's Research Group – Biomaterials, Biodegradables and Biomimetics, University of Minho, Headquarters of the European Institute of Excellence on Tissue Engineering and Regenerative Medicine, Guimaraes, Portugal
[4]ICVS/3B's – PT Government Associate Laboratory, Braga/Guimaraes, Portugal

Corresponding author:
Thomas Groth, Biomedical Materials Group, Institute of Pharmacy, Martin Luther University Halle-Wittenberg, Heinrich-Damerow-Strasse 4, 06120 Halle (Saale), Germany.
Email: thomas.groth@pharmazie.uni-halle.de

expression of focal adhesions and cytoskeletal structures. By contrast, cell adhesion and spreading were lower on aldehyde hyaluronan. Immunofluorescence staining of cells in contact with aldehyde hyaluronan revealed a stronger expression of CD44, which can represent an alternative route of cell adhesion. The results show that oxidised glycosaminoglycans can be successfully applied for the development of bioactive surface coatings. The created biomimetic microenvironment may be useful to engineer surfaces of implants and scaffolds for tissue regeneration.

Keywords
Glycosaminoglycans, sulphation degree, oxidation, surface immobilisation, bioactivity, fibroblast adhesion

Introduction

Historically, biomaterial surface engineering was used to generate biologically compatible surfaces that minimise the body's response to foreign devices. Nowadays, this approach has shifted to the design and development of biomimetic surfaces that specifically interact and respond to the in vivo environment at the implantation site, and thus, direct cell attachment, growth and differentiation.[1] Ideally, such surface engineering supports faster regeneration of damaged tissue with the formation of new blood vessels and/or better bonding of the implant material to the surrounding tissue.[2,3] Following this tendency, a large body of work has been devoted to the immobilisation of short peptide sequences that mimic bioactive portions from protein components of the extracellular matrix (ECM).[4] These short peptides activate selectively different integrin adhesion receptors triggering signalling pathways.[5,6] Although this approach represented a great progress in surface bioengineering, it addressed mainly integrins, while peptide sequences are less suitable to regulate the activity of receptors controlling cell growth and differentiation.[7]

Herein, we are exploring another class of bioactive molecules – glycosaminoglycans (GAGs). Similar to the proteins, GAGs (alone or as conjugates, i.e., proteoglycans) are important components of cell surface receptors and ECM – the natural surroundings of cells in tissues.[8] GAGs are linear polysaccharides made of disaccharide building blocks consisting of an amino sugar (*N*-acetylglucosamine or *N*-acetylgalactosamine) and an uronic acid (glucuronic acid or iduronic acid). There are four major types of GAGs: heparin (HEP)/heparan sulphate, chondroitin sulphate (CS)/dermatan sulphate, keratan sulphate and hyaluronan (HA). GAGs' chains are sulphated to various degrees with only one exception: HA is not sulphated and the only one that exists as a free GAG, that is, not as protein conjugate.[8] GAGs are able to bind non-covalently a plethora of proteins that possess specific binding sites for GAG sequences; ECM proteins, such as collagens, fibronectins and laminins that bind to integrin adhesion receptors belong to this group.[9] However, also chemokines and growth factors, such as stromal cell–derived factor 1 (SDF-1), fibroblast growth factors (FGFs), bone morphogenic proteins (BMPs) controlling migration, homing, growth and differentiation of cells have a high affinity particularly to sulphated GAGs.[10,11] A common mechanism of affinity is given by the presence of HEP-binding domains in these proteins, which indicates a high affinity to sulphated GAGs and like molecules.[12] HA also promotes cell activities such as initial cell attachment and migration via direct binding to cell receptors RHAMM and CD44.[13] Because of the multiple interactions of GAG with different classes of ECM proteins and cell surface receptors, they play not only a role in processes such as development, homeostasis and wound healing but also in pathological processes such as inflammation, cancer development and progression.[10,13–15]

Reprinted with permission from Journal of Bioactive and Compatible Polymers, Yuan Yang, Alexander Köwitsch, Ning Ma, Karsten Mäder, Iva Pashkuleva, Rui L. Reis, Thomas Groth (2015), Functionality of surface-coupled oxidised glycosaminoglycans towards fibroblast adhesion, 31 (2), 191-207.
 DOI: 10.1177/0883911515599999

Therefore, immobilisation of GAG on material surfaces is a promising approach to generate biomimetic coatings on medical implant materials and can also be useful for the development of in vitro models for studying interaction of GAG with growth factors and cells.[16–18] A major requirement for any immobilisation approach is not to compromise the biological activity of GAG. A common approach towards the immobilisation of glycans is the reaction between their reducing end and amino- or hydrazide-activated surfaces via reductive amination. However, this method is utilised mainly for monosaccharides or short oligosaccharides,[19] while the covalent binding of larger polysaccharides is difficult because of steric reasons. An alternative approach is a multivalent immobilisation that requires generation of multiple reactive species along the polysaccharide chain, which react with functional groups on material surfaces. Here, we used the oxidation of the uronic acid component of GAG to generate reactive aldehydes (aldehyde glycosaminoglycans (aGAGs)) that bind to amino-functionalised model surfaces by reductive amination. Our approach should demonstrate the feasibility of this simple method of immobilisation of GAGs on biomaterial surfaces. In particular, changes in physical surface properties were used to show that physical surface properties such as wettability and surface potential are changed by the immobilisation of aGAGs. Most important, however, were studies on human fibroblast (HF) adhesion to show that oxidation did not hamper the bioactivity of GAGs. The results are reported herein.

Materials and methods

Materials

HA sodium salt (molecular weight (Mw) 923 kDa) was provided by Kraeber & Co GmbH (Ellerbek, Germany). Hyaluronan sulphate, sodium salt (Mw 94 kDa, degree of sulphation (DS) 1.3, sulphated hyaluronan (HAS)) was synthesised according to Hintze et al.[20] and provided by INNOVENT e.V. (Jena, Germany). CS sodium salt (Mw 25 kDa) was purchased from Sigma–Aldrich (Schnelldorf, Germany). HEP sodium salt (Mw 15 kDa) was provided by Serva (Heidelberg, Germany). Sodium cyanoborohydride ($NaBH_3CN$) was purchased from Merck KGaA (Darmstadt, Germany). Sodium periodate ($NaIO_4$), Schiff's fuchsin–sulphite reagent, glutaric dialdehyde and Triton X-100 were obtained from Sigma–Aldrich. The dialysis bag (Spectra/Pore membrane; Mw cutoff = 3500), Roti-Histofix and organic solvents were provided by Roth (Karlsruhe, Germany). Other used compounds were 3-aminopropyltriethoxysilane (APTES) (ABCR GmbH & Co. KG, Karlsruhe, Germany) and phosphate buffered saline (PBS) prepared according to the following formulation: 2.7 mM KCl, 137 mM NaCl, 1.4 mM KH_2PO_4, 4.3 mM $Na_2HPO_4 \times 2H_2O$ and pH 7.4.

Preparation and characterisation of aGAGs

Preparation of aGAGs

The method used here was slightly modified to a previously described protocol.[21] HA (0.5 g), HAS (DS = 1.3, 0.5 g), CS (0.5 g) and HEP (0.5 g) were dissolved in 80 mL H_2O, respectively, in a flask that was wrapped with aluminium foil. Different amounts of $NaIO_4$ were added to the solutions of GAG. The reaction mixture was stirred for 6 h for HA, CS and HEP and 3 h for HAS at room temperature (RT) in the dark. Various feed mole of $NaIO_4$ and reaction times were applied based on previous studies[22] targeting similar oxidation degree of all GAGs leading to introduction of aldehyde groups. Therefore, all products are named aGAG in general and aldehyde hyaluronan (aHA), and so on specifically. The solutions were purified by dialysis against distilled water for 3 days. The final products were obtained by freeze-drying and stored at 4°C.

Reprinted with permission from Journal of Bioactive and Compatible Polymers, Yuan Yang, Alexander Köwitsch, Ning Ma, Karsten Mäder, Iva Pashkuleva, Rui L. Reis, Thomas Groth (2015), Functionality of surface-coupled oxidised glycosaminoglycans towards fibroblast adhesion, 31 (2), 191-207.
 DOI: 10.1177/0883911515599999

Characterisation of aGAGs

The quantity of aldehyde groups was determined using Schiff's reagent via ultraviolet–visible (UV-VIS) spectroscopy. A calibration curve for determination of the aldehyde content was established with glutaric dialdehyde as a standard substance. The procedure was carried out by adding 2.5 mL of Schiff's reagent to a sample of 0.5 mL of aGAG (4 mg/mL). The absorbance of the coloured complex was measured at 550 nm within 40 min. The chemical structures of aGAGs were analysed by Fourier transform infrared (FT-IR) (IFS 28; Bruker, Ettlingen, Germany). The sulphate content was measured by elemental analysis with a LECO CHNS-932 (LECO Instrumente GmbH, Mönchengladbach, Germany). The molecular weight and polydispersity of aGAGs were measured by asymmetrical flow field-flow fractionation (4F) equipped with a Dawn EOS detector (Wyatt Technology Corp. (Dernbach, Germany)) and an RI-Detector (Shodex; RI-101 (Munich, Germany)). All samples were measured in 50 mM NaCl containing 0.02% NaN_3 (w/v) to prevent bacterial growth. Molecular weights were calculated using Astra software (Wyatt Technology Corp.)

Functionalisation and characterisation of substrata

Preparation of model substrata

Glass cover slides (Menzel GmbH + Co KG, Braunschweig, Germany) were cleaned by immersion in freshly prepared Piranha solution of a mixture of H_2O_2 and H_2SO_4 (30/70 v/v) for 1 h. Afterwards, the glass surfaces were washed with Milli-Q water (0.055 mS/cm, 10 cycles for 6 min each) and dried under a stream of nitrogen. Silicon wafers (15 × 15 mm^2; Silicon Materials, Kaufering, Germany) were treated with a solution of NH_4OH (27%), H_2O_2 (30%) and water (1:1:5 v/v/v) at 70°C for 15 min and subsequently washed with copious amount of Milli-Q water. Afterwards, the silicon wafers were also dried with a stream of nitrogen.

Preparation of amino-terminated glass and silicon

The amino-terminated surfaces were prepared by immersion of clean glass or silicon in a solution of APTES in ethanol (1% v/v) for 1 h according to Faucheux et al.[23] Small amounts of concentrated acetic acid were added to the solution to accelerate the condensation reaction. Fresh APTES solution was prepared immediately before the silanisation was started. The surfaces were then rinsed extensively with copious amount of ethanol and Milli-Q water and finally dried with nitrogen flow.

Immobilisation of aGAGs

The immobilisation of aGAGs on NH_2-terminated surfaces (glass and silicon) was achieved by reductive amination. A solution of 1 mL aGAG (4.0 mg/mL in PBS, pH 7.4) was applied to NH_2-modified surfaces and kept for 24 h at RT. Then 1 mL $NaBH_3CN$ (3.0 mg/mL in PBS) was added to the same solution to create a stable bond by reducing Schiff's base. The solution was kept at 4°C for 24 h. Then, the aGAG-coated surface was rinsed by copious amounts of PBS and Milli-Q water and then dried with a stream of nitrogen.

Characterisation of aGAG-modified surfaces

Water contact angle

Static water contact angle (WCA) measurements were performed with an OCA 15 Plus device from DataPhysics (Filderstadt, Germany) applying the sessile drop method to measure the wetting

Reprinted with permission from Journal of Bioactive and Compatible Polymers, Yuan Yang, Alexander Köwitsch, Ning Ma, Karsten Mäder, Iva Pashkuleva, Rui L. Reis, Thomas Groth (2015), Functionality of surface-coupled oxidised glycosaminoglycans towards fibroblast adhesion, 31 (2), 191-207.
 DOI: 10.1177/0883911515599999

changes after surface modification of substrata and immobilisation of aGAGs. Five droplets of 3 µL ultrapure water were applied to each of the nitrogen-dried sample surfaces and the obtained values were used to calculate means and standard deviations.

Ellipsometry

The changes in layer thickness of the modified silicon surfaces were determined by ellipsometry (M-2000V; J.A. Woollam Co. Inc., Lincoln, NE, USA) at a range of angles from 65° to 85°. A refractive index of 1.45 was used for all samples which is recommended for such kind of surfaces.[24] The measurements were performed three times at different locations on the surface of dry samples and averaged. The experimental data were analysed with the WVase32 software provided with the equipment.

Zeta potential

Zeta potential was measured using a SurPASS device (Anton Paar, Graz, Austria). The glass cover slips with the immobilised aGAGs were placed in the equipment and the gap was adjusted to a distance that allows a flow rate between 100 and 150 mL/min under a maximum pressure of 300 mbar; 1 mM KCl was used as model electrolyte. Before starting the measurement, the pH value of the model electrolyte was adjusted to pH 10.5 using 1 N NaOH. The measurements were carried out in automated titration mode using 0.1 N HCl for a range from pH 10.5 to 4.0, which was adjusted by two titration steps: 0.03 mL from pH 10.5 to 5.0 and 0.25 mL from pH 5.0 to 4.0.

Atomic force microscopy

Atomic force microscopy (AFM) was performed with a 3D-Molecular Force Probe instrument (MFP-3D-BIO; Asylum Research, Santa Barbara, CA, USA) and ACT cantilevers (Applied NanoStructures Inc., Santa Clara, CA, USA) with a resonance frequency of 300 kHz and a spring constant of 40 N/m to monitor the surface morphology. Modified dry surfaces were probed with tapping mode under ambient conditions. Scans were carried out on a 0.7-µm^2 sized window. Roughness analysis was performed using the open source software Gwyddion (v2.39) and is calculated as the following formulas

$$R_a = \frac{1}{n}\sum_{i=1}^{n}|y_i| \quad (1)$$

$$R_{rms} = \sqrt{\frac{1}{n}\sum_{i=1}^{n}y_i^2} \quad (2)$$

where n is the total number of data points used in the calculation and y is the vertical surface position measure from the average surface height.

Cell adhesion studies on aGAG-modified surfaces

Cell culture

Human dermal fibroblasts (PromoCell, Heidelberg, Germany) were grown in Dulbecco's modified Eagle's medium (DMEM; Biochrom AG, Berlin, Germany) supplemented with 10% foetal bovine

Reprinted with permission from Journal of Bioactive and Compatible Polymers, Yuan Yang, Alexander Köwitsch, Ning Ma, Karsten Mäder, Iva Pashkuleva, Rui L. Reis, Thomas Groth (2015), Functionality of surface-coupled oxidised glycosaminoglycans towards fibroblast adhesion, 31 (2), 191-207.
 DOI: 10.1177/0883911515599999

serum (FBS; Biochrom AG), 1% antibiotic–antimycotic solution (AAS; Sigma–Aldrich) at 37°C in a humidified 5% CO_2/95% air atmosphere using a NUAIRE DH Autoflow incubator (NuAire Corp., Plymouth, MN, USA). Cells from confluent cultures were harvested by 0.25% Trypsin/0.02% ethylenediaminetetraacetic acid (EDTA) (Biochrom AG) for 5 min at 37°C. Trypsin was neutralised with DMEM containing 10% FBS. After centrifugation of cell suspension for 5 min at 900 r/min, HFs were re-suspended in culture medium without FBS and seeded on the NH_2- or aGAG-modified surfaces at a density of 2.5×10^4 cells/mL for 4 h.

Cell morphology and expression of adhesion structures

The test surfaces (different types of modified glass slides) were placed into 12-well tissue culture plates (Greiner Bio-One GmbH, Frickenhausen, Germany) and rinsed with sterile PBS twice. NH_2-terminated glass was used as control. HFs (2.5×10^4 cells/mL) were seeded on the surfaces and incubated for 4 h at 37°C in a humidified 5% CO_2/95% air atmosphere. After 4 h incubation, cells attached to the different surfaces were fixed with Roti-Histofix, followed by permeabilisation using 0.1% (v/v) Triton X-100 (Sigma) in PBS (pH 7.0) for 10 min. After rinsing the samples twice with PBS, the non-specific binding sites were blocked by incubation with 1% bovine serum albumin (BSA) for 30 min. Filamentous actin was directly stained by incubation with BODIPY phalloidin (Invitrogen, Germany) for 30 min at RT. The nuclei were stained with TO-PRO-3 (Invitrogen). Cells were then stained either for vinculin using a mouse monoclonal anti-vinculin primary antibody (Sigma) or CD44 (a cell surface receptor of HA) using a mouse monoclonal anti-CD44 primary antibody (Dianova, Hamburg, Germany) for 30 min at RT, respectively. Specific antibody binding was revealed by incubation with a Cy2-conjugated anti-mouse immunoglobulin secondary antibody (Dianova). All antibodies were diluted by 0.1% BSA dissolved in PBS. The samples were then washed with PBS, distilled water and finally mounted with Mowiol 4-88 (Calbiochem, Germany). Samples were examined with confocal laser scanning microscopy (LSM 710; Carl Zeiss MicroImaging GmbH, Germany) using a 63× objective.

Quantitative estimation of cell adhesion and spreading

HFs were seeded as described above for 4 h and then stained with crystal violet (0.5% w/v in methanol), followed by extensive washing with water and drying. Cells were photographed by a transmitted light microscope (Axiovert 100; Carl Zeiss MicroImaging GmbH) equipped with a charge-coupled device (CCD) camera (Sony, MC-3254; AVT-Horn, Aalen, Germany). Cell number and area were evaluated by ImageJ (v1.48) analysis software.

Statistical analysis

Data are reported as means ± standard deviations. Analysis of variance (ANOVA) and post Tukey's test were done to assess statistical significance of results. A p value of ≤ 0.05 was considered for significance and is indicated by asterisks in the figures.

Results and discussion

Synthesis and characterisation of aGAGs

Chemical modifications of GAGs such as oxidation or thiolation can introduce reactive groups into GAGs' backbone, thus allowing covalent immobilisation on functionalised surfaces or cross-linking

Reprinted with permission from Journal of Bioactive and Compatible Polymers, Yuan Yang, Alexander Köwitsch, Ning Ma, Karsten Mäder, Iva Pashkuleva, Rui L. Reis, Thomas Groth (2015), Functionality of surface-coupled oxidised glycosaminoglycans towards fibroblast adhesion, 31 (2), 191-207.
 DOI: 10.1177/0883911515599999

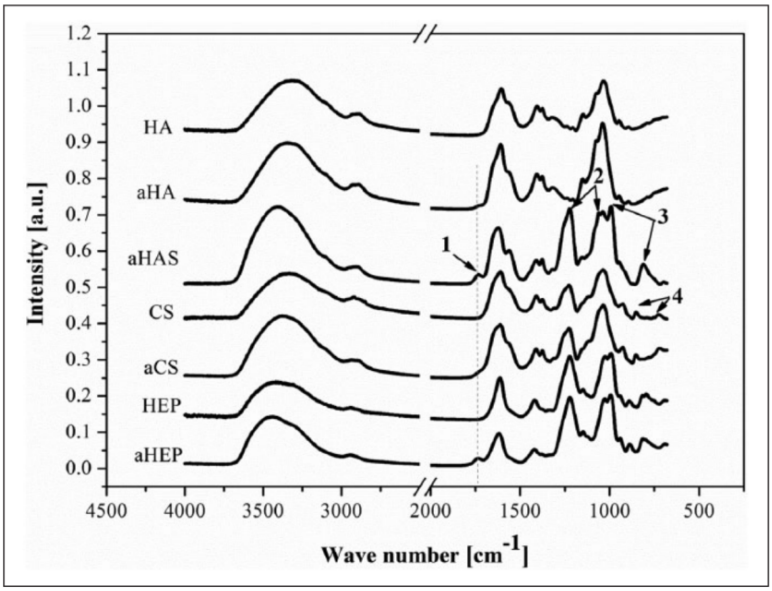

Figure 1. FT-IR spectra of native glycosaminoglycans and oxidised modified glycosaminoglycans.
HA: hyaluronan; aHA: aldehyde hyaluronan; aHAS: aldehyde hyaluronan sulphate (DS = 1.3); CS: chondroitin sulphate; aCS: aldehyde chondroitin sulphate; HEP: heparin; aHEP: aldehyde heparin; (1) C=O stretching vibration of aldehyde after oxidation; (2) S=O asymmetric and symmetric stretching vibrations of $-OSO^{3-}$ groups; (3) vibrations of equatorial $-OSO^{3-}$ groups; and (4) vibrations of axial $-OSO^{3-}$ groups on C4 of galactosamine residues.

of the GAGs.[22] Vicinal hydroxyl groups of the D-glucuronic acid (GlcA) of HA, HAS and CS or the L-iduronic acid (IdoA) of HEP can be oxidised by $NaIO_4$ to generate aldehyde groups. Aldehydes react with amino groups by formation of a Schiff base or imine bond,[25] which was used here to immobilise aGAGs covalently on amino-terminated glass or silicon surfaces.

The FT-IR spectra of native GAGs and oxidised aGAGs are shown in Figure 1. The spectra of native GAGs (Figure 1 - HA, CS, HEP) have typical peaks of saccharide alkyls at 2920 and 1415 cm^{-1} and alkoxyls at 1040 cm^{-1}. Additional peaks at 1224 and 1030 cm^{-1} appeared in the spectra of HAS, CS and HEP and these are associated with the presence of $O–SO_3^-$ groups.[26] The adsorption peaks of C–O–S group are near 990 and 820 cm^{-1}. When native GAGs were oxidised, a new weak infrared band associated with the C=O stretch vibration of aldehyde groups appeared at around 1732 cm^{-1} (Figure 1). The appearance of this characteristic band is in agreement with previous studies reporting the spectra of oxidised GAGs such as oxidised HA[22] or oxidised CS.[21]

The molar quantity of aldehydes introduced in the aGAGs backbone was determined with Schiff's reagent (Table 1). Aldehyde groups in aGAGs were in the range of $8.2–12.9 \times 10^{-4}$ mol/g, which is related to an oxidation degree of approximately 25%. The lowest oxidation degree was determined for aHA (around 17.5%) probably because the hydroxyl groups of HA are hindered by hydrogen bonds and thus are less sensitive to the oxidising reagent.[27] The molecular weights of aGAGs were determined by 4F with aqueous NaCl solution as the mobile phase (Table 1). Treatment of GAGs with different molar amounts of $NaIO_4$ led to a decrease in the molecular weights (from 923 to 103 kDa of HA, 94 to 69 kDa of HAS, 15 to 9 kDa of HEP) with only one exception: no significant change was observed for aldehyde chondroitin sulphate (aCS) when compared with the starting CS. The observed changes in molecular weight are due to break of glycosidic bonds as reported previously in other studies.[22]

Reprinted with permission from Journal of Bioactive and Compatible Polymers, Yuan Yang, Alexander Köwitsch, Ning Ma, Karsten Mäder, Iva Pashkuleva, Rui L. Reis, Thomas Groth (2015), Functionality of surface-coupled oxidised glycosaminoglycans towards fibroblast adhesion, 31 (2), 191-207.
 DOI: 10.1177/0883911515599999

Table 1. Reaction conditions for oxidation of GAGs and properties of aGAGs.

Sample	DS[a]	$NaIO_4$ (g)[b]	Reaction time (h)	DO_{th} (%)	DO_{exp} (%)[c]	CHO content ($\times 10^{-4}$ mol/g)[c]	Molecular weight (kDa)[d]		
							Mw	Mn	PDI
aHA	N/A	0.134	6	25	17.5	9.0	103	62	1.7
aCS	~0.8	0.107	6	25	32.6	12.9	26	22	1.2
aHAS	~1.3	0.214	3	25	21.7	8.2	69	40	1.7
aHEP	~1.6	0.332	6	30	25.5	9.0	9	6	1.5

GAG: glycosaminoglycan; aGAG: aldehyde glycosaminoglycan; DS: degree of sulphation; DO_{th}: theoretical degree of oxidation; DO_{exp}: experimental degree of oxidation; PDI: polydispersity index; aHA: aldehyde hyaluronan; aCS: aldehyde chondroitin sulphate; aHAS: aldehyde hyaluronan sulphate; aHEP: aldehyde heparin; UV-Vis: ultraviolet–visible.
[a]DS was determined by elemental analysis.
[b]The quantities of $NaIO_4$ were calculated from the DO_{th} and depend on GAGs' disaccharide repeating unit of different molecular weights in 1.0 g raw GAGs.
[c]Molar amount of aldehyde groups were determined by UV-Vis spectroscopy with Schiff's reagent in relation to the molar amount of GAGs' disaccharide repeating units.
[d]Molecular weights and PDI of oxidised GAGs were determined by field-flow fractionation with mobile phase of 50 mM NaCl.

Characterisation of aGAG-modified surfaces

Amino-terminated surfaces were exposed to aqueous solutions of aGAGs to allow formation of covalent links via Schiff's base or imine bonds. Because imine bonds are reversible, they were reduced to a secondary amine by addition of $NaBH_3CN$ to stabilise the bond between surface and aGAG according to previous protocols.[21] Since a covalent bond between the substratum and the aGAG is difficult to detect by spectroscopy due to similar bonds in GAG (e.g. N-acetyl bonds in HA, HAS, CS and partially HEP), only indirect evidence for the successful surface immobilisation of aGAG was collected by WCA and zeta potential measurements, ellipsometry and AFM.

Surface wettability determined by WCA

The wetting properties of the substrata after immobilisation of the different aGAGs were studied by static WCA measurements. The results are depicted in Figure 2.

The WCA increased when the cleaned glass cover slips (WCA$<20°$) were modified by APTES to generate amino-terminated surface (NH_2-glass, WCA$=55°\pm4°$), which is in agreement with previous reports.[23] After immobilisation of aGAGs on NH_2-glass, the WCA decreased tremendously and this decrease was dependent on the DS of aGAGs: from a WCA of about 35° for aHA (DS$=0$) and aCS (DS~0.8) to a WCA of about 15° for aldehyde hyaluronan sulphate (aHAS) and aldehyde heparin (aHEP) (DS>1.0). The DS of aGAGs estimated by elemental analysis obviously affects the wettability of the surfaces, although differences in the coating density of aGAGs on NH_2-glass could have an effect on the wetting properties.

Surface layer thickness determined by ellipsometry

The thickness of surface coatings of aGAG was measured by ellipsometry after silanisation of silicon with APTES using the same protocol as for glass (Figure 2). The basal layer of silicon oxide after Piranha cleaning of silicon was 1.80 ± 0.07 nm thick. After application of APTES, an

Reprinted with permission from Journal of Bioactive and Compatible Polymers, Yuan Yang, Alexander Köwitsch, Ning Ma, Karsten Mäder, Iva Pashkuleva, Rui L. Reis, Thomas Groth (2015), Functionality of surface-coupled oxidised glycosaminoglycans towards fibroblast adhesion, 31 (2), 191-207.
 DOI: 10.1177/0883911515599999

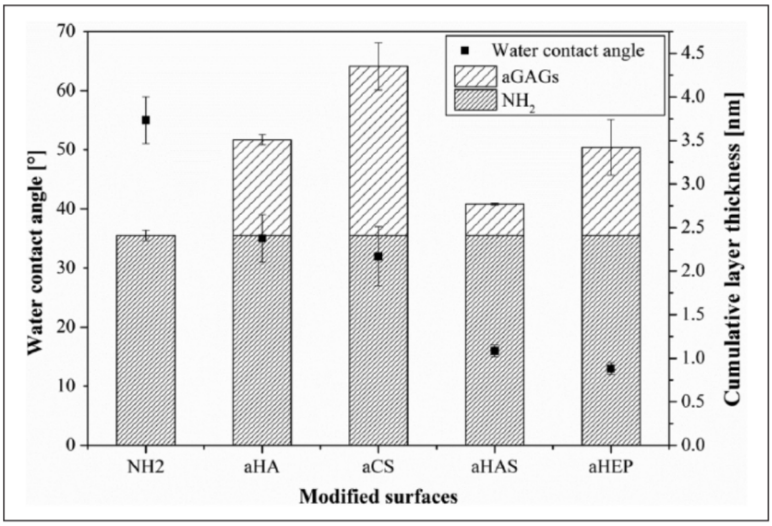

Figure 2. Effect of aGAG immobilisation on the properties of NH_2-functionalised surfaces: water contact angle measurements (left scale, black squares) and on thickness of surface layers measured by ellipsometry (right scale, bars). The wettability increased after immobilisation of aGAGs on NH_2-functionalised surfaces as indicated by a decrease in WCA while the thickness of the surface layer was increased as shown by ellipsometry measurements.
NH_2: amino-terminated glass or silicon; aHA: aldehyde hyaluronan; aCS: aldehyde chondroitin sulphate; aHAS: aldehyde sulphated hyaluronan; aHEP aldehyde heparin.

additional layer with a thickness of 0.61 ± 0.06 nm was obtained, which indicated the formation of a surface layer of aminopropyl chains in accordance with previous studies.[23] When the different aGAGs were bound to NH_2-Si, the layer thickness increased by 1.10 ± 0.06 nm for aHA, 1.94 ± 0.26 nm for aCS, 0.36 ± 0.06 nm for aHAS and 1.01 ± 0.32 nm for aHEP. The length of GAGs ranges in general from 17 nm to 1.6 μm,[28,29] which is far more than the measured thickness increases after aGAGs' immobilisation. Comparison of molecular weights shown in Table 2 reveals no correlation with the thickness increase. aHEP, which is the smallest molecule (Mw ~ 9 kDa), has no significantly lower thickness compared to aHA (Mw ~ 103 kDa). It was reported that single molecules of HA and HEP were 0.58 ± 0.17 nm in height measured by AFM.[30] Considering that the bound molecules were two to three times thicker than the GAGs in relaxed state as reported, one can draw the conclusion that aGAGs are attached side-on in a slightly coiled conformation with little differences in the coating density. This attachment can also be expected because the GAGs will have a more extended conformation due to the deprotonation at a physiological ionic strength and the existence of several aldehyde groups along the polysaccharide chain allowing multiple attachment sites on the surface.

Zeta (ζ) potential measurements

Zeta (ζ) potential measurements were used here as an indirect method to monitor the immobilisation of the different aGAGs on NH_2-glass surfaces (Figure 3 and Table 2). A typical decline of zeta potentials from acidic to basic pH values was observed for all surfaces (Figure 3). This decline is due to the deprotonation of sulphate and carboxylic groups with a characteristic levelling-off at basic pH values. Such behaviour is characteristic for surface with negatively charged groups as

Reprinted with permission from Journal of Bioactive and Compatible Polymers, Yuan Yang, Alexander Köwitsch, Ning Ma, Karsten Mäder, Iva Pashkuleva, Rui L. Reis, Thomas Groth (2015), Functionality of surface-coupled oxidised glycosaminoglycans towards fibroblast adhesion, 31 (2), 191-207.
 DOI: 10.1177/0883911515599999

Table 2. Zeta potential and roughness of plain and aGAG-modified surfaces.

Surface	ζ potential at pH 7.4[a]	Surface roughness (nm)[b]	
		R_a	R_{rms}
Bare glass/silicon	−82.6	0.29 ± 0.05	0.36 ± 0.05
NH_2-glass/silicon	−26.7	0.27 ± 0.03	0.35 ± 0.08
aHA	−38.6	0.53 ± 0.09	0.64 ± 0.09
aCS	−53.8	1.11 ± 0.13	1.55 ± 0.13
aHAS	−64.7	0.81 ± 0.20	1.20 ± 0.32
aHEP	−66.5	0.93 ± 0.34	1.33 ± 0.31

aGAG: aldehyde glycosaminoglycan; aHA: aldehyde hyaluronan; aCS: aldehyde chondroitin sulphate; aHAS: aldehyde hyaluronan sulphate; aHEP: aldehyde heparin; AFM: atomic force microscopy.
[a]Zeta potential of surfaces was determined by streaming potential measurements with SurPASS device.
[b]Surface roughness was determined from AFM images: R_a, average roughness; R_{rms}, root mean square roughness. Five different images of scan area 0.7 × 0.7 μm² were used for analysis.

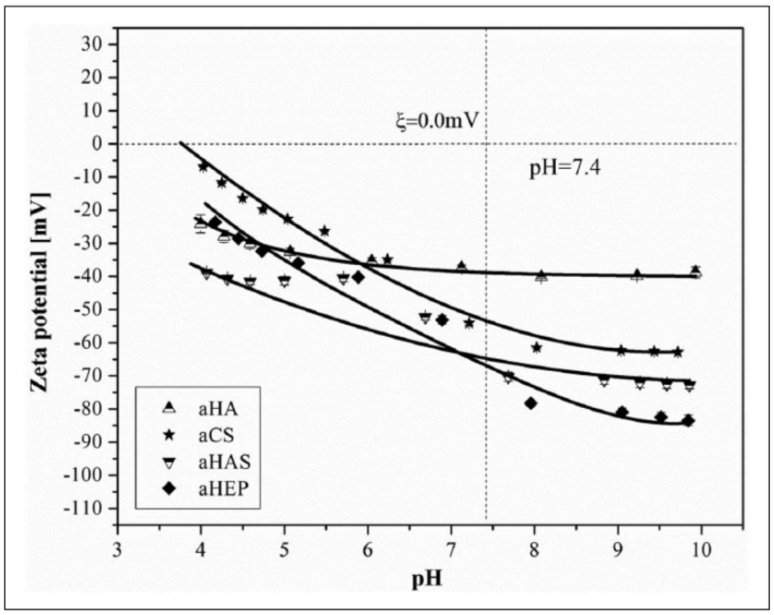

Figure 3. Effect of aGAG immobilisation on zeta potentials measured in 1 mM KCl at pH 4–10. The results show a decrease in zeta potentials with an increase in sulphation degree of the immobilised aGAGs at pH 7.4.
aHA: aldehyde hyaluronan; aCS: aldehyde chondroitin sulphate; aHAS: aldehyde sulphated hyaluronan; aHEP: aldehyde heparin.

previously reported.[31,32] At physiological pH, the zeta potential of NH_2-glass was the least negative (Table 2), which is expected due to the presence of amino groups. The zeta potentials of aGAGs coatings on NH_2-glass were related to the DS declining from aHA > aCS > aHAS ≥ aHEP, which is in accordance with the previously reported results for model surfaces with self-assembling monolayers with end sulphonic groups.[33]

Reprinted with permission from Journal of Bioactive and Compatible Polymers, Yuan Yang, Alexander Köwitsch, Ning Ma, Karsten Mäder, Iva Pashkuleva, Rui L. Reis, Thomas Groth (2015), Functionality of surface-coupled oxidised glycosaminoglycans towards fibroblast adhesion, 31 (2), 191-207.
 DOI: 10.1177/0883911515599999

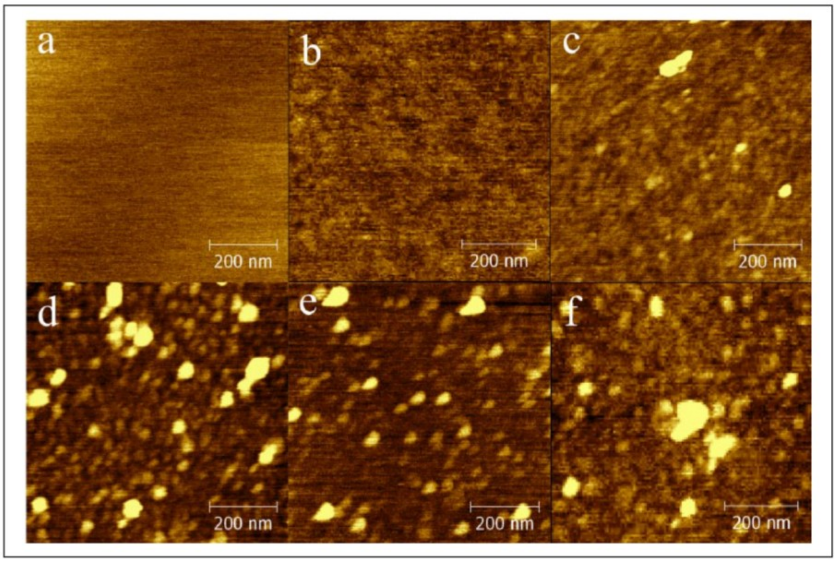

Figure 4. Atomic force micrographs of different surfaces taken in tapping mode (image size: $0.7 \times 0.7\,\mu m^2$): (a) bare silicon (b) amino-terminated silicon, (c) aldehyde HA on NH_2-Si,(d) aldehyde CS on NH_2-Si, (e) aldehyde HAS on NH_2-Si and (f) aldehyde HEP on NH_2-Si. An increase in surface roughness was detectable when aGAGs were used for coating the silicon surfaces.

Surface topography and roughness studies by AFM

The bare silicon surfaces were plane (Figure 4(a)) with low roughness values R_a and R_{rms} (Table 2). The coating of silicon with APTES did not change quantitative roughness values in comparison to bare silicon. However, some texture of the surface became visible that may indicate that no perfect monolayer coating was achieved (Figure 4(b)). This is indeed known for silanisation with short chain organosilanes.[23] The immobilisation of aHA resulted in surfaces with a granular structure and topography that was different from the sulphated aGAGs' surfaces (Figure 4(c)).

The topography of aHA surface might be related to some extent to the distribution of immobilised APTES. The quantitative roughness values of aHA-coated surface were slightly larger in comparison to APTES-coated silicon but significantly smaller than the roughness of surfaces after immobilisation of sulphated aGAGs (Table 2). The topography of surfaces with immobilised sulphated aGAGs was completely different (Figure 4(d) to (f)): larger globular structures and apparent aggregates in a size scale of about 50 nm were visible. The roughness values were significantly higher for all surfaces after immobilisation of sulphated aGAGs compared to aHA surfaces. The rough estimate of size of these structures does not match the size of any of the GAG molecules like HEP, for example, with 16.5 ± 1.80 nm in length and 1.07 ± 0.14 nm in width as reported previously.[29] Since the aGAG solutions used for surface modification had no turbidity, we assume that the formation of the globular domains occurred on the surface. A possible reason might be a condensation reaction of aldehydes via aldol reaction.[34] For the stabilisation of the formed Schiff base, we have applied $NaBH_3CN$ which is a strong base that is also able to remove acidic hydrogens from carbonyl groups to form enolates. The nucleophilic enolate is able to react with another carbonyl group like an aldehyde to form a new carbon–carbon bond. This can lead to cross-linking of aGAG chains. However, the apparent process of aggregation of the aGAGs does not represent

Reprinted with permission from Journal of Bioactive and Compatible Polymers, Yuan Yang, Alexander Köwitsch, Ning Ma, Karsten Mäder, Iva Pashkuleva, Rui L. Reis, Thomas Groth (2015), Functionality of surface-coupled oxidised glycosaminoglycans towards fibroblast adhesion, 31 (2), 191-207.
 DOI: 10.1177/0883911515599999

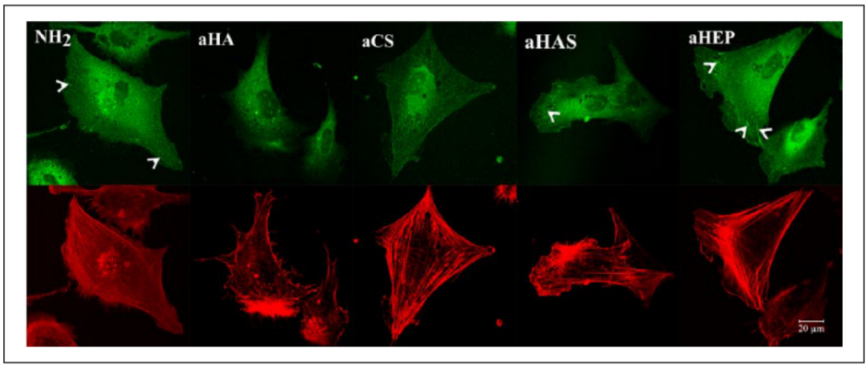

Figure 5. Immunofluorescence staining of vinculin (top row) and actin (bottom row) in fibroblasts cultured on NH_2-glass and aGAG-modified NH_2-glass in medium without serum for 4 h. Focal adhesions positive for vinculin are indicated by arrows.
aHA: aldehyde hyaluronic acid; aCS: aldehyde chondroitin sulphate; aHAS: aldehyde sulphated hyaluronic acid; aHEP: aldehyde heparin.

any disadvantage because it would increase the quantity of immobilised aGAGs and make the surface coating process more effective.

In summary, the results of surface characterisation techniques indicate that all surfaces generated by the immobilisation of the different aGAGs produce a stable coating of NH_2 surfaces that have wetting properties and surface potentials related to the charge density of the GAGs.

Effect of aGAG-modified surfaces on fibroblast adhesion

Sulphated GAGs such as HEP interact with different adhesive proteins such as fibronectin, laminin and others that possess specific binding domains, which promote adhesion, growth and function of cells.[8–11] Non-sulphated GAG such as HA may also promote initial adhesion of cells through the HA receptors such as CD44 and initiate signal transduction events related to cell migration and growth.[13] Since oxidation of GAGs changes their molecular structure, we were interested to study whether the bioactivity of GAGs is altered by the immobilisation process. The direct interaction of cell receptors after secretion of fibronectin by fibroblasts occurs quickly after seeding.[35] We therefore studied such interactions by performing short cell culture in the absence of serum and did not pre-adsorb adhesive proteins such as fibronectin to study direct interaction of cells with the aGAG-modified surfaces.

Immunofluorescence studies of fibroblast adhesion

As expectable from previous studies,[23] cells on amino-terminated glass (NH_2-GL) were largely spread after 4 h and had well-developed actin stress fibres (Figure 5). Indeed, vinculin staining was rather diffuse with very thin small focal adhesions in the peripheral zone of cells. The lack of larger focal adhesions is probably due to the lack of larger quantities of adhesive proteins such as fibronectin, which normally promotes assembly of focal adhesions.[36]

In contrast, adhesion and spreading of HFs on aHA bound surface were significantly suppressed, which is in good agreement with previous studies.[22,37] Cells appeared smaller and less polarised than on NH_2-GL. Actin was concentrated primarily at the cell edges and few stress fibres were visible. Also, no focal adhesions were detected. By contrast, cells on all sulphated aGAGs' surfaces

Reprinted with permission from Journal of Bioactive and Compatible Polymers, Yuan Yang, Alexander Köwitsch, Ning Ma, Karsten Mäder, Iva Pashkuleva, Rui L. Reis, Thomas Groth (2015), Functionality of surface-coupled oxidised glycosaminoglycans towards fibroblast adhesion, 31 (2), 191-207.
 DOI: 10.1177/0883911515599999

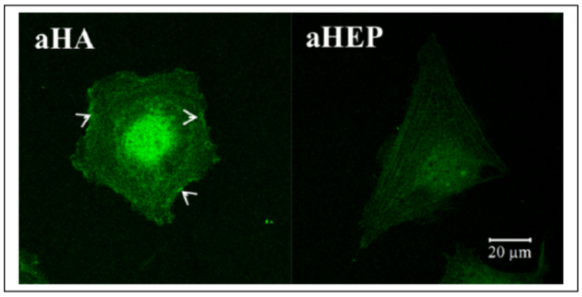

Figure 6. Immunofluorescence staining of hyaluronan-receptor CD44 in fibroblasts cultured on aHA- and aHEP-modified NH_2-glass in medium without serum for 4 h. The arrows indicate peripheral cell areas of increased CD44 expression.
aHA: aldehyde hyaluronan; aHEP: aldehyde heparin.

expressed a more spread, polarised phenotype (see Figure 5 as well). The expression of focal adhesions increased with the rising DS of aGAG. The most expressed focal adhesions were observed in fibroblasts cultured in contact with aHEP surface. The increased expressions of focal adhesions on more sulphated aGAGs and the corresponding stronger development of cytoskeletal structures have also been observed elsewhere on self-assembled monolayers with terminal sulphonic groups.[33,38] The emergence of focal adhesions on higher sulphated aGAGs can be explained with rapid secretion of fibronectin by fibroblasts[35] that can be adsorbed in a more active manner on sulphated aGAGs due to the presence of HEP-binding domains in fibronectin.[12]

On non-sulphated aHA-coated surfaces, an alternative adhesion mechanism can be activated via the HA receptors such as CD44, which is also expressed in fibroblast.[37,39] On both NH_2-GL and sulphated aGAGs' surfaces, CD44 staining was predominantly perinuclear as indicated by the staining around the nucleus of the cells (see Figure 6, right image). Less or faint peripheral staining of CD44 of spread cells was detected on these surfaces with aHEP shown here as an example. On the contrary, CD44 was present in the peripheral regions of cells cultured on aHA (see Figure 6, left image). There was a higher assembly of CD44 cluster in the periphery of spread HFs, indicating that the adhesion of fibroblasts on aHA is mediated via CD44–HA interaction as observed in previous studies.[22,37] In fact, in other studies on adhesion of adipose-derived stem cells and bone marrow–derived mesenchymal stem cells on aHA, a clear evidence for a participation of CD44 receptor was found.[40] Altogether, this supports strongly the idea that immobilisation of oxidised HA leads to a bioactive surface that addresses cell adhesion via CD44-mediated mechanisms.

Quantitative analysis of fibroblast adhesion and spreading

Apart from the effect of aGAGs' immobilisation on gross cell morphology, also a quantitative estimation of cell adhesion (cell number) and spreading (cell area) was done after staining cells with crystal violet, taking images by light microscopy and the quantitative analysis of micrographs with ImageJ software (Figure 7(a) and (b)).

The adhesion and spreading of fibroblasts were strongly dependent on the type of aGAGs immobilised on NH_2-glass. Analysis of initial cellular behaviour shows that adhesion and spreading of HFs were the highest on NH_2-GL compared with that on aGAG-modified NH_2-GL. This finding is well in line with previous studies and indicates that modification with APTES was successful.[23] Seeding of fibroblasts on aHA-modified NH_2-GL resulted in a significantly reduced number of cells of smaller size. By contrast, immobilisation of sulphated aGAGs led to an increase

Reprinted with permission from Journal of Bioactive and Compatible Polymers, Yuan Yang, Alexander Köwitsch, Ning Ma, Karsten Mäder, Iva Pashkuleva, Rui L. Reis, Thomas Groth (2015), Functionality of surface-coupled oxidised glycosaminoglycans towards fibroblast adhesion, 31 (2), 191-207.
 DOI: 10.1177/0883911515599999

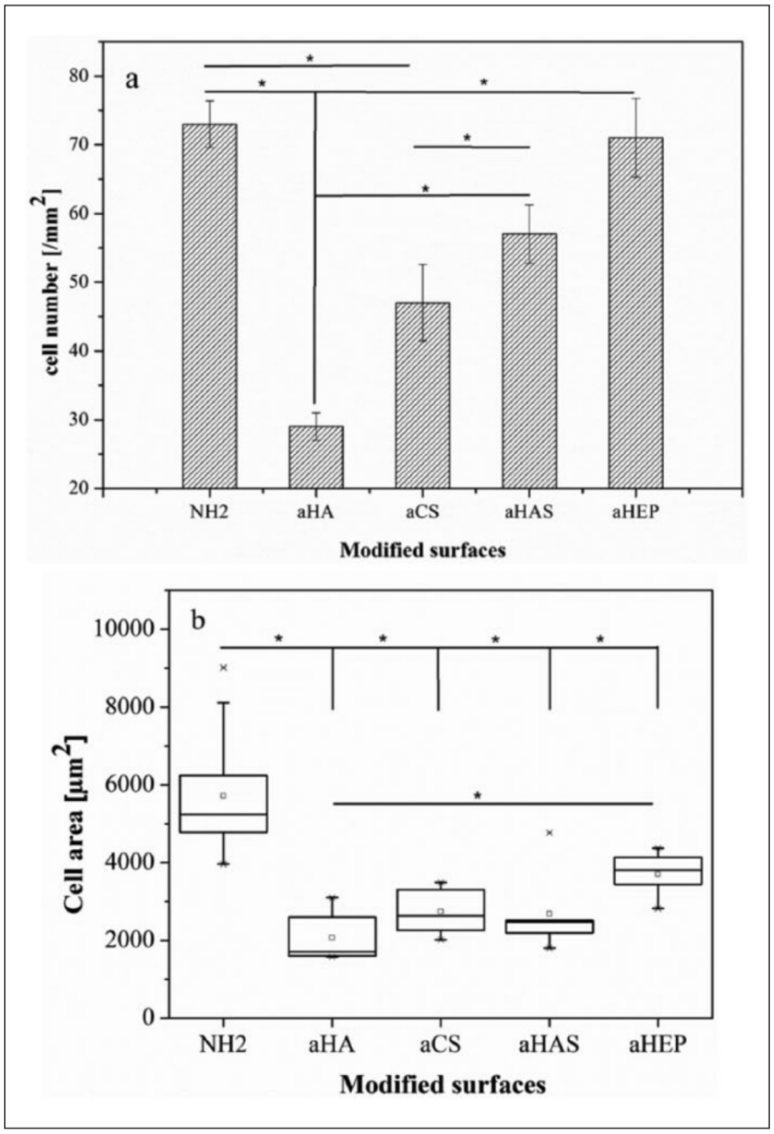

Figure 7. Analysis of adhesion and spreading behaviour of HFs on different aGAGs immobilised surfaces. Data were analysed from transmitted light microscopic images of HFs stained by crystal violet (0.5%v/v in methanol) through ImageJ software. (a) Cell number/mm² and (b) cell area of HFs after 4 h incubation on different aGAGs' immobilised surfaces.
HFs: human fibroblasts; aHA: aldehyde hyaluronic acid; aCS: aldehyde chondroitin sulphate; aHAS: aldehyde sulphated hyaluronic acid; aHEP: aldehyde heparin. Data represent means and standard deviations. Significance level of $p \leq 0.05$ is denoted by an asterisks (*).

in cell adhesion and spreading in relation to the DS with the following order: aHA(DS = 0) < aCS (DS = 0.8) < aHAS(DS = 1.3) < aHEP(DS = 1.6).

The results of adhesion and spreading studies confirmed the observations made by immunofluorescence in a quantitative manner. Adhesion and spreading on the NH_2-GL were highest due to the

Reprinted with permission from Journal of Bioactive and Compatible Polymers, Yuan Yang, Alexander Köwitsch, Ning Ma, Karsten Mäder, Iva Pashkuleva, Rui L. Reis, Thomas Groth (2015), Functionality of surface-coupled oxidised glycosaminoglycans towards fibroblast adhesion, 31 (2), 191-207.
 DOI: 10.1177/0883911515599999

presence of adhesion-promoting amino groups corresponding to previous studies.[23,35,41] An increased content of sulphate groups promoted an increase in number of adhering cells and their size. This observation is in line with other studies showing that sulphated GAGs promote adhesion of different cell types, most probably due to increased adsorption and bioactivity of pre-adsorbed and secreted or adhesive proteins such as fibronectin.[20,33,38,40]

Conclusion

The results of this study show that oxidation of GAGs (aGAGs) is a facile way to activate them for subsequent immobilisation on amino-functionalised surfaces, which can be produced by several techniques on a variety of biomaterials.[3,23,24,41] It can be assumed from this study that aGAGs were immobilised in a side-on conformation and formed an almost complete coating of the surface. The physicochemical properties of these surfaces were closely related to the molecular compositions and charge density of the GAGs. Particularly sulphated aGAGs possessed a remarkable bioactivity towards cells, which was indicated by increasing adhesion and spreading with an increase in DS of GAG. Also, a direct interaction of cell receptors such as CD44 in the case of surfaces modified with oxidised HA contributed to cell attachment most probably via a CD44-mediated pathway. This indicates strongly that the used oxidation process does not hamper the bioactivity of GAG to a large extent. Since GAGs are important modulators of protein functions, aGAGs may be useful to generate biomimetic surface coatings on biomaterials since they support, for example, fibrilisation of proteins such as collagen[42] and adsorption of other matrix proteins such as fibronectin, laminin and vitronectin and growth factors such as fibroblast growth factor homologous factor 2 (FHF-2), bone morphogenetic protein-2 (BMP-2) and vascular endothelial growth factor (VEGF) crucial for activity of cells.[10–12,40,43] In addition, such aGAGs may not only be useful to generate bioactive surface coatings on implants and scaffolds but also be useful for cross-linking reaction with other polyamines such as chitosan or matrix proteins to generate hydrogels for controlled drug delivery or tissue engineering applications.[1,7,44]

Acknowledgements

Y.Y. and A.K. contributed equally to this work. We are very thankful to Dr Matthias Schnabelrauch from INNOVENT e.V. for the kind supply of HAS.

Declaration of conflicting interests

The author(s) declared no potential conflicts of interest with respect to the research, authorship and/or publication of this article.

Funding

The author(s) disclosed receipt of the following financial support for the research, authorship, and/or publication of this article: This work was carried out under the scope of the EU 7th Framework Programme (FP7/2007-2013) under grant agreement no. NMP4-SL-2009-229292 (Find & Bind).

References

1. Shin H, Jo S and Mikos AG. Biomimetic materials for tissue engineering. *Biomaterials* 2003; 24: 4353–4364.
2. Ghanaati S, Webber MJ, Unger RE, et al. Dynamic in vivo biocompatibility of angiogenic peptide amphiphile nanofibers. *Biomaterials* 2009; 30: 6202–6212.
3. Schröder K, Finke B, Ohl A, et al. Capability of differently charged plasma polymer coatings for control of tissue interactions with titanium surfaces. *J Adhes Sci Technol* 2010; 24: 1191–1205.
4. Hersel U, Dahmen C and Kessler H. RGD modified polymers: biomaterials for stimulated cell

adhesion and beyond. *Biomaterials* 2003; 24: 4385–4415.
5. Lee JY, Choi YS, Lee SJ, et al. Bioactive peptide-modified biomaterials for bone regeneration. *Curr Pharm Des* 2011; 17: 2663–2676.
6. Hynes RO. Integrins: bidirectional, allosteric signaling machines. *Cell* 2002; 110: 673–687.
7. Lee K, Silva EA and Mooney DJ. Growth factor delivery-based tissue engineering: general approaches and a review of recent developments. *J R Soc Interface* 2011; 8: 153–170.
8. Ruoslahti E. Structure and biology of proteoglycans. *Annu Rev Cell Biol* 1988; 4: 229–255.
9. Hardingham TE and Fosang AJ. Proteoglycans: many forms and many functions. *FASEB J* 1992; 6: 861–870.
10. Afratis N, Gialeli C, Nikitovic D, et al. Glycosaminoglycans: key players in cancer cell biology and treatment. *FEBS J* 2012; 279: 1177–1197.
11. Kuschert GS, Coulin F, Power CA, et al. Glycosaminoglycans interact selectively with chemokines and modulate receptor binding and cellular responses. *Biochemistry* 1999; 38: 12959–12968.
12. Xu D and Esko JD. Demystifying heparan sulfate-protein interactions. *Annu Rev Biochem* 2014; 83: 129–157.
13. Toole BP. Hyaluronan: from extracellular glue to pericellular cue. *Nat Rev Cancer* 2004; 4: 528–539.
14. Wang Z, Sun B, Zhang M, et al. Functionalization of electrospun poly(ε-caprolactone) scaffold with heparin and vascular endothelial growth factors for potential application as vascular grafts. *J Bioact Compat Polym* 2012; 28: 154–166.
15. Chopra A, Murray ME, Byfield FJ, et al. Augmentation of integrin-mediated mechanotransduction by hyaluronic acid. *Biomaterials* 2014; 35: 71–82.
16. Guillame-Gentil O, Semenov O, Roca AS, et al. Engineering the extracellular environment: strategies for building 2D and 3D cellular structures. *Adv Mater* 2012; 22: 5443–5462.
17. Tsourdi A, Salbach-Hirsch J, Rauner M, et al. Glycosaminoglycans and their sulfate derivatives differentially regulate the viability and gene expression of osteocyte-like cell lines. *J Bioact Compat Polym* 2014; 29: 474–485.
18. Emami SH and Chaudhry MAS. Self-renewal and proliferation of murine embryonic stem cells: a study of glycosaminoglycans effect on feeder-free cultures. *J Bioact Compat Polym* 2007; 22: 314–322.
19. Sin I, Park S and Lee MR. Carbohydrate microarrays: an advanced technology for functional studies of glycans. *Chemistry* 2005; 11: 2894–2901.
20. Hintze V, Miron A, Möller S, et al. Sulfated hyaluronan and chondroitin sulfate derivatives interact differently with human transforming growth factor-β1 (TGF-β1). *Acta Biomater* 2012; 8: 2144–2152.
21. Wang DA, Varghese S, Sharma B, et al. Multifunctional chondroitin sulphate for cartilage tissue-biomaterial integration. *Nat Mater* 2007; 6: 385–392.
22. Köwitsch A, Yang Y, Ma N, et al. Bioactivity of immobilised hyaluronic acid derivatives regarding protein adsorption and cell adhesion. *Biotechnol Appl Biochem* 2011; 58: 376–389.
23. Faucheux N, Schweiss R, Lützow K, et al. Self-assembled monolayers with different terminating groups as model substrates for cell adhesion studies. *Biomaterials* 2004; 25: 2721–2730.
24. Booth BD, Vilt SG, McCabe C, et al. Tribology of monolayer films: comparison between n-alkanethiols on gold and n-alkyl trichlorosilanes on silicon. *Langmuir* 2009; 25: 9995–10001.
25. Margel S. Polyaldehyde microspheres as probes for cell membranes. *Ind Eng Chem Prod Res Dev* 1982; 21: 343–348.
26. Harada NS, Oyama HT, Bartoli JR, et al. Quantifying adsorption of heparin on a PVC substrate using ATR-FTIR. *Polym Int* 2005; 54: 209–214.
27. Morra M. Engineering of biomaterials surfaces by hyaluronan. *Biomacromolecules* 2005; 6: 1205–1223.
28. Jacoboni I, Valdre U, Mori G, et al. Hyaluronic acid by atomic force microscopy. *J Struct Biol* 1999; 126: 52–58.
29. Guo C, Wang B, Wang L, et al. Structural basis of single molecular heparin–FX06 interaction revealed by SPM measurements and molecular simulations. *Chem Commun* 2012; 48: 12222–12224.
30. Yeh ML and Luo ZP. The structure of proteoglycan aggregate determined by atomic force microscopy. *Scanning* 2004; 26: 273–276.
31. Werner C, Konig U, Augsburg A, et al. Electrokinetic characterization of biomedical polymers – a review. *Colloid Surface A* 1999; 159: 519–529.

Reprinted with permission from Journal of Bioactive and Compatible Polymers, Yuan Yang, Alexander Köwitsch, Ning Ma, Karsten Mäder, Iva Pashkuleva, Rui L. Reis, Thomas Groth (2015), Functionality of surface-coupled oxidised glycosaminoglycans towards fibroblast adhesion, 31 (2), 191-207.
 DOI: 10.1177/0883911515599999

32. Schweiss R, Wenzel PB, Werner C, et al. Dissociation of surface functional groups and preferential adsorption of ions on self-assembled monolayers assessed by streaming potential and streaming current measurements. *Langmuir* 2001; 17: 4304–4311.
33. Amorim S, Pires RA, Costa DS, et al. Interactions between exogenous FGF-2 and sulfonic groups: in situ characterization and impact on the morphology of human adipose-derived stem cells. *Langmuir* 2013; 29: 7983–7992.
34. Mlynarski J and Paradowska J. Catalytic asymmetric aldol reactions in aqueous media. *Chem Soc Rev* 2008; 37: 1502–1511.
35. Altankov G and Groth T. Fibronectin matrix formation by fibroblasts on surfaces varying in wettability. *J Biomater Sci Polymer Ed* 1997; 8: 299–310.
36. Altankov G and Grinnell F. Depletion of intracellular potassium disrupts coated pits and reversibly inhibits cell polarization during fibroblast spreading. *J Cell Biol* 1993; 120: 1449–1459.
Nebe JGB and Lüthen F. Integrin- and hyaluronan-mediated cell adhesion on titanium – hyaluronan-mediated adhesion. In: Breme J, Kirkpatrick CJ and Thull R (eds) *Metallic biomaterials interactions*. Hoboken, NJ: Wiley-VCH, 2008, pp. 179–182.
38. Da Costa DS, Pires RA, Frias AM, et al. Sulfonic groups induce formation of filopodia in mesenchymal stem cells. *J Mater Chem* 2012; 22: 7172–7178.
39. Svee K, White J, Vaillant P, et al. Acute lung injury fibroblast migration and invasion of a fibrin matrix is mediated by CD44. *J Clin Invest* 1996; 98: 1713–1727.
40. Da Costa DS, Marquez-Posadas MC, Araujo A, et al. Adhesion of adipose-derived mesenchymal stem cells to glycosaminoglycan surfaces with different protein patterns. *ACS Appl Mater Interfaces* 2015; 7: 10034–10043.
41. Faucheux N, Tzoneva R, Nagel MD, et al. The dependence of fibrillar adhesions in human fibroblasts on substratum chemistry. *Biomaterials* 2006; 27: 234–245.
42. Zhao M, Li L, Zhou C, et al. Improved stability and cell response by intrinsic cross-linking of multilayers from collagen I and oxidised glycosaminoglycans. *Biomacromolecules* 2014; 15: 4272–4280.
43. Rico P, Hernandez JCR, Moratal D, et al. Substrate-induced assembly of fibronectin into networks: influence of surface chemistry and effect on osteoblast adhesion. *Tissue Eng Part A* 2009; 15: 3271–3281.
44. Millan C, Cavalli E, Groth T, et al. Engineered microtissues formed by Schiff base crosslinking restore the chondrogenic potential of aged mesenchymal stem cells. *Adv Healthc Mater*. Epub ahead of print 9 April 2015. DOI: 10.1002/adhm.201500102.

Reprinted with permission from Journal of Bioactive and Compatible Polymers, Yuan Yang, Alexander Köwitsch, Ning Ma, Karsten Mäder, Iva Pashkuleva, Rui L. Reis, Thomas Groth (2015), Functionality of surface-coupled oxidised glycosaminoglycans towards fibroblast adhesion, 31 (2), 191-207.
 DOI: 10.1177/0883911515599999

Chapter 6

Summary – Novel mineralized heparin–gelatin nanoparticles for potential application in tissue engineering of bone:

In this publication nanoparticles (NPs) were produced by the cross-linking of succinylated gelatin (s-GL) with oxidized heparin (a-HEP) and subsequently used as a nano-template for the mineralization of hydroxyapatite (HAP).

Gelatin was partially succinylated with succinic anhydride to increase its solubility at room temperature. The uronic acid residues of heparin were partially oxidized with sodium periodate to generate aldehyde groups which can be used as a cross-linker that can react with s-GL to form nanoparticles via Schiff base linkage. The aldehyde group concentration of a-HEP and the amino group concentration of s-GL were determined with Schiff test and TNBS assay, respectively.

The polymer solution concentrations, feed molar ratios and pH conditions were varied to obtain a broad range of NPs. The preparation of NPs was conducted by using s-GL solutions of pH ranging from 2.5 to 10.0. Then, different ratios of a a-HEP solution (5% w/v in water) were added to the stirred s-GL solution. Nanoparticles were obtained with a spheroid shape of an average size of 196 nm at pH 2.5 and 202 nm at pH 7.4. These NPs had a positive zeta potential of 7.3±3.0 mV and a narrow distribution with PDI 0.123 at pH 2.5, while they had a negative zeta potential of -2.6±0.3 mV and formed aggregates (PDI 0.257) at pH 7.4. Thus, the NPs prepared at pH 2.5 with a mean particle size of 196 nm were further used for mineralization studies. Therefore, the pH of a s-GL/a-HEP NP-solution was adjusted to 10.0 with ammonium hydroxide and calcium nitrate and ammonium phosphate were added to obtain a CA/P-ratio of 1.67. Samples of the solution were taken out after different time points (0.5 h, 1 h, 4 h and 24 h), freeze-dried and applied to Fourier transform infrared (FT-IR) spectroscopy and X-ray diffraction (XRD). FT-IR showed the appearance of specific phosphate-associated bands which indicated the formation of HAP. Unlike for s-GL/a-HEP NPs which are composed of amorphous polymers lacking of a crystalline phase, it was found specific peaks in the XRD spectra after 24 h mineralization which could be associated with the formation of HAP.

HAP coated s-GL/a-HEP NPs developed in this study may be used as osteoinductive fillers enhancing the mechanical properties of injectable hydrogels or as potential multifunctional device for nanotherapeutic approaches.

J Mater Sci: Mater Med (2014) 25:669–680
DOI 10.1007/s10856-013-5111-2

Novel mineralized heparin–gelatin nanoparticles for potential application in tissue engineering of bone

Yuan Yang · Haihao Tang · Alexander Köwitsch · Karsten Mäder · Gerd Hause · Joachim Ulrich · Thomas Groth

Received: 6 May 2013 / Accepted: 29 November 2013 / Published online: 6 December 2013

Abstract Nanoparticles (NPs) were prepared from succinylated gelatin (s-GL) cross-linked with aldehyde heparin (a-HEP) and used subsequently as a nano-template for the mineralization of hydroxyapatite (HAP). Gelatin was functionalized with succinyl groups that made it soluble at room temperature. Heparin was oxidized to generate aldehyde groups and then used as a cross-linker that can react with s-GL to form NPs via Schiff's base linkage. The polymer concentrations, feed molar ratios and pH conditions were varied to fabricate NPs suspension. NPs were obtained with a spheroid shape of an average size of 196 nm at pH 2.5 and 202 nm at pH 7.4. These NPs had a positive zeta potential of 7.3 ± 3.0 mV and a narrow distribution with PDI 0.123 at pH 2.5, while they had a negative zeta potential of −2.6 ± 0.3 mV and formed aggregates (PDI 0.257) at pH 7.4. The NPs prepared at pH 2.5 with a mean particle size of 196 nm were further used for mineralization studies. The mineralization process was mediated by solution without calcination at 37 °C. The HAP formed on NPs was analyzed by Fourier transform infrared spectroscopy and X-ray diffraction. HAP coated s-GL/a-HEP NPs developed in this study may be used in future as osteoinductive fillers enhancing the mechanical properties of injectable hydrogel or use as potential multifunctional device for nanotherapeutic approaches.

Yuan Yang and Haihao Tang have contributed equally to this study.

Electronic supplementary material The online version of this article (doi:10.1007/s10856-013-5111-2) contains supplementary material, which is available to authorized users.

Y. Yang · H. Tang · A. Köwitsch · T. Groth (✉)
Biomedical Materials Group, Department of Pharmaceutical Technology and Biopharmacy, Institute of Pharmacy, Martin Luther University Halle-Wittenberg, Heinrich-Damerow-Str. 4, 06120 Halle (Saale), Germany
e-mail: thomas.groth@pharmazie.uni-halle.de

K. Mäder
Pharmaceutical Technology Group, Department of Pharmaceutical Technology and Biopharmacy, Institute of Pharmacy, Martin Luther University Halle-Wittenberg, Wolfgang-Langenbeck-Str. 4, 06120 Halle (Saale), Germany

G. Hause
Microscopy Unit, Biocenter, Martin Luther University Halle-Wittenberg, Weinberg Weg 22, 06120 Halle (Saale), Germany

J. Ulrich
Thermal Process Engineering, Center for Engineering Science, Martin Luther University Halle-Wittenberg, Hoher Weg 7, 06120 Halle (Saale), Germany

1 Introduction

Natural bone is composed of 30 % w/v organic collagen fibrils and 70 % inorganic calcium phosphate crystals, hierarchically organized at nanoscale, which has been used as model for different attempts to mimic the bone structure on a nanoscale level [1–3]. Composite polymeric matrices were developed that combine the inorganic component of bone namely calcium phosphates (CaP) like hydroxyapatite (HAP) with polymeric materials such as chitosan obtain injectable nanocomposite systems that possess compositional and partly structural analogies to natural bone [4, 5]. Classical HAP-polymer composites were fabricated at macroscale due to the requirement of critical size defects. Recently, HAP or CaP/polymer nanocomposites were developed, which enable these hybrid materials to extend their applications in the field of controlled drug delivery [6], minimal-invasive surgery and imaging [6, 7], which paves the way to new nanotherapeutic approaches. Particular HAP coated or mixed microspheres [8] or

nanoparticles (NPs) [2, 9] have attracted great interest, because of the feasibility to be used as regenerative filler or as a template for nucleation of new bone growth. However, only a few studies on engineering of CaP or HAP/gelatin NPs have been reported so far [2, 9]. The materials in these studies were fabricated using glutaraldehyde as a cross-linker via microemulsion technique, which resulted in NPs with a mean size of around 300 nm.

Gelatin is a protein produced by partial hydrolysis of collagen, which has been widely used as material in the pharmaceutics or food industry. Since collagen is a main matrix for bio-mineralization of HAP in nature, gelatin also evoked interest in the field of bone repair and regeneration. It can form transparent elastic thermo-reversible gels upon cooling around 35 °C due to the formation of collagen-like triple-helix [10], which can build up the shell of micro or nanocapsules for the controlled release of DNA [11] or growth factors [12, 13]. However, the gelatin shell layer is not stable enough in controlled release systems, because the body temperature is above the critical gel point or due to a decrease of extracellular pH value in tumor tissues [14]. Therefore, cross-linkers, like formaldehyde, glutaraldehyde or epoxy compounds are usually used to stabilize the particles or capsules during the formation procedure. However, the cytotoxity of these compounds has raised serious concerns about their safety and prompted research into the development of natural cross-linking reagents, like genipin [15]. Boanini et al. [8] also developed gelatin microspheres stabilized by dialdehyde alginate using an inverse microemulsion, but alginate lacks multiple bio-specific binding sites for growth factors or extracellular matrix proteins.

Heparin is a highly sulfated negatively charged glycosaminoglycan (GAG), which can non-covalently bind to various functional proteins, such as growth factors, extracellular matrix components and adhesion molecules, triggering multiple downstream signaling pathways [16] controlling cellular growth, differentiation and functions [17]. Thereby, the sulfation of heparin has a great influence on the interactions with proteins and cells. It has been reported that 2–O-sulfation from iduronic acid residues and 6–O-sulfation of glucosamine residues within heparin is essential in FGF-2 signal transduction [18, 19], while *N*-sulfate and 3–O-sulphation is required for its anticoagulant activity [19]. Heparin is also well known to interact with BMP-2, by which up-regulates the BMP-2-induced osteogenic activity through the contributions of BMP-2 antagonists and inhibitory Smads [20]. Jeon et al. [21] have synthesized heparin-conjugated nanospheres suspended in a fibrin gel, which can enhance BMP-2-induced ALP activity of osteoblasts and further stimulate bone formation and calcium deposition in vivo. Liu et al. [22] showed that polyelectrolyte nanoscale multilayers composed of HEP and chitosan promoted differentiation of hMSC towards osteoblasts, which further might promote bio-mineralization.

The vicinyl hydroxyl groups of GAGs can be oxidized and thereby generate active aldehyde groups, which can react with amino groups of other biopolymers, such as chitosan, gelatin or collagen. It has been also shown that oxidized GAGs like aldehyde hyaluronic acid is not cytotoxic up to 0.1 g/mL [23]. We also reported that immobilized aldehyde hyaluronic acid (HA) had similar bioactivity like native HA regarding the binding to its natural partner aggrecan [24]. In this work we generate aldehyde groups in heparin by oxidation, which shall act as biocompatible macromolecular cross-linker, to cross-link succinylated gelatin (s-GL) at room temperature and to form protein/GAG NPs by adjusting pH value and other parameter during the formation of particles. In addition, subsequent mineralization of NPs was performed using them as nucleation sites for complexing Ca^{2+} to acidic groups of s-GL and aldehyde heparin (a-HEP).

2 Materials and methods

2.1 Materials

Gelatin (Type A, bloom 80) was obtained from Fluka (Schnelldorf, Germany), heparin from Serva (Heidelberg, Germany) and succinic anhydride from Alfa Aesar (Karlsruhe, Germany). Sodium periodate, L-lysine, 2,4,6-trinitrobenzene sulfonic acid (TNBS) and Schiff's fuchsin-sulfite reagent were purchased from Sigma-Aldrich (Schnelldorf, Germany). The dialysis bag (Spectra/Por membrane, Mw cutoff = 3,500), acetone, glutaraldehyde, hydrochloric acid, sodium hydroxide and ammonia were obtained from Carl Roth GmbH (Karlsruhe, Germany). Sodium dodecyl sulfate (SDS) and Pluronic F68 were purchased from AppliChem (Gatersleben, Germany). Diammonium phosphate and calcium nitrate were bought from Merck (Darmstadt, Germany).

2.2 Preparation and characterization of protein and polysaccharide derivatives

2.2.1 Synthesis of s-GL and a-HEP

Succinylated gelatin was prepared (see Fig. 1a) as previously described [25]. Briefly, 50 mL of 5 % w/v gelatin solution was dissolved at 40 °C. The solution was adjusted to pH 9.0 by dropwise addition of 1 M NaOH solution. 0.625 g of succinic anhydride in 5 mL acetone was added to the gelatin solution, to obtain a ratio of 0.25 mg of succinic anhydride per milligram of gelatin. After addition

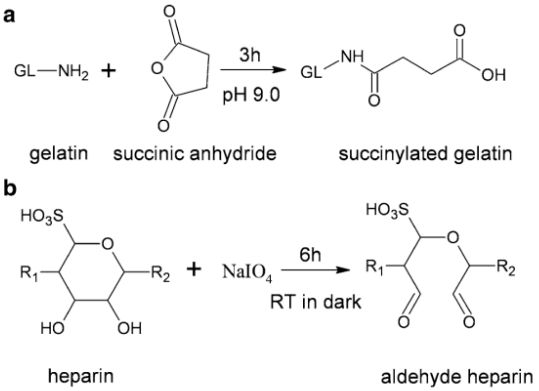

Fig. 1 Reaction scheme for the synthesis of components for the formation of NPs **a** succinylation of gelatin (s-GL) and **b** oxidation of heparin (a-HEP) (R_1, R_2 are vicinal saccharide units)

of succinic anhydride, the solution was stirred for 3 h at pH 9.0. s-GL was purified by dialysis against distilled water for 2 d and freeze-dried (ALPHA 1–2 LD plus, Christ, Osterode am Harz, Germany) overnight.

The method used for synthesis of a-HEP (Fig. 1b) was slightly modified compared to previous reports [24, 26]. A 0.4 % w/v heparin solution in distilled water was reacted with stoichiometric amounts of $NaIO_4$ at room temperature in the dark under constant stirring for 6 h. The amount of periodate was varied to obtain different degrees of oxidation. The solution was purified by dialysis against distilled water for 2 days. The final dry product was obtained by freeze-drying and stored at 4 °C.

2.2.2 *Characterization of s-GL and a-HEP*

2.2.2.1 Chemical structures and functional groups analysis The chemical structures of native molecules and their derivatives were analyzed by Fourier Transform Infrared (FTIR) spectroscopy (IFS 28, Bruker, Ettlingen, Germany). The functional groups, either amino groups or aldehyde groups, were determined by ultraviolet–visible (UV–Vis) spectroscopy using a modified procedure of TNBS assay [27] for amino groups and Schiff's reagent for aldehyde groups [24], respectively.

2.2.2.2 Molecular weight and polydispersity analysis The molecular weight and polydispersity of native molecules and their derivatives were measured by asymmetrical flow field-flow fractionation (FFF) equipped with a Dawn EOS detector (Wyatt Technology Corporation, Santa Barbara, CA, USA) and a refractive index (RI)-detector (Shodex RI-101, Showa Denko Europe GmbH, Munich, Germany). All samples with concentrations of 1 mg/mL were prepared in 50 mM NaCl with 0.02 % NaN_3 (w/v) to prevent bacterial growth. Molecular weights were calculated using Astra software (Wyatt Technology Corporation).

2.3 Preparation and characterization of s-GL/a-HEP NPs and HAP coated NPs

2.3.1 *Preparation of s-GL/a-HEP NPs*

To synthesize s-GL/a-HEP NPs, 10 mL of Pluronics F68 (0.1 and 1 % w/v) was prepared with MilliQ water and subsequently added to different amounts of s-GL (see result section) to obtain a final s-GLconcentration of 0.5 and 5 % w/v respectively according to previous work [28] After stirring for 0.5 h, the solution was filtrated with cellulose membrane (0.45 μm) and the pH was adjusted to 2.5 using 1 N HCl and 5.0, 7.4 and 10.0 with 1 N NaOH (for the parallel groups, respectively). 20 mL of acetone was dropped into the solution using a syringe pump (KDS 200, kdScientific, USA) at 1 mL/min dropping speed under stirring at 600 rpm for 20 min. The diameter of the needle was 0.5 mm. After stirring for 10 min, different amounts of a-HEP solution of concentration of 5 % w/v in DI water[n(–CHO)/n(–NH_2) = 10/2.3, 5/2.3, 1/2.3) were added to s-GL solution to form cross-linked NPs and stirred for 12 h. [9, 29] After that, acetone was evaporated over night at room temperature under a chemical hood and then the solution was centrifuged (Avanti J-26 XP, Beckman, USA) at 10,000 rpm for 5 min [30]. The sediment (particles bigger than 1 μm and some aggregates) was discarded and the solution was diluted to 25 mL with DI water. The nanoparticle solutions were stored at room temperature. The yield of NPs was calculated from the freeze-dried products and ended up with approximately 80 % w/w.

2.3.2 *Biomimetic HAP mineralization on s-GL/a-HEP NPs*

HAP mineralization on s-GL/a-HEP NPs was carried out as described previously [2, 8, 31]. 10 mL of s-GL/a-HEP nanoparticle solution was prepared. The pH was adjusted to 10.0 using $NH_3{\cdot}H_2O$. 0.0354 g $Ca(NO_3)_2{\cdot}4H_2O$ was added to the solution with a given ratio of 5 mmol Ca^{2+}/g s-GL/a-HEP NPs. The solution was stirred for 2 h at 37 °C. After that, to obtain Ca/P = 1.67, 5 mL of $(NH_4)_2HPO_4$ solution which contains 0.0238 g $(NH_4)_2HPO_4$ was dropped using syringe pump (KDS 200, kdScientific, USA) at 0.1 mL/min dropping speed under magnetic stirring at 600 rpm. The diameter of the needle was 0.5 mm. The pH of solution was then adjusted to 10.0 again using $NH_3{\cdot}H_2O$. At different reaction time points, 0.5, 1, 4 and 24 h, respectively, 3 mL of solution was removed and freeze-dried to obtain dry products for further analysis.

2.3.3 Characterization of s-GL/a-HEP NPs

2.3.3.1 Fourier transform infrared spectroscopy A FTIR spectrometer (IFS 28, Bruker, Ettlingen, Germany) was used to analyze the chemical composition of NPs and HAP coated NPs. The freeze-dried NPs were mixed with KBr to form pellets and examined on a spectrometer with a resolution of 2.00 cm^{-1} and recorded in the range of 4,000–400 cm^{-1}.

2.3.3.2 Dynamic light scattering (DLS) measurements Sizes and size distribution of NPs prepared at different pH conditions were characterized by DLS on a Zetasizer Nano NS (Malvern Instruments, Worcestershire, England), equipped with a detector to measure the intensity of the scattered light at 173° to the incident beam. The DLS measurements give a value called Z-average size (or cumulant mean), which is an intensity mean and the polydispersity index (PDI). The particle solution was measured in concentrations between 1 and 5 mg/mL at room temperature (25 °C).

2.3.3.3 Zeta-potential measurement Zeta-potentials of NPs at pH 2.5 and pH 7.4 were measured by Zetasizer Nano NS (Malvern Instruments, Worcestershire, England). All the samples of concentration of 1–5 mg/mL were dissolved in 10 mM NaCl in order to increase the conductivity which is between 1 and 5 mS/cm. The data were analyzed using the Malvern zetasizer v 6.30 software.

2.3.3.4 Transmission electron microscopy (TEM) Negatively stained samples were prepared by spreading 3 μL of the NPs dispersion onto a cupper grid (200 mesh) coated with a formvarfilm. After 1 min, excess liquid was blotted off with filter paper. The grid was then placed on a droplet of 1 % (w/v) aqueous uranyl acetate solution and drained off after 1 min. The dried specimens were examined with a Zeiss EM 900 transmission electron microscope at an acceleration voltage of 80 kV. Electron micrographs were taken with a slow scan camera (Variospeed SSCCD camera SM-1k-120, TRS, Moorenweis, Germany). The data were analyzed using Image J software.

2.3.3.5 Degree of cross-linking of NPs The free amino group content of NPs was quantified using a slightly modified TNBS test according to a previous report [32]. The NPs were dispersed in 4 % w/v $NaHCO_3$ to obtain 4 mg/mL sample solution. 1 mL of this solution was added with 1 mL of 0.1 % (w/w) TNBS in 4 % w/v $NaHCO_3$ (~pH 9.0). The mixture was stirred for 4 h at 40 °C. Then 1 mL of 10 % SDS and 0.5 mL of 1 M HCl were added to the mixture. 1 mL of 4 % w/v $NaHCO_3$ was used as a blank instead of a sample solution. The absorbance of the solution was measured at 365 nm using UV–Vis spectroscopy and compared to a plotted calibration curve using L-lysine as standard substance. The degree of cross-linking (D_c) of NPs was calculated from Eq. (1) by measuring the remaining free amino groups content within s-GL/a-HEP NPs.

$$D_c = \frac{(\text{Amino groups before crosslinking}) - (\text{Amino groups after crosslinking})}{(\text{Amino groups before crosslinking})} \times 100 \quad (1)$$

2.3.3.6 X-ray diffractometer (XRD) The mineralized NPs were investigated by XRD with a D4 ENDEAVOR XRD (BRUKER axs). A copper anode was used and the wavelength was 15.4 nm. 35 kV and 30 mA were used with the diffractometer. The XRD data were collected at room temperature (25 °C) over the 2-θ range of 10°–60° at step sizes of 0.02° and a count rate of 0.5 s/step. The software EVA v 8.0 was used for data analysis.

3 Results and discussion

3.1 Synthesis of s-GL and a-HEP

Gelatin type A used in this study can be dissolved in water at around 40 °C. At room temperature, it undergoes gelation due to the aggregation of collagen-like triple-helix. Gelatin was succinylated by using succinic anhydride (see Fig. 1a) to increase its water solubility [25] at room temperature, which is due to increased quantity of carboxylic groups and partially destruction of hydrogen bonds in the helix structure [25]. Vicinal hydroxyl groups of β-D-glucuronic acid or α-L-iduronic acid in heparin can be oxidized to dialdehydes in the presence of sodium periodate [24], which introduces these reactive groups to the sugar backbone (Fig. 1b) that can further react with amino group containing biopolymers.

The FTIR spectra of gelatin (GL), s-GL, heparin (HEP) and a-HEP are shown in Fig. 2. The spectrum of native GL (see Fig. 2c) has typical peaks at 1,634 and 1,533 cm^{-1}, which were associated to amide I [ν(C=O)] and amide II [δ(NH) and ν(N–C=O)] bands, respectively [25]. Compared with gelatin, a new weak absorption band (Fig. 2d)

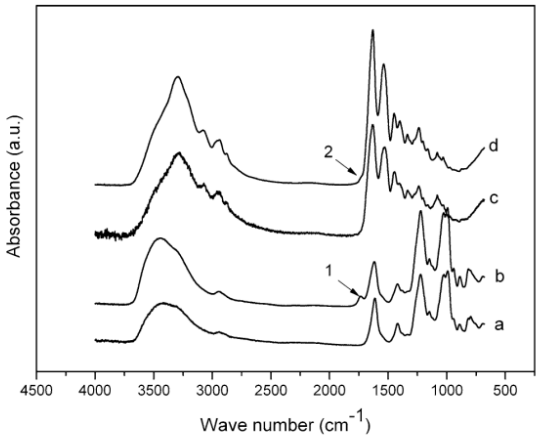

Fig. 2 FTIR spectra of *a* heparin, *b* a-HEP, *c* gelatin and *d* s-GL, and their new adsorption bands after chemical modification: (*1*)–C=O stretching vibration of aldehyde after oxidation, (*2*)–C=O stretching vibration of carboxyl groups after succinylation

Table 1 Active group contents (related to repeating disaccharide units) and weight average molecular mass (Mw), number average molar mass (Mn), and polydispersity index (PDI) of native molecules and their derivatives

Samples	Active groups contents		Molecular weight[b] (kDa)		
	$-NH_2$ group content[a] ($\times 10^{-4}$ mol/g)	–CHO group content[b] ($\times 10^{-4}$ mol/g)	Ww (kDa)	Wn (kDa)	PDI[c] (Mw/Mn)
GL	2.8	–	~190	~127	1.5
s-GL	1.1	–	~177	~42	4.2
HEP	–	–	~15.2	~14.0	1.1
a-HEP	–	10.0	~14.2	~12.4	1.1

[a] Amino groups content was determined via using TNBS assay by UV–Vis spectroscopy at 365 nm. L-lysine was used as the standard substance

[b] Molecular weights and PDI of native molecule and their derivatives were determined by field–flow fractionation with mobile phase of NaCl 50 mM

[c] Aldehyde content was determined via using Schiff's reagent by ultraviolet–visible (UV–Vis) spectroscopy at 550 nm. Glutardialdehyde was used as standard substance

appeared at 1,735 cm^{-1}, which was attributed to carboxyl groups (–COOH). This is in accordance with the work of Xiao et al. [25] and similar to the analogous synthesis of succinylated chitosan [33, 34], indicating that gelatin has been successfully modified. The spectrum of native heparin (see Fig. 2a) has typical peaks of saccharide alkyls at 2,920 and 1,415 cm^{-1}, alkoxyls at 1,040 cm^{-1} and sulfates at 1,231 and 1,029 cm^{-1} [35]. When heparin was oxidized, a new weak infrared band associated with the C=O stretch vibration of aldehyde groups appeared at 1,738 cm^{-1} (see Fig. 2b), which is in the agreement with the spectrum of oxidation of other GAGs, such as oxidized HA [24] or oxidized chondroitin sulfate (CS) [36].

Primary amino groups of GL and s-GL can react with TNBS (2,4,6-trinitrobenzenesulfonic acid) at alkaline pH conditions to form a color trinitrophenyl complex, which can be analyzed by UV–Vis spectroscopy at the wavelength of 365 nm [37, 38]. The amino group contents of gelatin and s-GL are shown in Table 1. The introduction of additional carboxyl groups to gelatin after succinylation can disturb hydrogen bonding, which in turn makes the protein more hydrophilic and anionic. It was found here that about 40 % of amino groups, 1.1 $\times$ 10^{-4} mol/g, of gelatin are still available after succinylation to react with aldehyde groups aHEP for NPs formation.

The controlled periodate oxidation of heparin should lead to the opening of the vicinal hydroxyls of glucuronic acid or iduronic acid rings, resulting in the formation of two aldehydes per ring. The amount of aldehydes of a-HEP was determined using Schiff's reagent and detected by UV–Vis spectroscopy at a wavelength of 550 nm within 40 min. The aldehyde groups of a-HEP had a molar concentration of 10.0 $\times$ 10^{-4} mol/g, which means approximately a 30 % degree of oxidation.

The molecular weights and PDI of the products were determined by FFF in 50 mM NaCl solution as the mobile phase. After succinylation, there were no significant molecular weight differences between gelatin and s-GL. After heparin oxidation, no significant degrease of a-HEP molecule weight was found. Since radicals may also break to glycosidic bonds and hence cause a decrease of molecular weight of GAG [24], it suggests that the oxidation procedure had little effect on the glycosidic bonds of heparin.

3.2 Synthesis of s-GL/a-HEP cross-linked NPs

Cross-linked s-GL/a-HEP NPs were prepared at different pH values probably by different reaction mechanisms according to Farris et al. [39]. At neutral or slightly alkaline conditions, the formation of NPs should be dominated by the formation of Schiff base linkage between non-protonated ε-NH_2 groups of s-GL and aldehyde groups of a-HEP (see Fig. 3a). By contrast, at acid condition (lower than 4.5), the reaction should take place between hydroxyl groups and aldehyde groups (see Fig. 3b). The acidic medium turns the α-carbon of the aldehyde into a highly reactive carbocation, and the –OH groups of hydroxyproline and hydroxylysine in gelatin (approximately 9.8 and 0.75 %, respectively, in type A gelatin) can attack it to form a hemiacetal. In addition, the electrostatic interactions between the positively charged $-NH_3^+$ and negatively charged $-COO^-$ or $-SO_3^{2-}$ groups may also contribute to

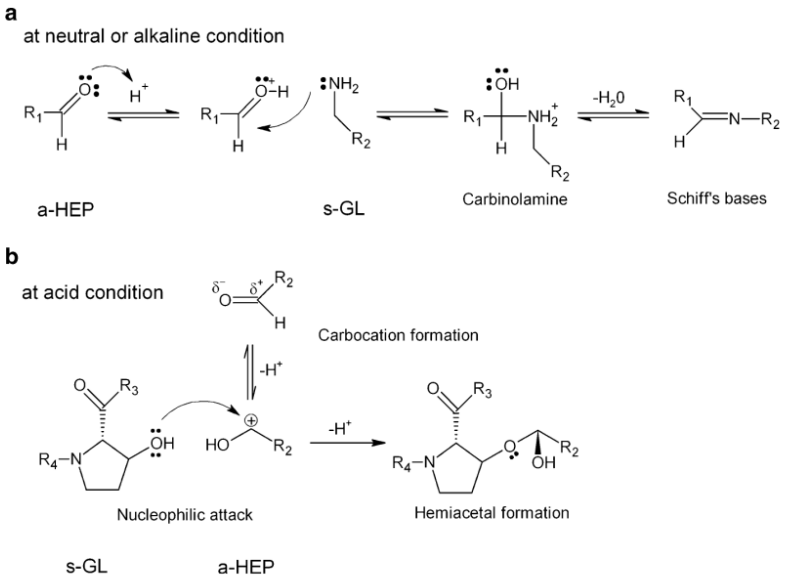

Fig. 3 Reaction mechanism **a** between amino groups of succinyl gelatin and aldehyde groups of a-HEP for the formation of Schiff base at pH 5.0, 7.4 and 10.0 and **b** between hydroxyl groups of s-GL and aldehyde groups of a-HEP at pH 2.5

stabilization of the NPs. At this acidic status, most of the amino groups are protonated and cannot react with aldehyde groups. But we assume that there are still some free amino groups involved in Schiff base reaction to form cross-linked NPs at equilibrium conditions.

Cross-linked s-GL/a-HEP NPs were prepared in water/acetone by simply adjusting pH values during the reaction. Parameters such as surfactant (Pluronics) concentration (0, 0.1 and 1 % w/v), s-GL concentration (0.5 and 5 % w/v), volume ratio of acetone/water (1:1, 2:1 and 3:1) and molar ratio of a-HEP/s-GL (10:2.3, 5:2.3 and 1:2.3) were varied to optimize the condition of NPs formation, which also influenced the stability of s-GL/a-HEP NPs suspensions. The results showed that a high concentration of s-GL (5 % w/v) without any surfactant lead to aggregation in water/acetone at either pH 2.5 or 7.4 before addition of the a-HEP as a cross-linker. Therefore, a lower concentration of s-GL of 0.5 % w/v was chosen and combined with two concentrations of surfactant (Pluronics F68), such as 0.1 and 1 % w/v. Pluronics F68 is a non-ionic surfactant, which contains a central hydrophobic block of polypropylene oxide (PPO) and two identical hydrophilic blocks of polyethylene oxide (PEO) at both sides. Without F68, the solution was unstable after the addition of the cross-linker (a-HEP), while after adding the surfactant, stable solutions were obtained. At low concentration of 0.1 % w/v, F68 contributed to stabilization of the s-GL emulsions at different pH value probably via the hydrophobic interaction between the PPO fragment and hydrophobic residues of s-GL [40], resulting in NPs of a size around 200 nm determined by DSL (Table 2). However, at high F 68 concentration of 1.0 % w/v, the particle size increased from 196.3 nm to 372.2 nm at pH 2.5 and from 202.4 nm to large aggregates at pH 7.4, respectively. The size distribution also increased significantly from 0.123 to 0.232 nm at pH 2.5 and from 0.257 to 0.646 nm at pH 7.4. The larger diameter and broader size distributions of NPs indicated that an excess of surfactant increased the diameter of cross-linked NPs. This was not beneficial to form NPs of a homogeneous size.

Table 2 Effects of pH conditions and Pluronics F68 concentrations on the Z-average diameter and polydispersity index (PDI) of s-GL/a-HEP NPs

pH	0.1 % (w/v) Pluronics F68		1 % (w/v) Pluronics F68	
	Z-average[a] (d. nm)	PDI[a]	Z-average[a] (d. nm)	PDI[a]
2.50	196.3	0.123	372.2	0.232
5.00	283.7	0.301	–	–
7.40	202.4	0.257	–	0.646
10.00	210.6	0.351	–	–

[a] Size (Z-average) and size distribution (PDI) determined by the DLS method

Aggregation of particles was also observed in the solution when the molar ratio of –CHO/–NH_2 was increased from 1:2.3 to 10:2.3 due to excess amount of cross-linker of a-HEP. In the end, 0.1 % w/v Pluronics F68, 0.5 % w/v s-GL, 2:1 v/v acetone/water and 1:2.3 of –CHO/–NH_2 (a-HEP/s-GL) were chosen for particle synthesis. Under this condition, four different pH values applied during particle

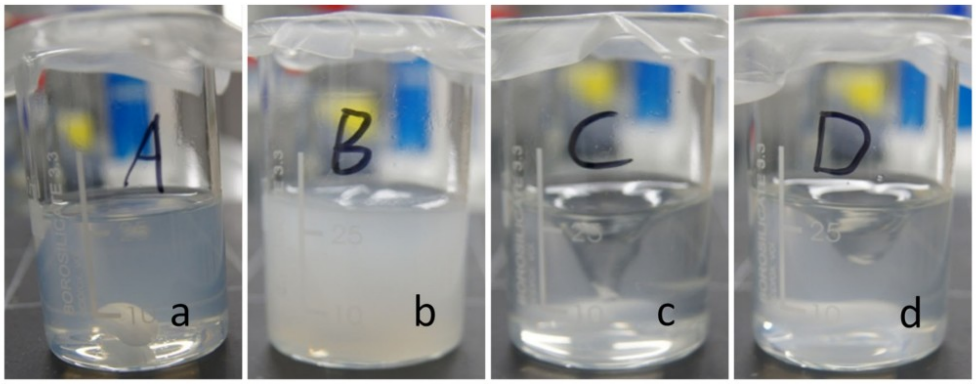

Fig. 4 Photos of s-GL solution containing 0.1 % (w/v) Pluronics F68 were cross-linked by a-HEP at **a** pH 2.5, **b** pH 5.0, **c** pH 7.4 and **d** pH 10.0

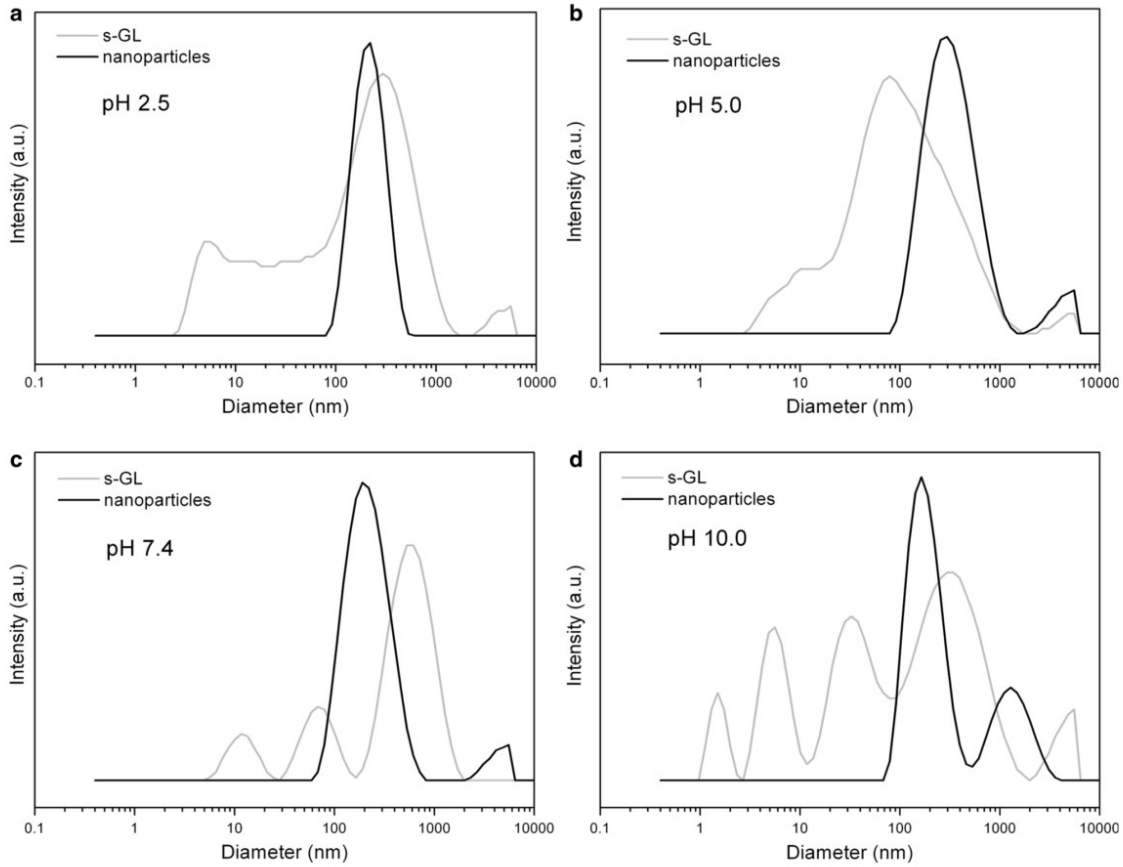

Fig. 5 DLS measurements of s-GL solution of concentration 1 mg/mL (*gray line*) and s-GL/a-HEP NPs of concentration 1–5 mg/mL (*black line*) at different pH values, **a** pH 2.5, **b** pH 5.0, **c** pH 7.4, **d** pH 10.0

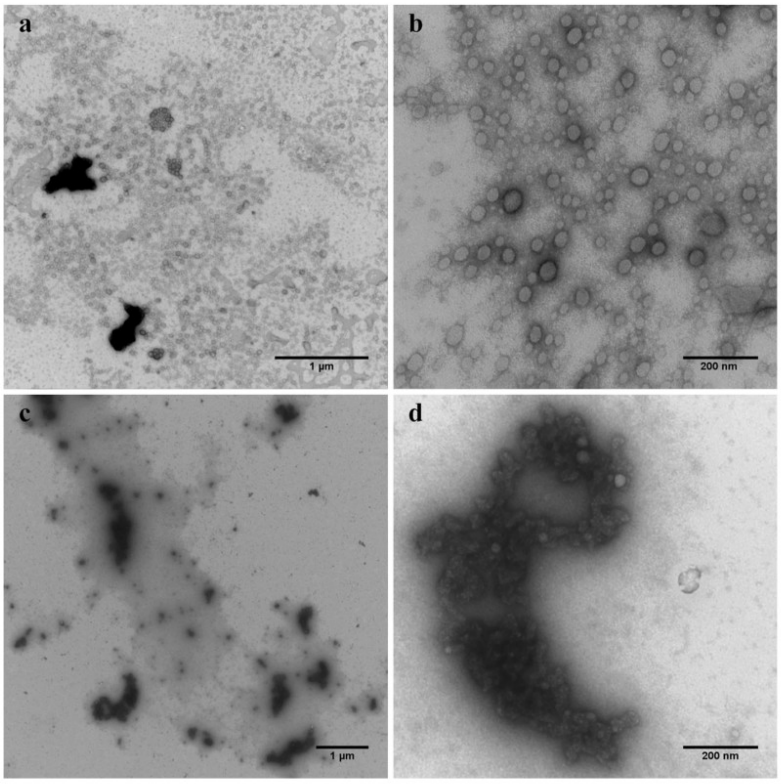

Fig. 6 TEM images of s-GL/a-HEP NPs prepared at different pH conditions **a**, **b** NPs well distributed at pH 2.5 and **c**, **d** NPs formed large aggregation at pH 7.4: **a**, **c** images over large regions of scale bar 1 μm and **b**, **d** images of characteristic regions of scale bar 200 nm, respectively

formation were compared. The macroscopic appearance of these solutions is shown in Fig. 4. At pH 5.0, aggregation in the solution was observed after addition of acetone. The isoelectric point (IEP) of s-GL is around 4.0 (see Fig. S1) and near this pH, s-GL has the minimum solubility. Far away from IEP of gelatin, stable emulsions were formed at pH 2.5, 7.4 and 10.0, respectively.

Figure 5 and Table 2 show the size distribution of s-GL and cross-linked s-GL/a-HEP NPs under various pH conditions. We can see that every peak of s-GL before cross-linking (PDI are nearly 1), whether single or multiple, are broad (grey lines in Fig. 5a–d). Gelatin is a hydrolysis product of collagen with large variance in molecular weight, thus it is a challenge to fabricate uniform NPs. Coester et al. [30] developed a two-step desolvation method and successfully formed uniform and stable NPs. In our study, we chemically modified the gelatin and then used dialysis to separate the gelatin of large molecular weight from small molecular weight ones. The gelatin no less than 177 kDa was kept for forming NPs. After cross-linking, s-GL/a-HEP NPs have narrow size distributions at all pH conditions (black lines in Fig. 5a–d).The diameters of s-GL/a-HEP NPs were in the range of 200–300 nm (see Table 2), depending on pH values. The net charge of s-GL in solution is strongly affected by the prevalent pH conditions, which led to the alterations in final particle size. At pH 2.5, the NPs have uniform particle size and a well dispersed character (Fig. 5a) (Z-average 196.3 nm, PDI 0.123), which is smallest among all. At pH 5.0, the produced NPs strongly tended to aggregation and precipitation, which ended up with an average size of 283.7 nm. The PDI is 0.301 (Fig. 5b), indicating high heterogeneity. s-GL is neutral at around pH 4.0. Under this condition, the remaining net charge of s-GL was too weak to prevent the freshly formed cross-linked NPs from large aggregation. Above pH 5.0, for example 7.4 and 10.0, cross-linked NPs slightly increased in size compared to those at pH 2.5, while the size distribution was broaden with pH increasing (Fig. 5c, d). The amino groups on NPs' surface are neutral and easily react with a-HEP, which might cause them

cross-linked to each other and form large aggregation, which were also observed from TEM, as shown in Fig. 6c, d.

The TEM images of s-GL/a-HEP cross-linked NPs in Fig. 6 further demonstrate that the change of pH value can lead to different morphology of NPs. At pH 2.5, the NPs showed a spherical shape of an average particle size ~50 nm (Fig. 6 a, b); while at pH 7.4, they showed large aggregation of size around 1 μm consisting of a number of smaller particles of sizes approximately 30–40 nm (Fig. 6 c, d). In general, during TEM the particles were shrinking largely (size approximately 50 nm) compared with the size in solution (approximately 200 nm, measured by DLS) at pH 2.5 and 7.4. The shrinking of NPs under dry condition was also observed by Coester et al. [30] when they used scanning electron microscopy to examine gelatin NPs.

The free amino group content of s-GL/a-HEP NPs prepared at different pH conditions was determined by TNBS test. The degree of cross-linking of NPs was then calculated from Eq. (1) and is listed in Table 3. The experimental degrees of cross-linking, 13.3 % and 19.4 %, were lower than the expected, 43.5 %. The degree of cross-linking at pH 2.5 (13.3 %) was lower than that at pH 7.4 (19.4 %), which may be due to the different cross-linking mechanisms [39]. At pH 2.5, most of amino groups are protonated ($-NH_3^+$) so that they cannot react with aldehyde groups and thus the NPs displayed a positive zeta potential 7.3 ± 3.0 mV (Table 3). Those $-NH_3^+$ groups were then deprotonated and tested by TNBS assay at pH 9. In additional, at acid condition, most of hydroxyl groups instead of amino groups were cross-linked with aldehyde groups and there quantity cannot be easily measured. On the other hand, at neutral or alkaline condition, primary amino groups reacted with aldehyde groups and raised the degree of cross-linking over the one at lower pH, according to TNBS test. After cross-linking, the remaining amino groups of s-GL were in neutral status, while the carboxyl groups (from s-GL and a-HEP) and sulfate groups (from a-HEP) were deprotonated. Therefore, the NPs showed a negative zeta potential of −2.6 ± 0.3 mV at pH 7.4. Due to different mechanisms, the real cross-linking degree cannot be detected easily, especially at acidic condition.

Table 3 Theoretical (D_{th}) and experimental (D_{exp}) degree of cross-linking and zeta potentials of s-GL/a-HEP NPs at different pH conditions

pH	Free $-NH_2$ groups of s-GL ($\times 10^{-4}$ mol/g)	Free $-NH_2$ groups of s-GL/a-HEP NPs ($\times 10^{-4}$ mol/g)[a]	D_{th} (%)	D_{exp} (%)	Zeta-potential (mV)[b]
2.5	1.08	0.936	43.5	13.3	7.3 ± 3.0
7.4	1.08	0.870	43.5	19.4	−2.6 ± 0.3

[a] The remaining amino groups content of s-GL/a-Hep NPs was determined via using TNBS assay by UV–Vis spectroscopy at 365 nm. L-lysine was used as the standard substance

[b] Zeta-potential measured by a zetasizer with three trials

3.3 Hydroxyapatite mineralization on cross-linked NPs

The particles synthesized at pH 2.5 were used for further mineralization. The whole process is shown in Fig. 7. (a) s-GL/a-HEP NPs formed at pH 2.5 with a positive zeta potential due to the protonation of amino groups and carboxylic acid groups within s-GL. (b) When pH increased to 10.0 with $NH_3 \cdot H_2O$, $-NH_3^+$ became $-NH_2$ and –COOH or $-SO_3H$ were deprotonated. Therefore, NPs displayed a negative charge. (c) $Ca(NO_3)_2$ was added and the negatively charged particles attracted Ca^{2+} due to Coulomb attraction [2]. (d) $(NH_4)_2HPO_4$ was added and PO_4^{3-} interacted with Ca^{2+} to start mineralization. Finally, HAP was formed on the cross-linked NPs [2, 8].

At different time points of reaction (0.5, 1, 4 and 24 h), a certain amount of sample solution was recovered, kept in −80 °C freezer for 2 days and subsequently freeze-dried overnight. The mineralized products were analyzed by FTIR and XRD and the results are shown in Figs. 8 and 9. For s-GL/a-HEP NPs (Fig. 8a), the adsorption bands at 1,657; 1,542; and 1,239 cm^{-1} were associated to amide I [ν(C=O)], amide II [δ(NH) and ν(N–C=O)] bands of s-GL, respectively. The typical peaks at 1,235 cm^{-1} [overlay with ν(N–C=O)] and 1,032 cm^{-1} related to symmetric and

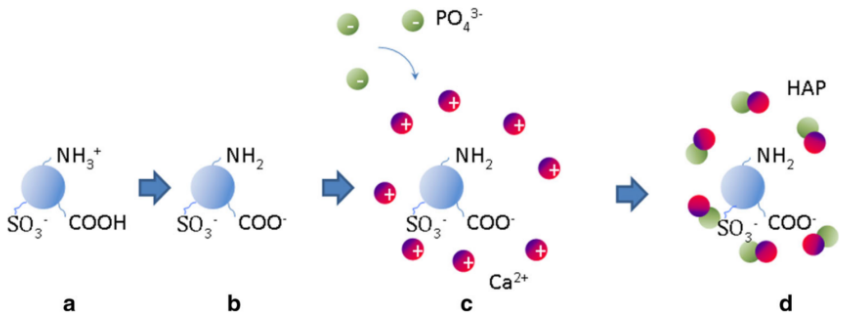

Fig. 7 Schematic picture of bio-mineralization process on s-GL/a-HEP NPs

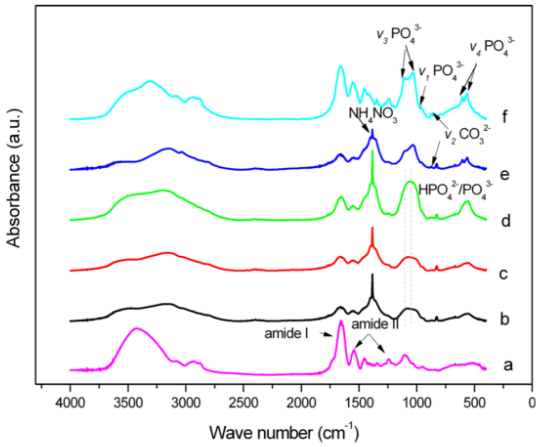

Fig. 8 FTIR spectrums of (*a*) s-GL/a-HEP NPs, and HAP mineralization on s-GL/a-HEP NPs at different time intervals (*b*) at 0.5 h, (*c*) at 1 h, (*d*) at 4 h, (*e*) at 24 h before dialysis (*f*) at 24 h and subsequently dialysis for 24 h

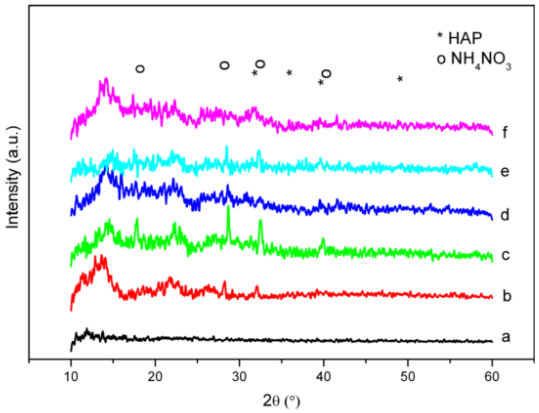

Fig. 9 X-ray diffraction spectrum of (*a*) s-GL NPs, and HAP mineralization on s-GL/a-HEP NPs at different time intervals (*b*) at 0.5 h, (*c*) at 1 h, (*d*) at 4 h, (*e*) at 24 h before dialysis, and (*f*) at 24 h and subsequently dialysis for 24 h

asymmetric stretching absorptions of sulfate groups within a-HEP. Therefore, intermolecular and/or intramolecular bridges between s-GL are formed through the cross-linking by a-HEP and result in the stable shell of NPs.

Comparing to the FTIR spectra of s-GL/a-HEP NPs (Fig. 8a), after mineralization for different periods of time, a broad band appeared in the region of 1,115 to 1,030 cm^{-1} after 0.5–4 h, which might be related to HPO_4^{2-}/PO_4^{3-} mixed phase [31], indicating the formation of a precursor of HAP. After 24 h mineralization (Fig. 8 e, f), this broad band split into two distinguished peaks at 1,093 and 1,033 cm^{-1}, respectively, which were associated to v_3 asymmetric stretching of PO_4^{3-} ions, suggesting the transformation of HPO_4^{2-}–PO_4^{3-} (Fig. 8f). In addition we also observed the weak band of v_1 symmetric stretching PO_4^{3-} at 970 cm^{-1}, degenerated v_4 bending PO_4^{3-} at 604 and 563 cm^{-1}, respectively, suggesting the presence of a apatite-like phase [6, 41, 42]. Figure 8e shows that NH_4NO_3 was formed and showed a peak at 1,384 cm^{-1} due to N–O covalent bond, but after dialysis it was removed from the particles (Fig. 8f) [43]. During the co-precipitation process of HAP on s-GL/a-HEP NPs, the Ca^{2+} ions can interact with $–COO^-$ of s-GL and a-HEP, as well as $-SO_3^{2-}$ of a-HEP. The doubly degenerated v_2 CO_3^{2-} bending mode at 877 cm^{-1} (Fig. 8 e–f) indicated the formation of a B-type carbonate HAP on the NPs [41, 44], which is the main biological apatite found in the bone or tooth [45]. Unlike gelatin or collagen inducing HAP that only provide $R\text{-}COO^-$ nucleation site, we assume that the additional $-SO_3^{2-}$ groups of a-HEP can provide a new nucleation site for the growth of HAP crystals. There is a very weak band at 672 cm^{-1}, which might be associated to calcium sulfate complex [46]. But its typical bands at around 1,010 cm^{-1} were overlaid by the bands of PO_4^{3-} [46]. Therefore, to confirm such complex, the samples should be further subjected to Raman spectroscopy. Moreover, the cross-linking induces to shorten the distances between s-GL/a-HEP network and so more amount of Ca^{2+} have a chance to bind to protein/GAG matrix, which might be favor to form the well-ordered HAP crystals.

There is no characteristic sharp peak found in the spectra of organic s-GL/a-HEP NPs, which is typical for amorphous polymer lacking of crystalline phase (Fig. 9a). Figure 9b–f shows that the peaks at 25.9°(002), 32.1°(211), 40.0°(310) and 50°(004) were associated to HAP according to XRD database JCP 2.2 CA, indicating that HAP formation on NPs over time. s-GL/a-HEP NPs acting as individual nano-template are suitable for HAP crystallization. The NPs are loaded with calcium ions by complexation with the carboxyl or sulfate groups present either in s-GL or in a-HEP chains. Further addition of phosphate ions leaded to the formation of calcium phosphate.

The solution composed of $Ca(NO_3)_2{\cdot}4H_2O$ and $(NH_4)_2HPO_4$ can be mediated to transform HAP, which is thermodynamically stable. The time dependent crystallite growth can also be determined with the sharpness of the peaks in Fig 9 b–e. NH_4NO_3 as a side product also have peaks at 17.7°, 22.3°, 28.6° and 39.3° based on XRD database. However, after dialysis, all its characteristic peaks disappeared. The HAP peaks show that its intensity is very low, which may be the result of little HAP in the sample. But it is important to note that the local Ca^{2+} concentration around the NPs surfaces is higher than that in the surrounding solution, which can be in favor of its

bounding to functional groups of NPs, and thus nucleation takes place. Combining the results from FTIR and XRD, we demonstrate that HAP has been formed.

4 Conclusions

In this study NPs were formed by cross-linking s-GL with oxidized heparin via Schiff's base linkage. The obvious advantage of this method is that small toxic cross-linkers like glutardialdehyde are not needed while the aldehyde groups of the larger oxidized GAG do not express a toxicity in vitro as shown in previous investigations [24].The process of nanoparticle formation could be optimized here regarding particle size and colloidal stability selecting a pH of 2.5, 0.5 % w/v s-GL and a ratio of 1:2.3 n(–CHO)/n(–NH_2) to obtain a mean particle size of 198 nm. These NPs were further used as nano-reactor for promoting the growth of HAP crystals. The mineralization process was done in a solution composed of $Ca(NO_3)_2$ and $(NH_4)_2HPO_4$. The NPs provided probably nucleation sites through their carboxyl and sulfate groups to form thermally-stable B-type HAP on them without calcination. Future studies with these NPs will be conducted to test their applicability for controlled release of growth factors with heparin-binding domains like BMP-2 or FGF-2 and their intermixing with hydrogels, which can be injected into bone defects.

Acknowledgments We are very thankful to Dr. Hendrik Metz for zeta potential experiment, Mrs. Ute Mentzel for FFFF and DLS measurements and Ms. Kristin Wendt for XRD analysis. This work was supported by the European Union Seventh Framework Program (FP7/2007–2013) under Grant agreement no. NMP4-SL-2009-229292 ("Find and Bind").

References

1. Ryu J, Kim SW, Kang K, Park CB. Mineralization of self-assembled peptide nanofibers for rechargeable lithium ion batteries. Adv Mater. 2010;22(48):5537–41. doi:10.1002/adma.201000669.
2. Scholler K, Ethirajan A, Zeller A, Landfester K. Biomimetic route to calcium phosphate coated polymeric nanoparticles: influence of different functional groups and pH. Macromol Chem Phys. 2011;212(11):1165–75. doi:10.1002/macp.201100109.
3. Zietz C, Bergschmidt P, Lange R, Mittelmeier W, Bader R. Third-body abrasive wear of tibial polyethylene inserts combined with metallic and ceramic femoral components in a knee simulator study. Int J Artif Organs. 2013;36(1):47–55. doi:10.5301/ijao.5000189.
4. Liu H, Li H, Cheng WJ, Yang Y, Zhu MY, Zhou CR. Novel injectable calcium phosphate/chitosan composites for bone substitute materials. Acta Biomater. 2006;2(5):557–65.
5. Legeros RZ, Lin S, Rohanizadeh R, Mijares D, Legeros JP. Biphasic calcium phosphate bioceramics: preparation, properties and applications. J Mater Sci. 2003;14(3):201–9.
6. Li WM, Chen SY, Liu DM. In situ doxorubicin-CaP shell formation on amphiphilic gelatin-iron oxide core as a multifunctional drug delivery system with improved cytocompatibility, pH-responsive drug release and MR imaging. Acta Biomater. 2013;9(2):5360–8. doi:S1742-7061(12)00460-6.
7. Azami M, Samadikuchaksaraei A, Poursamar SA. Synthesis and characterization of a laminated hydroxyapatite/gelatin nanocomposite scaffold with controlled pore structure for bone tissue engineering. Int J Artif Organs. 2010;33(2):86–95.
8. Boanini E, Bigi A. Biomimetic gelatin–octacalcium phosphate core-shell microspheres. J Colloid Interface Sci. 2011;362(2):594–9.
9. Ethirajan A, Ziener U, Chuvilin A, Kaiser U, Colfen H, Landfester K. Biomimetic hydroxyapatite crystallization in gelatin nanoparticles synthesized using a miniemulsion process. Adv Funct Mater. 2008;18(15):2221–7.
10. Nitta SK, Numata K. Biopolymer-based nanoparticles for drug/gene delivery and tissue engineering. Int J Mol Sci. 2013;14(1):1629–54.
11. Kadengodlu PA, Aigaki T, Abe H, Ito Y. Cationic cholesterol-modified gelatin as an in vitro siRNA delivery vehicle. Mol Biosyst. 2013;9(5):965–8. doi:10.1039/c2mb25424g.
12. Tan GK, Tabata Y. Effect of gelatin microsphere size and cell/microsphere ratio on transforming growth factor-beta-3-induced chondrogenesis of human mesenchymal stem cells. J Tissue Eng Regen Med. 2012;6:67.
13. Solorio LD, Vieregge EL, Dhami CD, Dang PN, Alsberg E. Engineered cartilage via self-assembled hMSC sheets with incorporated biodegradable gelatin microspheres releasing transforming growth factor-beta 1. J Controlled Release. 2012;158(2):224–32.
14. Lee ES, Gao ZG, Bae YH. Recent progress in tumor pH targeting nanotechnology. J Controlled Release. 2008;132(3):164–70.
15. Kawadkar J, Jain R, Kishore R, Pathak A, Chauhan MK. Formulation and evaluation of flurbiprofen-loaded genipin cross-linked gelatin microspheres for intra-articular delivery. J Drug Target. 2013;21(2):200–10. doi:10.3109/1061186X.2012.745549.
16. Guillame-Gentil O, Semenov O, Roca AS, Groth T, Zahn R, Voros J, et al. Engineering the extracellular environment: strategies for building 2D and 3D cellular structures. Adv Mater. 2010;22(48):5443–62. doi:10.1002/adma.201001747.
17. Hudalla GA, Murphy WL. Biomaterials that Regulate Growth Factor Activity via Bioinspired Interactions. Adv Funct Mater. 2011;21(10):1754–68.
18. Lever R, Page CR. Novel drug development opportunities for heparin. Nat Rev Drug Discov. 2002;1(2):140–8.
19. Raman K, Mencio C, Desai UR, Kuberan B. Sulfation patterns determine cellular internalization of heparin-like polysaccharides. Mol Pharm. 2013;. doi:10.1021/mp300679a.
20. Kanzaki S, Ariyoshi W, Takahashi T, Okinaga T, Kaneuji T, Mitsugi S, et al. Dual effects of heparin on BMP-2-induced osteogenic activity in MC3T3-E1 cells. Pharmacol Rep. 2011;63(5):1222–30.
21. Jeon O, Song SJ, Yang HS, Bhang SH, Kang SW, Sung MA, et al. Long-term delivery enhances in vivo osteogenic efficacy of bone morphogenetic protein-2 compared to short-term delivery. Biochem Biophys Res Commun. 2008;369(2):774–80.
22. Liu ZM, Gu QY, Xu ZK, Groth T. Synergistic effect of polyelectrolyte multilayers and osteogenic growth medium on differentiation of human mesenchymal stem cells. Macromol Biosci. 2010;10(9):1043–54.
23. Kisiel M, Martino MM, Ventura M, Hubbell JA, Hilborn J, Ossipov DA. Improving the osteogenic potential of BMP-2 with hyaluronic acid hydrogel modified with integrin-specific fibronectin fragment. Biomaterials. 2013;34(3):704–12.
24. Kowitsch A, Yang Y, Ma N, Kuntsche J, Mader K, Groth T. Bioactivity of immobilized hyaluronic acid derivatives regarding protein adsorption and cell adhesion. Biotechnol Appl Biochem. 2011;58(5):376–89.

25. Xiao JW, Zhu YC, Ruan QC, Liu YY, Zeng Y, Xu FF, et al. Biomacromolecule and surfactant complex matrix for oriented stack of 2-dimensional carbonated hydroxyapatite nanosheets as alignment in calcified tissues. Cryst Growth Des. 2010;10(4):1492–9.
26. Jia XQ, Burdick JA, Kobler J, Clifton RJ, Rosowski JJ, Zeitels SM, et al. Synthesis and characterization of in situ cross-linkable hyaluronic acid-based hydrogels with potential application for vocal fold regeneration. Macromolecules. 2004;37(9):3239–48.
27. Sashidhar RB, Capoor AK, Ramana D. Quantitation of epsilon-amino group using amino-acids as reference-standards by trinitrobenzene sulfonic-acid—a simple spectrophotometric method for the estimation of hapten to carrier protein ratio. J Immunol Methods. 1994;167(1–2):121–7.
28. Croy SR, Kwon GS. The effects of Pluronic block copolymers on the aggregation state of nystatin. J Control Release. 2004;95(2):161–71.
29. Ethirajan A, Schoeller K, Musyanovych A, Ziener U, Landfester K. Synthesis and optimization of gelatin nanoparticles using the miniemulsion process. Biomacromolecules. 2008;9(9):2383–9.
30. Coester CJ, Langer K, van Briesen H, Kreuter J. Gelatin nanoparticles by two step desolvation—a new preparation method, surface modifications and cell uptake. J Microencapsul. 2000;17(2):187–93. doi:10.1080/026520400288427.
31. Kim DW, Cho IS, Kim JY, Jang HL, Han GS, Ryu HS, et al. Simple large-scale synthesis of hydroxyapatite nanoparticles. In situ observation of crystallization process. Langmuir. 2010;26(1):384–8.
32. Habeeb AFS. Determination of free amino groups in proteins by trinitrobenzenesulfonic acid. Anal Biochem. 1966;14(3):328. doi:10.1016/0003-2697(66)90275-2.
33. Lu SY, Liu MZ, Ni BL. An injectable oxidized carboxymethylcellulose/*N*-succinyl-chitosan hydrogel system for protein delivery. Chem Eng J. 2010;160(2):779–87.
34. Sui WP, Wang YH, Dong S, Chen YJ. Preparation and properties of an amphiphilic derivative of succinyl-chitosan. Colloids Surf A. 2008;316(1–3):171–5.
35. Harada NS, Oyama HT, Bartoli JR, Gouvea D, Cestari IA, Wang SH. Quantifying adsorption of heparin on a PVC substrate using ATR-FTIR. Polym Int. 2005;54(1):209–14.
36. Wang DA, Varghese S, Sharma B, Strehin I, Fermanian S, Gorham J, et al. Multifunctional chondroitin sulphate for cartilage tissue-biomaterial integration. Nat Mater. 2007;6(5):385–92.
37. Kale R, Bajaj A. Ultraviolet spectrophotometric method for determination of gelatin crosslinking in the presence of amino groups. J Young Pharm. 2010;2(1):90–4. doi:10.4103/0975-1483.62223.
38. Bubnis WA, Ofner CM. The determination of epsilon-amino groups in soluble and poorly soluble proteinaceous materials by a spectrophotometric method using trinitrobenzenesulfonic acid. Anal Biochem. 1992;207(1):129–33.
39. Farris S, Song J, Huang Q. Alternative reaction mechanism for the cross-linking of gelatin with glutaraldehyde. J Agric Food Chem. 2010;58(2):998–1003. doi:10.1021/jf9031603.
40. Griffiths PC, Fallis IA, Teerapornchaisit P, Grillo I. Hydrophobically modified gelatin and its interaction in aqueous solution with sodium dodecyl sulfate. Langmuir. 2001;17(9):2594–601.
41. Dasgupta S, Banerjee SS, Bandyopadhyay A, Bose S. Zn- and Mg-doped hydroxyapatite nanoparticles for controlled release of protein. Langmuir. 2010;26(7):4958–64. doi:10.1021/la903617e.
42. Rehman I, Bonfield W. Characterization of hydroxyapatite and carbonated apatite by photo acoustic FTIR spectroscopy. J Mater Sci. 1997;8(1):1–4.
43. Wu HB, Chan MN, Chan CK. FTIR characterization of polymorphic transformation of ammonium nitrate. Aerosol Sci Technol. 2007;. doi:10.1080/02786820701272038.
44. Chang MC, Tanaka J. FT-IR study for hydroxyapatite/collagen nanocomposite cross-linked by glutaraldehyde. Biomaterials. 2002;23(24):4811–8.
45. LeGeros RZ. Calcium phosphates in oral biology and medicine. Monogr Oral Sci. 1991;15:1–201.
46. Rodriguez A, Eremin K, Khandekar N, Stenger J, Newman R, Bazeta F, et al. Characterization of calcium sulfate grounds and fillings of applied tin-relief brocades by Raman spectroscopy, Fourier transform infrared spectroscopy, and scanning electron microscopy. J Raman Spectrosc. 2010;41(11):1517–24.

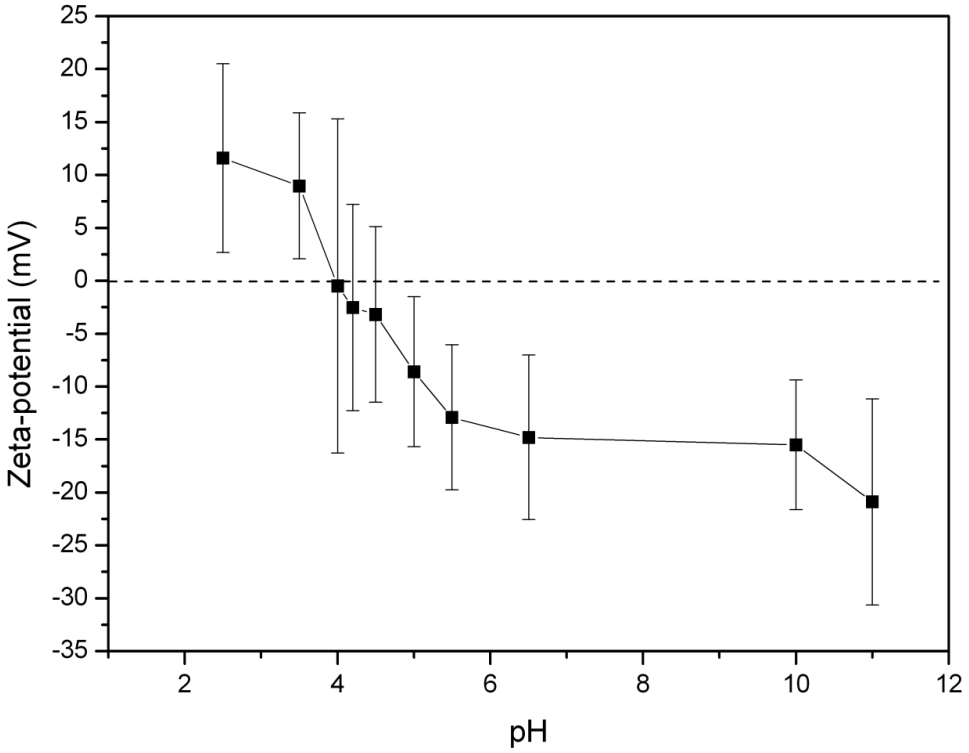

Figure S1: Zeta potential of succinylated gelatin at 1 mg/mL in 50 mM NaCl solution.

Reprinted with permission from Springer Science + Business Media and Journal of Materials Science: Materials in Medicine, 25, 2013, 669-680, Novel mineralized heparin–gelatin nanoparticles for potential application in tissue engineering of bone, Yuan Yang, Haihao Tang, Alexander Köwitsch, Karsten Mäder, Gerd Hause, Joachim Ulrich, Thomas Groth.
 DOI: 10.1007/s10856-013-5111-2

Chapter 7

Summary and future perspectives

This PhD thesis was aimed to develop stable material coatings consisting of the natural biopolymers called glycosaminoglycans (GAG). Therefore, two different modification strategies were applied to generate reactive and functional GAG. The selected GAG represented heparin, chondroitin sulfate, hyaluronic acid (HA) and a chemically sulfated HA. In the first approach, a small cross-linker was introduced to a portion of the GAG carboxyl groups and then subsequently cleaved to generate free thiol species. On the other hand, the carbon-carbon bond of the uronic acid saccharide moieties was cleaved by sodium periodate to generate free aldehyde functionalities. Both strategies were applied at two different ratios to obtain GAG with different amount of reactive functional groups. Consequently, the modified GAG were applied to different model substrata (glass, silicon and gold) to produce “glycanized” substrata that reflect the specific properties of the applied GAG. The immobilization of the functional GAG was achieved by covalent attachment of thiolated GAG to vinyl-terminated glass or silicon via thiol-ene click reaction or the reductive amination of the aldehyde GAG to amino-terminated substrata. Further, it was shown that the thiolated GAG can be immobilized in a heterogeneous manner via microcontact printing. The characterization of the modified substrata demonstrated an increased layer thickness as well as specific topographical structures for the different type of GAG that were immobilized. In addition, the surfaces represented the increasing sulfation of the immobilized GAG by an increase in surface wettability and a more negative zeta potential.

To determine the bioactivity of the fabricated GAG coatings, their interaction with natural binding proteins fibronectin (FN) and aggrecan was assessed by in situ measurements with surface plasmon resonance monitoring. It was found that an increased sulfation of the immobilized GAG improved the binding of FN and that aggrecan was bound to the modified HA derivatives in comparable amounts as to the native HA. Furthermore, cell adhesion and cell growth experiments were conducted to investigate the biological activity and the cytotoxicity of the glycanized substrata. Moreover, it was shown that cell adhesion on the HA coated surfaces was possibly mediated by the specific interaction of HA with its cell surface receptor ligand CD44.

Cell viability and cell growth studies revealed that especially the GAG having a lower degree of modification retained their bioactivity indicated by support of cell adhesion and proliferation on the GAG-modified substrata.

The activation of GAG by either oxidation or thiolation is a facile way to obtain reactive biopolymers that can be subsequently used for covalent surface grafting as well as cross-linking to other reactive species. The ability to control the degree of modification by thiolation or oxidation is offering a wide range of possible applications combining them with biological derived or synthetic materials. Since thiols can be transformed to disulfides by pH variation or under mild oxidizing conditions the cross-linking of the thiolated GAG can be applied for the subsequent stabilization of multilayer coatings or for the generation of hydrogels. Furthermore, the thiols are able to bind several proteins and growth factors which also offer free thiol moieties. The aldehyde heparin was applied as a cross-linker of succinylated gelatin to form nanoparticles as a template for the mineralization of hydroxyapatite. The use of oxidized heparin is avoiding the necessity of an additional cross-linking agent and allowing an additional uploading of growth factors exhibiting a heparin-binding domain e.g. FGF-2 or BMP-2. These approaches might also be use to guide stem cell differentiation into osteogenic or chondrogenic lineage, thus, being capable of promoting tissue regeneration. Furthermore, it is possible to use the oxidized GAG for the formation of hydrogels or scaffolds by cross-linking them with (poly)amine or hydrazide compounds.

The presented surface modification approaches represent a promising tool to produce stable GAG coatings for biomedical implants in the field of tissue engineering. Moreover, the generation of heterogeneous GAG coatings by microcontact printing represents a fast approach to produce biosensing tools that might be useful for the detection of the metastatic activity of cancer cells.

Acknowledgment

First of all, I would like to express my deepest gratitude to Prof. Dr. Thomas Groth who gave me the opportunity to work in his group and helped me to gather the knowledge needed to compose this thesis. Furthermore, I want to thank him for the fruitful discussions, the freedom to fulfill my scientific aims and the possibility to collaborate with an international scientific community.

I would like to thank all my former and current colleagues of the Biomedical Materials Group, for their collaboration, support and the familiar atmosphere which always helped to keep me motivated, focused and balanced.

Furthermore, I would like to acknowledge all my co-authors and collaborators. Dr. Georgios Michanetzis and Prof. Dr. Yannis Missirlis from the Biomedical Engineering Lab of the University of Patras for the opportunity to perform numerous AFM measurements. Prof. Dr. Karsten Mäder and the Pharmaceutical Technology Group of the Martin Luther University Halle-Wittenberg for the measurements of molecular weights with Field-Flow Fractionation. Martin Hielscher and Prof. Dr. Steffen Fischer from the Institute of Plant and Wood Chemistry at the University of Technology in Dresden for doing the FT-IR and Raman measurements.

The European Union Seventh Framework Programme (FP7/2007-2013, NMP4-SL-2009-229292; PIAP-GA-2012-324386) and the German Academic Exchange Service (DAAD) are acknowledged for partly supporting the successful fulfillment of my experimental work.

I am truly grateful to my family and my friends for their ongoing support and the continual encouragements.

Finally, I would like to express my gratitude to all who made a contribution to this work and that have not been explicitly mentioned here.

Publication list with declaration of self-contribution to research articles

1. A. Köwitsch, G. Zhou, T. Groth, Medical application of glycosaminoglycans – A review, Submitted to *Journal of Tissue Engineering and Regenerative Medicine*, **2016.**

My contribution was about 80%. I assembled and wrote all parts except for the part 3 “Survey on medical application of native glycosaminoglycans” which was mainly written by G. Zhou. Prof. Dr. T. Groth helped in planning and revising the manuscript.

2. A. Köwitsch, Y. Yang, N. Ma, J. Kuntsche, K. Mäder, T. Groth, Bioactivity of immobilized hyaluronic acid derivatives regarding protein adsorption and cell adhesion, *Biotechnology and Applied Biochemistry* **2011**, *58*, 376 - 389.

My contribution was about 50%. I performed the synthesis, characterization and measurements related to thiolated hyaluronic acid and wrote the major part of the manuscript. Also I performed the AFM measurements. The synthesis and most of the characterization of oxidized hyaluronic acid were done by Dr. Y. Yang. The cell adhesion experiment were performed by N. Ma. The measurements of molecular weight were measured by Dr. J. Kuntsche from the group of Prof. Dr. K. Mäder.

3. A. Köwitsch, M. Jurado Abreu, A. Chhalotre, M. Hielscher, S. Fischer, K. Mäder, T. Groth, Synthesis of thiolated glycosaminoglycans and grafting to solid surfaces, *Carbohydrate Polymers* **2014**, *114*, 344 - 351.

My contribution was about 75%. I wrote the manuscript with help of Prof. T Groth who helped me planning the experiments and revised the manuscript. I performed all experiments except for the microcontact printing which was done by M. Jurado Abreu and A. Chhalotre and the measurements of molecular weight were measured in the group of Prof. Dr. K. Mäder. Further, Raman spectroscopy was performed by M. Hielscher from the group of Prof. Dr. S. Fischer.

4. A. Köwitsch, M.S. Niepel, G.P. Michanetzis, Y.F. Missirlis, T. Groth, Effect of immobilized thiolated glycosaminoglycans on fibronectin adsorption and behavior of fibroblasts, *Macromolecular Bioscience* **2016**, *16*, 381 - 394.

My contribution was about 80%. I conducted all experimental work. M.S. Niepel contributed to the biological evaluation of the paper. Dr. G.P. Michanetzis assisted me in performing the AFM measurements at the group of Prof. Dr. Y.F. Missirlis. Prof. Dr. T. Groth supported the planning of experiments and also contributed during the revision of the manuscript.

5. Y. Yang, A. Köwitsch, N. Ma, K. Mäder, I. Paskuleva, R.L. Reis, T. Groth, Functionality of surface-coupled oxidised glycosaminoglycans towards fibroblast adhesion, *Journal of Bioactive and Compatible Polymers* **2015**, *31*, 191 – 207.

My contribution was about 40%. I mainly contributed to the surface grafting and surface characterization, like Ellipsometry and AFM measurements and wrote the related paragraph. I also primarily contributed in writing and revising of the manuscript.

6. Y. Yang, H. Tang, A. Köwitsch, K. Mäder, G. Hause, J. Ulrich, T. Groth, Novel mineralized heparin-gelatin nanoparticles for potential application in tissue engineering of bone, *Journal of Materials Science: Materials in Medicine* **2014**, *25*, 669 – 680.

My contribution was about 20%. I mainly contributed in writing and revision of the manuscript. I also contributed to the synthesis and the evaluation of the chemical composition of the succinylated gelatin and the oxidized heparin (FT-IR, Molecular weight).

Other publications that are not involved in this thesis

1. L. Heller, S. Schwarz, V. Perl, A. Köwitsch, B. Siewert, R. Csuk, Incorporation of a Michael acceptor enhances the antitumor activity of triterpenoic acids, *European journal of medicinal chemistry* **2015**, *101*, 391 - 399.
2. S.E. Majd, R. Kuijer, A. Köwitsch, T. Groth, T.A. Schmidt, P.K. Sharma, Both hyaluronan and collagen type II keep proteoglycan 4 (lubricin) at the cartilage surface in a condition that provides low friction during boundary lubrication*, Langmuir* **2014**, *30*, 14566 - 14572.
3. B. Siewert, J. Wiemann, A. Köwitsch, R. Csuk, The chemical and biological potential of C ring modified triterpenoids, *European journal of medicinal chemistry* **2014**, *72*, 84 - 101.
4. M.C. Márquez-Posadas, J. Ramiro, J. Becher, Y. Yang, A. Köwitsch, I. Pashkuleva, R. Díez-Ahedo, M. Schnabelrauch, R.L. Reis, T. Groth, S. Merino, Surface microstructuring and protein patterning using hyaluronan derivatives, *Microelectronic Engineering* **2013**, *106*, 21–26.
5. Z. Li, A. Köwitsch, G. Zhou, T. Groth, B. Fuhrmann, M. Niepel, E. Amado, J. Kressler, Enantiopure chiral poly(glycerol methacrylate) self-assembled monolayers knock down protein adsorption and cell adhesion*, Advanced Healthcare Materials* **2013**, *2*, 1377-87.

Book Chapter

1. M.S. Niepel, A. Köwitsch, Y. Yang, N. Ma, N. Aggarwal, G. Guduru, T. Groth

   Generic Methods of Surface Modification to Control Adhesion of Cells and Beyond, In: Taubert A, Mano JF, Rodríguez-Cabello JC (eds.), *Biomaterials Surface Science* **2013**, Wiley-VCH, Weinheim, Chapter 15, pp. 443 - 468.

Published Abstracts

1. A. Köwitsch, Y. Yang, T. Groth, Dependence of protein adsorption and cell adhesion on glycosaminoglycan sulfation degree, *International journal of artificial organs* **2013**, 36, 550.
2. Z. Li, A. Köwitsch, G. Zhou, T. Groth, B. Fuhrmann, M. Niepel, E. Amado, J. Kressler, Chirality of poly(glycerol methacrylate) brushes affects protein adsorption and cell adhesion*, Abstracts of papers of the american chemical society* **2013**, *245*, 523.
3. Y. Yang, N. Ma, A. Köwitsch, T. Groth, Controlling mesenchymal stem cell proliferation and differentiation through glycosaminoglycan engineered surfaces, *Journal of tissue engineering and regenerative medicine* **2012**, *6*, Suppl. 2, TS010.
4. Y. Yang, J. Becher, N. Ma, A. Köwitsch, M. Schnabelrauch, T. Groth, Sulfate groups effect on protein adsorption and cell adhesion, *International journal of artificial organs* **2011**, *34*, 637 - 38.
5. A. Köwitsch, J. Kuntsche, N. Ma, Y. Yang, T. Groth, Biomimetic modification of surfaces by thiolated glycosaminoglycans, *International journal of artificial organs* **2011**, *34*, 665.

Oral presentations

1. A. Köwitsch, Y. Yang, T. Groth, Dependence of protein adsorption and cell adhesion on glycosaminoglycan sulfation degree, *40th Congress of the European Society for Artificial Organs*, 11th – 14th September **2013**, Glasgow, Scotland.
2. A. Köwitsch, M. Jurado Abreu, Y. Yang, J. Ramiro, M.C. Márquez-Posadas, S. Merino, T. Groth, Immobilized thiolated glycosaminoglycans to control protein adsorption and cell behavior, *Annual Meeting of the German Society for Biomaterials*, 1st – 3rd November **2012**, Hamburg, Germany.
3. Y. Yang, H. Kindi, A. Köwitsch, T. Groth, An in situ injectable polysaccharide-based hydrogel with potential for cartilage repair and regeneration, *Annual Meeting of the German Society for Biomaterials*, 1st – 3rd November **2012**, Hamburg, Germany.
4. A. Köwitsch, Y. Yang, N. Ma, G.P.A. Michanetzis, Y.F. Missirlis, T. Groth, Effects of immobilized thiolated glycosaminoglycans on protein adsorption and cell adhesion, *39th Congress of the European Society for Artificial Organs*, 26th – 29th September **2012**, Rostock, Germany.
5. Y. Yang, S. Möller, N. Ma, A. Köwitsch, J. Becher, M. Schnabelrauch, T. Groth, Sulfation of glycosaminoglycans affects cell adhesion, proliferation and differentiation, *Summer School on Biomaterials and Regenerative Medicine*, 9th - 13th July **2012**, Riva del Garda, Italy.

Posters

1. A. Köwitsch, Y. Yang, B. Tulabandula, H. Kindi, T. Groth, Hydrogels from Glycosaminoglycans for Cartilage Renewal, *19th Congress of the European Society for Biomechanics*, 25th – 28th August **2013**, Patras, Greece.
2. A. Köwitsch, Y. Yang, N. Ma, T. Groth, Effect of immobilized thiolated Glycosaminoglycans on cell adhesion, *4th International Symposium Interface Biology of Implants (IBI)*, 9th – 11th May **2012**, Warnemünde, Germany.
3. A. Köwitsch, Y. Yang, N. Ma, T. Groth, Effect of immobilized thiolated glycosaminoglycans on cell adhesion, *3rd Congress BioNanoMed*, 1st – 2nd March **2012**, Krems (Danube), Austria.
4. A. Köwitsch, J. Kuntsche, N. Ma, Y. Yang, T. Groth, Biomimetic modification of surfaces by thiolated glycosaminoglycans, *4th Joint ESAO-IFAO Congress*, 9th – 12th October **2011**, Porto, Portugal.
5. A. Köwitsch, J. Kuntsche, N. Ma, Y. Yang, T. Groth, Surface modification with thiolated glycosaminoglycans to study protein adsorption and cell behavior, *Advanced Summer School "Interrogations at the biointerface"*, 20th – 24th June **2011**, Porto, Portugal.
6. A. Köwitsch, Y. Yang, T. Groth, Characterization and immobilization of thiolated heparin for biomimetic modification of gold surfaces, *ESAO Winter School*, 26th – 29th January **2011**, Semmering, Austria.

Curriculum vitae

Personal data

Name:	Alexander Köwitsch
Address:	Fischerstecherstr. 5, 06120 Halle (Saale), Germany
Date of birth:	17. August 1982 in Salzwedel, Germany
Academic degree:	Dipl.-Chem. (Diplom-Chemiker)

Work Experience

04/2014 – 03/2016	Research and teaching assistant (Pharmacy, Pharmaceutical Biotechnology, Biomedical Engineering), Institute of Pharmacy, Martin-Luther-University Halle-Wittenberg
10/2014 – 12/2014	Research fellow at BioElpida (Lyon, France)
12/2009 – 03/2010	Research assistant at Biomedical Material Group, Institute of Pharmacy, Martin-Luther-University Halle-Wittenberg

Education

04/2010 – 03/2016	PhD student in the group of Prof. Dr. rer. nat. habil. Thomas Groth, Institute of Pharmacy, Martin-Luther-University Halle-Wittenberg
10/2008 – 09/2009	Diploma student in the group of Prof. Dr. techn. habil. Rene Csuk Institute of Chemistry, Martin-Luther-University Halle-Wittenberg Title of diploma thesis: “Synthese von antitumoraktiven Ursol- und Oleanolsäurederivaten”
10/2003 – 09/2008	Chemistry student at Martin-Luther-University Halle-Wittenberg

07/2002 – 03/2003 Military service in Schleswig

08/1998 – 06/2002 Secondary School “Geschwister Scholl” in Gardelegen

08/1993 – 07/1998 Secondary School J. F. Danneil in Kalbe/Milde

Awards / Grants

10/2012	DAAD research fellow, Institute of Biomechanics and Biomedical Engineering, University of Patras, Greece
03/2012	Poster award (Erwin Schrödinger Gesellschaft) BioNanoMed 2012 Krems (Austria)
10/2011 - 11/2011	DAAD research fellow, Institute of Biomechanics and Biomedical Engineering, University of Patras, Greece
06/2011	Termis Travel Grant „Advanced summer school - Interrogations at the biointerface“, Porto (Portugal)

Halle (Saale), 18. April 2016

Alexander Köwitsch

Selbstständigkeitserklärung

Hiermit erkläre ich gemäß § 5 der Promotionsordnung der Naturwissenschaftlichen Fakultät I der Martin-Luther-Universität Halle-Wittenberg, dass ich die Ergebnisse der vorliegenden kumulativen Dissertationsarbeit

Immobilization of functionalized glycosaminoglycans

to regulate protein adsorption and cell behavior

am Institut für Pharmazie in der Arbeitsgruppe Biomedizinische Materialien unter Anleitung von Prof. Dr. rer. nat. habil. Thomas Groth selbständig erarbeitet und die Dissertation ohne fremde Hilfe verfasst habe.

Weiterhin erkläre ich, dass ich keine anderen als die von mir angegebenen Quellen und Hilfsmittel zur Erstellung meiner Dissertation verwendet habe. Den benutzen Werken wörtlich oder inhaltlich entnommene Stellen sind als solche gekennzeichnet.

Ferner erkläre ich, dass ich mich mit der vorliegenden Dissertationsarbeit erstmals um die Erlangung eines Doktorgrades bewerbe.

Halle (Saale), den 18. April 2016

Dipl.-Chem. Alexander Köwitsch